Impact and blast response of polymer matrix laminates- finite-element studies

Impact and blast response of polymer matrix composite laminates: finite-element studies

by

Vaibhav A. Phadnis

A doctoral thesis submitted in a partial fulfilment of the requirements for the award of Doctor of Philosophy at Loughborough University

Wolfson School of Mechanical and Manufacturing Engineering

December 2013

To my parents, Adv. Anant and Meghana Phadnis, and sister Ms. Maitreyee Phadnis

ABSTRACT

Polymer matrix composites (PMCs) offer several advantages compared to traditional metallic counterparts when employed in high-performance products that need to be lightweight, yet strong enough to sustain harsh loading conditions - such as aerospace components and protective structures in military applications- armours, helmets, and fabrications retrofitted to transport vehicles and bunkers. These are often subjected to highly dynamic loading conditions under blast and ballistic impacts. Severe impact energy involved in these dynamic loading events can initiate discrete damage modes in PMCs such as matrix cracking, matrix splitting, delamination, fibre-matrix debonding, fibre micro-buckling and fibre pull-out. Interaction of these damage modes can severely reduce the load carrying capacity of such structures. This needs to be understood to design structures with improved resistance to such loading.

In this regard, the current study focuses on the FE modelling of the impact and blast response of PMC laminates. To facilitate this, 3D continuum dynamic failure criteria, based on the theory of continuum damage mechanics (CDM), were proposed to accurately estimate initiation and evolution of damage of PMC laminates. These criteria are capable of differentiating between the damage modes of matrix and fibre materials distinctly under tension and compression loading states. Non-linear shear behaviour of the polymer matrix was modelled using the classical plasticity approach while accounting for the strain-rate-sensitive response of the material. These criteria were incorporated as a user-defined subroutine VUMAT in ABAQUS/Explicit. Interply delamination was modelled using cohesive zone elements (CZE). The developed material model was employed to analyse the response of PMC laminates under two distinctively different dynamic loading events - ballistic-impact and blast loading.

First, FE model was developed to study ballistic-impact response of hybrid composite laminates made of plain-weave E-glass woven fabric/epoxy composite and 8H satin weave woven fabric/epoxy composite and their hybrids. Four cases – two parents and two hybrids – were studied to analyse their ballistic limit velocity, energy absorption capacity, and discrete damage modes. In the second case, air-blast performance of curved quasi-isotropic laminate - AS4/3501-6 - was studied. Appropriate fluid-structure interaction (FSI) was considered to model the loss of blast energy to surrounding air in a shock tube. The effect of varying radius of curvature of these panels on their energy absorption capacity, and modes of deformation was studied. It was shown that the current FE modelling approach can be effectively used to model mechanical behaviour of PMC composite laminates under such transient dynamic loading events.

Keywords – Polymer matrix composite; FE model; blast; ballistic impact; VUMAT; damage; cohesive-zone model; failure

ACKNOWLEDGEMENT

I would like to express my deepest gratitude to my supervisors Professor Vadim Silberschmidt and Dr Anish Roy for their invaluable guidance throughout the course of this study. Their positive outlook, suggestions, constructive criticism and confidence in my research work catalysed the accomplishment of this thesis.

Special thanks to Professor Arun Shukla and Dr Puneet Kumar (University of Rhode Island, USA) for providing the experimental data of blast behaviour of curved CFRP panels. I am also grateful to Prof Niranjan Naik and Mr Kedar Pandya (Indian Institute of Technology, Mumbai, India) for their support in the experimental study of ballistic performance of woven-fabric composites.

Many thanks to all the members of Mechanics of Advanced Materials (MOAM) research group for their boundless companionship and fruitful discussions.

Finally, very special thanks to my parents Mr Anant Phadnis, Mrs Meghana Phadnis and my sister Ms Maitreyee Phadnis for their endless love, patience and encouragement throughout this study. I dedicate this thesis to them.

PUBLICATIONS

JOURNAL PAPERS

Phadnis, V. A., Kumar, P., Shukla A., Roy, A. and Silberschmidt, V. V. (2013). Air blast response of curved FRP composites: experiments and numerical analysis. Materials and Design. Submitted.

Phadnis, V. A., Makhdum, F., Roy, A. and Silberschmidt, V. V. (2013). Drilling in carbon/epoxy composites: Experimental investigations and finite element implementation. *Composites Part A - Applied Science and Manufacturing*. 47, pp. 41-51.

Makhdum, F., Phadnis, V. A., Roy, A. and Silberschmidt, V. V. (2013). Effect of ultrasonically-assisted drilling on carbon-fibre-reinforced plastics, Journal of Sound and Vibration. Submitted

Phadnis, V. A., Roy, A. and Silberschmidt, V. V. (2013). A Finite Element Model of Ultrasonically Assisted Drilling in Carbon/Epoxy Composites. *Procedia CIRP*. 8, pp. 140-145.

Phadnis, V. A., Roy, A. and Silberschmidt V. V. (2013). Finite element analysis of drilling in carbon fibre reinforced polymer composites. *Journal of Physics: Conference Series*. 382(1), pp. 120-128.

Phadnis, V. A., Pandya K. S., Naik N. K., Roy, A. and Silberschmidt V. V. (2013). Ballistic-impact behaviour of hybrid woven fabric composites: Experimental study and finite element analysis. *Journal of Physics: Conference Series*. Accepted.

Phadnis, V. A., Roy, A. and Silberschmidt V. V. (2013). Ultrasonic assisted drilling: A finite element model incorporating acoustic softening effects. *Journal of Physics: Conference Series*. Accepted.

Phadnis, V. A., Kumar, P., Shukla A., Roy, A. and Silberschmidt V. V. (2013). Blast

response of curved carbon/epoxy composite panels. *Journal of Physics: Conference Series*. Accepted.

Phadnis, V. A., Kumar, P., Shukla A., Roy, A. and Silberschmidt V. V. (2013). Finite element analysis of blast response of CFRP panels. *Key Engineering Materials*. Accepted.

Phadnis, V. A., Roy, A. and Silberschmidt V. V. (2013). Ultrasonically assisted drilling of CFRPs: FE model. *Key Engineering Materials*. Accepted.

Phadnis, V. A., Kumar, P., Shukla A., Roy, A. and Silberschmidt V. V. (2013). Response of curved carbon/epoxy composite panels to air blast loading: Experimental investigation and finite-element analysis. *Composite Science and technology*. Submitted.

Phadnis, V. A., Roy, A. and Silberschmidt V. V. (2013). Ballistic-impact behaviour of hybrid woven fabric composites: Experimental study and finite element analysis. C*omposites Part A: Applied Science and Manufacturing*. Submitted.

Phadnis, V. A., Makhdum, F., Roy, A. and Silberschmidt, V. V. (2012). Experimental and Numerical Investigations in Conventional and Ultrasonically Assisted Drilling of CFRP Laminate. *Procedia CIRP*. 1, pp. 455-459.

Phadnis, V. A., Makhdum, F., Roy, A. and Silberschmidt, V. V. (2012). Drilling-Induced Damage in CFRP Laminates: Experimental and Numerical Analysis. *Solid state phenomena*. 188, pp. 150-7.

CONFERENCE CONTRIBUTIONS

Phadnis, V.A., Kumar, P., Shukla A., Roy, A. and Silberschmidt V. V. (2013). Blast response of curved CFRP panels. *Deformation and Fracture of Composites (DFC-12) & Structural Integrity and Multi-scale Modelling (SI-6)*. Cambridge, UK.

Phadnis, V.A., Roy, A. and Silberschmidt, V. V. (2013). Finite element analysis of UAD in CFRP composites. *14th CIRP conference on Modelling of machining operations*. Torino, Italy.

Phadnis, V.A., Roy, A. and Silberschmidt, V. V. (2013). Finite element analysis of UAD in CFRP composites. *10th International conference on damage assessment of*

structures, DAMAS. Dublin, Ireland.

Phadnis, V.A., Kumar, P., Shukla A., Roy, A. and Silberschmidt V. V. (2013). Modelling air-blast response of curved carbon/epoxy panels. *10th International conference on damage assessment of structures, DAMAS*. Dublin, Ireland.

Phadnis, V.A., Makhdum, F., Roy, A. and Silberschmidt, V. V. (2012). Finite element analysis of drilling in CFRP composites. *5th CIRP conference on High Performance Cutting*. Zurich, Switzerland.

Phadnis, V.A., Makhdum, F., Roy, A. and Silberschmidt, V. V. (2012). Ultrasonically assisted drilling in carbon/epoxy composites. *15th European conference on composite materials, ECCM'15*. Venice, Italy.

Phadnis, V.A., Makhdum, F., Roy, A. and Silberschmidt, V. V. (2012). Drilling of CFRP composites for aerospace applications: advantages of a new technique. *1st Annual EPSRC Manufacturing the Future Conference*. Loughborough, UK.

Phadnis, V.A., Roy, A. and Silberschmidt, V. V. (2011). Delamination in CFRP composites: Effect of dynamic loading. *Deformation and Fracture of Composites (DFC-11) & Structural Integrity and Multi-scale Modelling (SI-5)*. Cambridge, UK.

Phadnis, V.A., Makhdum, F., Roy, A. and Silberschmidt, V. V. (2011). Drilling induced damage in CFRP laminate: Experiment and numerical analysis. *21st International Workshop on computational mechanics of materials, MPSVA'11*. Timisoara, Romania.

Phadnis, V.A., Makhdum, F., Roy, A. and Silberschmidt, V. V. (2011). Ultrasonically assisted drilling in advanced composites. 21st International Workshop on Computational Mechanics of Materials (IWCMM21), Limerick, Ireland.

CONTENTS

LIST OF FIGURES

LIST OF TABLES

SYMBOLS

Symbols related to elasticity and strength of laminates

E_c	Elastic modulus of a composite
E_f	Elastic modulus of fibre
E_m	Elastic modulus of matrix
V_f	Volume fraction of fibre
V_m	Volume fraction of matrix
E_{11}, E_{22}, E_{33}	Elastic moduli of a lamina in fibre direction and transverse (in-plane and out-of-plane) directions
$\nu_{12}, \nu_{13}, \nu_{23}$	Poisson's ratio of a lamina in-plane 1-2, 1-3 and 2-3
G_{12}, G_{13}, G_{23}	Shear moduli of a lamina in-plane 1-2, 1-3 and 2-3
X_{1t}, X_{2t}, X_{3t}	Tensile strengths in fibre-direction and transverse directions (in-plane and out-of-plane)
X_{1c}, X_{2c}, X_{3c}	Compressive strengths in fibre-direction and transverse directions (in-plane and out-of-plane)
S_{12}, S_{13}, S_{23}	Shear strengths in-plane (1-2) and out-of-plane (plane 1-3 and 2-3)
S_{is}	In-situ shear strength
α	Non-linear shear parameter
X^{qs}	Quasi-static strength of a ply
X^{dyn}	Dynamic strength of a ply
$\tilde{\sigma}_{y0}$	Initial effective shear yield stress
$\bar{\varepsilon}^{pl}$	Equivalent plastic stain due to shear deformation
C, p	Coefficients in strain-hardening equation (Eq. 4.14)

Symbols related to finite-element analysis

P	External forces applied to the node
I	Internal forces on the node
m	Mass of a structure
$\ddot{u}$	Acceleration of a structure
l_e	Characteristic length of a meshed element

Symbols related to delamination

K	Stiffness of a cohesive interface
δ	Separation between adjacent laminae
$\sigma_{IO}, \sigma_{IIO}, \sigma_{IIIO}$	Interlaminar normal tensile strength (mode I), and shear strengths (mode II and III)
G	Energy release rate (ERR), total, in 3D
G_I, G_{II}, G_{III}	Energy release rate (ERR) of modes I, II and III
G_c	Critical energy release rate (ERR), total, in 3D
η	Mode-mixity parameter
d	One-dimensional damage state variable

Symbols related to damage

σ_{ij}	Stress tensor
ε_{kl}	Strain tensor
C_{ijkl}	Stiffness tensor
σ	Effective stress
D_{ij}, d_{ij}	Damage tensor
D, d	Damage variable
$\bar{\sigma}$	Undamaged stress
m	Weibull modulus
$E(D)$	Effective modulus
$\bar{E}$	Undamaged (virgin) modulus

$p_{12}^{+}, p_{12}^{-}, p_{22}^{-}$	Puck's inclination parameters
A_0	Damaged area
E_d	Damaged elastic modulus
G_d	Damaged shear modulus
Y_{22}^{0}	Strain threshold for transverse direction at the initiation of damage in MLT model
Y_{12}^{0}	Strain threshold of plane 1-2 at the initiation of damage in MLT model
Y_{22}^{C}	Strain threshold for transverse direction at damage saturation in MLT model
$Y_{brittle}$	Effective strain threshold indicating brittle behaviour in MLT model
δ_{eq}^{fi}	Equivalent separation at the evolution of damage variable for i^{th} damage mode, where $i = 1,\ 2,\ 3,\ 4$
δ_{eq}^{0}	Equivalent separation at the initiation of damage for damage variable at respective damage mode
σ_{eq}^{fi}	Equivalent stress at the evolution of damage variable for i^{th} damage mode, where $i = 1,\ 2,\ 3,\ 4$

ACRONYMS

2D	Two-dimensional
3D	Three-dimensional
A-FEM	Augmented finite-element method
CDM	Continuum damage mechanics
CFRP	Carbon fibre/fabric –reinforced polymer
CLT	Classical laminate theory
CZE	Cohesive zone element
CZM	Cohesive zone model
DCB	Double cantilever beam
DIC	Digital image correlation
DOF	Degree of freedom
ENF	End-notched fixture
FEM	Finite element method
FSDT	First-order shear deformation theory
FSI	Fluid-structure interaction
GFRP	Glass fabric –reinforced polymer
HPVI	Hyper-velocity impact
HSDT	Higher-order shear deformation theory
HVI	High-velocity impact
IVI	Intermediate-velocity impact
LVI	Low-velocity impact

MMB	Mixed-mode bending
PMC	Polymer matrix composite
RVE	Representative volume element
SHPB	Split Hopkinson pressure bar
SPH	Smooth particle hydrodynamics
UD	Uni-directional
UMAT	User defined material subroutine
VCCT	Virtual crack closure technique
VUMAT	Vectorised user defined material subroutine
WWFE	World-wide failure exercise
XFEM	Extended finite-element method

CHAPTER 1

INTRODUCTION

1.1 Background

Over several past decades, the use of laminated polymer-matrix composite (PMC) materials has proliferated in various commercial applications - aerospace, locomotive, marine, sports and defence related industries. Thanks to their excellent mechanical properties - high specific stiffness, excellent fatigue and corrosion resistance, and better energy absorption capacity - PMCs continue replacing metallic materials and have emerged as major trend-setters in modern manufacture. For example, AIRBUS, a giant aircraft manufacturer uses over 50% by weight of PMCs in its new aircraft - A350 - that resulted in considerable 20% weight reduction (Marsh, 2008).

PMCs used in aerospace and defence structures can be subjected to extremely hostile loading conditions such as impact and blast. This research area attracted attention of research community over recent decades, though further investigation regarding their mechanical response under such loading conditions is still needed to design structures with improved impact and blast resistance. Real time experiments are the apparent means to study these highly dynamic events; though they are rather complex to carry out due to difficulty in obtaining reliable output data.

Recently, finite-element (FE) based numerical models have evolved as a virtual alternative to study such complex events, thanks to the improved computational power. A robust FE model validated using the real-life experimental data provides a convenient tool to study mechanical behaviour of PMCs, including their damage modes, failure characteristics and energy-absorbing mechanisms. Moreover, such computer simulations can provide a valuable insight into the effect of various design parameters on the blast and impact resistance of PMCs.

Computational techniques have been used to evaluate highly dynamic (such as crash) response of metallic structures since the 1970s in order to shorten their design time and reduce development costs. Damage modes and energy absorption mechanisms of metallic structures are now well understood and rendered reasonably accurately in computer simulations. However, accurate prediction of failure initiation in laminated composite materials has not yet reached maturity (Hinton and Soden, 1998; Hinton *et al.*, 2002, 2004; Soden *et al.*, 2004).

Damage of composites under dynamic loading conditions has different characteristics than that of quasi-static loading conditions, for example - a composite structure impacted by a high-velocity, low-mass projectile tends to induce more localized form of damage resulting in energy dissipation over a comparatively small region when compared to a low-velocity, large-mass impact, as in case of drop weight impact test. Additionally, some PMCs may exhibit strain-hardening behaviour under high-deformation rates. In these regard, material-property degradation and energy absorbed through failure has been the subject of research for several years now. While failure criteria still require enhancements, the post-failure behaviour of material is rarely addressed.

Thus a better understanding of PMC's degradation and failure under highly dynamic events as ballistic impact and blast is needed to gain an acceptable confidence level in their simulated responses to design structures with improved survivability.

1.2 Research aim and objectives

The aim of this thesis is to analyse the impact and blast response of polymer matrix composite laminates (PMC) numerically using finite-element method. In general terms, this should also allow modelling of PMC's mechanical behaviour under a wide regime of impact loading conditions – low to high velocity.

To fulfil this aim, continuum-level numerical criteria will be proposed capable of studying failure of PMC under dynamic loading conditions - such as impact and

blast. This will be then implemented into a commercial FE code ABAQUS/Explicit to model responses of PMCs to highly dynamic impact and blast loading events. The FE models will then be employed to study geometric effects of structures to improve their design for better resistance to such loading.

In order to achieve the aim of this study, the following objectives are defined.

1. Review of existing numerical models to analyse damage and failure of unidirectional (UD) polymer matrix composites (PMC)
2. Suggestion of modifications to nominated numerical failure criteria for its use in the analysis of response of UD PMCs under dynamic loading conditions, such as impact and blast - based on the experimental results
3. Implementation of modified dynamic failure criteria in ABAQUS/Explicit
4. Development of 3D finite-element (FE) model of ballistic-impact response of woven fabric-reinforced polymer composite laminates to analyse damage modes and energy absorption mechanisms
5. Development of 3D FE model of air blast response of curved carbon fibre-reinforced polymer (CFRP) composite to analyse modes of deflection of panels and energy distribution during this event

1.3 Research methodology

A schematic layout of the research methodology adopted here is shown in Figure 1.1. The thesis covers six main areas – introduction, literature review, experimentation, failure criteria for PMCs, simulations, and conclusions and future work. These areas are linked to each other in such a way that information from the former was used to form the basis of later. This work resulted in seven chapters. A brief description of the chapters will be given in the following section. The rest of this section is focused on the interaction between the elements of research methodology. It is mainly comprised of numerical simulations, while the experiments were carried out in Indian Institute of Technology, Bombay and University of Rhode Island, USA and their details are provided at the start of each

chapter. The insight into these results initiated the need of improved dynamic failure criteria for UD PMCs. In this regard, existing numerical models analysing mechanical behaviour of UD composites and their damage modes, were critically reviewed, and consequently a failure criteria based on the combined work of Hashin (1980) and Puck (1992) was nominated to extend its functionality to assess response of UD PMCs under dynamic loading conditions, such as impact and blast. Two numerical case studies – ballistic-impact response of woven fabric-reinforced composite laminates and air blast loading on the CFRP composites were performed using a commercial FE code ABAQUS /Explicit. Intraply damage was modelled using proposed dynamic failure criteria and interply damage was modelled using cohesive zone elements (CZE).The computational results were validated using experimental data. In the first case study, the damage at the front and back face of the laminates was analysed and compared with experimental data. The contribution of different damage modes in energy absorption capacity of a laminate was assessed. In the second case study, damage modes of curved CFRP panels under blast load were analysed and the energy distribution during this event is discussed. A parametric study was also carried out to optimise the CFRP panel curvature for improved blast resistance. Finally, the conclusions are provided, research areas requiring further attention were identified and recommendations for future research discussed.

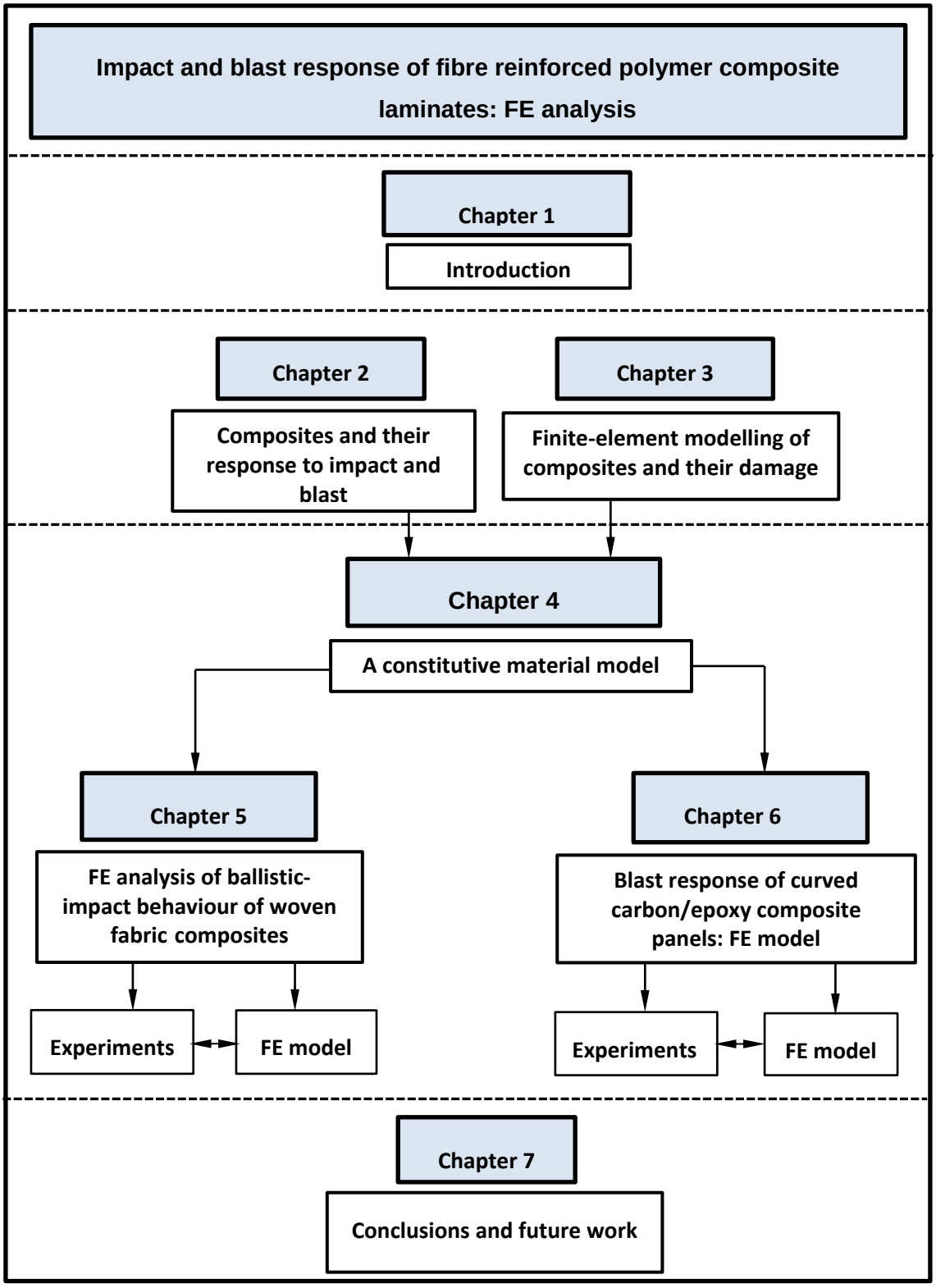

Figure 1.1. Research methodology

1.4 Thesis outline

A brief description of the remaining chapters of this thesis is given below.

Chapter 2 Composites and their response to impact and blast

This chapter is divided into three parts. In the first part, composite materials and their classification is discussed briefly. Two main PMC composites - UD CFRP and woven fabric-based - are focussed on in this study and reviewed to understand their ply architecture. In the second part, a review of impact responses of these composites is presented. In the third part, different damage mechanisms in such composites under impact - and blast - like conditions are discussed.

Chapter 3 Finite-element modelling of composites and their damage

This chapter is also divided into three parts. Firstly, the basics of FE methods regarding modelling of composite laminates are presented, starting with an equivalent-single-layer theory followed by a continuum-based 3D elasticity theory. Different length scales and finite-element solvers are also discussed. Secondly, various theoretical approaches employed in FE modelling for discrete damage mechanisms of composites are discussed. In the last part, a critical review of existing continuum-level damage models is performed and their merits and shortcomings are listed. It should be noted that the presented review does not attempt to list all material models but rather seeks to show important developments in the domain of finite-element modelling of penetrating impacts and blasts on laminated composite structures.

Chapter 4 A constitutive material model

An improved material model addressing some of the identified short-falls is presented in Chapter 4. This material model is kept as straightforward as possible to facilitate its use in engineering environment. The material parameters are chosen such that they can be easily measured and possess a physical significance. Distinctive measures are taken to allow this constitutive model to be

used for strain-rate-sensitive PMC materials. At the end, the implementation of this material model into ABAQUS/Explicit is discussed.

Chapter 5 Finite-element analysis of ballistic-impact behaviour of woven-fabric composites

This chapter represents the first case study using the dynamic failure criteria proposed in Chapter 4. A brief introduction of this research topic is provided first followed by the description of experimental details. The mechanical behaviour of hybrid woven fabric-reinforced composite laminates subjected to ballistic-impact is assessed using the developed FE modelling approach. The details of FE model development are discussed. The results and discussions are presented next.

Chapter 6 Modelling blast response of curved CFRP composite panels

This chapter represents the second case study using the dynamic failure criteria proposed in Chapter 4. A brief introduction of this research topic is provided first followed by the description of experimental details. The response of UD CFRP composite panels under air blast is examined using the FE modelling approach. The details describing FE model development are provided followed by the results and discussions.

Chapter 7 Conclusions and future outlook

This chapter summarizes the findings of this research study. Conclusions are drawn regarding the precision improvement provided by the proposed material model and a number of recommendations are proposed to improve numerical simulations of impact and blast performance of composite structures.

CHAPTER 2

COMPOSITES AND THEIR RESPONSE TO IMPACT AND BLAST

2.1 Introduction

Over the last few decades, the use of composite materials has become increasingly popular in various structural applications especially in aerospace and automotive industry. Composites are preferred above conventional monolithic materials like metals because of several advantages including high specific strength to weight ratio, good fatigue and corrosion resistance and flexibility in their design capabilities. Moreover, thanks to their lightweight and superior mechanical properties, composite materials are often used as protective structures in military and marine applications where they are often exposed to the hostile conditions such as impact and blast. Thus it is an imperative task to study the response of composite materials under such conditions in order to facilitate deign of structures with improved impact and blast resistance.

In this regard, this chapter provides the review of the earlier work regarding the impact and blast response of polymer composite (PMCs) materials. First, an introduction to PMCs is made and their classification is briefly discussed. This is followed by a review of the impact behaviour of composites under low, intermediate and high velocity regimes. A detailed account of various damage mechanisms ensued by such loading conditions is presented next. Later, a blast response of PMCs is discussed with the focus on the blast through air. Finally, a summary of the key decisions made to formulate the research methodology is given.

Thus the main focus of this chapter is to understand the mechanical response of PMCs and apply this knowledge to develop a finite-element modelling tool that could adequately predict their behaviour under impact and blast loading.

2.2 Composite materials

The pursuit for stronger, stiffer, durable, light-weight and tailor-made structures and components is ever increasing to meet various needs and demands of the human life. Composite structures have the potential to fulfil these requirements. A composite material is a combination of two or more materials on macroscopic scale with significantly different properties of its constituents that remain separate and distinct within (Chawla, 2007). In many cases, composites are generally understood as a combination of high-strength brittle fibres and a weaker matrix. The fibres are particularly stronger and stiffer than the matrix, thus, governing the mechanical characteristics of the composite such as its strength and stiffness (Daniel *et al.*, 2003). The mechanical properties of composites - stiffness, strength, weight, corrosion resistance, thermal properties, fatigue life and wear resistance - can be tailored through combinations of matrix and fibre systems and ply layups.

Composite materials have a long history of application. Nature itself presents various forms of composite structures such as wood. In ancient times, man-made composites appeared in the form of mud bricks strengthened by straw; similarly medieval swords and armours were constructed of layers of different metals. Plywood was fabricated when it was realised that the traditional wood can be rearranged to achieve superior material properties.

Recently, PMCs that offer advantages like high strength-to-weight and stiffness-to-weight ratios have posed as an important candidate in the design of light-weight and strong structures such as aerospace, automotive, defence and civil products. Especially the aircraft industry is enormously benefited from the use of such composites in the various parts of an aeroplane, e.g., the Boeing Dreamliner 787 introduced in the international air traffic in late 2009, consisted

of composites in proportion of 50% by volume reducing its overall weight by 1.3 to 1.8 tonnes compared to their rivals. This enabled 787 to use 20% less fuel resulting in 18% less emissions (Norris and Wagner, 2005).

The composite materials can be primarily categorised in three classes based on the nature of their reinforcement (Jones, 1999):

- particulate composites having particles in a matrix such as concrete, metal-matrix and ceramic-matrix composites;
- fibrous composites having fibres in a matrix; and
- laminated composites consisting of layers of various materials bonded together.

Presently, fibrous composites have found wide application in industry. The principal fibres used for engineering applications are glass, carbon, aramid and boron. The reinforcing fibres in the fibrous composites should have the following properties:

- high modulus of elasticity;
- high ultimate strength;
- low variation of strength between individual fibres;
- stability and retention of strength during handling and fabrication;
- uniform fibre cross-section;

Moreover, fibres themselves are unable to withstand the loads in engineering applications unless bound by continuous medium called the ‘matrix’. The matrix is required to have the following characteristics:

- support and bind the fibres together;
- transfer the load to the fibres;
- arrest a crack propagation straight through a mass of fibres;
- provide protection to the fibres from damage during handling and in-service, including environment;
- chemically and thermally compatible with the fibres.

The most widely used matrix materials for fibrous composites are polymers. Hence, the term fibre-reinforced plastic/polymer (FRP) is used for such composites. A type of fibres used during fabrication of composite materials may be unidirectional (UD) such as unidirectional tows or tapes; two-dimensional (2D) such as woven fabrics and three-dimensional (3D) such as fabrics with fibres oriented along many directions, e.g. 3D interlock weaves. The architecture of two most important classes of composite materials, namely, unidirectional fibre and woven fabric composites is reviewed next.

(A) Unidirectional-fibre composites

A unidirectional composite is shown schematically in Fig. 2.1. Several unidirectional layers can be stacked in a specified sequence of orientation (θ) to fabricate a laminate that will meet design strength and stiffness requirements. Each layer of unidirectional composite may be referred to as *layer, ply* or *lamina*.

The direction parallel to fibres is called as *longitudinal direction* (axis 1).The direction perpendicular to fibre (in-plane and out-of plane of a lamina) is called the *transverse direction* (in this case axis 2 and 3). These axes are also called material axes of a ply.

A ply depicted in Fig 2.1 shows only one fibre through thickness, though in practise, a ply may have several fibres through its thickness. These fibres are distributed randomly throughout the cross-section and may be in contact with each other at some locations. The plies are generally constructed from single-end or multiple-end rovings impregnated into the polymer matrix. The fibre diameter varies typically from 8 to 10 μm. Thus the ply thickness to fibre diameter ratio ranges between 10 and 15.

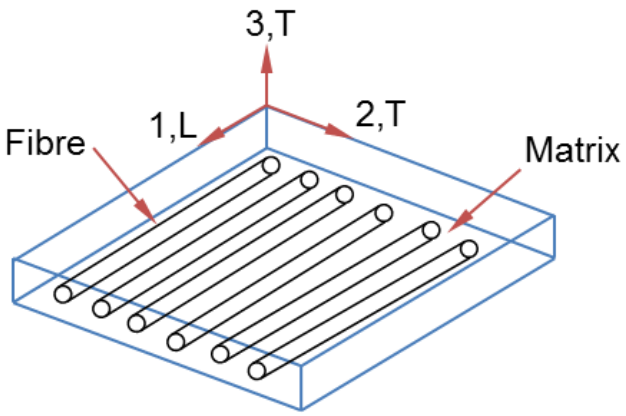

Axis 1, L – longitudinal direction

Axis 2, T – transverse direction (in lamina plane)

AXIS 3, T- transverse direction (out-of lamina plane)

Figure 2.1 Schematic representation of a unidirectional composite ply

Due to its structure, a unidirectional composite shows different properties in the longitudinal and transverse directions. The mechanical properties of a composite are governed by the relative proportion of the matrix and reinforcing materials. These relative proportions are given as the weight fractions or volume fractions where mechanical properties of a composite laminate are calculated by using the *law of mixtures* based on following assumptions:

- Fibres are uniform, parallel and continuous
- There exists a perfect bonding between fibre and matrix
- The load applied in fibre direction produces equal strain in fibre and matrix
- The load applied in fibre direction is shared between fibre and matrix

For example, elastic modulus of a unidirectional composite can be calculated using *law of mixtures* as:

$$Ec = E_f V_f + E_m V_m , \tag{2.1}$$

Here Ec, E_f and E_m are elastic moduli of a composite, fibre and matrix respectively; whereas V_f and V_m are volume fractions of fibre and matrix respectively.

Generally, desirable mechanical properties (e.g. stiffness and strength) of a laminate can be achieved by varying its layup sequence. Some commonly employed ply configurations are described below.

- Balanced laminate: If for each $+\theta$ ply, a laminate has an identical ply of same thickness with $-\theta$ orientation, such laminates are known as balanced laminates. e.g., $[0/+45/-45/90/0_2]_T$. Here T denotes *total* laminate sequence.
- Symmetric laminate: If a laminate has plies stacked in a way such that through its thickness the plies are symmetric about the mid-plane. Such laminates would not exhibit any extension-bending coupling. e.g., $[0/\pm30/45_2/90_2/45_2/\pm30/0]_T$ or $[0/\pm30/45_2/90]_S$, where subscript S denotes *symmetry* about mid-plane.
- Cross ply laminate: If the plies are stacked in two orthogonal directions, i.e. in longitudinal (0^0) and transverse directions (90^0), the laminate is called as cross ply laminate e.g.,$[0_2/90_4/0_2]_T$.
- Quasi-isotropic laminate: If plies of identical properties and thickness are oriented in a way that angle between two adjacent plies is equal to π/n, where n is the number of plies equal to or greater than three, it is called as quasi-isotropic laminate. This type of laminate exhibits isotropy in the in-plane material properties e.g., $[0/+45/90/-45]_S$.

(B) Woven-fabric composites

Mechanics of woven structural composites can be best studied by taking into account their hierarchical organization. There are usually four important levels in a manufacturing process of woven composites:

fibre > yarn > fabric > composite

A selection of fibres represents the first step in fabrication of woven composites. The fibres are grouped in a specific pattern and impregnated with resin to form yarns. The size of yarns is usually expressed as filament count which is the number of fibres (usually in thousands) in a single yarn. The yarns are then interlocked in specific patterns to form fabrics. Fabrics are classified as woven nonwoven, knitted, braided, 2D and 3D. 2D means that the woven fabric features only in-plane reinforcing properties. Fabric preforms are stacked on top of each other in a specific stacking sequence to obtain thickness. The fabrics are impregnated with the matrix and cured forming a composite laminate. A laminate is thus a collection of laminae where each lamina is reinforced with a layer of fabric (Barbero, 2010).

The woven structure is characterized by the interlacing of two sets of yarns called the warp (0^{o}) and weft (90^{o}) yarns in a regular pattern or weave style. The fabric's integrity is maintained by the mechanical interlocking of the yarns. The weft tows run perpendicular to the direction of the warp tows. The woven fabrics are usually balanced and symmetric. A balanced fabric is one where the number and weight of fibres in yarns along the warp and weft directions are the same (Daniel *et al.*, 2003). The material is therefore identical along these two directions. The warp and fill directions play equal roles affecting the thermo-mechanical properties of the composite laminate.

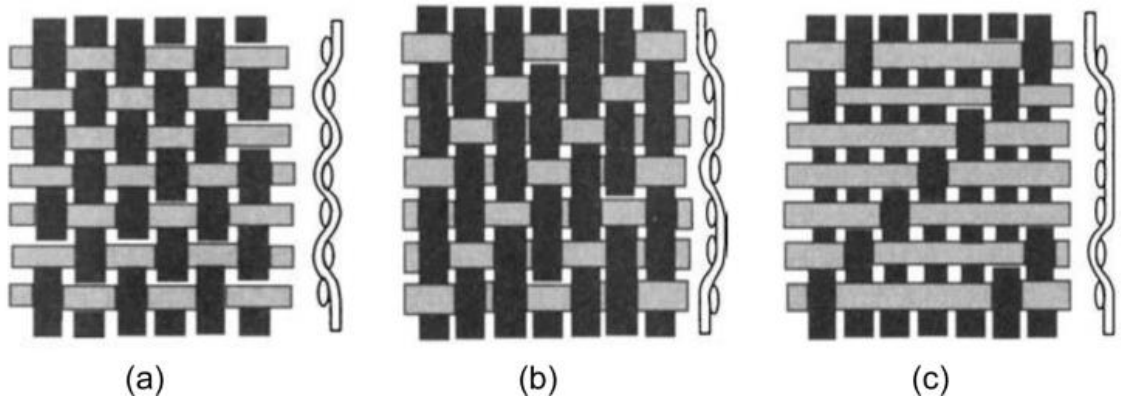

Figure 2.2 Architecture of woven fabrics: (a) plain weave; (b) twill weave; (c) satin-weave (Daniel *et al.*, 2003)

An unbalanced fabric may be used to obtain different mechanical properties along the warp and weft directions. Weave patterns such as plain weave, twill weave, and satin-weave are the common forms of woven architectures and are shown in Fig.2.2. In plain weaves (Fig. 2.2a), each weft yarn goes over a warp yarn then under a warp yarn and so on. Due to the alternative interlacing, there is a high level of waviness or yarn crimp, which imparts relatively low mechanical properties such stiffness and strength of the composite compared to other weave styles. Plain weaves are not very drapable. Twill weave, as shown in Fig. 2.2b, is formed by weaving one or more warp yarns over and under two or more weft yarns in a regular repeated manner.

In a 5-harness satin-weave (Fig. 2.2c), each weft yarn goes over 4 warp yarns before going under the fifth one. Here, low waviness of yarns results in good mechanical properties. The satin-weave is asymmetric, where one side of the fabric is predominantly warp yarns and the other is weft. Exchange sites also break symmetry because they bend yarns in an asymmetric way. Bending and stretching in a satin-weave ply are consequently coupled. There is also coupling between stretching and in-plane shear, because exchange locations are not symmetric about either in-plane axis (Fig. 2.2c). Coupling between bending and stretching tends to cause warping during cure because of thermal strains (Cox and Flanagan, 1997).

A selection of a weave for a specific application involves manufacturing considerations as well as final mechanical properties. The type of weave affects dimensional stability and conformability of the fabric over complex surfaces. Further, weaves with more yarn crimps such as plain weave offer low stiffness and strength. On the other hand, satin-weaves have less crimp and good conformability, but their shear resistance is low due to the increased straight segments of yarns. Since the composites are often subjected to bending deformations during impact causing shear damage of laminates in the form of delamination, thus, an optimum composite material is a polymer matrix reinforced with a symmetric balanced twill 2/2 woven fabric. The elastic

properties of the fabrics can be estimated by considering these to consist of two UD plies crossing at 90^0 angles with each other (Daniel *et al.*, 2003).

2.3 Impact response of FRP laminates

With increasing use of composites in military air, ground and sea-borne vehicles, commercial aircrafts, shipping industry, infrastructure and sports goods, understanding their impact and dynamic behaviour is critical to designers and end-users. A wealth of knowledge has been published on dynamic impact response of composite materials and structures, though with continuously emerging materials and structures, systematic structure-property-performance relationships that could provide guidelines on the dynamic impact behaviour of composites are not well established.

In general, composite structures are often exposed to dynamic loads under service conditions. Aerospace structures, for example, can receive impacts during maintenance operations, or during service such as hailstones or other kind of debris. A dynamic behaviour of composites is greatly influenced by the damage processes driven by impact loading. Generally components subjected to impacts are designed to absorb energy by undergoing damage. Damage in composites under dynamic impact conditions is complex phenomena that demands better understanding. Thus, it is important to study the impact characteristics of composites and the underlying damage modes to enable design of better energy absorbing structures.

Impact response of materials can be categorized into low velocity (large mass), intermediate velocity, high velocity (small mass) and hyper-velocity regimes. These regimes are shown in Fig.2.3 and briefly described below.

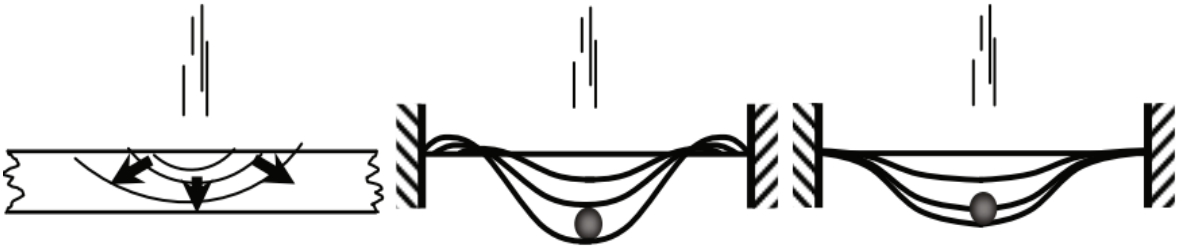

(a) (b) (c)

Figure 2.3 Classification of impact regimes: (a) high velocity impact, very small impact time with dilatational wave dominated response (b) intermediate-velocity response, short impact times with flexural and shear wave dominated response; (c) low-velocity impact, long impact times with quasi-static response (Olsson, 2000)

2.3.1 Low-velocity impact (LVI)

LVI can be treated as a quasi-static event, the upper limit of which may vary from 1 m/s to 10 m/s depending upon target stiffness, material properties and the impactor mass and stiffness (Sjoblom *et al.*, 1998).

The response of a target material is controlled by impactor/target mass ratio rather than impact velocity (Olsson, 2000). Here, the dynamic structural response of the target is important since the contact duration is long enough for the entire structure to respond to the impact and consequently, energy is absorbed elastically.

Though LVI is recognised to be treated as quasi-static event, the scientific community share different opinions about this. Some (Cantwell and Morton, 1991) classified low velocity up to 10 m/s using test techniques such as Charpy, Izod, and drop-weight impact. Few other researchers (Liu and Malvern, 1987) suggested that the type of impact can be classified by the assessment of damage occurred. A large group of researcher defined LVI as being one in which the through-thickness stress wave plays no significant part in stress distribution. The failure modes in LVI highly depend on the specimen size, stiffness and boundary conditions (Abrate, 1991, 1998; Richardson, 1996). The

impact energy for an underlying composite specimen under LVI is absorbed primarily in the form of strain energy, in addition to the energy dissipated towards various failure modes such as matrix cracking, fibre breakage and delamination. These are discussed in Section 2.6.

2.3.2 Intermediate-velocity impact (IVI)

It is considered to fall between the low and high velocity impact regimes. The range of impact velocities falling in this category is not clear (Abrate, 1986, 2011). Depending on the projectile mass, large deformation may occur in IVI range, but it may differ from LVI in terms of loading rate and momentum. Typically IVI arises from the events such as road debris impact on automobiles, lower end velocity bullet impact, hail impact or even baseball bat striking a ball.

2.3.3 High-velocity (ballistic) impact (HVI)

FRP composites are being extensively involved in ballistic armour applications, and understanding the penetration mechanism and failure is important. Abrate (2011) defines the HVI regime as the ratio between the impactor velocity and the transverse compression wave velocity that is greater than the failure strain in that direction.

This kind of response is dominated by the stress wave propagation through the thickness of the material, where a structure does not get enough time to respond, leading to a localised damage. Boundary condition effects are of petite importance, since the impact event passes before the stress waves reach the boundary as shown in Fig. 2.3. Cantwell and Morton (1991) found that this small mass, high velocity impact is more detrimental to CFRP laminates than low velocity drop tower impact. They also provided a guideline when an impact event can be considered as a high velocity impact. According to this – if a velocity of impact is higher than 10% of the wave speed in that material, it can be considered as HVI. Following this rule of thumb, Abrate (2011) mentioned the range of HVI to be from 50 m/s to 1000 m/s depending upon the impact system (impactor and target structure).

2.3.4 Hyper-velocity impact (HPVI)

It is typically considered to take place in the range of > 1 Km/s, where projectile moves with a very high velocity and target behaves as a fluid (Abrate, 2011). This type of impact is mostly studied to develop protection against micrometeorites of objects and personnel in low earth orbit (LEO). The research regarding finite-element modelling of HPVI on composites is still in its initial phase due to lack of availability of reliable experimental data. Also complex non-linear equation of state properties (orthotropic material properties in case of ply level modelling of composite materials) must describe the shock impedances for accurate prediction of compression and release states with phase changes and spallation target structures, which are difficult to obtain (Riedel *et al.*, 2006). The response of target structures under such impact is often dominated by the pressure created by the shock wave ahead of the projectile, and the structure may fail before actual physical contact when the pressure exerted exceeds the ultimate strength of material. This event is generally accompanied by the generation of high temperature and may result in phase changes of material. (Clegg *et al.*, 2006)

Next, terminologies used in assessing damage are mentioned and various damage modes commonly observed in laminated composites are discussed.

2.4 Damage in FRP laminates

The heterogeneity of microstructure as well as the underlying anisotropy provides different characteristics of composite materials in how they deform or fail, in comparison to monolithic materials like metals. At this stage, several terms concerning damage in composites needs to be defined that characterise their behaviour (Talreja and Singh, 2012).

- *Fracture*: Conventionally fracture is understood to be breakage of material, or at a more fundamental level, breakage of atomic bonds. Examples of fracture in composites include fibre breakage, matrix cracking, fibre/matrix debonding and separation of adjacent plies (delamination).

- *Damage*: Here, damage refers to a unification of irreversible changes in a material brought about by a set of energy dissipating mechanisms. The damage itself may be established by the atomic bond breakage and in general it implicates to distributed changes. The examples of damage in composites include multiple fibre-bridged matric cracking, multiple delaminations.
- *Failure*: The failure is an inability of a given material system (here composites) to perform its designated function. Fracture is an example of damage, though material can fracture locally and still be able to perform its function, e.g. upon undergoing damage in the form of multiple matrix cracking, a composite material may still continue to carry load thereby meeting the load-bearing requirements.

Overall, the failure of a composite material is a seriously complex phenomenon; since in reality, composite material may fail by progressive occurrences and interaction of various damage mechanisms. Damage mechanisms commonly found in FRPs under impact loading conditions are discussed next.

2.5 Damage mechanisms

The heterogeneous microstructure of composites, the large difference between properties of the constituents, the presence of interfaces and orientations of reinforcement that introduces anisotropy in overall composite properties, are the reasons for the distinctively different damage mechanisms observed in FRPs when exposed to hostile loading conditions that is rarely observed in their homogeneous metallic counterparts.

For example, specific damage mechanisms encountered in fabric-reinforced composites include: intra-ply delamination (i.e. delamination between overlapping tows of the same woven ply), transverse normal and shear failure modes under axial loading, and failure of pure matrix regions (Adumitroaie and Barbero, 2011). In textile composites, damage begins at micro-scale with matrix cracking, fibre-matrix debonding and fibre failure within the ply. This is followed

by meso-scale damage such as intra-yarn cracking and inter-ply delamination. On the macro-scale, composite failure is characterised by a strong interaction of intra-ply cracking and inter-ply delamination and ultimate fabric rupture (Daggumati *et al.*, 2010). Consequently, this interaction of various damage mechanisms leads to a degradation of stiffness and strength properties of the composite material, resulting in a loss of its structural integrity. Thus it is necessary to understand initiation and evolution of these damage mechanisms during a period of laminate failure. A brief description of these damage mechanisms under LVI is given next.

(A) Matrix cracking

Fibre-reinforced composites offer high strength and stiffness properties in the longitudinal direction. However, their properties in the transverse direction are generally low and result in readily developing cracks. These cracks are usually the first observed form of damage in fibre-reinforced composites (Nairn, 2000). Matrix cracks also referred as transverse cracks, intralaminar cracks and ply cracks appear first in the layers transverse to the loading direction, traversing through the ply thickness and running parallel to the fibres in that ply. Matrix cracks are an intralaminar form of damage, and involve cracks or voids between fibres within a single composite lamina.

The initiation and growth of matrix cracks is dependent on the loading scheme and composite's lay-up, and usually a single matrix crack may develop a series of cracks within a lamina at a characteristic spacing. In low-velocity impacts, matrix cracks in upper layers of composite laminate initiate at the contact edges of an impactor. A typical example of matrix crack in UD FRP laminate is shown in Fig.2.4.

Initiation and development of transverse cracks and their effect on structural integrity and durability of laminated composites were extensively studied by many researchers (Berthelot and Le Corre, 2000).

Figure 2.4 Example of matrix cracks observed in continuous fibre composite laminates (Talreja, 2011)

Among the earliest researches, Parvizi *et al.* (1978) carried out extensive experiments to study transverse cracks. They observed that transverse crack spacing decreased with increasing applied stress and increased with the increase in transverse ply thickness. They also noted that cracks formed in a direction parallel to transverse reinforcement and thickness of the transverse layer influence initiation and propagation of the matrix cracking process. Silberschmidt (2006) presented that a random spatial distribution of fibres results in variations of local properties of composite laminates. This non-uniformity not only affects the effective properties of composite materials but is also a crucial factor in initiation and evolution of damage and fracture processes that are also spatially random. Such randomness in microstructure and in damage evolution is responsible for non-uniform distributions of stresses in composite specimens even under externally uniform loading, resulting in a random distribution of matrix cracks in cross-ply laminates. Crack density, which is the number of cracks per unit length, increases abruptly with the applied load after initiation of cracking, until cracking comes to saturation state called a *characteristic damage state*. Matrix cracking gradually reduces stiffness and strength of the laminate and changes its coefficient of thermal expansion, moisture absorption and structure's natural frequency (Kashtalyan *et al.*, 2005).

(B) Interfacial debonding

The next intralaminar micro-level damage mode is fibre-matrix debonding, where a debond parallel to the fibres' direction, separates the constituents from each other; thus, the matrix support to the fibres in that region is eliminated. An interface between fibres and matrix resin plays a significant role in load transfer between fibres and matrix, with interface adhesive properties controlling the performance of composite. Debonding occurs at a weak interface between fibre and matrix. This damage mode initiates at the constituent level and gradually evolves into a macro level as the applied load increases, with all the layers in the laminate readjusting the load they carry in order to properly redistribute the stress released by damage. Although matrix cracking and fibre-matrix debonding do not cause ultimate structural failure of laminated composites, they can result in significant degradation of material's stiffness and can also trigger more severe forms of damage such as delamination and fibre breakage (Soutis, 2000, 2005). Fibre-matrix debonding in fibre reinforced composite under tensile load is shown in Fig. 2.5.

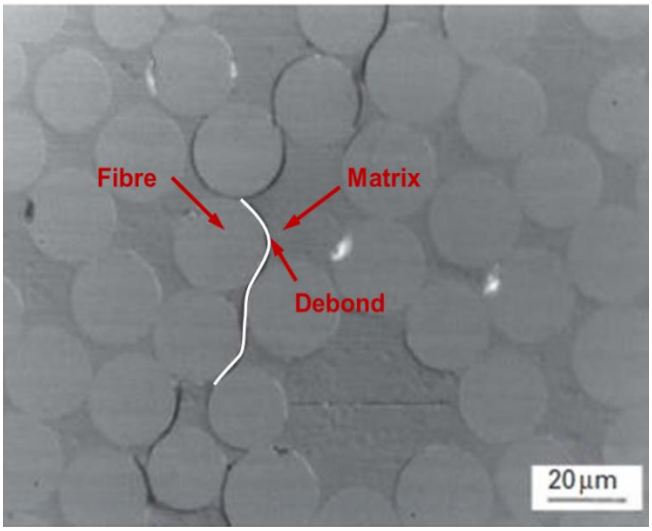

Figure 2.5 Debonds in fibre-reinforced composite (Gamstedt and Sjögren, 1999)

Interfacial sliding or fibre pull-out can occur when different displacement fields are imposed on different constituents (Talreja and Singh, 2012). One example

of this is the case of thermal loading; due to different coefficients of thermal expansion, the fibres and the matrix will be under different loading conditions. Interfacial strength plays a very important role also in this case for the existence of this kind of damage mechanism. Sliding of fibres against the matrix can cause further damage due to frictional wear. Fibre pull-out can also occur when brittle or discontinuous fibres are embedded in a tough matrix.

(C) Delamination/inter-ply cracking

As discussed earlier, with the onset of damage, a ply weakens, and the adjacent plies take on additional loads and, subsequently, undergo damage-initiation and evolution processes. First matrix cracks are formed randomly, and then they coalesce and lead to delaminations at interfaces between layers. Delaminations are separations between internal layers of a composite laminate due to the lack of reinforcement in the thickness direction. These delaminations are caused by high through-thickness shear and normal stresses, a mismatch in the Poisson's ratio between the layers and a presence of geometric discontinuity between layers of laminated composites. Similarly edge delaminations initiate at load–free edges of the composite laminate due to a mismatch in the Poisson's ratio and transverse shear stresses close to these edges. In the vicinity of free edges, stresses are three-axial consisting of in-plane and out-of-plane stresses; hence, the classical laminate theory (CLT) based on a plane-stress assumption becomes invalid. These out-of-plane stresses (also called interlaminar stresses) depend on a stacking sequence of plies and are primarily due to the mismatch of engineering properties such as the Poisson's ratios and shear-coupling coefficients between adjacent plies. These interlaminar stresses produce matrix cracks at the free edges, from which they propagate into the laminate and initiate delaminations, leading to stiffness degradation, strength loss and failure of laminated structures (Soutis, 2000). Delamination can also occur near any stress risers in the laminate such as holes and cut-outs in addition to free edge effects. Impact loading is also a

major cause of delamination failure in fibre-reinforced composites, resulting in reduction of compressive residual strength of laminates.

In transverse dynamic loading, intralaminar shear and bending stresses are the major causes of delamination (Abrate, 2011; Cantwell, 1986). Once interlaminar damage is initiated, its propagation and residual strength of the structure depend on the toughness of interlaminar layers and the level of energy that is required to propagate the crack. A matrix forms the weakest link in a laminate's through-thickness direction which is responsible for delamination cracking. In general, brittle resins favour delamination while tougher resins tend to induce kink-band formation and overall shear failure. Interply delamination resulted from the joining of two adjacent matrix cracks in FRP composite laminate is shown in Fig.2.6.

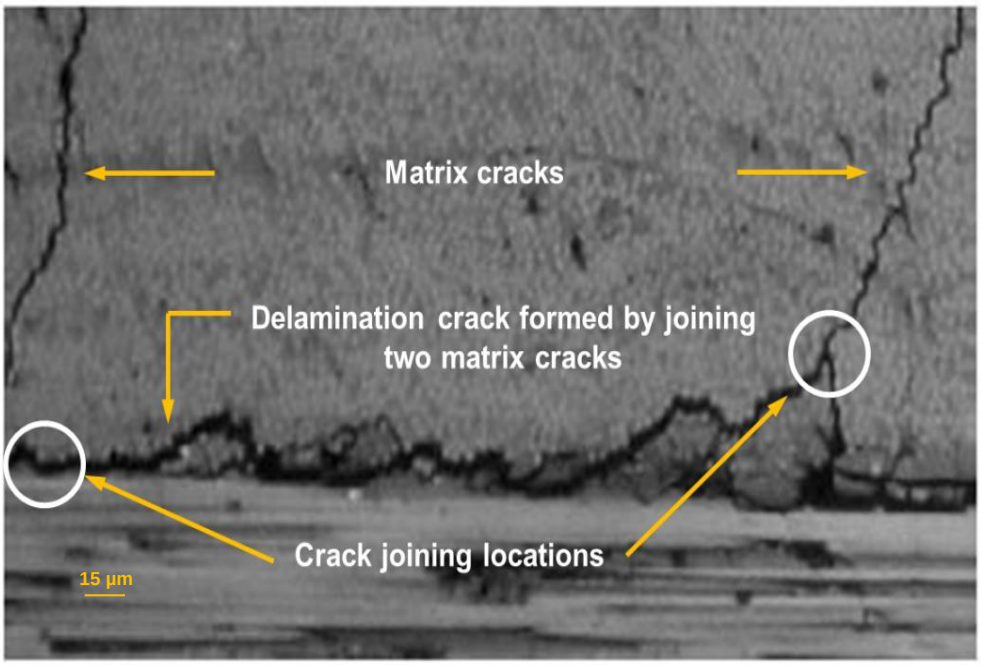

Figure 2.6 Interply delamination crack formed due to joining of two adjacent matrix cracks in fibre-reinforced composite laminate (Talreja and Singh, 2012)

Delamination has a more detrimental effect on structural integrity of composite laminates than transverse cracking. Delamination can render a structure

incapable of load-carrying and trigger the structural failure if it grows in size under an increasing load. On the other hand, this is not generally the case with transverse cracking where neighbouring plies can constrain the effect of this damage and maintain residual load-carrying capability of the structure (Bunsell and Renard, 2005). Delamination can be reduced by either improving the fracture toughness of the material or increasing interlaminar strength of the laminate by modifying the fibre orientation and ply stacking sequence as well as Z-pins stitching.

The problem of delamination has also been investigated widely, and many studies have been published addressing this failure mode. The first analytical model to predict the energy release rate associated with the growth of delamination induced by a transverse crack was developed by O'Brien (1982). Wang *et al.* (1985) used a three-dimensional finite-element analysis to evaluate the energy released with the delamination growth, by considering delamination induced by transverse cracks and free edges of the laminate. Nairn and Hu (1992) investigated the initiation and growth of crack-induced delaminations based on variational approach (Hashin, 1980; Nairn, 1989) for transverse cracking in cross-ply laminates. The variational-mechanics analysis predicted that transverse cracking developed until the crack density reached some critical density for delamination. A substantial amount of research was carried out in the investigation of delaminations induced by various mechanisms within composite laminates and presented in review papers. Garg (1988) reviewed the state of the art of delamination behaviour since 1970s to 1980s discussing some aspects such as causes of delamination and its effect on structural performance, analytical and experimental techniques to predict its behaviour and some of the preventive measures to delay the delamination so as to make the structure more damage-tolerant. Pagano and Schoeppner (2000) conducted critical reviews of many selected papers, especially the pioneering works on delamination research. Tay (2003) reviewed major developments in the analysis and characterization of buckling-driven delamination from 1990 to 2001. Brunner *et al.* (2008) reviewed the developments leading towards new

standardized test procedures for determination of delamination resistance or fracture toughness of fibre-reinforced polymer–matrix composites.

(D) Fibre kinking

Fibre failure in compression occurs due to micro-buckling and formation of kink bands, when a unidirectional or orthogonal woven composite laminate is subjected to a compressive load (Talreja and Singh, 2008). When an on-axis composite laminate is loaded in longitudinal compression, there is a phenomenon of local instability caused by failure of the matrix supporting fibres leading to formation of a kink band. Hence, fibres start buckling due to the lack of lateral support.

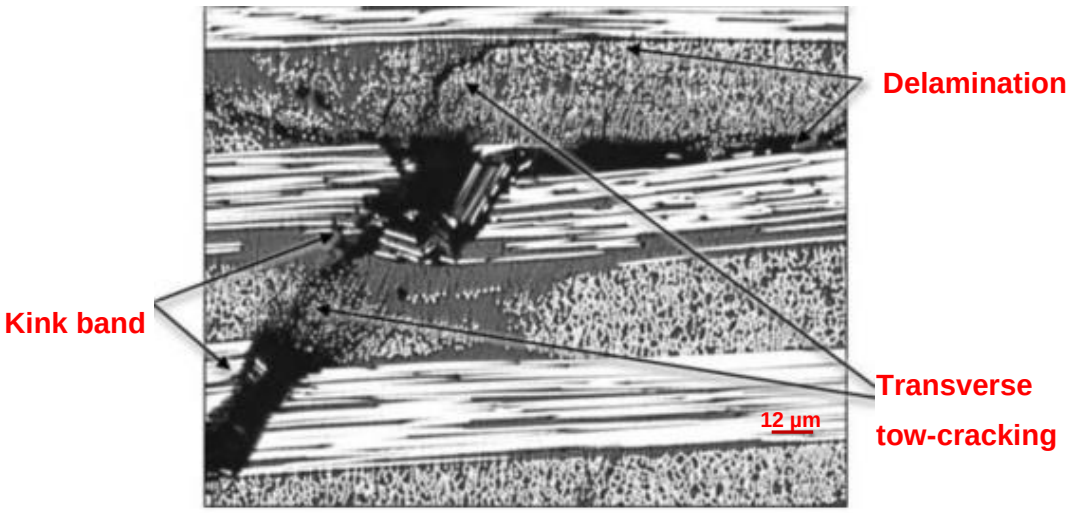

Figure 2.7 Different damage modes in a 5H satin-weave CFRP laminate under compression: delamination between the tows, cracking of transverse tows and kinking of load-aligned tows (De Carvalho *et al.* , 2011)

As the applied load is increased, the fibres/tows reach a critical buckling load and initial fibre/tow fracture occurs in the compression side. Finally, the kink band is fully formed when fibres/tows fail at the top side of the kink band as shown in Fig. 2.7. The critical buckling load is thus a function of the properties of fibres/tows, matrix and their adhesion.

(E) Fibre breakage

The initiation of fibre fracture is often considered as the ultimate failure mode of the laminate, as a drastic reduction in the load-carrying capacity occurs at this stage because fibres act as the principal load-bearing constituent, and resist most types of the applied loads. As the applied load is increased, progressive matrix cracks lead to fibre-matrix debonding and delamination resulting in a complex stress state. Now, as the matrix is debonded and shattered, the only load-carrying members are the fibres, which start to fail when the laminate's strain reaches the fibre's fracture strain resulting in multiple fibre cracks. In low-velocity impact events, fibre failure occurs just below the impactor due to high local stresses and indentation effects; and on non-impacted face due to high bending tensile stresses (Abrate, 2011). Accumulation of individual fibre fractures within tows and, subsequently, plies leads to ultimate laminate's failure when there are not enough fibres remaining intact to carry the required load. Damage progression becomes catastrophic and the material's ultimate strength is achieved.

The performance and development of the above mentioned damage mechanisms leading to failure of any composite structure depend on a range of parameters including the geometry, material, lay-up, loading conditions, load history and failure modes. Each damage mechanism has a different governing length scale and evolves differently when the applied load is increased. The damage scenario becomes more complicated when there is interaction between individual mechanisms. As the loading increases, load transfer takes place from high damage regions in the laminate to those with low damage, and the composite failure results from the criticality of the last load bearing element. These damage parameters are highlighted in a recent experimental study by De Carvalho *et al.* (2011) of two different woven composites - twill and satin-weaves - subjected to compression. They concluded that tows behaved as structural elements at the reinforcement level, damage morphology was affected by the weave architecture and geometry, and tows tended to fail at the

crimp region. It was found that kink-band formation, matrix cracking and transverse tow cracking were the predominant damage propagation mechanisms in compression. Similarly, damage observed in woven laminates as a consequence of tensile loading was in the form of transverse matrix cracking and delamination at the crimp regions (Gao *et al.*, 1999). However studies of damage mechanisms induced by large-deflection bending in woven composites are very limited. Thus, variability of woven composites due to their reinforcement architecture promotes interaction between different micro-mechanical damage mechanisms, increasing the difficulty to study their failure. Also, as these damage mechanisms are often embedded within the plies of a composite laminate, they may easily escape detection.

(F) Penetration

Penetration is a macroscopic failure mode and occurs when the fibre failure reaches a critical extent that enables an impactor to completely penetrate the target material (Abrate, 2011). The threshold impact energy required to penetrate the specimen increases with increase in its thickness. The major energy absorbing mechanisms during penetration are shear-out (also called shear-plug), delamination and elastic flexure. The shear-out (shear plug) mechanism is discussed here – during HVI, the high velocity impact energy is dissipated over a smaller region of target composite material giving rise to damage mechanism at higher velocities known as the shear plug.

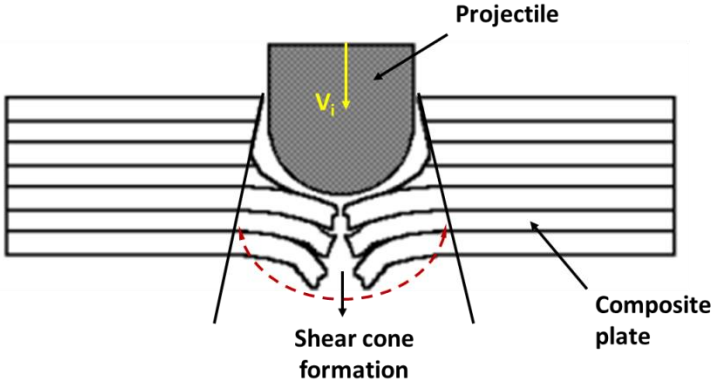

Figure 2.7 Shear-out/shear-plug formation in composites

Due to the high stresses created at the point of impact, the material around the perimeter of the projectile is sheared and pushed forward causing a hole or "plug" slightly larger than the diameter of the projectile and its size increases as it penetrates the composite as shown in Fig. 2.7.

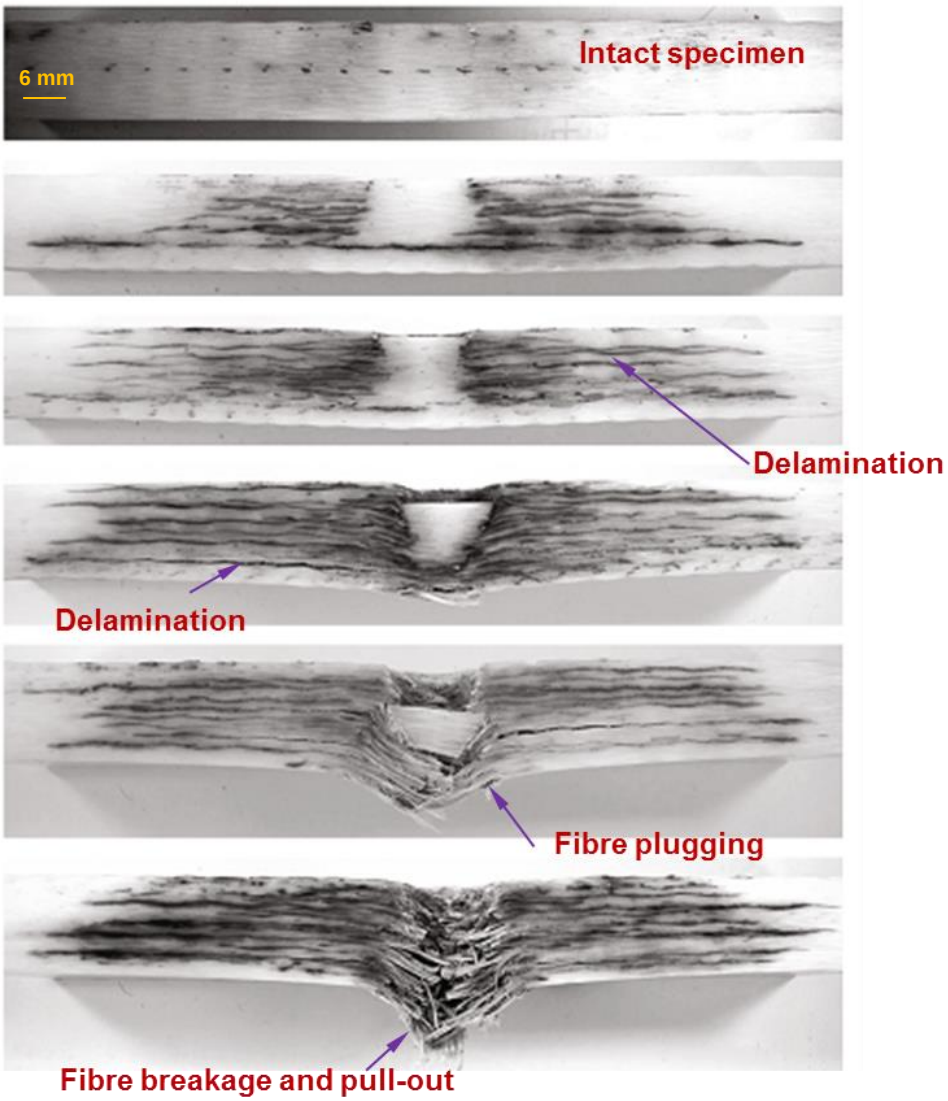

Figure 2.8 A typical penetration process observed in S-glass/epoxy composite (Xiao *et al.*, 2007)

It is noteworthy that shear-out mechanism accounts for 50-60% of total energy absorption depending upon the laminate thickness. (Abrate, 2011; Naik *et al.*, 2006, 2008). Apart from thickness of a laminate, various other factors such as

fibre volume ratio, tow size, orientation, weave architecture; matrix type and interface pose an influence on the penetration process (Abrate, 1991; Cantwell, 1986).

A typical penetration process observed in plain-weave S2-glass/epoxy composite impacted by a cylindrical projectile at 194m/s is shown in Fig.2.8. It can be seen that fibre plugging, fibre breakage and fibre pull-out are the major failure modes (Xiao *et al.*, 2007).

2.6 Blast response of FRP laminates

Thin, laminated composite structures are attractive for many lightweight applications such as military vehicles and civil infrastructures due to their durability, versatility and high mechanical performance. One of the technical challenges in their design is to determine the level of blast protection.

They may undergo large deflection dynamic motion under high-pressure explosive blast loads and experience progressive material damages and even a structural collapse. Recently, Tekalur *et al.* (2008) conducted an experimental study of material behaviour and damage evolution for E-glass vinyl ester and carbon composites subjected to static and blast loads. Their findings in the case of the blast loads were limited to qualitative descriptions of the different damage evolutions for the two composite materials. Perhaps more importantly, they acknowledged that the response of composites to explosives and air blast is a complex phenomenon to implement in a laboratory setting and thus is rarely studied experimentally.

As a result, the level of understanding of the response of these materials at high loading rates, as would normally be observed in blast events is not yet well established as that under static conditions (LeBlanc and Shukla, 2011) due to inadequacy of experimental data. This typically results in composite structures being conservatively designed with large safety factors to ensure that damage will not occur. This inherent conservativeness leads to overdesigns which do not afford the full weight savings possible with composites and hence

development of finite-element schemes capable of sufficiently modelling these events is necessary.

Historically, two experimental methodologies are used to impart shock loading conditions to structures: (1) explosives and (2) shock tubes (Le Blanc and Shukla, 2011; Tekalur *et al.*, 2008; Arora *et al.*, 2010). Although the use of explosives offers an ease of use, there are associated deficiencies such as spherical wave fronts and pressure signatures which are often spatially complex and difficult to capture. Shock tubes offer the advantage of plane wave fronts and wave parameters that are easily controlled and repeated.

When composite materials are subjected to blast loading conditions they may experience damage in the form of several distinct mechanisms occurring in the in-plane and through thickness directions. In general terms, in blast events, the in-plane damage mechanisms consist of fibre breakage and matrix cracking, while the through thickness damage is dominated by delamination of the plies. These are discussed in Section 2.5 and hence are not reiterated here, though some relevant studies are mentioned to exhibit their features particular to blast loading.

Experimental studies on shock loading of materials have examined the material response over a range of loading rates. Nurick *et al.* (1995, 1996) have studied the effects of boundary conditions on plates subjected to blast loading and identified distinct failure modes depending on the magnitude of the impulse and standoff. Tekalur *et al.* (2008) investigated the effects of shock loading on both E-Glass and Carbon based laminates. This study used a shock tube to impart pure shock loading as well as a small scale explosion tube to consider the shock load combined with the effects of the heat generated during combustion of the explosive materials. Mourtiz (1995, 1996) has studied the effect of shock loading on the flexural and fatigue properties of composite laminates when subjected to underwater shock loading.

These studies have shown that under relatively low impulsive loading the material sustains little damage (primarily matrix cracking) and the mechanical properties remain the same as for undamaged laminates. However, once a critical loading threshold is exceeded then the panels experience fibre breakage and the material strengths are significantly degraded. Mouritz (2001) studied the effectiveness of adding a light weight, through thickness stitching material to increase the damage resistance of composites. LeBlanc *et al.* (2007) have studied the effects of shock loading on 3D woven composite materials. Recently, there has been an increased interest in the study of the effect of shock loading on sandwich structures. These studies include the effects of shock and impact loading conditions (Jackson and Shukla, 2011); Schubel *et al.* (2007); Arora *et al.* (2010).

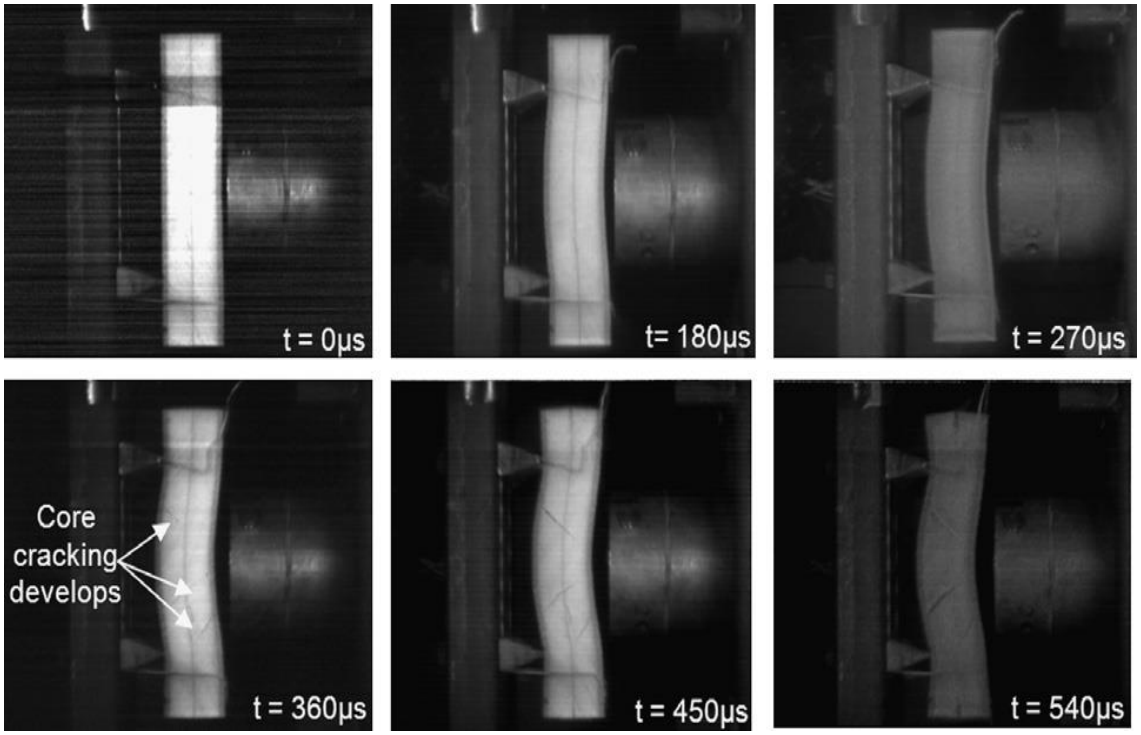

Figure 2.9 Blast response of a sandwich composite made of E-glass woven laminate face sheet and SAN foam core (Jackson and Shukla, 2011)

A time-history of typical response of a sandwich composite under blast load obtained by Jackson and Shukla (2011) is shown in Fig. 2.9. In general, it

should be noted that this research area is still relatively new and a limited number of research studies are conducted previously.

2.7 Summary

Composite materials are one of the most crucial aspects of current and future engineering technologies. Thanks to their excellent mechanical properties, they are finding their applications in plethora of commercial fields. In this chapter the mechanical behaviour of laminated composites and the ensued damage modes under impact loading scenario were reviewed in detail. The summary is presented below.

In their service life, composites are often subjected to impact loading conditions that trigger various damage mechanisms depending upon the extent of impact. The laminated composites subjected to LVI often absorb the impact energy through matrix cracking and delamination. These damage modes, though, do not result into the ultimate failure of a laminated structure, can significantly reduce its load-carrying capacity.

On the other hand, the composite laminates subjected to a HVI exhibit all the damage modes as in case of LVI, along with the fibre fracture, fibre crushing and penetration. Fibre failure is the extreme damage mode in laminated composites and at this stage the structure fails. This failure can be catastrophic or progressive depending upon the type of fibre reinforcement employed in the laminated composite structure. The numerical studies to characterise the mechanical behaviour and damage in such composites under impact and blast loading are still very limited.

The blast events are difficult to study experimentally since they can produce pressure signatures which are spatially complex and difficult to measure. Thus very sophisticated laboratory instruments are required to account for these. This gives rise to a lack of availability of reliable experimental data that can be used to validate a finite-element model of such dynamic events. Moreover the observation of damage initiation and evolution of composite materials is very

difficult due to the transient nature of this event where the entire event takes place in less than few milliseconds. Further blast is a highly dynamic event and modelling the mechanical behaviour of composites under such loading is a challenging task, mainly due to complications associated with respect to the complex interaction between fluid and structural domains (in this case air and CFRP plate), and accurate representation of dynamic response of composite plates shock induced loading. Further to this, under blast and ballistic impact conditions, structures made of composite materials often undergo extreme deformations and the underlying mesh in finite-element models may become highly distorted to the point where it may possibly yield unreliable results.

In this phenomenon, composites are often exposed to high loading rates, at which their response can be substantially different as compared to that under static loading. At low impulse blast loading, matrix cracking and delamination are dominant modes while at high impulse loading, composite structures may fail by undergoing fibre breakage and penetration.

In this respect, this study focuses on the finite-element (FE) modelling of laminated composites and their damage under impact and blast loading conditions. The basic aspects of FE modelling of composite laminates and various damage modelling schemes are discussed in the next chapter.

CHAPTER 3

FINITE-ELEMENT MODELLING OF COMPOSITES AND THEIR DAMAGE

3.1 Introduction

In recent decades, numerical methods have been employed increasingly in the analysis of composite laminates and evaluation of their damage modes, thanks to the availability of the improved computational power. Most of these approaches have made an attempt to analyse composites within the framework of a 2D boundary value problem using an assumption of plane-stress or generalized plane-strain conditions (Abrate, 1991; Jones, 1999) and hence are not effective means to analyse resulting through-thickness stress-states and underlying damage modes.

Damage in composites is a complex phenomenon and its inspection, especially within the laminate, can be problematic with the use non-destructive techniques. In recent years, the finite-element method has attracted much attention to model such phenomena at various scale levels. An accurate prediction of fracture in composite laminates often depends on modelling a progressive development of all modes of damage, such as matrix cracking and delamination, as well as their interactions. The combined effect of various damage modes acting concurrently on complex shaped composite structures subjected to arbitrary loading conditions cannot be handled properly with analytical techniques. The problem becomes even more complicated if one has to account for stresses induced due to processing, thermal loading and moisture absorption. Therefore, one has to resort to numerical techniques such as the finite-element method to predict the damage behaviour of composite structures accurately. With advances in computing resources, damage

modelling at various length scales and its effect on the macroscopic failure of laminated structures has become the focus of research. In this chapter, methodologies for modelling composite laminates and investigation of damage in these materials based on the finite-element method are presented.

3.2 Finite-element method

The finite-element method (FEM) is an approximate numerical technique for solution of continuum-mechanics problems. The continuum is discretised into a finite number of parts called *elements* connected at their common points called *nodes*. The finite-element discretization transforms a continuous boundary-value problem into an algebraic system of equations for discrete nodal variables of a given finite-element mesh. Variational principles are used to transform the governing differential equations of the problem under study to a weak form (integral form). In numerical methods, there are generally two approaches of formulating kinematics of continuum mechanics - Lagrangian or the material description of behaviour, and Eulerian or the spatial behaviour. In the Lagrangian approach, the material is associated with an element throughout the entire analysis, and the material cannot flow across element boundaries. In the Eulerian approach, elements are fixed in space and the material flows through them (Hibbit *et al.*, 2011). Thus, in the Lagrangian mesh, the mass in each element is constant while its volume varies; in the Eulerian, the mass can vary in each element, but not its volume. The Lagrangian formulation is preferable in simulations, where boundary conditions have to be fixed, contacts defined between the solids, or if an analysis is to be made of solids formed of several layers of material as in composite laminates. The Lagrangian mesh allows the history of the material to be followed which is particularly useful for the study of damage behaviour of composite materials (Abrate, 2011). Although the Lagrangian approach suffers from large-deflection of structures, when the mesh is highly distorted, still, the mesh control techniques available in the FE codes, e.g. Abaqus, resolve this issue. Eulerian methods are used commonly in fluid mechanics simulations. In this study, continuum elements based on the

Lagrangian formulation are used for the analysis of damage in woven and multidirectional composites.

The finite-element method has found an increasing application in the solution of complicated engineering problems. The most attractive feature of the FEM is its versatility and ability to handle complicated geometries under various loading scenarios with relative ease (Cook *et al.*, 2001). It is powerful tool for solving problems having no exact analytical solutions. Although it is an approximate solution method, the approximation can easily be improved by refining the mesh at regions where field gradients are high or if edge effects are to be included in the analysis. This local mesh refinement is known as *h-refinement*. The solution accuracy can also be increased by using elements with higher-order shape functions known as *p-refinement*. Combination of both these refinements is most efficient for simulating complex structures with irregular shapes and boundary conditions. It should be noted that the choice of element and mesh is problem dependent. When solving a specific problem using FEM, the accuracy of mesh refinement can be checked by carrying out a series of runs with different mesh densities or different element types and checking the results for convergence. On the other hand, modelling, discretisation and numerical errors affect greatly the solution of the problem.

Most real world composite structures do not admit exact solutions, requiring one to find approximate but representative solutions (Ochoa and Reddy, 1992). FEM is an effective approximate method for predicting the response of composite laminates. Application of FEM to composites requires specific element formulations that adequately represent their orthotropic behaviour, stiffness and strength, as well as the lamination of plies often used. Unlike isotropic materials, composites exhibit complicated mechanical behaviour requiring knowledge of anisotropic elasticity, lamination theories, and failure and damage criteria. This complex behaviour of composites results in need of in-depth research for their design and application. The next section highlights various approaches for the analysis of composite laminates using FEM.

3.3 FE modelling of composite laminates

Fibre-reinforced composites are manufactured in the form of thin layers bonded together to form a laminate with desired geometry and material properties. The properties of a laminate are very much dependent on properties of individual plies and their corresponding angles. Thickness of these laminates is usually small compared with their other dimensions so that it forms a plate type structure. Therefore, two-dimensional theories are used to analyse composite laminates for stresses and subsequent failure. Zhang and Yang (2009) classified the laminated plate theories into the two categories: equivalent single layer shell theories and a continuum-based 3D elasticity theory. Computational modelling of composites in the commercial FE softwares is usually based on elements formulated according to these theories. A short description of these modelling approaches is given below.

3.3.1 Equivalent-single-layer shell theories

Formulation of shell finite-elements is usually based on a classical lamination theory (CLT), a first-order shear deformation theory (FSDT) (also called *Mindlin plate theory*) and higher-order shear deformation theory (HSDT). The two-dimensional classical lamination theory (CLT) derived from the three-dimensional elasticity theory is found to be adequate for most applications where the thickness of a laminate is small and shear deformation effects are negligible (Ochoa and Reddy,1992). This theory is based on assumptions that the in-plane displacements vary linearly through the thickness and the transverse displacement is assumed to be constant through the thickness. Stiffness coefficients of the laminate are derived from stiffnesses of individual plies using CLT. Usually, stress-strain relations for a thin lamina of orthotropic material are written down, and subsequent transformation and integration procedures yield stiffness moduli for the whole laminate. Determination of laminate's stiffness moduli has been made easy by the application of FEM. Since, the material properties vary from ply to ply, the stress variation through thickness of the composite laminate will be discontinuous. That is why a

laminate theory is used instead of simple material stiffness for a laminated material (Cook *et al.*, 2001). Further, the theory ignores edges whereas real-life plates have edges subjected to stresses. Therefore, CLT should not be used for composites that are likely to fail in transverse shear and delamination. In a commercial FE package Abaqus, formulation of thin conventional shell elements is based on CLT (Kirchhoff) theory (Matthews *et al.*, 2000). The conventional shell is a planar 2D representation of a solid element, even if deformable in a 3D space. Thickness is attributed to a planar element by assigning a section or a composite layup. Since, the geometry is defined in the two-dimensional space, thus an element cannot be assigned to each ply of the composite. A continuum shell element is also available for modelling thick solid parts in Abaqus; however, its kinematic and constitutive behaviour is similar to conventional shell. Continuum shell also has a single element through its thickness, which contains multiple plies defined in the layup (Hibbit *et al.*, 2011).

The first-order shear deformation theory (FSDT) or Mindlin shell theory is used for thin and moderately thick laminated plates, providing a balance between computational efficiency and accuracy for the structural response of the laminated composites. But this theory does not predict local effects such as interlaminar stress distribution between layers and delamination. To overcome these deficiencies, higher-order shear deformation (HSDT) theories have been developed, that satisfy free boundary conditions of the transverse shear stresses on the upper and lower ply surfaces. Interlaminar stresses can be predicted accurately but at the expense of computational cost as the number of unknowns depends on the number of plies of the laminate. Thus, 3D representation of each ply in the FE model is necessary.

3.3.2 Continuum based 3D elasticity theory

Composite laminates are typically modelled using elements based on shell theories, which are limited in modelling their through-thickness behaviour. Through-thickness bonding between the plies is provided by a weak matrix, which is susceptible to delamination caused by high transverse shear stresses.

The solid elements formulated on 3D continuum-based elasticity theory have a capability to predict delamination and interlaminar shear as well as normal stresses in a composite laminate. In such layer-wise modelling, each separate layer of the laminate is explicitly represented by at least one continuum element with its own degrees of freedom (DOFs). The 3D continuum-based modelling approach relies classically on the use of solid brick elements that are stacked on each other so as to form the whole laminate. In Abaqus, if the FE model contains multiple continuum solid elements through the thickness of a region, correct results can be obtained by sectioning the solid region of the composite for each ply and defining a separate composite layup for each layer of elements (Cook *et al.*, 2001). Since, this description introduces a number of DOF that depends on the number of layers constituting the laminate, the computational cost for 3D models becomes higher.

The fibre direction in a ply and the stacking sequence of plies forming a composite laminate have a significant effect on its response (Matthews *et al.*, 2000). While defining a composite laminate in a FE package, the fibre direction, number of plies and their stacking sequence are specified in the pre-processor. Similarly, the orthotropic material properties of each lamina are also defined in the material model. Most composite laminates are manufactured by stacking sheets of material with the fibres directions changing from ply to ply. In this type of structure, all the fibres are at known fixed angles to each other, and the direction of the reference ply is defined to specify the alignment in the lay-up. The fibre direction is controlled by the angle with respect to the reference ply and the global coordinate system. By incorporating appropriate boundary and loading conditions, the structural problem is solved as in the case of isotropic material model. In post processing, the obtained results are viewed and manipulated at ply level, and each ply failure is thus investigated using an appropriate failure criterion.

Composite structures may be subjected to nonlinear behaviours in various ways. Structures made of thin laminates are prone to a large-deflection nonlinear response in static as well as dynamic loading scenarios. This

geometric nonlinear behaviour is modelled employing large-deflection options in FE packages. Buckling instability of thin structures is also one of geometric nonlinear problems. Similarly, material nonlinearity has a significant effect on stability and failure of composite structures. Many composite structures are made of brittle materials and thus can exhibit a nonlinear behaviour involving brittle fracture. Delamination modelling based on material's softening behaviour also poses a nonlinear phenomenon in FE models. A macroscopic behaviour of composite materials is determined by the properties of their constituents, i.e. fibres and matrix, at microscopic level. Fibrous composites show a high degree of spatial variation in their microstructure, resulting in their non-uniform and anisotropic properties. In contrast to more traditional homogeneous materials like metals and ceramics, composites demonstrate multiple modes of fracture and damage due to their heterogeneity and microstructure. Damage evolution affects both their in-service properties and performance that can deteriorate with time. Therefore, to design and engineer composite materials for specific end uses, an in-depth knowledge of material properties at various length scales is required. Thanks to availability of high-performance computing resources, FEM is largely used to model composite materials at various scales. The next section highlights modelling strategies for fibrous composites using FE techniques at various length scales.

Finite-element formulations based on CLT, FSDT, HSDT and layer-wise theories are capable to predict in-plane failure of composite plates. They are generally used to investigate a mechanical behaviour and failure of laminated composite based on first-ply failure criterion. However, in this research study, structures are subjected to transverse dynamic loading, and the major failure mode is that of fibre damage and delamination due to high interlaminar stresses. Therefore, finite-element models based on the 3D elasticity theory are used to investigate the behaviour of a 3D stress field at the edges of laminated plate and to predict through-thickness failure of composite laminates.

3.4 Modelling composite laminates at various length scales

The advantage of fibre-reinforced composites as structural components lies in the fact that the material's behaviour can be tailored. Desired properties of composites at macroscopic level can be obtained by manipulating the constituents at microscopic level. Since the mechanical behaviour of composite laminates varies at different length scales, it is required to study their behaviour at various scales. Micromechanical analysis facilitates understanding of the effect of local properties of constituents and their arrangement on macroscopic material and structural behaviour, thereby accelerating the development cycle of a material system for a specific application. The task of micromechanics is to link mechanical relations at various scales. Microstructural mechanics combines approaches of computational mechanics and materials sciences to estimate local deformation mechanisms in heterogeneous materials at the level of heterogeneity, to predict overall properties of heterogonous materials based on homogenisation techniques and to simulate local damage in heterogeneous materials (Zohdi and Wriggers, 2005). Multi-scale material models are employed to predict the properties at various scale levels and then correlate those using approaches of continuum mechanics. With a rapid growth in computational power of computers, multi-scale modelling of fibre-reinforced composites has become an important means of understanding the behaviour of such materials.

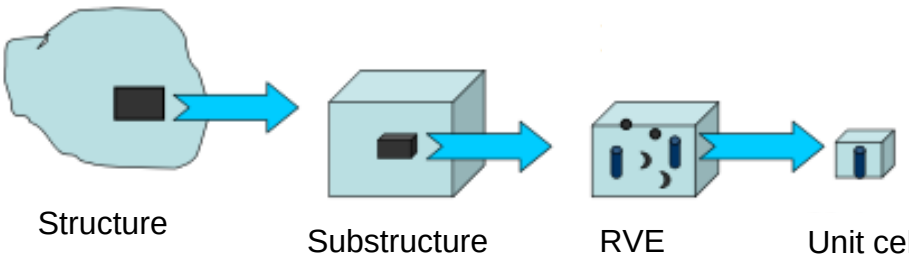

Figure 3.1 A multi-scale approach: from structural scale moving down to lower scales (Talreja, 2006)

A multi-scale approach considers three scale levels (Fig. 3.1) for the analysis of heterogeneous composite materials (Talreja and Singh, 2008) as described below:

1. Micro-scale: The micro-scale is the lowest observation scale taking into account the behaviour of constituents (fibres and matrix) of the material. Here, fibre and matrix phases are modelled separately, and the average properties of a single reinforced layer are determined based on properties of individual constituent using a homogenisation technique. Interaction between constituents and the resulting behaviour of the composite (fields of micro-strain and -stress) is the main concern at this scale. In woven composites, damage mechanisms such as matrix micro-cracking, fibre/matrix debonding and fibre failure within tows can be modelled at micro-scale.
2. Meso-scale: The meso-scale considers the ply as a basic homogeneous continuum entity for mechanical analysis of, and failure prediction in laminated composites. Each ply is modelled separately as a homogeneous material and the fibre direction is taken into account in terms of orthotropy of the homogenous material. The ply's mechanical and elastic properties can be determined through experimentation, but modelling at this scale does not provide any information about a character of interaction between the constituents. However, this scale can be much more easily implemented in analysis of large structures than the micro-scale due to lower computational effort. In woven composites, damage such as intra-yarn cracking and inter-ply delamination is normally predicted using this scale. In this approach, a virtual laminate is built by stacking plies with different fabric orientations, and the FE model explicitly includes each ply as well as interfaces between them. Meshing of the laminate is carried out with solid elements for the plies, while cohesive interface elements can be used to account for ply interfaces in the model. This modelling strategy presents two main advantages. Firstly, full 3D stress states can be considered contrary to

simulations based on the use of shell elements for composite plies, which are limited to 2D stress states. Secondly, intralaminar and interlaminar damage can be introduced separately together with a complex interaction between them. However, the main limitation of this approach lies in computational power required to carry out such simulations for large structures (Llorca *et al.*, 2011). Ladeveze (1995) was among the pioneers to propose meso-level modelling approach for damage in composites

3. Macro-scale: The macro-scale is defined at the level of components at which the structure is a completely homogeneous continuum and its material behaviour is described by an anisotropic constitutive law. The overall structural response to external loading makes a continuum mechanics problem and can be investigated by using FE models with effective (average) material properties. At this scale, composite's failure is characterised by a strong interaction of intra-ply cracking and inter-ply delamination and ultimate fabric rupture (Shyr and Pan, 2003). Main advantages of macro-scale models are their simplicity as well as capability to be adapted to different geometries and types of fabric reinforcements, provided the respective mechanical tests that define them are performed. The main disadvantage is that since the reinforcement is not modelled explicitly, the actual damage mechanisms are not captured, leading to an arguable lack of physical representativeness (De Carvalho *et al.*,2012)

Multi-scale modelling is based on two different analysis procedures of homogenisation and localisation. The homogenisation technique allows the behaviour of heterogeneous material to be regularised (homogenised) as a continuum. This technique is designed to estimate the effective properties of composite materials at macro-scale based on the known properties of several constituents and microstructural morphology. The approach is to compute a constitutive relation between volume-averaged field variables. Then, the homogenised properties can be used in a macroscopic analysis of the material.

The volume averaging takes place over a statistically representative sample of the studied material referred to as a *representative volume element* (RVE). This statistical representative volume has to be large enough to reproduce information concerning the material's global behaviour. The choice of RVE depends upon the detail required to characterise the phenomena occurring inside the material (Bunsell and Renard, 2005). However, the homogenisation process based on average values does not account for damage at micro level triggered by localised stress field. Therefore to deal with physical events in the microstructure such as fibre damage etc., a localisation technique or a periodic micro-field approach can be used to evaluate local stresses and strains at micro-scale. Analysis of periodic materials is based on the repeating unit cell concept (RUC) and the associated periodic boundary conditions. Here, spatial placements of the reinforcements are assumed at regular locations in space. Numerical simulations of the mechanical response of a unit cell with prescribed loading and boundary conditions are carried out to determine the material's macroscopic properties (Pindera *et al.*, 2009; Segurado *et al*, 2006). Apart from the material characterisation and constitutive modelling, the micromechanical approach is also used to study local phenomena in heterogeneous materials such as initiation and evolution of microscopic damage, nucleation and growth of cracks, effects of local instabilities, stresses at intersections between macroscopic interfaces and free surfaces, and the interactions between phase transformations and micro-stresses (Böhm, 2005). Ernst *et al.* (2010) carried out multi-scale progressive failure analysis of woven laminates. They first determined the material constants by using micro-scale RVEs and then implemented the material data in a macro-scale model of three-point bending test. Finite-element models incorporating various damage modes at the constituent scale of yarns and matrix in woven composites were developed in (Daggumati *et al.*, 2010; López-Puente and Li, 2012; De Carvalho *et al.*, 2012; Römelt and Cunningham, 2012) among others, yet the problem domain was limited to a representative volume or unit cell and the full laminate was not modelled. The meso-level modelling approach was employed (Iannucci and Willows, 2006; Johnson *et al.*, 2009; Menna *et al.*, 2011; Gamma and Gillespie,

2011; Sokolinsky *et al.*, 2011) to characterise the damage behaviour of fabric-reinforced composite structures.

However, this hierarchical multi-scale approach faces major difficulties in selecting length scales for damage-initiation and progression, and modelling multiple damage modes occurring simultaneously and interacting with each other. Talreja (2006) proposed a synergistic damage mechanics approach, an alternative to hierarchical approach, combining continuum damage mechanics for macro- and meso-scale modelling and micro damage mechanics for microstructure modelling. Silberschmidt (2008) showed that the effect of random distribution of fibres in composite laminates resulted in non-uniformity of damage processes and cracking evolution and their effect on the composite's response to external loading using multi-scale damage models.

As mentioned earlier, computational modelling is used to investigate damage at various scale levels. Subsequently, multi-scale modelling transfers the damage information from lower to higher scale to predict the catastrophic collapse of laminates. However, multi-scale failure analysis using finite-element models combining coarse meshes and finer meshes at the macro and micro levels respectively is still computationally costly because of a large volume of calculations. Further, a complex weaving architecture as well as multiple modes of damage at various length scales in textile laminates makes micro-mechanics based constituent-level modelling more computationally expensive for problems of real life. Therefore, meso-level models coupled with continuum damage mechanics are efficient in design and failure prediction of composite laminates: it is also employed in this work. In the following section, the analysis procedures for FE modelling of composites and there damage are described.

3.5 Implicit *vs*. explicit solvers in FE modelling

Implicit and explicit techniques are widely used in finite-element methods to solve linear and nonlinear systems of equations (Crisfield, 1994). Implicit methods are based on static equilibrium. The basic statement of static equilibrium is that the internal forces exerted on the nodes I (resulting from the

element stresses) and external forces P acting at every node must balance (Hibbit *et al.*, 2011):

$$P - I = 0 \tag{3.1}$$

The solution procedure iterates successively until convergence is achieved. This incremental-iterative solution technique is usually based on the Newton-Raphson method as in Abaqus-standard. The method is unconditionally stable i.e. any size of increments can be used. This method requires a solution of a banded set of simultaneous equations at a series of load increments, and needs constant updating of a global stiffness matrix and a series of iterations in order to achieve convergence. However each iteration requires a tangent stiffness matrix that needs careful handling in numerical aspects for its solution. One of the most challenging issues in the cohesive-zone method using the implicit solver is convergence of the FE model during its softening behaviour (Turon *et al.*, 2007) Also, implicit methods require much more computational resources and a higher computation time per cycle than explicit methods. Large matrices need to be stored and a large system of algebraic equations should to be solved in each cycle. Consequently, implicit methods are mostly used for static and low-rate dynamic analyses.

An explicit method uses a central difference rule to integrate the equations of motion explicitly with regard to time, using kinematic conditions at one increment to calculate the force at the next increment. The explicit methods are based on dynamic equilibrium which includes the inertial forces:

$$P - I = m\ddot{u} \ , \tag{3.2}$$

where m is the mass and $\ddot{u}$ is the acceleration of the structure. The explicit method does not deal with the tangent stiffness matrix, and, therefore convergence is more likely to achieve. Though it is conditionally stable, i.e. for the solution to be stable, the time step has to be small enough such that information does not propagate across more than one element per time step. Thus, this method needs very small time increments in order to have stable

solutions in time, leading to higher CPU times for time-dependent loading (Crisfield, 1994). This restriction makes the explicit method inadequate for long duration dynamic problems. The explicit formulation is often appropriate in cases with severe changes in stiffness matrix, such as analysis with failure or degradation of the material. An explicit dynamic analysis approach is typically adapted to model large deflections, material nonlinearities and contact behaviours in high-velocity transients but it can be also employed effectively in modelling dynamic phenomena with severe discontinuities in the structural response, as is the case in unstable crack propagation. Since time integration is easy to implement, the material nonlinearity can be cheaply and accurately treated, and the computational resources required are small even for large problems. Menna *et al.* (2011) performed numerical simulations of low-velocity impact tests on glass fabric/epoxy laminates through the explicit FE code LS-DYNA. Iannucci and Willows (2006) modelled impact induced damage such as delamination in woven composite using the explicit code LS-DYNA 3D. Similarly, Johnson *et al.* (2009) studied impact damage in woven GFRP composites panels for marine applications using Abaqus/Explicit solver. The method can also be used for quasi-static analyses by artificially increasing the load rate or material's mass to increase the stable time increment for fast solutions. Pinho *et al.* (2006) employed the explicit method to model mixed-mode delamination in composites using cohesive-zone elements under quasi-static loading conditions. Gözlüklü *et al.* (2012) modelled delamination propagation in L-shaped laminated CFRP composites under quasi-static bending using the explicit solver of Abaqus. Based on the advantages, the explicit method is ideal for nonlinear dynamic problems such as impact and penetration and large-deformation quasi-static simulations and it is employed in this study. The following section highlights various FE modelling and analysis techniques for damage behaviour of composite laminates.

3.6 Finite-element modelling of damage mechanisms

Failure prediction of fibre-reinforced composite laminates is complicated due to inherent heterogeneous nature, which gives rise to multiple cracks, interacting

strongly as failure progresses. These damage mechanisms may cause significant redistribution of stresses and thus affect the load level, at which final structural failure occurs. Design and certification of most composite structures are based on empirical approaches because of the difficulty of complete damage-process prediction, with relatively little use of simulations. Therefore, there is a need for models, capable to simulate the entire damage process from its initiation through evolution to complete failure of the composite structure. The use of analytical models is practical only for simplified cases and cannot be used to model this complex process, initiating from matrix cracking, evolving in delamination and fibre breakage to composite structural ultimate failure. The most promising and suitable tool is a computational approach based on the finite-element method (FEM). This approach unlocks a full potential of composites resulting in more rational and optimised designs of composite laminated structures. However, the development of proper numerical model representing the physics of damage mechanisms is a challenging task (Van der Meer *et al.*, 2009)

Reliable and accurate simulations of discrete damage behaviour of composite laminates require guidance from experimental and theoretical studies of damage mechanisms. Understanding a sequence of different damage modes in ply-scale damage and defining physical parameters in material's constitutive laws that determine which mode will dominate is a challenge of respective simulations. According to Cox and Yang (2006), the difficulty in composite damage modelling is linked not only to insufficient computational power. A more serious challenge is to categorise and characterise many possible mechanisms of damage and represent them in a model in a realistic and physical way. Similarly, understanding the origins of numerical instabilities that often occur in simulations of heterogeneous materials poses another challenge. It is critical to know whether these instabilities are due to numerical approximations or rather they reflect physically unstable damage propagation, such as the dynamic crack propagation that is often observed in experiments. Modelling of cracking sequences and potential instabilities successfully in a computationally cost-

effective way is of key interest to developing tools for use as virtual tests (Zhou *et al.*, 2010). Various approaches are implemented in finite-element models to characterise the onset and progression of damage for analysis of composite structures. The studies involve monitoring of a particular type of parameter such as stiffness degradation for prediction and monitoring of damage growth. In the next section, various damage characterisation and analysis approaches based on numerical techniques are presented.

The damage in composite laminates is a complex phenomenon and results in various failure modes that interact in a unique pattern. Usually, failure of the first ply represents the damage-initiation and evolution of the composite laminate, but does not lead to the ultimate structure failure. According to Puck and Schürmann (1998) analysis of damage-initiation and evolution in composite laminates requires (a) analysis of strains and stresses ply by ply; (b) failure criteria for single lamina; (c) degradation models to include the effects of damage, which often does not lead to ultimate failure of the laminate; and (d) a computer program, which simulates the gradual failure process by applying above sequences. The approaches to model crack initiation and damage evolution are discussed below.

3.6.1 Strength-based approaches

Strength of a material can be used to characterise the onset of damage in composite laminates. Strength-based failure criteria predict the onset of different damage mechanisms in composites and, depending on the material, its geometry and the loading conditions, can also predict final structural collapse. According to this approach, micro-cracks form when the stress reaches the transverse strength of the ply material or some multi-axial stress criterion is satisfied (Parvizi and Bailey, 1978; Parvizi *et al.*, 1978). Application of the strength approach is based on defining one or more strength criteria, and the structure is deemed to have been irreversibly damaged once these criteria are met. These models fail to account for difference in crack initiation and progression for specimens of different ply thicknesses since the stress state at

the onset of transverse cracking is not constant for different laminates. Moreover, the main drawback of strength-based criteria is a lack of agreement with the experimental predictions as shown by the failure exercise of Hinton and Soden (1998). It is important to note that strength-based characterisation of damage is most commonly applied to define the damage-initiation, and not the progression of an existing damage region such as delaminations between plies (Orifici *et al.*, 2008). A large number of strength-based criteria have been derived to relate stresses and experimental measures of material strength to the onset of failure. One of the first models to predict micro-cracking was based on the first ply failure theory, where it is assumed that the first crack develops when the applied strain in the plies reaches the ply's failure strain. Another simplest approach is the ply discount method, which completely neglects transverse stiffness of the cracked plies; it underestimates stiffness of the cracked laminate. Predictions based on both these models were not in agreement with experimental observations (Talreja and Singh, 2008).

Another approach included a shear-lag (Cox, 1952) analysis model developed for the prediction of stress recovery in a broken fibre embedded in a matrix composite. The term shear lag is based on the assumption that all of the load transfer from matrix to fibre occurs via shear stresses acting on the cylindrical interface between the two constituents. The stress distribution in the fibre is determined by relating shear strains in the matrix around the fibre to the macroscopic strain of the composite.

Fibres are treated as one-dimensional, axial load-carrying springs. Other simplifications can be made, but the universal characteristic of shear-lag models is that a three-dimensional fibre is assumed to act like a one-dimensional entity. Shear-lag models of varying degrees of complexity have been used to determine the stresses in a broken fibre. Highsmith and Reifsnider (1982) developed shear lag models based on the principle of stress transfer between cylindrical fibres surrounded by matrix material, where a load transfer between plies was assumed to take place in shear layers between neighbouring plies. The shear lag theory neglects variations in the stresses and strains through ply

thickness. However, this theory is based on approximations that may render predictions subject to error. To overcome these limitations, Hashin (1985) and Nairn (1989) developed models of stress transfer in cracked cross-ply laminates based on variational method. This approach attempts to solve a two-dimensional boundary value problem, and thus yields much better results than shear lag models. Prediction of thermomechanical parameters such as stiffness, local ply stresses and coefficients of thermal expansion of cross-ply laminates with regularly spaced ply cracks based on these models were in good agreement with experimental data. Failure criteria such as the maximum stress, Hashin, Hoffman, Yamada-Sun, Puck, Tsai-Hill and Tsai-Wu were developed over the past five decades (Liu and Zheng, 2010) for strength and failure analysis of laminates, but no universally accepted failure criterion exists. Among these, interactive failure criteria such as Hashin (1980), Puck (1998) and Tsai-Wu (1971) are widely used to characterise separate damage types in composites. Chang and Chang (1987) developed a progressive damage model for notched laminated composites subjected to tensile loading, capable of assessing damage in laminates with account for material's nonlinearity.

Most of these failure criteria are implemented in commercial FE codes such as Abaqus and Ansys, to name a few, to determine whether a composite structure will fail. Numerous researchers have applied strength-based criteria to predict damage in woven composites. Daggumati *et al.* (2010) detected damage-initiation at yarns with Hoffmann criteria in a meso-level FE model of 5-harness satin woven composite subjected to tension. Menna *et al.* (2011) employed Tsai-Wu criteria to predict intra-ply damage in simulations of woven GFRP laminates under impact loading. Santiuste *et al.* (2010) developed a progressive failure model based on Hou and Hashin criteria in Abaqus/Explicit to predict failure modes of composite laminated beams subjected to low-velocity impacts in a three-point bending configuration. However, the use of strength-based failure criteria for composite materials has a drawback that the scale effect relating to the length of cracks subject to the same stress field cannot be modelled correctly. In other words strength based failure criteria can be an

effective mean to model damage initiation in laminated composites, though it does not allow to model its propagation before complete failure. Hence, the use of fracture mechanics- or energy-based approaches is attractive for modelling of matrix cracks or delaminations (Iannucci, 2006).

3.6.2 Fracture-mechanics-based approaches

Strength and failure analysis of laminated composites is rather different from the analysis of strength of a single ply. Failure of laminates usually involves matrix cracking and delamination between the plies. It has become a common practice to investigate progression of these damage modes using fracture mechanics-based approaches. Fracture mechanics deals with the influence of defects and cracks on the strength of a material or structure. The main objective of fracture mechanics analysis is to predict the onset of crack growth for a structure containing a flaw of a given size. It has generally been assumed that the size of a plastic zone at the crack tip is small compared to the crack length while calculating the critical load for a cracked composite. Linear elastic fracture mechanics has been found useful for certain types of cracks in composites, i.e., interlaminar cracks such as delamination, or matrix cracks in a unidirectional composite (Adams *et al.*,2003). In the fracture mechanics theory, the growth of a macroscopic defect is controlled by the rate of strain energy released in propagation, as compared to a threshold maximum strain energy release rate for that material, also known as *material toughness* (Orifici *et al.*, 2008) The strain energy released in crack propagation is typically split into three components linked to separate mechanisms of crack growth. Mode I refers to opening or peeling of crack surfaces, Mode II refers to sliding, and Mode III refers to tearing as shown in Fig.3.2. This approach has proved to be highly successful, when complemented with an accurate stress analysis approach for damage-initiation. However, the fracture mechanics approach cannot be easily incorporated into a progressive failure methodology (Iannucci, 2006).

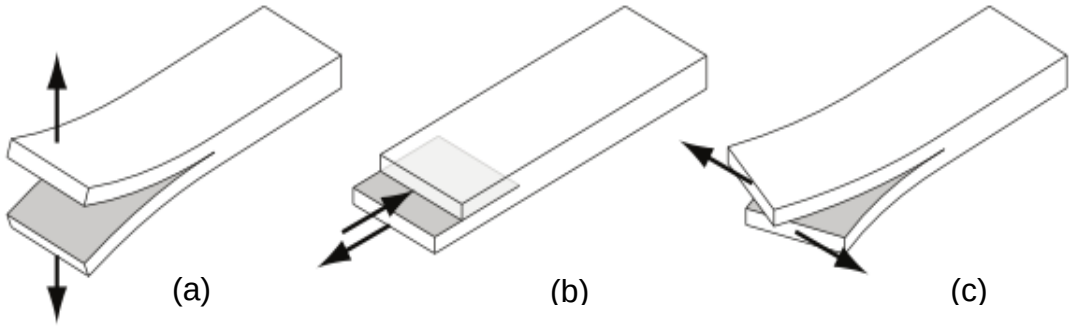

Figure 3.2 Modes of crack growth (a) Mode I (opening); (b) Mode II (sliding); (c) Mode III (tearing) (Orifici *et al.*, 2008)

Fracture mechanics analysis has been limited in this respect due to complexities involved in monitoring crack growth and a typical requirement for a fine mesh around the crack front, which usually means either a highly dense mesh or computationally expensive re-meshing (Orifici *et al.*, 2008). Further, prediction of fracture properties requires special techniques such as J-integral proposed by Rice (Rice, 1968). But this approach cannot be employed to calculate the energy release rate for complex 3D laminated structure since it is limited only to the case for plane structure and also requires a high quality dense mesh at the crack tip when using finite-element method. These factors make the application of fracture mechanics techniques limited to predicting the initiation of crack growth and not its progression (Orifici *et al.*, 2008). However, recent approaches based on fracture mechanics such as virtual crack closures technique (VCCT) were developed and implemented successfully in commercial FE codes such as Abaqus, for crack propagation analysis. This technique is applied during every increment of a nonlinear analysis, and uses single-mode and mixed-mode fracture criteria to determine when attached nodes should be released to represent crack growth.

The VCCT was initially proposed by Rybicki and Kanninen (1977) based on Irwin's crack tip energy analysis for linear elastic materials (Irwin, 1957). The method employs an assumption that the strain energy released in the process of crack growth by a certain amount is the same as that required to close the

crack by the same amount. The VCCT is widely used to compute the energy release rates at the crack tip based on results from continuum (2D) and solid (3D) finite-element analyses to provide the mode separation energy required when using the mixed-mode fracture criterion (Krueger, 2004). Further, this technique does not require a high mesh density like other fracture mechanics based approaches such as J-integral. Pereira *et al.* (2005) implemented the VCCT in Abaqus using 3D 8-node brick C3D8R elements to determine the energy released in Mode I double cantilever beam (DCB) tests performed on woven glass/epoxy multidirectional laminates. Shindo *et al.* (2009) employed the VCCT in a FE model to calculate the energy release rate in Mode II fatigue delamination growth in woven GFRP laminates at cryogenic temperatures. Hallet *et al.* (2008) used VCCT to determine the applied load that would cause free edge delamination in modelling interaction between matrix cracks and delamination in scaled quasi-isotropic specimens under tensile loading. Marsavina and Sadowski (2007, 2009) determined stress intensity factors at the tip of a crack in bi-material ceramic interfaces under bi-axial state of stress using finite-element method.

3.6.3 Cohesive-zone models

Computational simulation of delamination requires a capability to model initiation and progression of damage during analysis. Delamination initiation in composite laminates is usually assessed by strength-based criteria. Several techniques based on fracture-mechanics are employed in the finite-element method to simulate a delamination growth such as the J-integral, the virtual crack extension technique and the virtual crack closure technique (VCCT) (Wimmer *et al.*, 2009). Fracture-mechanics analysis is limited in this respect since it neglects material's nonlinearity in most cases and requires a position of delamination crack to be known in advance (Alfano and Crisfield, 2001). Further, typically, a fine mesh around the crack front is required, which makes the analysis of three-dimensional composite structures rather computationally expensive. Therefore, numerical prediction of the effects of interlaminar damage

on the behaviour of composite laminate requires a finite-element scheme that is capable to model strength as well as toughness of the inter-ply layers.

A reliable and promising approach to overcome the above issues and model the material as well as geometric nonlinearities is to employ cohesive elements at the interface between the composite laminae. Cohesive-zone elements are based on the model proposed by Dugdale (1960), who introduced the concept that stresses in the material are limited by the yield stress and that a thin plastic zone is generated in front of the crack. Barenblatt (1962) introduced an idea of cohesive forces on a molecular scale in order to solve the problem of equilibrium in elastic bodies consisting of cracks.

(A) Traction-separation laws

Cohesive-zone damage models define relationships between tractions and displacement at an interface, where a crack may occur. Various constitutive models defining the traction-displacement behaviour of cohesive elements have been developed. Needleman (1987) was one of the first to use polynomial and exponential types of cohesive-zone models to describe the process of void nucleation from initial debonding to complete decohesion in metal matrices. Tvergaard and Hutchinson (1992) proposed a trapezoidal law to calculate the crack growth resistance in elasto-plastic materials, whereas Cui and Wisnom (1993) defined a perfectly plastic rule. The irreversible, bi-linear, softening constitutive behaviour used in this study, was developed in previous works by Mi *et al.* (1998), Alfano and Crisfield (2001), and Camanho and Davila (2002). Other formulations have been proposed such as Yang and Cox (2005) developed cohesive models for damage evolution in laminated composites.

Damage-initiation in the bi-linear cohesive law is related to interfacial strength, i.e., the maximum traction on the traction–displacement jump relation, at which reduction of material's stiffness starts as shown in Fig 3.3. Stiffness degradation continues until the interface elements attain zero stiffness, corresponding to complete separation of adjacent layers. After this, the interface elements act only as a contact region without transferring load. The work required to reduce

the material's stiffness to zero is equal to its fracture toughness, i.e. the area under the traction-separation curve (*Turon et al.*, 2006). The bi-linear relationship is generally preferred due to its simplicity and often used for modelling the interfacial response of quasi-brittle polymer composites. It can be defined as,

$$\sigma = \begin{cases} K\delta & \delta \le \delta_0 \\ (1-d)K\delta & \delta_0 < \delta < \delta_f \\ 0 & \delta \ge \delta_f \end{cases} \tag{3.3}$$

Here, d is a stiffness degradation parameter and is defined as,

$$d = \frac{\delta_f(\delta - \delta_0)}{\delta(\delta_f - \delta_0)}\ ,\ 0 < d < 1 \tag{3.4}$$

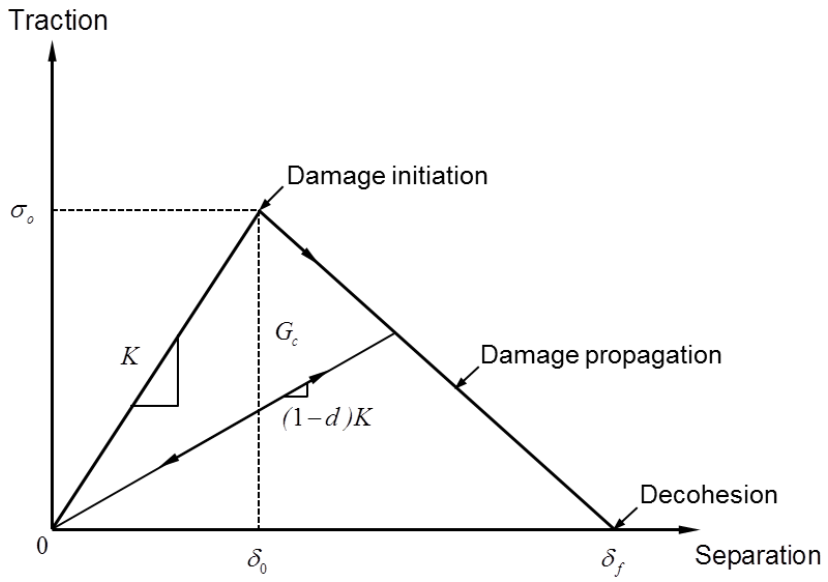

Figure 3.3 Bilinear traction-separation law (Meo and Thieulot, 2005)

The traction-relative displacement curve shown in Fig. 3.3 can be divided into three main parts that are described below (Meo and Thieulot, 2005):

(a) The portion for $\delta \le \delta_0$ presents the *elastic part* where the traction across the interface increases linearly until it reaches the maximum. The stress in this

portion of the law is linked to the relative displacement via the interface penalty stiffness K described by the first part of Eq. (3.3).

(b) The part of the curve for displacements $\delta_0 < \delta < \delta_f$ is known as the *softening part*. Here, the traction across the interface decreases until it vanishes and the two layers begin to separate. The damage accumulated at the interface is characterized by a variable *d* (see Eq. 3.4), which has a zero value in the undamaged state and reaches a value of one when the material is fully damaged.

(c) The portion of the graph for $\delta > \delta_f$ is called the *decohesion part*. Separation (or decohesion) of the two layers is complete, and there is no more bond between them. Interpenetration is prevented by reapplying only normal stiffness, in the case when a crack closure is detected.

The interfacial maximum strength in either Mode I or II for the bi-linear softening law can be determined as:

$$\sigma_o = K\delta_0 \tag{3.5}$$

Similarly, the critical energy dissipated per unit area of the softening curve which is equal to the fracture toughness G_c for either Mode I or II can be determined as:

$$G_c = \frac{\sigma_0 \ . \ \delta_f}{2} \tag{3.6}$$

Thus, at least five properties are required to define the interfacial behaviour of composites under quasi-static conditions: penalty stiffness K (generally it is assumed that there exists rigid bonding between adjacent composite plies and contact stiffness is infinite; though in FEA of delamination a reasonable value of such stiffness – penalty stiffness - needs to be selected such that it does not affect the numerical results, e.g. very high value of such stiffness will induce spurious oscillation in the results , while its lower value may indicate the weaker interface) corresponding fracture toughnesses in Mode I and II, G_{Ic} and G_{IIc}; the

corresponding interlaminar normal tensile and shear strengths σ_{Io} and σ_{IIo}, respectively. In dynamic simulations of damage, the interface material density will also be required.

(B) Damage-initiation and propagation

The fracture mechanisms that the cohesive law represents are often mode-dependent, and, in general, a cohesive law should be defined for both normal and shear tractions as a function of both normal and shear openings. A delamination growth is likely to occur under mixed-mode loading in structural applications of composites, in which crack faces simultaneously open and slide relative to each other. Therefore, a general formulation for cohesive elements dealing with an onset and propagation of mixed-mode delamination is also required (Camanho and Dàvila, 2002).

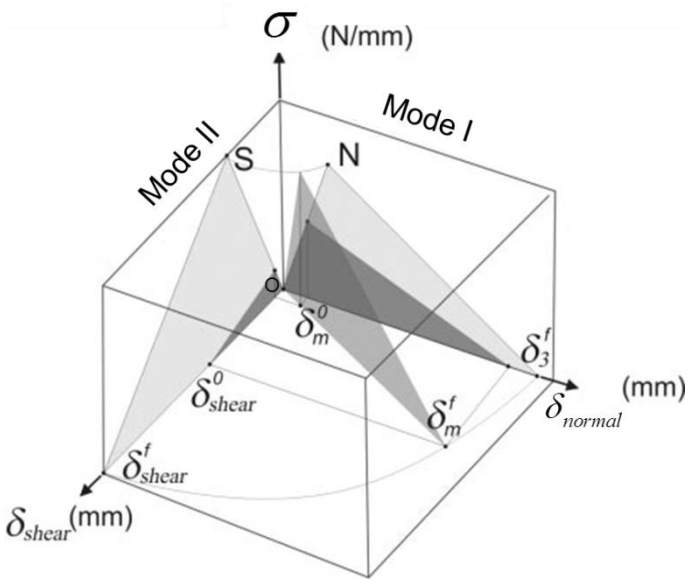

Figure 3.4 Bi-linear mixed-mode traction-separation law **(**Benzeggagh and Kenane, 1996)

A mixed-mode traction separation law shown in Fig. 3.4 is used when a structure fails under combined fracture modes such as in bending. Its formulation (Fig. 3.4.) can be illustrated using a single three-dimensional map by representing the normal opening mode (mode I) on the $O-\sigma-\delta_{normal}$ plane,

and the shear mode (mode II) on the $O-\sigma-\delta_{shear}$ plane. The triangles $O-N-\delta_3^f$ and $O-S-\delta_{shear}^f$ are the bi-linear response in Mode – I and shear mode respectively. In this 3D map, any point on the $O-\delta_{shear}-\delta_{normal}$ represents a mixed mode relative displacement.

Various strength-based criteria are developed for damage-initiation such as a maximum nominal stress criterion and quadratic stress criterion. Cui *et al.* (1992) highlighted the importance of mode mixity for interlaminar stress components when predicting delamination. It was shown that poor results were obtained using the maximum stress criterion. Therefore, the mixed-mode quadratic stress criterion accounting for the effect of interaction of traction components in the onset of damage proposed by Cui *et al.* (1992) was used in this study.

The nominal quadratic stress criterion for damage-initiation used in this study is given as:

$$\left[\frac{\langle\sigma_I\rangle}{\sigma_{I0}}\right]^2+\left[\frac{\sigma_{II}}{\sigma_{II0}}\right]^2=1 \tag{3.7}$$

where σ_{I0} and σ_{II0} are the cohesive interface strengths in opening Mode I and shear modes II and III respectively. The Macaulay's operator $\langle\ \rangle$ ensures that compressive normal tractions do not affect the damage-initiation.

Delamination propagation is usually predicted by criteria established in terms of interlaminar critical fracture energy under mixed-mode loading. Traditionally, two types of fracture energy based criteria are employed; one is the power law criterion proposed by Reeder (1992) and the second developed by Benzeggagh and Kenane (B-K) (1996). Camanho and Davila (2002) recommended the use of the B-K criterion for epoxy and thermoplastic based polymer composites. The B-K criterion used in this study for damage propagation is given as:

$$G_C = G_{IC} + (G_{IIC} - G_{IC})\left[\frac{G_S}{G_T}\right]^{\eta} \tag{3.8}$$

where, G_T is the work done by the interface tractions, $\left(\frac{G_S}{G_T}\right)$ is the fraction of the cohesive energy dissipated by shear tractions, G_S is the work done by the shear components of interface tractions; G_{IC} and G_{IIC} are the energy release rates in mode-I and II directions respectively. η is mode-mixity parameter and is a material property. It can be found using curve fitting technique where material's fracture toughness is plotted under different mode ratios.

The double-cantilever beam (DCB) test is used to characterise the mode-I strain-energy release rate, end-notched-flexure (ENF) test is employed to characterise the mode-II strain-energy release rate while mixed-mode bending (MMB) test gives mixed-mode strain-energy release rate. Their schematic is shown in Fig.3.5 (In Fig. 3.5, L - distance between applied centre of application of load and support, a - initial crack length). These tests provide the necessary input to FE models for simulating mode-I, mode-II, and mixed mode delamination. Further details regarding the experimental procedures to analyse these damage modes and their finite-element implementation can be found in Zureick and Nettles (2002) and Turon *et al.* (2010).

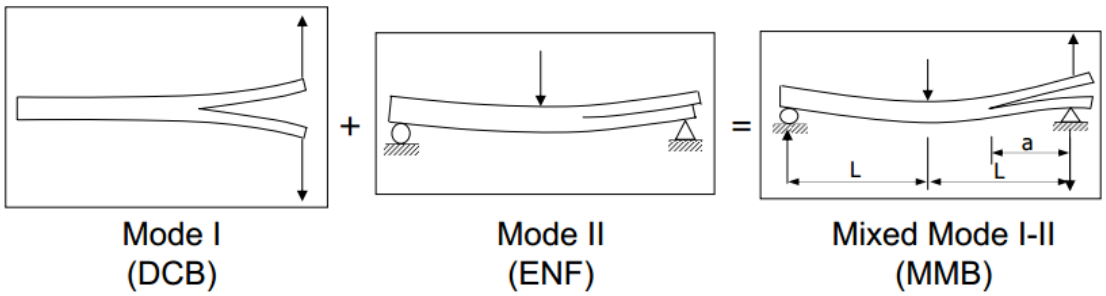

Figure 3.5 Experimental tests used to measure interlaminar strain-energy release rate of laminated composites

3.6.4 Damage mechanics approach

Strength-based failure criteria are commonly used to predict initiation of different failure mechanisms in composite laminates and can predict the ultimate structural failure depending on the given geometry, material and loading conditions. Since, composite structures accumulate damage before their ultimate collapse; the application of failure criteria is insufficient to predict this behaviour. The simplest way to model this damage behaviour is based on continuum damage mechanics (CDM) first proposed by Kachanov (1958). Damage mechanics approach has been widely used to predict the stiffness degradation and damage evolution in composite laminates. Damage can be interpreted as the creation of micro-cracks and micro-voids in a loaded material. Such microscopic damage behaviour is characterized by reduction of material stiffness at macroscopic level. According to Talreja and Singh (2012), damage mechanics is "a subject dealing with mechanics-based analysis of microstructural events in solids responsible for changes in their response to external loading". Hence, it is an approach for modelling a material response that attempts to quantify the physical events contributing to the evolving damage state. The application of damage mechanics involves introducing a phenomenological damage variable D in the material's constitutive model to represent initiation and progression of damage, which is monitored throughout the analysis. Multiple damage variables can be implemented to represent separate damage mechanisms, or a single damage variable can be used to capture the effects of all types of damage. A constitutive model relating the stress tensor σ to strain ε for a damaged composite laminate is given as,

$$\sigma = (1 - D)E \tag{3.9}$$

where $0 \le D \le 1$ and E is material stiffness. When the damage variable $D = 0$ it corresponds to a perfect undamaged material, and $D = 1$ to a completely damaged material. After initiation of laminate damage, the applied loads are resisted only by the undamaged ligaments such as fibres in the laminate. Stresses in fibres continue to increase until all fibres are severed and the

laminate fails. In progressive failure analysis based on CDM analysis, mechanical properties of damaged material are replaced with those of a homogeneous material by associating the damage mechanisms with their effects on the mechanical behaviour of laminated materials. The failure of the first layer indicates initiation of failure and damage evolution in the composite, but it does not represent the ultimate damage since the composite has still residual load-bearing ability (Liu and Zheng, 2010).

Various continuum damage models were developed by many researchers, e.g. Talreja (1985), Matzenmiller *et al.* (1995) and Miami *et al.* (2007) among others. Some of these models are discussed in-depth In Section 3.7. In these models, various damage modes generally found in composites were assumed and constitutive relationships between the damage tensor, conjugate forces and internal stress/strains were formulated to describe a progressive failure process and to interpret stiffness degradation of composite laminates. However, such thermomechanics-based models were usually developed for elastic-brittle behaviour, neglecting the effect of plasticity in some matrix-dominated off-axis laminates such as ±45 symmetric ones, and were usually limited to plane structures. Barbero (2002) presented a model by coupling CDM with a classical thermodynamic theory to predict inelastic effects such as reduction of stiffness and increments of damage and unrecoverable deformation; unrecoverable deformations and damage were coupled by the concept of effective stress. Talreja (1986) used an alternative approach based on CDM to describe the mechanical behaviour such as stiffness degradation of cracked laminates. The reduction of laminate stiffness was modelled in terms of internal damage state parameters. It was necessary to fit certain parameters to experimental or numerical data for application of this model. CDM-based modelling has found a wide application in analysis of damage and fracture of woven composites subjected to static and dynamic loads. Johnson *et al.* (2001) developed a CDM model for fabric-reinforced composites as a framework within which both in-ply and delamination failures in impact loading were modelled using FE code Pam-Crash. The fabric ply was modelled as a homogeneous orthotropic elastic or

elastic-plastic (in-plane shear) material with damage, whose properties were degraded on loading by microcracking prior to ultimate failure, giving a good agreement with experiments. Iannucci and Willows (2006) presented an energy-based damage mechanics model for woven carbon composites under impact loading by introducing various damage variables for in-plane damage along the warp and weft directions as well as shear nonlinearity into the FE code Ls-Dyna (Halquist, 2006).

The evolution of each mode of damage was controlled by a series of damage-strain equations, thus allowing the total energy dissipated for each damage mode to be set as a material parameter. Hochard *et al.* (2009) developed a CDM-based model and a non-local ply scale criterion for failure prediction for woven CFRP. The model was implemented in Abaqus using a user-defined material routine (UMAT) and validated with experiments for a notched composite plate. Johnson *et al.* (2009) implemented a CDM-based model in Abaqus/explicit employing a user-defined material subroutine VUMAT to study the in-plane damage whereas inter-ply delamination was modelled with cohesive-zone elements in woven GFRP composites under impact loading. A recent approach of modelling damage in composites is that of combining the CDM approach for the intralaminar (bulk) damage and cohesive-zone models (CZMs) for interlaminar damage in the commercial FE codes.

3.6.5 Other techniques

Apart from the methods mentioned above, there are some other new techniques that can be applied to simulate damage using different approaches, such as extended finite-element method (XFEM), augmented finite-element method (AFEM) and phantom node techniques.

XFEM makes modelling of cracks easier and accurate and does not require a mesh to match the geometry of discontinuities (cracks) and partitioning of geometry at the crack location as in the case of CZMs. This can be used to simulate initiation and propagation of a discrete crack along an arbitrary, solution-dependent path without the requirement of remeshing and can also be

employed in conjunction with the CZMs or VCCT. Predefined element boundaries are not needed for crack propagation as it fractures the element's interior. XFEM extends the piecewise polynomial function space of conventional FEM with extra functions called "enrichment functions". The numerical technique was introduced by Belytschko and Black (1999) based on the partition of unity method of Melenk and Babuska (1996). Applications of this technique include modelling of bulk fracture and failure in composites. Moës and Belytschko (2002) employed XFEM to simulate growth of arbitrary cohesive cracks, governed by a requirement for the stress intensity factors at the tip of the cohesive-zone to be vanished. Motamedi and Mohammadi (2012) used XFEM for dynamic propagation analysis of moving cracks in composites by introducing time-independent orthotropic enrichment functions. Kästner *et al.* (2011) developed a multi-scale XFEM-based model to simulate the inelastic material behaviour of textile GFRP composites. Abdel-Wahab *et al.* (2012) analysed the fracture of cortical bone at various scales using XFEM in the FE code Abaqus, however mentioned that this method cannot be used in the problems where crack branching occurs and location of a primary crack has to be known a priori.

3.7 Formulation of damage models for composites

A large number of failure criteria, material models and constitutive laws exist and aim to predict the failure of laminated composite materials. A selection of relevant material models is presented in this section. These models were selected on the basis of their innovation and prominence in the scientific literature. A short description of noteworthy aspects of these material behaviour models is also given, highlighting their strengths and weaknesses.

3.7.1 Lamina failure criteria

Unidirectional CFRP failure criteria evaluation was conducted from 1998 to 2004 in the work referred to as the World Wide Failure Exercise (WWFE). During this period, researchers representing the best available composite failure models were asked to participate in an evaluation of their respective models.

Each failure model was compared to an extensive set of experimental results. The merits and weaknesses of each model were exposed and recommendations were drafted to allow for improvement of composite material failure prediction. The failure prediction of most theories differed significantly from the experimental results, proving that much remains to be done in the field of composite failure theory.

Strength theories generally see the occurrence of failure as sudden events in which material parameters are degraded in an abrupt manner. However, the meaning of failure seems to vary from one theory to another as does the implication of failure of a lamina. The following will identify strengths and weaknesses of key material models proposed to deal with composite damage and failure.

(A) Maximum stress and maximum strain criterion

The maximum stress and maximum strain criteria, as their name imply, are based on maximum allowable values of stress or strain in the two directions, tension and compression, as well as in shear. These five criteria are fully decoupled, and material behaviour in one direction is independent of stress in the other normal directions. As a result, they do not take into account the coupled effects of stresses applied in other directions. These criteria are still widely used to estimate first ply failure for their simplicity, even though they do not reflect experimentally observed behaviour of unidirectional composites. Their mathematical formulation is given next.

According to the maximum stress criterion, material failure occurs if following condition is satisfied;

$$\left(\frac{\sigma_{11}}{S_{11,T}}\right) or \left(\frac{\sigma_{11}}{S_{11,C}}\right) or \left(\frac{\sigma_{22}}{S_{22,T}}\right) or \left(\frac{\sigma_{22}}{S_{22,C}}\right) or \left(\frac{\tau_{12}}{S_{12}}\right) \geq 1 \tag{3.10}$$

where $S_{11,T}$, $S_{11,C}$, $S_{22,T}$, $S_{22,C}$ and S_{12} are tensile and compressive strengths in fibre direction, tensile and compressive strengths in transverse direction and in-

plane shear strength respectively. This terminology is used throughout this section.

According to the maximum strain criterion, material failure occurs if following condition is satisfied;

$$\left(\frac{\varepsilon_{11}}{\varepsilon_{11,T}}\right) or \left(\frac{\varepsilon_{11}}{\varepsilon_{11,C}}\right) or \left(\frac{\varepsilon_{22}}{\varepsilon_{22,T}}\right) or \left(\frac{\varepsilon_{22}}{\varepsilon_{22,C}}\right) or \left(\frac{\varepsilon_{12}}{\varepsilon_{12}^{f}}\right) \geq 1 \tag{3.11}$$

where $\varepsilon_{11,T}$, $\varepsilon_{11,C}$, $\varepsilon_{22,T}$, $\varepsilon_{22,C}$ and ε_{12}^{f} are ultimate tensile and compressive strains in fibre direction, ultimate tensile and compressive strains in transverse direction and ultimate in-plane shear strain respectively.

(B) Tsai – Hill criterion

The Tsai-Hill criterion, proposed by Tsai (1965) was derived from theories developed in the 1950's to predict the yield of metals (Hill, 1963). The Tsai-Hill criterion is quadratic in nature and cites that failure occurs if,

$$\left(\frac{\sigma_{11}}{S_{11}}\right)^2 - \left(\frac{\sigma_{11}\,\sigma_{22}}{S_{11}^{\ 2}}\right) + \left(\frac{\sigma_{22}}{S_{22}}\right)^2 + \left(\frac{\tau_{12}}{S_{12}}\right)^2 \geq 1 \tag{3.12}$$

As the failure mechanics of laminated composites very different from that of metals, the physical pertinence of this model is at best doubtful. The merits of the model lie in the fact that it is extremely simple and mathematically convenient.

(C) Tsai – Wu criterion

Tsai-Wu (1971) failure criterion is a phenomenological criterion, i.e. based on observation rather than derived from fundamental theories. It was derived in an attempt to predict the failure of a material by assessing its stress invariants. As such, a single polynomial expression is used to express the advent of failure. This criterion does not distinguish between failure modes. Similar single expression criteria have been proposed by Tsai (1965), Azzi and Tsai (1965)

and Hoffman (1967). The Tsai-Wu criterion remains one of the most widely used failure criterion for composite material.

The Tsai-Wu criterion for composite lamina is expressed as;

$$F_1\sigma_{11} + F_2\sigma_{22} + F_{11}\sigma_{11}^{\ 2} + F_{22}\sigma_{22}^{\ 2} + F_{66}\tau_{12}^{\ 2} + 2F_{12}\sigma_{11}\sigma_{22} \geq 1 \tag{3.13}$$

for

$$F_1 = \frac{1}{S_{11,T}} + \frac{1}{S_{11,C}};\ F_2 = \frac{1}{S_{22,T}} + \frac{1}{S_{22,C}};\ F_{11} = -\frac{1}{S_{11,T}} + \frac{1}{S_{11,C}};$$
$$F_{22} = -\frac{1}{S_{22,T}} + \frac{1}{S_{22,C}};\ F_{12} = f\sqrt{F_{11}F_{22}};\ F_{66} = \frac{1}{S_{12}^{\ 2}} \tag{3.14}$$

Here f is an interaction parameter of magnitude varying between 1 and -1 and is determined experimentally. This single mathematical expression for failure cannot be justified physically. Laminated composites fail according to different mechanisms depending on the orientation of loading. This class of criteria is nevertheless convenient, as only one criterion needs to be implemented, which explains why it has been programmed in numerous FEM codes.

(D) Hashin-Rotem criterion

The model proposed by Hashin and Rotem (1973) is one of the first widely used failure models proposed specifically for unidirectional composite lamina. While the maximum stress based failure criteria was fully decoupled, the Hashin-Rotem criteria are partially coupled, i.e. failure can involve normal and shear stresses.

This model distinguishes between fibre direction failure and matrix direction failure, in both tension and compression. Tensile fibre failure occurs if

$$\left(\frac{\sigma_{11}}{S_{11,T}}\right)^2 \geq 1 \tag{3.15}$$

Compressive failure occurs if

$$\left(\frac{\sigma_{11}}{S_{11,C}}\right)^2 \geq 1 \tag{3.16}$$

Tensile matrix failure occurs if

$$\left(\frac{\sigma_{22}}{S_{22,T}}\right)^2 + \left(\frac{\tau_{12}}{S_{12}}\right)^2 \geq 1 \tag{3.17}$$

and compressive matrix failure occurs if

$$\left(\frac{\sigma_{22}}{S_{22,C}}\right)^2 + \left(\frac{\tau_{12}}{S_{12}}\right)^2 \geq 1 \tag{3.18}$$

(E) Hashin's criterion

The Hashin criteria are a modification to the Hashin-Rotem criteria to account for the beneficial influence of compressive stresses on the matrix strength (Hashin, 1980). According to Hashin, the plane stress tensile fibre failure criterion now becomes

$$\left(\frac{\sigma_{11}}{S_{11,T}}\right)^2 + \left(\frac{\tau_{12}}{S_{12}}\right)^2 \geq 1 \tag{3.19}$$

The compressive fibre failure criterion remained unaltered

$$\left(\frac{\sigma_{11}}{S_{11,C}}\right)^2 \geq 1 \tag{3.20}$$

Tensile matrix failure is also unchanged and occurs if

$$\left(\frac{\sigma_{22}}{S_{22,T}}\right)^2 + \left(\frac{\tau_{12}}{S_{12}}\right)^2 \geq 1 \tag{3.21}$$

and compressive matrix failure incorporated an additional term, taking the form:

$$\left(\frac{\sigma_{22}}{2S_{23}}\right)^2+\left[\left(\frac{S_{22,C}}{2S_{23}}\right)^2-1\right]\left(\frac{\sigma_{22}}{S_{22,C}}\right)+\left(\frac{\tau_{12}}{S_{12}}\right)^2\geq 1 \tag{3.22}$$

Here, S_{23} is shear strength of a ply in plane 2-3.

(F) Puck's criterion

After a vigorous review of numerous UD failure prediction methods (Soden *et al.*, 2004), one of the concluding remarks of the WWFE was the better prediction capability of the Puck theory with the experimental results analysed, thus validating the physical approach taken by Puck. The first iteration of this model was proposed in 1969 by Puck and Schneider. Puck later modified his theory to incorporate ideas from Hashin's theory (Hashin, 1980) to identify the UD material fracture plane (i.e. angle in the direction 2-3 plane) based on a modified Mohr-Coulomb theory (Puck, 1992, 1996). The Puck models are part of a continuing attempt by German research groups to predict failure according to physically meaningful parameters. It is now said to be the standard for composite failure prediction of the German aviation industry (París, 2001). The Puck (1996) theory consists in five different criteria covering five identified, distinct failure mechanisms. These include fibre tensile failure, fibre compressive failure, and three failure modes in shear, namely, combined shear and tensile failure, pure shear failure and combined shear and compression.

According to Puck, tensile fibre failure occurs if;

$$\left(\frac{\sigma_{11}}{S_{11,T}}\right)\geq 1 \tag{3.23}$$

Compressive failure occurs if

$$\left(\frac{\sigma_{11}}{S_{11,C}}\right) \geq 1 \tag{3.24}$$

Tensile matrix failure occurs if

$$\sqrt{\left(\frac{\tau_{12}}{S_{12}}\right)^2 + \left(1 - p_{12}^{+}\frac{S_{22,T}}{S_{12}}\right)^2 \left(\frac{\sigma_{22}}{S_{22,T}}\right)^2} + p_{12}^{+}\frac{\sigma_{22}}{S_{12}} \geq 1 \tag{3.25}$$

Compressive matrix failure occurs if

$$\frac{1}{S_{12}}\sqrt{\tau_{12}^2 + \left(p_{12}^{-}\sigma_{22}\right)^2} + p_{12}^{-}\sigma_{22} \geq 1 \tag{3.26}$$

and

$$\left[\left(\frac{\tau_{12}}{2(1+p_{22}^{-})S_{12}}\right)^2 + \left(\frac{\sigma_{22}}{S_{22,C}}\right)^2\right]\frac{S_{12}}{-\sigma_{22}} \geq 1 \tag{3.27}$$

Here p_{12}^{+}, p_{12}^{-} and p_{22}^{-} are the Puck inclination parameters, which cannot be determined by simple experiments. The procedure to obtain these parameters is formulated in Puck *et al.* (2002).

The Puck's criterion (Puck, 1996) was motivated by the experimental observation of failure of CFRP and GFRP laminates in shear (Fig 3.6a). He observed that when the combination of transverse tensile stress (σ_{22}) and in-plane shear stress (τ_{12}) act simultaneously and their ratio (σ_{22}/τ_{12}) exceeds certain value, the fracture occurs at certain angle $\theta_{fp} \neq 0$ (Fig 3.6b). The fracture angle increases as the stress ratio ($\sigma_{22}^{c}/\tau_{12}$) increases and reaches to $\pm 54^0$ for pure transverse compressive stress. This phenomenon defines a completely smooth failure envelope in the shear stress-matrix stress space ($\tau_{12} - \sigma_{22}$ space), while still identifying the distinct failure mechanism termed as inter fibre failure (IFF) mechanisms as illustrated in Fig 3.7. These are discussed below.

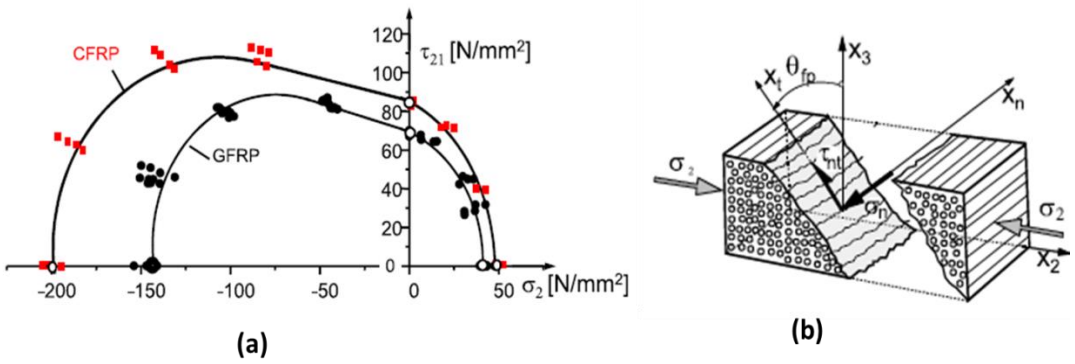

Figure 3.6 (a) Fracture limits for ($\sigma_{22} - \tau_{21}$) stress combinations (b) Schematic showing Puck's fracture plane concept

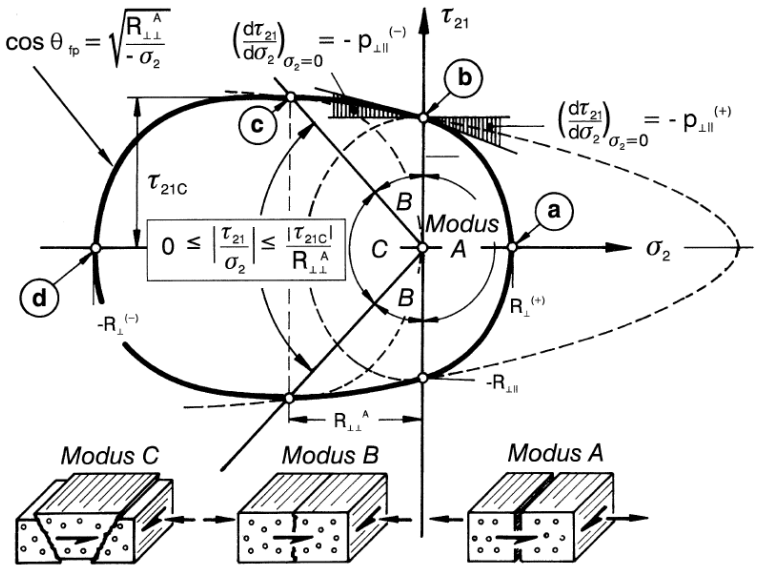

Figure 3.7 Puck failure envelope and failure modes in $\tau_{12} - \sigma_{22}$ space (adopted from Puck, 1996)

The analysis of the fracture behaviour by Puck works with the stresses on the action plane and not with the lamina stresses σ_2, σ_3, τ_{23}, τ_{31}, τ_{21}. This is a fundamental fact and leads to the approach to formulate fracture criteria using the stresses of the action plane.

Mode A: Transverse tensile stressing $\sigma_{\perp}^{t}$ or longitudinal shear stressing $\tau_{\perp\parallel}$ cause fracture acting either alone or in combination. In the case of a 2D-state of stress with σ_1, σ_2, τ_{21} the cracks run in thickness direction and thus in the

common action plane of the lamina stresses σ_2 and τ_{21}. The fracture surfaces are separated from each other due to the tensile stressing. This leads from a macroscopic point of view to a degradation of both the Young's modulus $E_\perp$ and the shear modulus $G_{\perp\parallel}$.

Mode B: Fracture is caused by longitudinal shear stressing $\tau\perp\parallel$. This fracture occurs on the action plane of the external shear stress τ_{21}. In contrast to Mode A, the transverse normal stressing $\sigma_{\perp c}$ which acts on the fracture plane simultaneously with $\tau_{\perp\parallel}$ is a compressive stressing. Thus the crack does not open and the fracture surfaces are pressed on each other. Consequently the degradation of stiffness due to IFF Mode B is much less significant than that due to IFF Mode A. An IFF Mode B occurs as long as the ratio of the compressive stress at fracture and the transverse compressive strength $|\sigma^c\perp fr/R^c\perp|$ is smaller than roughly 0.4. Here R denotes the resistance of the fracture plane against its fracture or simply, the strength.

Mode C: If the ratio of the compressive normal stressing at fracture and the transverse compressive strength $|\sigma^c{}_{\perp fr}/R^c\perp|$ exceeds roughly 0.4, the action plane of the external shear stress $\tau 21$ is no longer the fracture plane. Instead fracture occurs on a plane inclined by an angle $|\theta_{fp}| \neq 0°$ to the action plane of σ_2 and τ_{21}. The fracture angle $|\theta_{fp}|$ increases in the case of a plane state of stress (σ_1, σ_2, τ_{21}) from 0° at the threshold between Mode B and Mode C to roughly |54°| for pure transverse compression ($\tau_{21} = 0$). IFF Mode C implies the risk of delamination between the broken layer and adjacent layers.

These failure mechanisms of UD laminated composites are not expected to change abruptly as assumed in the maximum stress or maximum strain criteria. The physical reasoning of the Puck criteria therefore better matches the experimentally observed behaviour of laminated composites.

It should be noted that the Puck criteria are three dimensional and further descriptions can be found in Puck (1996), Puck and Schürmann (1998), Puck and Schürmann (2002). For simplification purposes, the equations presented in 3.23 to 3.27 are those of the equivalent in-plane criteria. In the 3D formulation,

the normal direction compression loading has the same effect on shear failure behaviour as does the transverse compression loading. The Puck's criteria can be expressed in a generalised form as below,

$$\left[\left(\frac{\sigma_{22}}{X_{2t}}\right)^2+\left(\frac{\sigma_{12}}{S_{12}}\right)^2+\left(\frac{\sigma_{23}}{S_{23}}\right)^2\right]+\sigma_{22}\left(\frac{1}{X_{2t}}+\frac{1}{X_{2c}}\right)=1\ . \tag{3.28}$$

$\sigma_{22}+\sigma_{33}>0,\ d_{mt}=1$ (matrix tensile failure)

$\sigma_{22}+\sigma_{33}<0,\ d_{mc}=1$ (matrix compressive failure)

Here, X_{2t}, X_{2c} and S_{12}, S_{12} are tensile and compressive strengths in transverse directions, and in-plane and out-of plane shear strengths respectively.

The Puck criteria are being used by many researchers (Dàvila and Camanho, 2003; Cuntze, 2004; Cuntze and Freund, 2004) as a basis for failure prediction improvement. The Puck criteria were used as a basis for NASA's attempt to improve composite failure criteria. NASA's Langley Research Centre criteria are named LaRC02 and are meant to improve the physical meaning of the parameters involved (Dàvila and Camanho, 2003). Furthermore, the LaRC02 criteria do not employ any fitting parameters (inclination parameters). The authors of the LaRC02 criteria acknowledge that Puck's failure envelope seems to better fit the loading cases presented in the WWFE, but believe that the use of the LaRC02 criteria is justified by its relative ease of characterization and its independence of non-physically parameters (parameters without physical significance, which cannot be measured directly).

3.7.2 Progressive failure models for lamina

Chang and Chang model originated in 1987 and was only applicable to study tensile and shear failure modes (Chang and Chang, 1987a, b). It is an extension of the model developed by Yamada and Sun (1978), which itself is based on the Hashin-Rotem model. Hashin-Rotem model was modified by Chang and Chang (1987 a, b) to include progressive degradation of material properties to predict laminate strength.

The degradation rules dictate behaviour of a laminate ply after failure allowing for a better representation of its residual strength. Plies are not removed altogether from a calculation. Instead upon failure, engineering constants were degraded distinctly depending on the type of failure. A material that fails in matrix tension (direction-2) is still capable of carrying loads in the fibre direction (direction-1).

For matrix tension, the failure criteria take the following form:

$$\left(\frac{\sigma_{22}}{S_{22,T}}\right)^2 + \left(\frac{\frac{\tau_{12}^2}{2G_{12}} + \frac{3}{4}\alpha\sigma_{12}^4}{\frac{S_{12}^2}{2G_{12}} + \frac{3}{4}\alpha S_{is}^4}\right) \geq 1 \tag{3.29}$$

Here S_{is} is the 'in-situ' shear strength measured from cross-ply laminate which differs from the lamina shear strength S_{12} and α is a non-linear shear parameter to be determined by fitting to experimentally obtained shear stress-strain curve.

Chang and Chang (1987a, b) defined 'in-situ' shear strength as the shear strength of UD ply obtained through rail-shear test (Whitney *et al.*, 1971).

Matrix compression failure occurs if

$$\left(\frac{\sigma_{22}}{2S_{is}}\right)^2 + \left[\left(\frac{S_{22,C}}{2S_{is}}\right)^2 - 1\right]\left(\frac{\sigma_{22}}{S_{22,C}}\right) + \left(\frac{\frac{\sigma_{12}^2}{2G_{12}} + \frac{3}{4}\alpha\sigma_{12}^4}{\frac{S_{is}^2}{2G_{12}} + \frac{3}{4}\alpha S_{is}^4}\right) \geq 1 \tag{3.30}$$

Fibre pull-out and breakage occurs if

$$\left(\frac{\sigma_{11}}{S_{11,T}}\right)^2 + \left(\frac{\frac{\tau_{12}^2}{2G_{12}} + \frac{3}{4}\alpha\sigma_{12}^4}{\frac{S_{12}^2}{2G_{12}} + \frac{3}{4}\alpha S_{12}^4}\right) \geq 1 \tag{3.31}$$

The material properties related to matrix failure E_{22}, G_{12} , ν_{12} and ν_{21} are reduced to zero instantaneously, while elastic modulus in fibre direction E_{11} remains unchanged. Thus the stiffness matrix takes the form:

$$\begin{pmatrix} \frac{E_{11}}{1-\nu_{12}\nu_{21}} & \frac{E_{22}}{1-\nu_{12}\nu_{21}} & 0 \\ \frac{E_{11}}{1-\nu_{12}\nu_{21}} & \frac{E_{22}}{1-\nu_{12}\nu_{21}} & 0 \\ 0 & 0 & G_{12} \end{pmatrix} \Rightarrow \begin{pmatrix} E_{11} & 0 & 0 \\ 0 & 0 & 0 \\ 0 & 0 & 0 \end{pmatrix} \tag{3.32}$$

However when fibre failure is achieved E_{22}, ν_{12} and ν_{21} are again reduced to zero though values of E_{11} and G_{12} are gradually reduced following degradation law based on the Weibull distribution function:

$$\begin{aligned} E_{11}^{d} &= E_{11} \exp\left[-\left(\frac{A}{A_0} \right)^{\beta} \right] \\ G_{12}^{d} &= G_{12} \exp\left[-\left(\frac{A}{A_0} \right)^{\beta} \right] \end{aligned} \tag{3.33}$$

These material degradation rules are based on a micro-mechanics approach for fibre bundle failure. The authors have not specifically stated how the parameters in Eq, (3.33) were determined from experiments, where (A/A_0) represented the ratio of damaged area as damage evolution took place to that at damage initiation, while β was defined to be Weibull parameter and was obtained through curve fitting and E_{11}^{d} and G_{12}^{d} are damaged elastic and shear moduli. Following its publication, this material model was implemented in numerous commercial finite element codes. LS-DYNA (Halquist, 2006) and other implementations vary extensively from the one discussed in the original articles by Chang and Chang (Chang and Chang, 1987a, b). In the LS-DYNA implementation, the moduli are linearly degraded to zero over 100 time steps for numerical stability reasons.

As a result, Chang and Chang introduced two more unitless, non-physical parameters through progressive degradation rules; however, the idea of degradation rule for brittle composite materials bridged the gap between failure criteria and the continuum damage models. These are discussed next.

3.8 Continuum Damage Model

The Continuum Damage Mechanics (CDM) approach focuses on the effect of the presence of micro-failures in the material rather than tracking crack propagation and initiation as done in the fracture mechanics approach

The application of CDM to composite failure analysis was popularized by Talreja (1985a, b). This theory describes the damage, which considered as the appearance of cracks, as a state variable that can be expressed as a scalar or tensor to quantify the isotropic or anisotropic damage. The presence of cracks in the material diminishes the relative area of material capable of withstanding loads, thereby increasing the stress in the undamaged material under a given strain. This leads to the concept of effective stress, which implies that a damaged material subjected to a load σ under a certain strain ε can be modelled as an equivalent undamaged material also subjected to the same strain ε under a modified load $\hat{\sigma}$ (Fig. 3.6) so that,

$$\{\hat{\sigma}\} = [M]\{\sigma\} \ , \tag{3.34}$$

where $[M]$ is effective damage tensor.

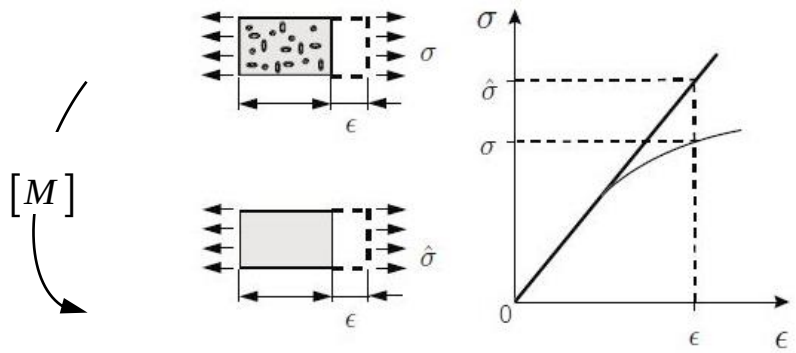

Figure 3.8 Hypothesis of effective stress (Simo and Ju, 1987)

Typical in-plane damage tensor takes the form

$$[M]=\begin{pmatrix} \frac{1}{1-d_{11}} & 0 & 0 \\ 0 & \frac{1}{1-d_{22}} & 0 \\ 0 & 0 & \frac{1}{1-d_{12}} \end{pmatrix}, \tag{3.35}$$

where d_{ij} are internal state variables that represent damage. Their magnitude varies from 0 to 1 and represent the reduction in the area that corresponds to the damage in the material such that

$$d_{ij}=\begin{cases} 0 & \text{... undamaged state} \\ 1 & \text{... fully - damaged state} \end{cases}, \tag{3.36}$$

The stress-strain relationship for a damaged material takes the form

$$\{\hat{\sigma}\}=[M]^{-1}[C]\{\varepsilon\}, \tag{3.37}$$

where $[C]$ is the stiffness tensor.

Continuum damage models can be derived from thermodynamics theories (Chaboche, 1988 a, b; Edlund and Volgers, 2004). This approach involves deriving the degradation rules from thermodynamics laws and using expressions of the Helmholtz free energy of the material (Kosevich *et al.*, 1984). Other simpler approach consists of directly defining the effective strain or stress to damage relation (Floyd, 2004). The latter approach is used by quite a few researchers; some of these are discussed next. This approach is used for the model proposed in Chapter 4.

3.8.1 Model of Ladevèze and Le Dantec

The CDM material model proposed by Ladevèze and Dantec (1992) has been used as a framework for the development of damage models by numerous authors since its publication. The material behaviour is dictated by damage evolution laws that affect the matrix and shear directions. These two damage modes represent matrix micro-cracking (direction-22) and matrix-fibre debonding (direction-12).

The lamina stress-strain relation is defined as,

$$\begin{bmatrix} \varepsilon_{11} \\ \varepsilon_{22} \\ \varepsilon_{12} \end{bmatrix} = \begin{pmatrix} \frac{\sigma_{11}}{E_{11}} & -\frac{\nu_{12}\sigma_{11}}{E_{11}} & 0 \\ -\frac{\nu_{21}\sigma_{22}}{E_{22}} & \frac{\sigma_{22}}{E_{22}(1-d_{22})} & 0 \\ 0 & 0 & \frac{\tau_{12}}{G_{12}(1-d_{12})} \end{pmatrix} . \tag{3.38}$$

Damage evolution law for matrix micro-cracking is expressed as,

$$d_{22} = \begin{cases} \dfrac{\left\langle Y_{22} - Y_{22}^{0} \right\rangle}{Y_{22}^{c}} & \text{... if } d_{22} < 1 \text{ and } Y_{12} < Y^{brittle} \\ 1 & \text{... fully-damaged state} \end{cases} . \tag{3.39}$$

Similarly damage evolution law for matrix-fibre debonding in shear plane is expressed as,

$$d_{12} = \begin{cases} \dfrac{\left\langle Y_{12} - Y_{12}^{0} \right\rangle}{Y_{12}^{c}} & \text{... if } d_{12} < 1 \text{ and } Y_{12} < Y^{brittle} \\ 1 & \text{... fully-damaged state} \end{cases} . \tag{3.40}$$

Here Y_{22} and Y_{12} are measured effective strains, Y_{22}^{0} and Y_{12}^{0} are strains at the initiation of damage, while Y_{22}^{c} and Y_{12}^{c} are the variables for strains at damage

saturation and $Y_{brittle}$ is an effective strain magnitude indicating brittle behaviour and has to be obtained experimentally.

Contrary to the Chang and Chang model (1987 a, b), this CDM material model allows for gradual degradation of material properties in direction-22 and direction-12. It has a thermodynamic basis to dictate the damage evolution rate. This material model also allows elastic unloading past the strain at peak stress. Variations of this model are available in the commercial explicit finite element code PAM-CRASH (ESI, 2004).

3.8.2 Model of Matzenmiller-Lubliner-Taylor (MLT)

Similar to Ladevèze and Dantec model, the Matzenmiller-Lubliner-Taylor (Matzenmiller *et al.*, 1995), or MLT model, is also the basis of numerous material model developments. In this material model, the stress-strain curve of the material takes the form of a Weibull function, allowing for strain softening of the damaged material. Typical stress-strain curves obtained with this material model are shown in Fig.3.7. Damage affects the warp, weft and shear directions. The stress-strain relationship takes the form,

$$\begin{bmatrix} \varepsilon_{11} \\ \varepsilon_{22} \\ \varepsilon_{12} \end{bmatrix} = \begin{pmatrix} \dfrac{\sigma_{11}}{E_{11}(1-d_{11})} & -\dfrac{\nu_{12}\sigma_{11}}{E_{11}} & 0 \\ -\dfrac{\nu_{21}\sigma_{22}}{E_{22}} & \dfrac{\sigma_{22}}{E_{22}(1-d_{22})} & 0 \\ 0 & 0 & \dfrac{\tau_{12}}{G_{12}(1-d_{12})} \end{pmatrix} . \tag{3.41}$$

Damage evolution law is expressed as,

$$d = 1\text{- } \exp\left[-\frac{1}{me}\left(\frac{\varepsilon}{\varepsilon_f} \right)^m \right] , \tag{3.42}$$

where ε_f is the nominal failure strain, m is a parameter to be obtained from experiments (Fig. 3.9) and e is the natural logarithmic base.

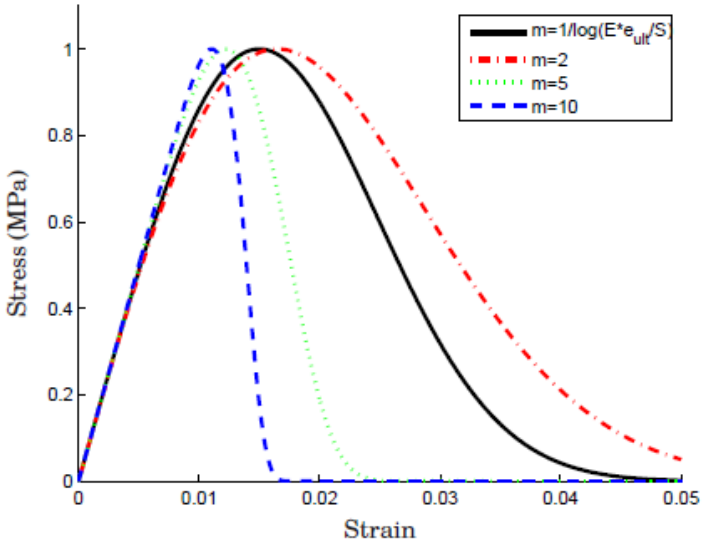

Figure 3.9 Typical stress-strain curves for the MLT model

The shape of Weibull function in tension and compression is governed by internal parameters (m) that dictate damage and post failure behaviour of the material. These parameters can be calculated so that the stress-strain curve peak matches the measured strain at maximum stress using equation 3.43.

$$m = \frac{1}{\ln\left(\frac{E}{S}\varepsilon\big|_{\sigma_{\max}}\right)} \quad . \tag{3.43}$$

Following equation (3.42), it can be seen that the strain softening behaviour is completely dictated by the elastic parameters: E is the material's elastic modulus, $\varepsilon\big|_{\sigma_{\max}}$ is the strain level at threshold (peak) stress (peak stress before initiation of damage) and S is its strength. When complete failure of the material is encountered, this strain softening behaviour leads to damage localization and mesh-size dependence of the solution.

Williams and Vaziri (2001) showed that parameter m plays a major role in the accuracy of non-penetrating normal impact simulation. Modelling of post-failure (strain softening) behaviour is found to be essential in the energy absorption of

laminated composites under impact. Furthermore, strain-rate dependencies were highlighted by the use of the MLT material model, showing that higher impact velocities require higher m values for accurate predictions since the material shows more brittle behaviour at higher strain rates. This strain-rate dependency of the strain softening behaviour of the material was also observed by Randles and Nemes (1992) and Nemes and Speciel (1996).

3.8.3 Multi-continuum theory (MCT)

Numerous attempts have been made to model the behaviour of woven composites using CDM combined with a multi-continuum approach (Barbero *et al.*, 2006; Hochard *et al.*, 2006; Thollon and Hochard, 2009; Key *et al.*, 2007). The MCT approach considers modelling individual fibres and the matrix, for UD or woven composites. The idea behind this lies in the fact that the elasticity and strength of the material modelled in this manner can be obtained by simply knowing the properties of these constituents.

The elastic properties of the composite can be calculated for a repetitive unit cell, using Classical Laminated Theory (CLT) and uniform stress and uniform strain analogies. Failure criteria and degradation rules are then applied to both fibre and matrix to obtain the failure envelope of the equivalent homogeneous material.

This approach is also sometimes referred as “unit cell-decomposition method" (Zheng *et al.*, 2003), "two-phase", "three-phase" or "multi-phase" constitutive model (Abdel *et al.*, 2000) or "multi-scale" constitutive model (Lua *et al.*, 2006). In most cases, this approach neglects the fibre-sizing (coating) that is especially formulated to ensure a proper bond between fibre and matrix. Since exact material behaviour cannot be obtained without the knowledge of the sizing used on specific fibres, composite coupon tests are required to determine the sizing properties. This requirement negates the benefit of this approach. Moreover, in most cases, these approaches do not provide information about the post-failure behaviour and thus are not applicable to perforating impact simulations.

3.9 Summary

A background and the basic notion behind FE modelling of composite laminates in 2D based on shell theory and 3D elasticity theory were described. Modelling of the damage mechanisms of these materials at various length scales under static and dynamic conditions were also described. The difference between implicit and explicit FE solvers is presented in terms of their approach to obtain the numerical solution.

As discussed in Chapter 2, discrete damage modes are observed at varying length scales in composites due to their heterogeneity and anisotropy. Regarding this, from a computational point of view; a systematic, efficient and reliable approach needs to be established that provides a reasonable trade-off between the computational resources needed to model these physical events properly and computational accuracy desired. This justifies the adoption of a macro or meso-scale modelling approach used in this study.

The basic principles behind various damage modelling techniques such as strength-based criteria, VCCT, CZMs and some latest numerical approaches were reviewed and their advantages and disadvantages were stated. It is evident that there is no definitive failure strength based criterion for composites, though; damage mechanics-based models have shown significant success in modelling structural degradation in laminated composites.

Moreover, it can be seen that an extensive amount of work has been done regarding the modelling and analysis of damage in laminated composites, where the underlying failure modes were modelled using CZM, CDM and/or combination of both. Among these techniques, CZM seems to be promising as it combines both strength and toughness-based fracture criteria to simulate various damage and fracture modes. Further, these damage modes are strongly interacting due to heterogeneity of composites, which are analysed in the context of CDM-based models. On the other hand, due to the inherent homogenisation in the CDM models, they cannot take into account coupling of various damage mechanisms explicitly, though it can be incorporated into the

mathematical formulation of damage and failure of such composites that often needs to be implemented into FE codes through user-defined subroutines. In general, the solutions obtained using both CZM and CDM based models are strongly mesh-dependent and require extensive mesh study, though, one of the biggest disadvantages of CZM approach lies in the fact that, here, in order to model fracture , its location must be known a priori. This is the motivation behind the development of CDM based criteria that can provide a valuable tool to assess damage and failure in laminated composites both qualitatively and quantitatively.

A few CDM based criteria applicable to model highly dynamic phenomena such as impact and blast response of laminated composites are discussed to examine their advantages and shortcomings in the second part of this chapter. They range from simple, linear elastic form to complex laws involving progressive, strain-rate dependent, bi-linear degradation rules based on orthotropic equivalent strain formulations with delamination capabilities and localisation mitigation schemes. For comparison of the material model's relative complexity, the number of material parameters required by each investigated material model is shown in Table 3.1.

Some of the failure criteria, while being very popular, do not accurately represent the physics behind composite's failure. In addition, most failure theories are formulated for UD composites and do not apply sufficiently well to laminated fabrics. As previously mentioned, failure of laminated composite materials is far from being completely understood. The WWFE (Hinton and Soden, 2004) has allowed for an evaluation of the best available techniques for unidirectional CFRP failure prediction. A similar enterprise would be greatly beneficial to the understanding of woven composite failure mechanisms.

To model impact and blast response of laminated composite under impact accurately and efficiently, material models require:

- Representation of all possible failure modes under impact and blast
- Progressive-damage of constituents

- Strain-rate dependent behaviour under high velocity loading conditions
- Mesh-size influence mitigation scheme
- Relatively simple characterisation

Table 3.1 Assessment of reviewed damage models for laminated composites according to the input parameters required under plane stress assumption

Material model	Total number of parameters	No. of non-physical parameters
Maximum Stress and Maximum Strain	4 elastic + 5 failure	0
Tsai-Hill	4 elastic + 5 failure	0
Tsai-Wu	4 elastic + 6 failure	1
Hashin-Rotem	4 elastic + 5 failure	0
Hashin	4 elastic + 6 failure	0
Puck	4 elastic + 8 failure	3
Chang and Chang	4 elastic + 9 failure	2
Ladeveze and Le Dantec	4 elastic + 5 failure	0
Matzenmiller-Lubliner-Taylor	4 elastic + 10 failure	5

A generally accepted theory has not yet emerged that considers all of the above stated requirements to simulate the mechanical behaviour of CFRP composites under impact and blast. The material models presented in this chapter lack features necessary to model the mechanical response of laminated composites

under high-rate loading. E.g., it was observed that most of the above discussed numerical criteria (MLT, Chang and Chang, Tsai- Wu, Tsai-Hill) were designed to model the in-plane behaviour of laminated composites, and damage of plies arising thereby. However upon the high-velocity impact, composites may undergo high compressive stresses in the thickness-direction; thus it is imperative to consider the through-thickness stress components and the underlying damage mechanisms such as delamination. Along with this at high load-rates, the laminated composites often exhibit strain-hardening due to the presence of viscous matrix material, which was not accounted for in these models. These effects may be explicitly modelled using MCT theory, though in most cases, this approach do not provide information about the post-failure behaviour of materials and thus may not be applicable to impact simulations involving material degradation due to penetration. Finally, many material models (refer Table 3.1), requires the use of non-physical material parameters (fitting/calibration parameters) that may not be obtained easily through the experiments.

Furthermore, it is difficult to address these specifications with a fairly simple, yet reasonably accurate CDM based material model. The prime attention needs to be paid so that the added accuracy would not overshadow the usability.

In this respect, the next chapter introduces an improved material model that combines the advantages of Hashin's (1980) and Puck's (1982) criteria to assess the mechanical behaviour of laminated composites under ballistic-impact and blast events. This model attempts to fulfil the requirements identified in this chapter. An effort is made to retain a level of simplicity and usability in the formulation of this model.

CHAPTER 4

A CONSTITUTIVE MATERIAL MODEL

4.1 Introduction

Chapter 3 highlighted some of the shortcomings associated with the existing material models, especially those based on the CDM approach. These include:

- A requirement of an overwhelming number of parameters for certain models;
- Difficulties in characterisation of parameters required in simulations;
- A lack of physical significance of certain parameters used for simulations;
- Unrealistic instantaneous failure of lamina (e.g., a brittle behaviour of certain models does not account correctly for a dissipated energy);
- Mesh-sensitivity issues due to strain softening;
- No account for a strain-rate effect.

The material model should be relatively easy to use and contain parameters that can be reasonably easily obtained experimentally and are of physical significance. It should be noted that there is no specific CDM based numerical criteria available to model impact/blast like response of laminated composite materials in the literature, though recently (Abrate, 2011; Thollon and Hochard, 2009; Shi *et al.*, 2012) a trend is seen that consists of modifying the existing numerical criteria (refer Sections 3.7 and 3.8) to suit their application for various loading scenarios. Thus to improve on the previously described lamina failure laws, the constitutive law presented in this chapter is designed with the following aim:

To fulfil this aim, the following objectives were recognised.

- A limited number of parameters should be required;

- Only physically meaningful parameters should be used;
- Mesh-size dependence should be minimal;
- The model should be capable of modelling full degradation and element erosion to allow for perforation of the target;
- The model should be able to take into account the strain-rate response at high loading rates.

This lamina model's main objective is to model high-velocity impact and blast responses of composite structures reasonably accurately. A prediction of the mechanical response, the extent of damage and the energy-absorption capacity of PMCs are of particular interest. It should be noted that this material model is initially designed considering the mechanical behaviour of a UD composite ply. This is later extended for the case of a woven fabric-reinforced composite ply using the equivalence of its continuum scale behaviour with the former. The details regarding its constitutive relationship, damage-initiation laws, damage evolution and element erosion are discussed next.

4.2 Elastic stress-strain relationship

Here, the elastic stress-strain relationship for a UD composite ply is expressed assuming the orthotropic damaged elasticity response. Its constitutive behaviour before damage is expressed using a generalised Hooke's law in the tensorial form as

$$\{\sigma\} = C\{\varepsilon\} \ . \tag{4.1}$$

In matrix notation, Eq. (4.1) can be written as

$$\begin{bmatrix} \sigma_{11} \\ \sigma_{22} \\ \sigma_{33} \\ \tau_{12} \\ \tau_{23} \\ \tau_{13} \end{bmatrix} = \begin{bmatrix} C_{11} & C_{12} & C_{13} & 0 & 0 & 0 \\ C_{12} & C_{22} & C_{23} & 0 & 0 & 0 \\ C_{13} & C_{23} & C_{33} & 0 & 0 & 0 \\ 0 & 0 & 0 & 2G_{12} & 0 & 0 \\ 0 & 0 & 0 & 0 & 2G_{23} & 0 \\ 0 & 0 & 0 & 0 & 0 & 2G_{13} \end{bmatrix} \begin{bmatrix} \varepsilon_{11} \\ \varepsilon_{22} \\ \varepsilon_{33} \\ \gamma_{12} \\ \gamma_{23} \\ \gamma_{13} \end{bmatrix} . \tag{4.2}$$

Here, C_{ijkl} is the fourth-order stiffness tensor and σ_{ij} and ε_{kl} are the second-order stress and strain tensors, respectively.

It should be noted that the material model presented in this chapter is based on the CDM approach discussed in Section 3.8. According to this approach, the effective stress $\bar{\sigma}$ in the equivalent homogeneous material is related to the stress in the damaged material through a damage tensor $\mathbf{d}$ such that

$$\{\bar{\sigma}\} = [\mathbf{d}]\{\sigma\} \ . \tag{4.3}$$

Thus substituting Eq. (4.1) in (4.3), the stress tensor can be expressed as

$$\{\sigma\} = [\mathbf{d}]^{-1} C^0 \{\varepsilon\} = C(\mathbf{d})\{\varepsilon\} \ . \tag{4.4}$$

The following damage variables are introduced to model failure modes in matrix and fibre: d_{ft}, d_{fc}, d_{mt}, and d_{mc} . These represent fibre failure modes in tension and compression; and matrix failure modes in tension and compression respectively. The global fibre and matrix failure modes d_f and d_m are thus expressed as:

$$\begin{aligned} d_f &= (1-d_{ft})(1-d_{fc}), \\ d_m &= (1-d_{mt})(1-d_{mc}). \end{aligned} \tag{4.5}$$

Another damage variable d_s is introduced to account for the stiffness degradation due to non-linear behaviour of matrix in shear failure.

Thus, undamaged elastic constants $\mathbf{C_0}$ and the damage variables d_f and d_m are substituted in Eq. (4.4) to calculate elastic constants $\mathbf{C(d)}$ of a damaged material. They are listed below:

$$
\begin{aligned}
C_{11} &= (1-d_f)\ C_{11}^0\ ; \\
C_{22} &= (1-d_f)\ (1-d_m)\ C_{22}^0\ ; \\
C_{33} &= (1-d_f)\ (1-d_m)\ C_{33}^0\ ; \\
C_{12} &= (1-d_f)\ (1-d_m)\ C_{12}^0\ ; \\
C_{23} &= (1-d_f)\ (1-d_m)\ C_{23}^0\ ; \\
C_{13} &= (1-d_f)\ (1-d_m)\ C_{13}^0; \\
G_{12} &= (1-d_s)\ 2G_{12}^0\ ; \\
G_{23} &= (1-d_s)\ 2G_{23}^0\ ; \\
G_{13} &= (1-d_s)\ 2G_{13}^0\ .
\end{aligned}
\tag{4.6}
$$

These damage variables d_f, d_m *and* d_s are linked to the damage-initiation in fibre and matrix such that their magnitudes vary between 0 and 1. When the material is intact, their magnitude is 0 and 1 when damage is initiated under given loading conditions. This is discussed next.

Figure 4.1 illustrates a generic loading diagram including damage and unloading. Damage occurs along path OMA, with unloading and compression from A to B. Reloading is performed along the same path from B to A. Further loading past point A causes additional damage. Complete damage is attained at point C.

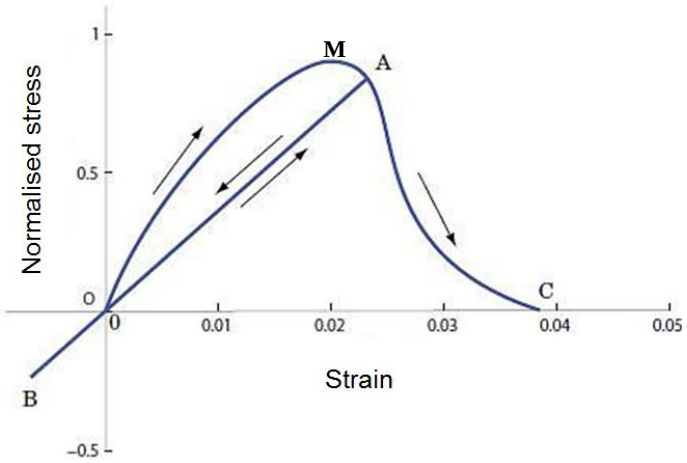

Figure 4.1 A generic loading path with damage

This material model does not account for residual strain due to incomplete crack closure or permanent deformations similar to plasticity in metals since it is mainly intended to model response of quasi-brittle composite laminates.

4.3 Strain-rate sensitivity

Numerous studies have been performed to document the effect of the loading rate on the response of laminated CFRP composites (Li and Lambros, 2000; Hsiao *et al.*, 1999; Daniel *et al.*, 2011). While the test methods and result interpretation vary greatly, researchers have in numerous cases found evidence of increased stiffness and increased strength with higher strain rates.

Numerical simulations of these strain rate effects require complex loading-unloading laws. The parameters that are affected by strain-rate need to be determined for each material system studied. Strain-rate influence on elastic moduli and strengths needs to be defined in order to accurately account for high strain-rate response of laminated composite materials. It should be noted that the strain-rate effects for carbon/epoxy like systems, where carbon fibres are brittle and show no strain-rate dependence (Li and Lambros, 2000; Hsiao *et al.*, 1999; Daniel *et al.*, 2011), the strain-hardening at higher loading rates is entirely

due to epoxy matrix; while in glass/epoxy like systems both glass fibres and epoxy matrix may contribute towards this.

Here the strain-rate effects in the elastic and shear moduli are defined by Eq. (4.7).

$$E(\dot{\varepsilon}) = E(\dot{\varepsilon}_0)\left[m_e \log\left(\frac{\dot{\varepsilon}}{\dot{\varepsilon}_0}\right)+1\right], \quad \dot{\varepsilon} = \{\dot{\varepsilon}_{ij}\} \text{ and } E(\dot{\varepsilon}) = \{E_{ii}\, G_{ij}\} \tag{4.7}$$

where $E(\dot{\varepsilon})$ is the elastic modulus at a specific strain-rate, $E(\dot{\varepsilon}_0)$ is elastic modulus at the reference strain-rate $\dot{\varepsilon}_0$, m_e is a material parameter obtained by fitting a curve to experimentally obtained data. E_{ii} are elastic moduli in all three directions ($i = 1, 2, 3$), while G_{ij} are shear moduli ($ij = 12, 23, 13$) in three planes. The effects of strain-rate on the ply strength are discussed in following sections where initiation of different damage modes is considered. It should be noted that there exists no clear conscience in the literature about the effect of strain-rates on the fracture energy (Koerber *et al.*, 2010; Daniel *et al.*, 2011). ; thus in this work it is not considered.

4.4 Damage-initiation

Modelling of composites and their damage at a laminate level typically requires input of several parameters, including homogenised ply properties, interply strength and information about the laminate lay-up. Here, a layer-by-layer modelling strategy is adopted to capture failure in each ply. This offers several advantages. First, full 3D stress states can be analysed. Typically, FE models of composite deformation involve the use of 2D shell elements to represent composite plies, which do not allow for accurate representation of stress through the composite thickness. Secondly, intraply and interply damage can be

introduced discretely along with phenomenological models that account for the complex interaction between them.

In 1973, Hashin, based on his experimental observations of failure of tensile specimens, proposed a criterion that recognised two different failure modes in a unidirectional composite ply, one related to fibre failure and the other to matrix failure. This criterion assumed a quadratic interaction between the tractions acting on the plane of failure. In 1980, he introduced fibre and matrix failure criteria that distinguished between tension and compression failure modes. Given the difficulty in obtaining the plane of fracture for the matrix-compression mode, Hashin employed a quadratic interaction between the stress invariants. Such derivation was based on logical reasoning rather than micromechanics. These two failure criteria proposed by Hashin in 1973 and 1980 are summarised in Table 4.1.

Table 4.1. Hashin's failure criteria with plane stress assumption (Hashin 1973, 1980)

Year	Failure criteria
1973	$F=\left(\frac{\sigma_T}{Y}\right)^2+\left(\frac{\tau}{S}\right)^2$
1980	For matrix $F_{mt}=\left(\frac{\sigma_{22}}{S_{22}}\right)^2+\left(\frac{\tau_{12}}{S_{12}}\right)^2$ $F_{mc}=\left(\frac{\sigma_{22}}{2S_{22}}\right)^2+\left[\left(\frac{S_{22}}{2S_{12}}\right)-1\right]^2$
	For fibre $F_{ft}=\left(\frac{\sigma_{11}}{S_{11}}\right)^2+\left(\frac{\tau_{12}}{S_{12}}\right)^2$ $F_{fc}=-\left(\frac{\sigma_{11}}{S_{11}}\right)$

In table 4.1., F_{mt}, F_{mc}, F_{ft} and F_{fc} refer to failure modes of matrix in tension and compression and tension; and those of fibre in tension and compression respectively.

Numerous studies (Hinton and Soden, 1998; Dávila *et al.*, 2003; Soutis *et al.* 2012) conducted over the past decade indicate that the stress interactions proposed by Hashin do not always fit the experimental results, especially in the case of matrix compression. It is well known, for instance, that moderate transverse compression ($\sigma_{22} < 0$) increases the apparent shear strength of a ply, which is not predicted by the Hashin's criterion. In addition, the Hashin's fibre-compression criterion does not account for the effects of in-plane shear, which significantly reduces the effective compressive strength of a ply, hence over-predicting the failure envelope. Several researchers have proposed modifications to Hashin's criteria to improve their predictive capabilities (Hinton and Soden, 1998, Dandekar *et al.*, 2012).

Moreover, three-dimensional effects are predominant at the ply edges and limit applicability of the planar approach. This statement is true in case of Hashin's 2D damage model for modelling progressive damage in long-fibre composites, available in the ABAQUS/Explicit material model library. Hence, modification in this material model is inevitable to include 3D effects in order to capture accurately through-thickness stresses in case of thick FRP laminates.

In this regard, a Puck's criterion (Puck and Schürmann, 1998) was shown to provide a reasonably good estimate of damage in epoxy matrix under compressive mode both qualitatively and quantitatively (refer Section 3.7). Thus, in this chapter, a material model offering a combination of Hashin's (1980) and Puck's failure criteria (Puck and Schürmann, 1998) is proposed to implement the advantages of both. The Hashin's criteria are employed to estimate damage in carbon fibres while damage in epoxy matrix is modelled using the Puck's criteria. The empirical forms of these criteria are discussed in Section 3.7.

In order to model damage-initiation in the impact - and blast - like events, involving large deformations and high strain gradients, the rate-dependent

behaviour of a polymer matrix is considered in this study. Fibre and matrix failures are described with two damage variables each. Interaction between these damage modes is also considered.

It should be noted that this material model does not account for the damage-initiation and propagation at the interface of the neighbouring plies, which is modelled explicitly using a concept of cohesive-zone element (CZE) (refer Section 3.6).

4.4.1 Fibre compressive failure

Longitudinal compressive failure of UD composites is driven by shear mechanisms in an intricate way. A first crack may be started by shear fracture of the fibres followed by rotation of the fibres and in-plane shearing of the matrix at the crack tip, which in turn promotes kink-band development (Gutkin *et al.*, 2010).

Thus, compressive-failure envelopes for combined compression/shear are strongly dependent on the material investigated, e.g. in Fig. 4.2, a selection of experimental results available in the literature is shown (Jelf and Fleck, 1994; Soden *et al.*, 2002; Michaeli *et al.*, 2009). The scatter of this data was related to the defects in tested specimens.

As discussed in Chapter 3, stress-interaction failure criteria for composites have been developed from polynomials based on stress-tensor expansions, a technique originally proposed for failure analysis of metals (Gol'demblat and Kopnov, 1968) by including anisotropic strength parameters (Tsai and Wu, 1971). These classes of criteria can be also expressed in terms of stress invariants and assume a perfectly aligned fibre arrangement implicitly (Hashin, 1980).

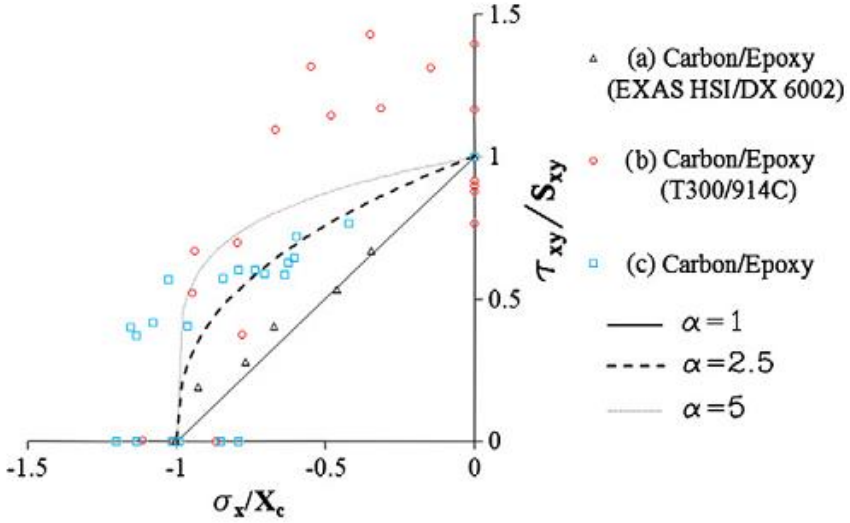

Figure 4.2 Failure envelopes for combined longitudinal/in-plane shear showing their variability according to different composite material systems (a) Jelf and Fleck (1994) (b) Soden *et al.* (2002) (c) Michaeli *et al.* (2009) : Quasi-static loading conditions

A large scatter in the available strength data can have various reasons. An explanation of the scatter would be the present failure mode. As explained in Chapter 3, specimens fail due to various failure modes in compression. Many of the observed failure modes are not representative for the material, but an artefact of the specimen geometry. Assessment of the results thus requires an accurate observation of the failure mode. This poses no difficulty in quasi-static tests (as test can be interrupted) though it is significantly more difficult in high-rate experiments. The scatter in the Fig. 4.3 can be explained on this basis.

Different carbon/epoxy composite systems will show different rate dependent behaviour. However, a certain similar pattern can be observed. Initially, the material properties do not seem to change dramatically. At a certain strain rate that can be different for each epoxy resin, the moderate almost linear increase of properties switches to an exponential increase.

A few phenomenological expressions have been proposed for predicting pure longitudinal compressive strength from shear strength (related by the interaction

parameter α , and assume an initial fibre misalignment (Argon, 1972; Budiansky, 1983; Dávila *et al.*., 2005; Pinho *et al.*, 2006), though they require a non-physical material parameter. The later has to be identified from curve-fitting of failure envelopes for a particular composite material and hence needs extensive experimental data for its validation. Thus, to avoid complexity, initial fibre misalignment is not considered in this study.

When considering the shear nature of compressive failure mechanisms, it is not a surprise that most of the published data in the literature indicates that the longitudinal compressive strength of UD composites is greatly affected by the strain-rate (Li and Lambros, 1999; Woldesenbet and Vinson, 1999; Woldesenbet *et al.*1999; Hsiao and Daniel, 1998; Pae and Karlson, 1998; Hsiao *et al.*, 1998; Koerber and Camanho, 2011). It was also seen that the shear yield strength increased more with the strain-rate than does the shear failure strength (Koerber *et al.*, 2012).

In order to incorporate such rate-sensitive behaviour of a laminated composite in a material model, a scaling parameter K is defined:

$$K = \frac{S_{12}^{dyn}(\dot{\gamma}_{12})}{S_{12}^{qs}} = \frac{S_{23}^{dyn}(\dot{\gamma}_{13})}{S_{13}^{qs}}. \tag{4.8}$$

Here, $S_{12}^{dyn}(\dot{\gamma}_{12})$ and $S_{23}^{dyn}(\dot{\gamma}_{23})$ are in-plane and out-of-plane shear strengths of a ply in dynamic loading condition at a given strain rate and S_{12}^{qs} and S_{23}^{qs} are its shear strengths in quasi-static loading condition. Thus dynamic longitudinal compressive strength X_{1C}^{dyn} of UD lamina is expressed as,

$$X_{1c}^{dyn} = \mathrm{K}\left(\dot{\varepsilon}\right)\mathrm{X}_{qs} \ , \tag{4.9}$$

where X_{qs} is quasi-static strength of a lamina, $\dot{\varepsilon}$ is a strain-rate and K is a scaling parameter for strength and derived from fitting shear strength *vs*. shear strain data, i.e.

Thus, the following criterion is proposed to model fibre compressive failure:

$$\left(\frac{\sigma_{11}}{X_{1c}^{dyn}}\right)+\left(\frac{\tau_{12}}{S_{12}^{dyn}}\right)+\left(\frac{\tau_{13}}{S_{13}^{dyn}}\right)\geq 1,\quad df_{c}=1; \tag{4.10}$$

Substituting Eq. (4.10) in Eq. (4.11), the final form appears as follows:

$$\left(\frac{\sigma_{11}}{K(\dot{\varepsilon})X_{1c}^{qs}}\right)+\left(\frac{\tau_{12}}{K(\dot{\gamma})S_{12}^{qs}}\right)+\left(\frac{\tau_{13}}{K(\dot{\gamma})S_{13}^{qs}}\right)\geq 1,\quad d_{fc}=1; \tag{4.11}$$

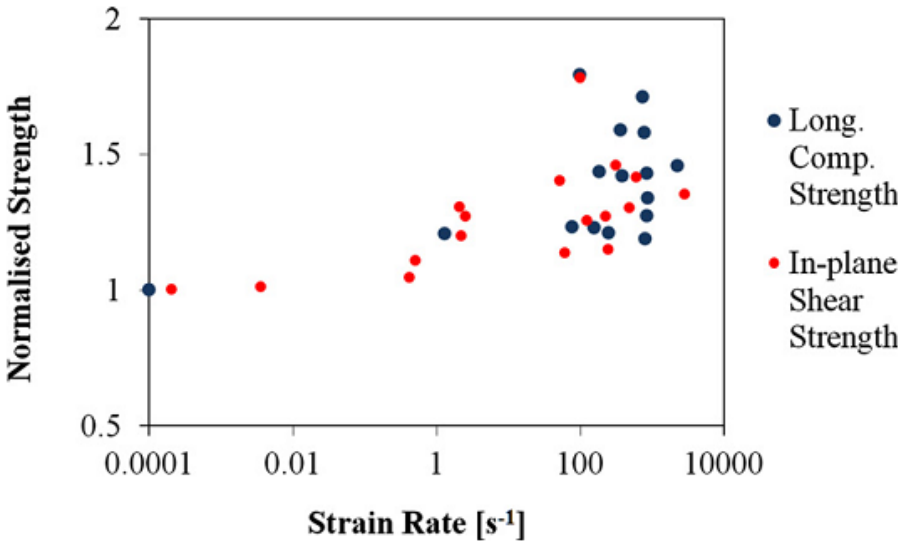

Figure 4.3 Normalised longitudinal compressive and in-plane shear strength *vs*. strain rate from various experiments in literature as collected in Wiegand (2008)

The typical normalised values of both longitudinal compressive strength and in-plane shear strength for various UD carbon/polymer composites are plotted versus strain rate in Fig. 4.3. The systems of composite materials employed in this study are different from the one used in this example. Thus it should be noted that this example is presented only to showcase the strain-rate induced variation of the shear dominated strength properties of laminated composites and the difficulties related to their accurate measurement.

These values were taken from Wiegand (2008), in which experimental results from various works published in the literature were collected.

4.4.2 Fibre tensile failure mode

Here, fibre tensile failure is defined as a function of tensile strength of lamina along the fibre direction as well as shear strength in transverse directions (in and out-of plane). The empirical relation is expressed in the following form:

$$\left(\frac{\sigma_{11}}{X_{1t}}\right)^2+\left(\frac{\sigma_{12}}{S_{12}}\right)^2+\left(\frac{\sigma_{13}}{S_{13}}\right)^2 \geq 1, \quad d_{ft}=1\,; \tag{4.12}$$

where X_{1t} is the tensile strength of the composite in the fibre direction identified with the index X. Here, X_{1t} is assumed equal to its quasi-static magnitude since fibres show negligible or no strain-rate dependence at high loading rates (Weeks and Sun, 1998; Barre *et al.*, 1996; Harding and Welsh, 1983; Zhou *et al.*, 2001).

4.4.3 Matrix failure

The phenomenological matrix-failure criteria for 3D QS failure analysis of UD composites were previously formulated by Puck and Schürmann (1998) (refer Section 3.7). These criteria forms a basis of the research work presented in this and in the next section. In these sections, the applicability of the tensile and compressive failure criteria proposed by Puck and Schürmann (1998) for quasi-static loading conditions is extended to dynamic loading conditions.

The polymer matrix material in a CFRP composite demonstrates strain-rate-sensitivity at high strain rates (~10^3 s^{-1}), which are typical for high-velocity impact- and blast- like events. This effect becomes significant, particularly in transverse directions, where the polymer matrix is a primary load-bearing member (Ochola *et al.*, 2004; Raimondo *et al.*, 2012; Koerber *et al.*, 2010; Daniel *et al.*, 2011). Many test methods have been developed to facilitate the

dynamic characterisation of composite materials at high deformation rates. Previous test studies highlighted an increase in stiffness and strength of composites with the increasing strain rate in the matrix-dominated regions (Gómez *et al.*, 2005; Ochola *et al.*, 2004; Raimondo *et al.*, 2012; Koerber *et al.*, 2010). In some cases, explicit empirical relations were formulated to derive such material properties for corresponding strain-rates (Koerber *et al.*, 2010; Daniel *et al.*, 2011).

A similar approach as employed in modelling fibre compressive failure is adopted here to account for strain-rate sensitivity. Moreover, it should be noted that tensile strength of a pure polymer resin is strain-rate dependent (Gerlach *et al.*, 2008). However, transverse tensile strength is dominated by strength of a weaker fibre/matrix interface, which would greatly depend on the material system and fibre packing arrangement and not only on the matrix properties. The conservative approach adopted here accounts for the load-rate sensitivity of the polymer matrix.

The following criteria are proposed to model failure in the matrix material in compression and tension.

$$\left[\left(\frac{\sigma_{22}}{K\,X_{2t}^{qs}(\dot{\varepsilon})}\right)^2+\left(\frac{\sigma_{12}}{K\,S_{12}^{qs}(\dot{\gamma})}\right)^2+\left(\frac{\sigma_{23}}{K\,S_{23}^{qs}(\dot{\gamma})}\right)^2\right]+\sigma_{22}\left(\frac{1}{K\,X_{2t}^{qs}(\dot{\varepsilon})}+\frac{1}{K\,X_{2c}^{qs}(\dot{\varepsilon})}\right)=1 \tag{4.13}$$

$\sigma_{22}+\sigma_{33}>0, dm_t=1$ (matrix tensile failure)

$\sigma_{22}+\sigma_{33}<0,\ dm_c=1$ (matrix compressive failure)

The final form of these criteria appears as:

$$\left[\left(\frac{\sigma_{22}}{X_{2t}^{dyn}}\right)^2+\left(\frac{\sigma_{12}}{S_{12}^{dyn}}\right)^2+\left(\frac{\sigma_{23}}{S_{23}^{dyn}}\right)^2\right]+\sigma_{22}\left(\frac{1}{X_{2t}^{dyn}}+\frac{1}{X_{2c}^{dyn}}\right)=1 \tag{4.14}$$

$\sigma_{22}+\sigma_{33}>0, dm_t=1$ (matrix tensile failure)

$\sigma_{22}+\sigma_{33}<0,\ dm_c=1$ (matrix compressive failure)

Here $\sigma_{11}, \sigma_{22}, \sigma_{33}, \sigma_{12}$ and σ_{23} are components of the stresses at an integration point of an element; dm_t and dm_c are the damage variables associated with failure modes of matrix in tension and compression respectively. X_{1t}, X_{2t} and X_{2c} are tensile failure stress in the fibre direction, tensile failure stress in the direction transverse to the fibre orientation and compressive failure stress in the direction transverse to the fibre orientation, respectively, while S_{11}, S_{12} and S_{13} are shear strengths in 1–2, 2–3 and 1–3 planes, respectively, while K is calculated from Eq. (4.8).

4.4.4 Shear response

The in-plane shear response of a composite laminate is often dominated by a non-linear behaviour of the matrix that exhibits both stiffness degradation due to matrix micro-cracking and plasticity. The elastic part (OA in Fig. 4.4) of the shear response was calculated using Eq. 4.1. In this section, the plastic shear response, leading to permanent deformations in the ply upon unloading (BCD in Fig. 4.4) of the material is discussed.

The shear response is usually calibrated with a cyclic tensile test on a ±45 laminate, where the strains along the fibre directions can be neglected. Fig. 4.4a shows the typical shear response of a fabric reinforced composite. It is noted that the unloading/reloading paths in this figure correspond to an idealization of the actual response, which usually exhibits hysteretic behaviour. For each unloading curve in Figure 4.4a, the plastic strain at the onset of unloading is determined from the value of residual deformation in the unloaded state. The values of at the onset of unloading are then used to fit the parameters of the hardening curve, as illustrated in Figure 4.4b.

A classical plasticity model with a hardening law applied to the effective stresses in the damaged material is used (Fig. 4.4b). The hardening law is of the form:

$$\tilde{\sigma}_0(\bar{\varepsilon}^{pl}) = \tilde{\sigma}_{y0} + C(\bar{\varepsilon}^{pl})^p \tag{4.15}$$

where $\tilde{\sigma}_{y0}$ is the initial effective shear yield stress; C and p are coefficients; and $\bar{\varepsilon}^{pl}$ is the equivalent plastic stain due to shear deformation .The damage in shear is simply calculated as,

$$d_s = \left\{ \frac{\sigma_{12}}{S_{12}}, \frac{\sigma_{13}}{S_{13}}, \frac{\sigma_{23}}{S_{23}} \right\} . \tag{4.16}$$

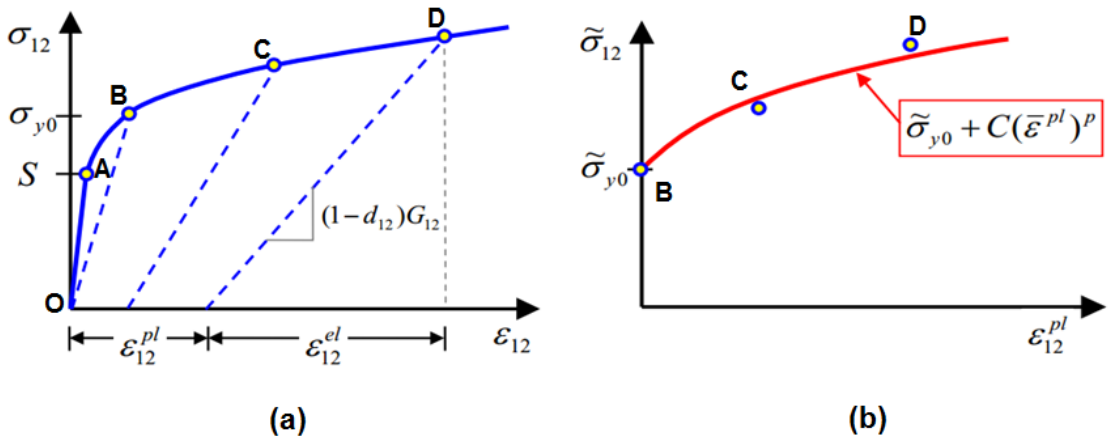

Figure 4.4 (a) Schematic representation of a typical in-plane shear response of a fabric reinforced composite (b) calibration of the shear hardening curve

Here σ_{12}, σ_{13} and σ_{23} are the effective shear stress while, S_{12}, S_{13} and S_{23} are the in-plane and out-of-plane shear strengths of a ply. Thus the evolution of the plastic work during yielding is given as,

$$\dot{U}_{pl} = \sigma_{12}\dot{\varepsilon}_{12}^{pl} + \sigma_{13}\dot{\varepsilon}_{13}^{pl} + \sigma_{23}\dot{\varepsilon}_{23}^{pl} \tag{4.17}$$

4.5 Damage evolution

To alleviate mesh dependency during strain softening, a characteristic length of a finite element is introduced into the formulation so that the constitutive law is expressed as a stress-displacement relation.

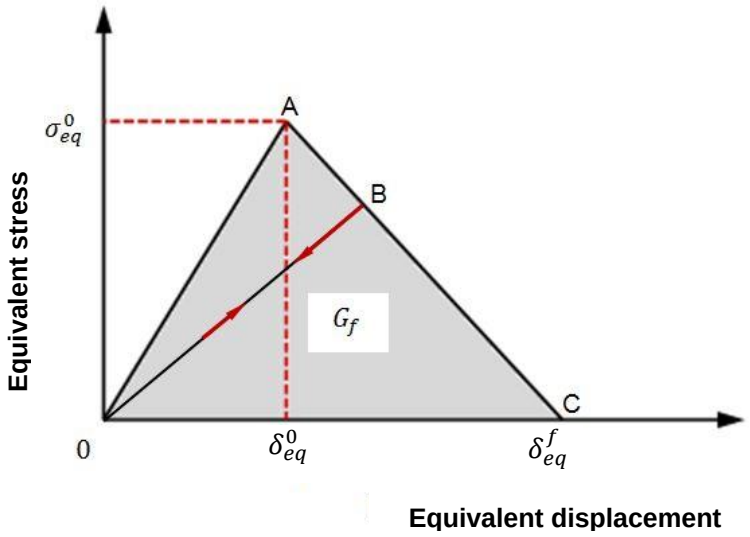

Figure 4.5 Concept of equivalent stress *vs.* equivalent displacement in evolution of damage variable

For example, for a linear-elastic brittle material like CFRP, the damage variable will evolve in such a way that the stress-strain behaviour follows the curve as shown in Fig. 4.5 in each of the four failure modes. The positive slope of the stress-displacement curve prior to damage-initiation corresponds to a linear-elastic material behaviour; while the negative slope after damage-initiation is achieved by evolution of damage parameter d as following.

$$d_i = \frac{\varepsilon_{eq}^{fi}(\varepsilon_{eq} - \varepsilon_{eq}^{0})}{\varepsilon_{eq}(\varepsilon_{eq}^{fi} - \varepsilon_{eq}^{0})}, \tag{4.18}$$

Here, ε_{eq}^{0} is the strain at the damage initiation, and ε_{eq}^{f} is the strain at which the material is completely damaged. $i = f_t, f_c, m_t, m_c$ corresponds to damage

variables associated with failure modes of fibre and matrix material in tension and compression, respectively, as discussed in Section 4.3.

For example, damage variable d for fibre tensile failure mode, can be written as:

$$d_{ft} = \frac{\varepsilon_{eq}^{f_{ft}}(\varepsilon_{eq} - \varepsilon_{eq}^{0_{ft}})}{\varepsilon_{eq}(\varepsilon_{eq}^{f_{ft}} - \varepsilon_{eq}^{0_{ft}})}\ , \tag{4.19}$$

Unloading from a partially damaged state, such as point B in Fig. 4.4 occurs along a linear path towards the origin; this path is followed back to point B upon reloading. Due to this irreversibility of the damage variable d , the strain calculated at each time step is defined as $\varepsilon_{eq} = \max\ (\varepsilon_{eq}\ ,\ \varepsilon_{eq}^{0})$. The damage parameter d varies from 0 to 1. The integer 0 represents the state of damage initiation while 1 represents the state of a material as fully-damaged. This is presented graphically in Fig. 4.6.

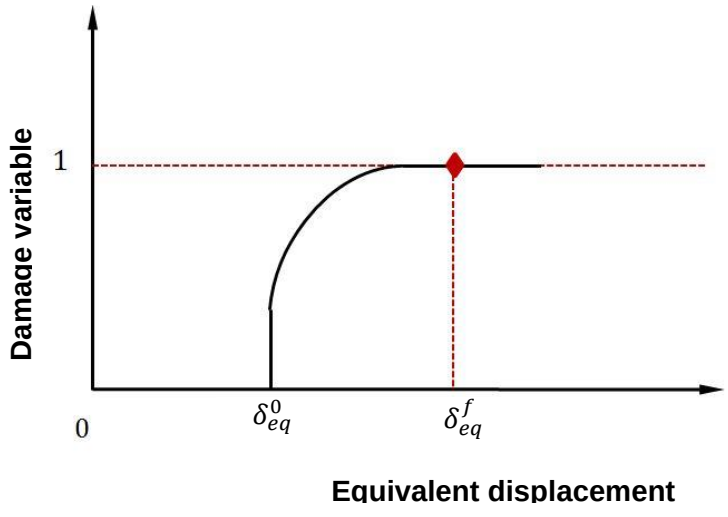

Figure 4.6 Graphical presentation of damage variable variation with equivalent displacement

The values of ε_{eq}^{0} for various modes depend on elastic stiffness and strength parameters specified as part of the damage-initiation definition in Section 4.3 and given by Eq. (4.20).

$$\varepsilon_{eq}^{0} = \frac{X_t}{E^0} \ , \tag{4.20}$$

where X_t is the equivalent stress at damage initiation and E^0 is the undamaged elastic modulus. The calculation of failure strain ε_{eq}^{f} using fracture energy G_f is discussed below.

The fracture energy G_f (expressed in J/m^2 or N/m) was idealised as, work required to open a unit area of a crack under given displacement and expressed as,

$$G_f = \int_0^{\delta_f} \sigma(u).\, du = \frac{1}{2}\sigma_{eq}^{f}.\, \delta_{eq}^{f} \ . \tag{4.21}$$

From Eq. (4.20),

$$\delta_{eq}^{f} = \frac{2G_f}{\sigma_{eq}^{f}} \ . \tag{4.22}$$

The mesh dependency of the final solution was alleviated by relating the characteristic length of a meshed element, L_c with the equivalent strain at failure ε_{eq}^{f} such that $\delta_{eq}^{f} = L_c.\varepsilon_{eq}^{f}$. Thus ε_{eq}^{f} can be calculated as :

$$\varepsilon_{eq}^{f} = \frac{2G_f}{\sigma_{eq}^{f}.\, L_c} \ . \tag{4.23}$$

The use of L_c assured a constant energy release rate per unit area of a crack thus making the final resultws independent of the FE mesh size. In this work, the approach developed by Bažant and Oh (1983) was employed, where for a solid element L_c is given by :

$$L_c = \frac{\sqrt{A_{ip}}}{\cos(\theta)} \ , \ |\theta| \leq 45^{\circ} \ . \tag{4.24}$$

Here, A_{ip} is the area associated with an integration-point of a meshed element, while θ is the angle between the mesh line and the direction of crack. This method is computationaly effcient and shown to work well for solid elements (Lapczyk and Furtado, 2007; Shi *et al.*, 2012). Typically L_c is a length of a line across a first-order element. It should be noted that this method does not cure the mesh dependency physically, though represents one way in which this issue can be tackled.

4.6 Element removal

The element-deletion approach used to remove the failed elements from the mesh was based on the magnitude of damage variables, d_i, $i = f_t, f_c, m_t, m_c$ as calculated using Eq. (4.17) applied to discrete damage modes in the composite laminate. The element was removed when the magnitude of either of the damage variables associated with the fibre failure reaches $d_{\max}(=1)$, refer Fig. 4.5) at an integration point of an element. When this condition is satisfied, the element is removed from the mesh, and it offered no subsequent resistance to deformation.

4.7 Failure criteria for woven fabric laminates

Architecture of a woven fabric ply differs from that of a UD-fibre based-ply in the sense that the fibre bundles are interlaced with each other as discussed in Section 2.2.2.

It should be noted that the composite ply is modelled as a homogeneous, orthotropic entity and, hence, an analogy can be drawn between the failure criteria proposed for laminated formed with UD composite plies and woven-fabric plies. For example, as seen in Section 4.3, all failure criteria are expressed in terms of stress components based on the ply-level stresses (σ_{11}, σ_{22}, σ_{33}, τ_{12}, τ_{13}, τ_{23}) and elastic moduli E_{11}, E_{22}, E_{33}, G_{12}, G_{13}, G_{23} . Here, indices 11, 22, 33, 12, 13, 23 denote the fibre direction, in-plain transverse and out-of-plane directions, respectively, in case of UD composite ply and in-plane fill, in-plane warp and out-of-plane directions, respectively, for a fabric composite ply. It should also be noted that the orientation of fibres is assumed orthogonal to each other here. The failure criteria for a fabric composite ply is listed below in Table 4.2.

Table 4.2 Dynamic failure criteria for woven-fabric reinforced composite ply

For tensile failure in fabric along fill direction	$\left(\frac{\sigma_a}{X_{at}}\right)^2+\left(\frac{\sigma_a}{S_{ab}}\right)^2+\left(\frac{\sigma_a}{S_{ac}}\right)^2\geq 1,\ \ df_{\text{ta}}=1;$
For tensile failure in fabric along warp direction	$\left(\frac{\sigma_b}{X_{bt}}\right)^2+\left(\frac{\sigma_b}{S_{ab}}\right)^2+\left(\frac{\sigma_b}{S_{ac}}\right)^2\geq 1,\ \ df_{\text{tb}}=1;$
For compressive failure in fabric along fill direction	$\left(\frac{\sigma_a}{K(\dot{\varepsilon})X_{ac}^{qs}}\right)+\left(\frac{\tau_{ab}}{K(\dot{\gamma})S_{ab}^{qs}}\right)+\left(\frac{\tau_{ac}}{K(\dot{\gamma})S_{ac}^{qs}}\right)\geq 1,\ \ df_{ca}=1;$

For compressive failure in fabric along warp direction	$\left(\frac{\sigma_b}{K(\dot{\varepsilon})X_{ac}^{qs}}\right)+\left(\frac{\tau_{ab}}{K(\dot{\gamma})S_{ab}^{qs}}\right)+\left(\frac{\tau_{ac}}{K(\dot{\gamma})S_{ac}^{qs}}\right)\geq 1,\ \ df_{cb}=1;$

For matrix failure

$$\left[\left(\frac{\sigma_{bb}}{X_{bt}^{dyn}}\right)^2+\left(\frac{\sigma_{ab}}{S_{ab}^{dyn}}\right)^2+\left(\frac{\sigma_{bc}}{S_{bc}^{dyn}}\right)^2\right]+\sigma_{22}\left(\frac{1}{X_{bt}^{dyn}}+\frac{1}{X_{bc}^{dyn}}\right)=1$$

$\sigma_{bb}+\sigma_{cc}>0, dm_t=1$ (matrix tensile failure)

$\sigma_{bb}+\sigma_{cc}<0,\ dm_c=1$ (matrix compressive failure)

In table 4.2, indices a, b and c denote the fill, warp and through-thickness directions respectively. The damage evolution was calculated using the procedure as described in Section 4.4.

4.8 User-defined subroutine

The user-defined subroutine was written in a vectorised from in FORTAN and implemented in the ABAQUS/Explicit (ABAQUS, 2010) solver owing to its ability to account for the time-dependent loading, complex contact interactions and inertia effects, as discussed in Section 3.5. Its implementation process for the 3D solid elements follows the steps below:

(a) Call a VUMAT subroutine with the previous strain vector as well as the iterative increment in strains, and trial values for the constitutive matrix at this material point.

(b) Update the total elastic strain for this iteration by summing the total strains from the previous increment and the corresponding iterative increments of strain.

(c) Compute the strain-rate and adjust the elastic moduli.

(d) Compute the updated stresses using the constitutive matrix and the total strains at this material point as well as adjust the strength values.

(e) Perform the failure initiation check using the Hashin's and Puck's failure criteria with adjusted elastic modulus and strength values in previous steps and determine whether any material failure had initiated. If so, perform the material degradation step.

(f) Perform the material degradation step. If material failure is detected, then degrade the material properties by degrading the entries in the constitutive matrix, so that the appropriate stress component will approach zero after failure initiation.

(g) Re-compute the constitutive matrix and the stresses, update the solution-dependent variables, and return to ABAQUS.

A flowchart of this code is presented in Figs. 4.7-4.10. Figure 4.7 presents the general structure of VUMAT subroutine. Figure 4.7 exhibits the stress and strain update technique that includes the damage-initiation loop based on the Hashin's and Puck's theories as discussed in Section 4.3 and damage evolution based on the criteria discussed in Section 4.4. Finally, these two loops are explicitly shown in Fig. 4.9 and 4.10, while the element-deletion strategy is shown in Fig. 4.9. Typical material properties employed in this VUMAT are listed in Table 4.3.

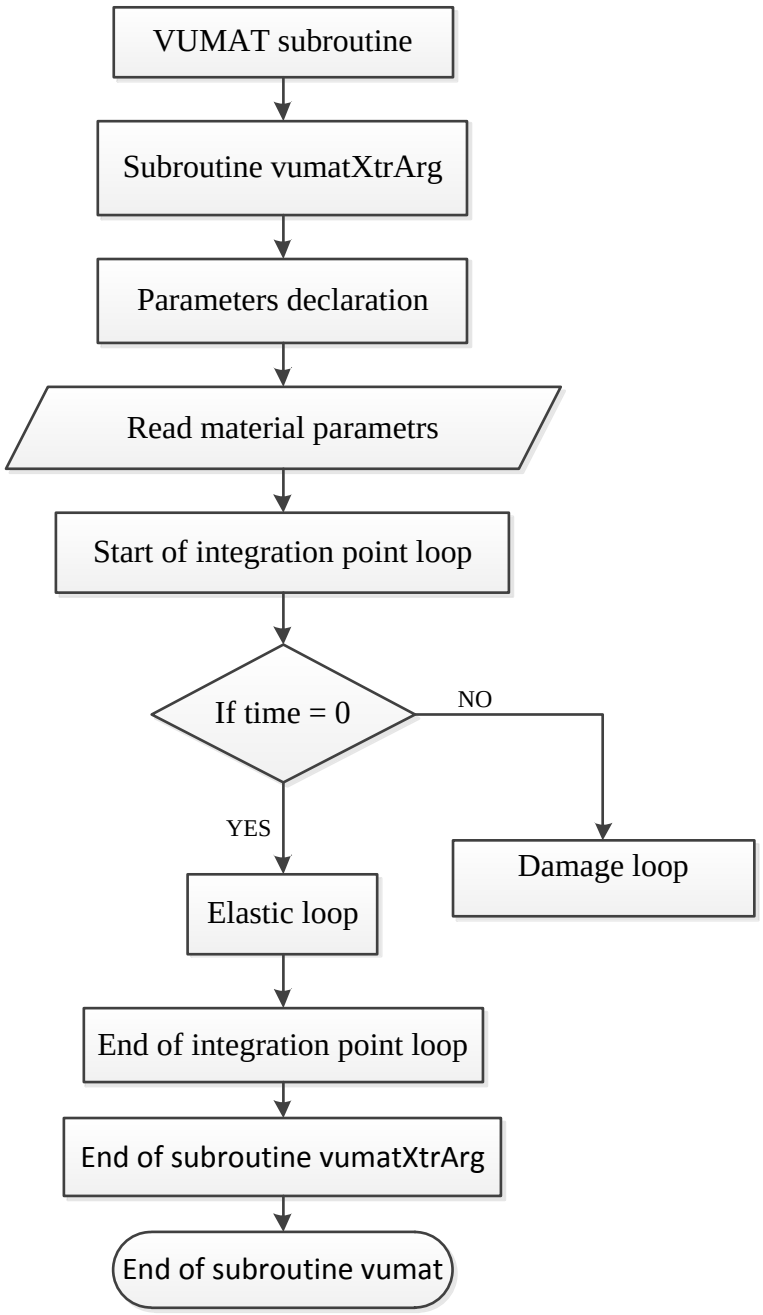

Figure 4.7 General structure of VUMAT to model damage

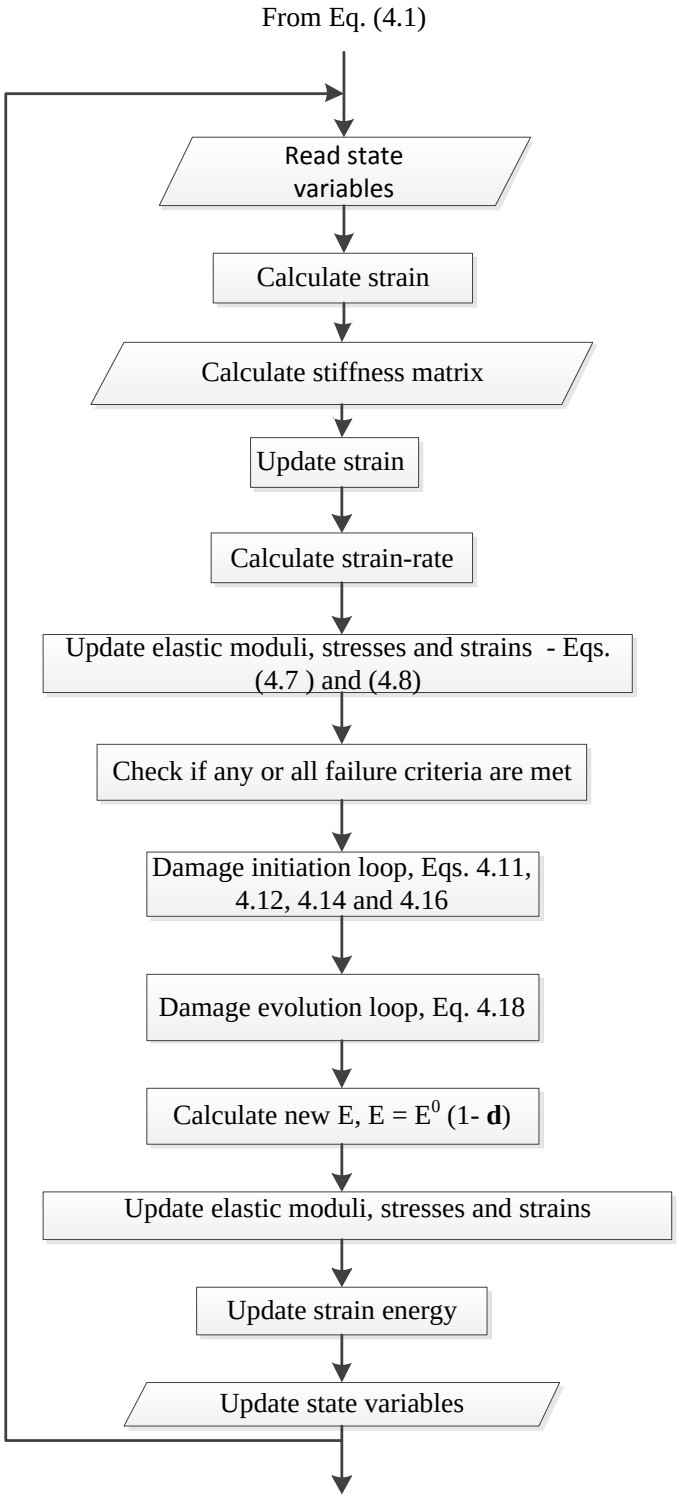

Figure 4.8 Structure of VUMAT: stress and strain update

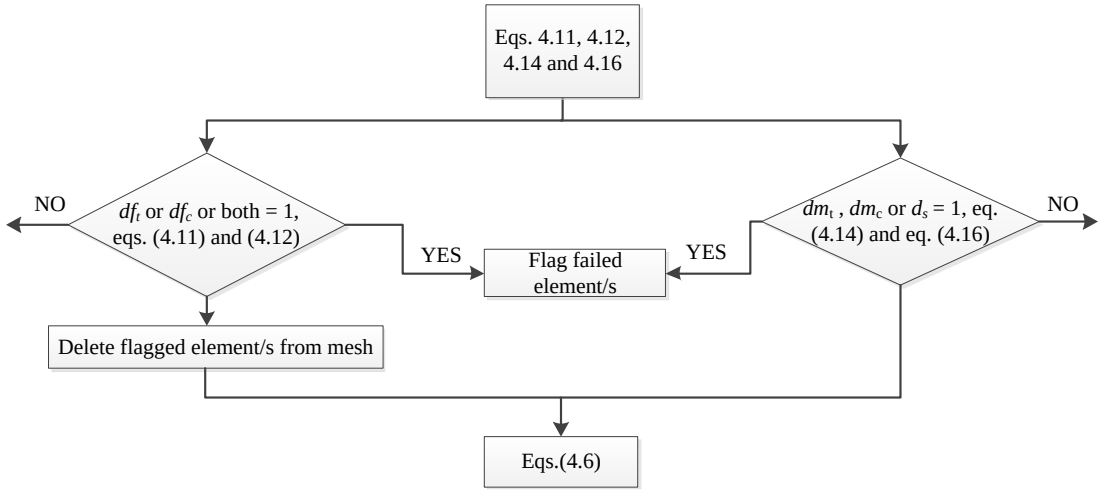

Figure 4.9 Flowchart of material model: determination of damage parameter

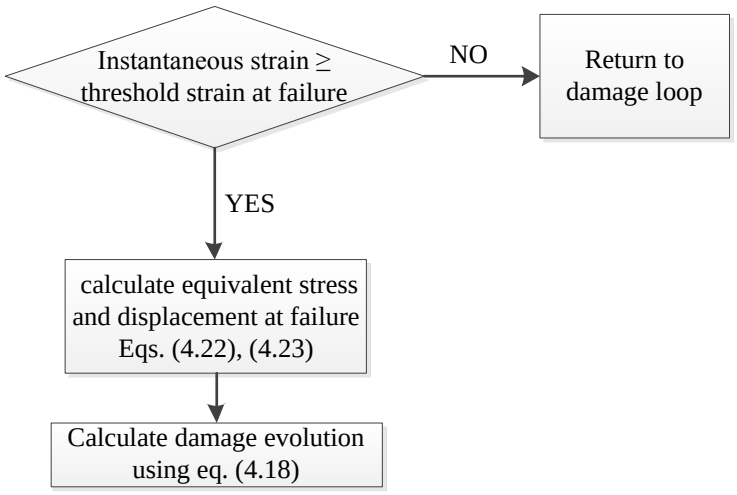

Figure 4.10 Flowchart of material model: evolution of damage parameter

The material properties and the corresponding output variables used in this VUMAT are listed below.

Table 4.3 Material properties of typical UD composite ply required for VUMAT

a) Elastic properties

E_{11}	Elastic modulus in fibre direction (GPa)
E_{22}	Elastic modulus in transverse direction (in-plane) (GPa)
E_{33}	Elastic modulus in transverse direction (out-of-plane) (GPa)
υ_{12}	Poisson's ratio in 1-2 plane
υ_{13}	Poisson's ratio in 1-3 plane
υ_{23}	Poisson's ratio in 2-3 plane
G_{12}	Shear modulus in 1-2 plane (GPa)
G_{13}	Shear modulus in 1-3 plane (GPa)
G_{23}	Shear modulus in 2-3 plane (GPa)

b) Damage-initiation and -evolution properties

X_{1t}	Tensile strength in fibre direction (MPa)
X_{1c}	Compressive strength in fibre direction (MPa)
X_{2t}	Tensile strength in transverse direction (in-plane) (MPa)
X_{2c}	Compressive strength in transverse direction (in-plane) (MPa)
X_{3t}	Tensile strength in transverse direction (out-of-plane) (MPa)
X_{3c}	Compressive strength in transverse direction (out-of-plane) (MPa)

S_{12} Shear strength in 1-2 plane (MPa)

S_{13} Shear strength in 1-3 plane (MPa)

S_{23} Shear strength in 2-3 plane (MPa)

G_{ft}^{1} Energy of tensile fracture in fibre direction, (J/m^2)

G_{fc}^{1} Energy of compressive fracture in fibre direction, (J/m^2)

G_{ft}^{2} Energy of tensile fracture in transverse direction (in-plane) , (J/m^2)

G_{fc}^{2} Energy of compressive fracture in transverse direction (in-plane) , (J/m^2)

G_{ft}^{3} Energy of tensile fracture in transverse direction (out-of-plane) , (J/m^2)

G_{fc}^{3} Energy of compressive fracture in transverse direction (out-of-plane) (J/m^2)

c) Shear plasticity coefficients

$\tilde{\sigma}_{y0}$ Initial effective shear yield stress (MPa)

C Coefficient in hardening equation

p Power term in hardening equation

$\dot{\varepsilon}$ Reference strain-rate

K Fitting parameter from shear stress-strain curve at different loading rates

d) Controls for material failure

$\tilde{\sigma}_{y0}$	Initial effective shear yield stress (MPa)
lDelFlag	Element deletion flag:
	0 - Element is not deleted
	1 - Element is deleted
$d_{\max}$	Maximum value of damage variable used (generally, it is assumed to be 0.99 to allow gradual loss of material's stiffness)

e) Output variables

SDV1	Tensile damage along fibre direction 1
SDV2	Compressive damage along fibre direction 1
SDV3	Tensile damage along transverse direction (in-plane)
SDV4	Compressive damage along transverse direction (in-plane)
SDV5	Tensile damage along transverse direction (out-of-plane)
SDV6	Tensile damage along transverse direction (out-of-plane)
SDV7	Shear damage
SDV8	Material point status (0 - intact, 1 - failed)
SDV9-13	Components of plastic stain
SDV14-19	Components of elastic strain

To demonstrate a successful implementation of proposed criteria, a simple case of dynamic compression loading of a CFRP laminate made of AS4/3501-6 UD ply (60% fibre volume fraction) using a Split Hopkinson pressure bar (SHPB) is simulated. A stress-strain response of a CFRP laminate with quasi-isotropic properties (layup sequence - $[\pm 45/0/90]_s$) was obtained at a strain rate of 860 s^{-}

[1]. The results of the FE analysis were then compared to experimental data. The experimental details can be found in Gómez-del Rio *et al.* (2005). The schematic representation of a meshed quarter-symmetric FE model is shown in Fig. 4.11.

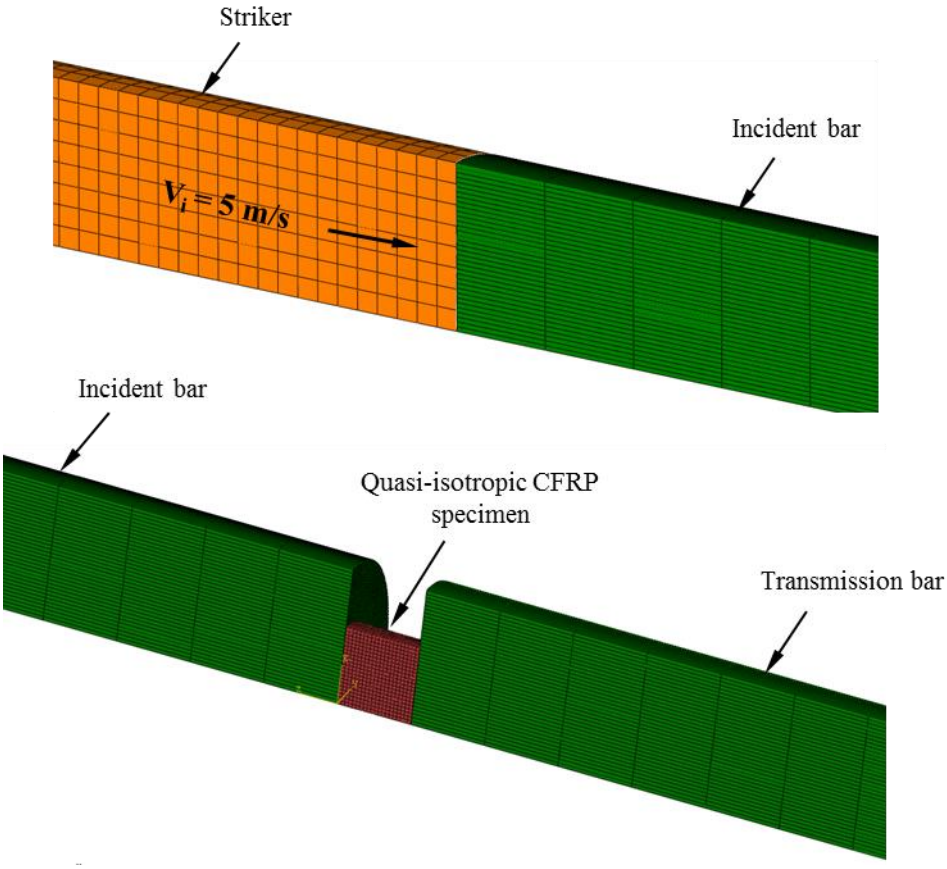

Figure 4.11 Dynamic compression of CFRP specimen using SHPB setup: FE model for a case of strain-rate of 860s^{-1}

The striker, incident bar and transmission bar were meshed with eight-node, isoparametric, hexahedral elements C3D8R. The incident and transmission bars were discretised with 80000 elements each; the striker bar with 12500 elements. The mesh used here is optimised based on a vigorous mesh-sensitivity analysis. The element size of 0.2 mm was found to be optimal for the specimen of thickness 2 mm. The initial velocity of a striker is 5 m/s that

correspond to the strain-rate of 860 s^{-1}. The static material properties are given in Table 4.4, while dynamic material properties were taken from Daniel *et al.* (2003).

Table 6.1 Mechanical properties of AS4/3501-6 UD composite laminate (Sánchez *et al.,* 2002; Daniel *et al.*, 2011)

Elastic moduli	$E_{11}=131$ GPa, $E_{22}=E_{33}=9$ GPa, $G_{12}=G_{13}=4.8$ GPa				
Tensile strength in fibre direction, X_{1t}	2137 MPa				
Compressive strength in fibre direction, X_{1c}	1425 MPa				
Tensile strength in transverse direction, X_{2t}	90 MPa				
Compressive strength in transverse direction, X_{2c}	200 MPa				
In–plane shear strength, S	75 MPa				
Stiffness of cohesive zone, K (N/mm^3)	5×10^6				
Interlaminar traction in normal direction, τ_n (MPa)	53.78				
Interlaminar traction in shear-1 and 2 direction, $\tau_s = \tau_t$ (MPa)	86.88				
Mode-I critical fracture energy, G_{IC} (N/mm)	0.08				
Mode II critical fracture energy, G_{IIC} (N/mm)	0.55				
Power law coefficient, β	1.8				
Strain-rate dependent properties	Average strain-rates, $\dot{\varepsilon}$ (s^{-1})				
	0.0001	1	400	2400	3800
Transverse modulus, E_{22} (GPa)	9	10.3	11.5	[11.8]	[12.2]

Shear modulus, G_{12} (GPa)	4.8	5.2	7	[7.6]	[7.8]
Transverse tensile strength, F_{2t} (MPa)	90	108	112	[117]	[119]
Transverse compressive strength, F_{2c} (MPa)	200	265	330	[365]	[379]

Note: Numbers in brackets denote extrapolated values.

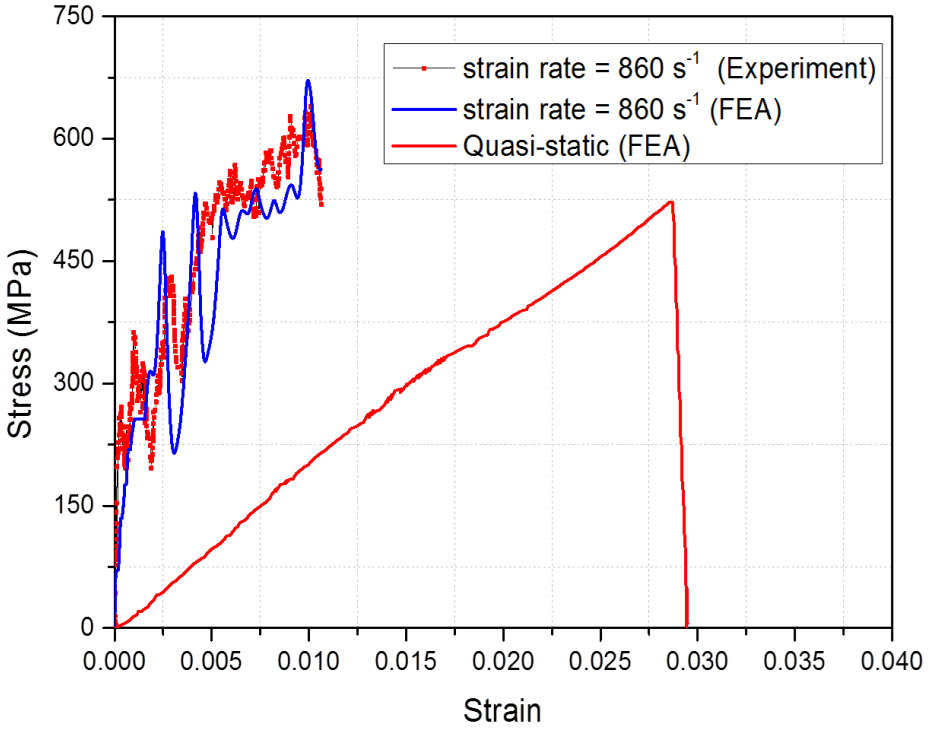

Figure 4.12 Quasi-static and high-strain-rate responses of QS CFRP laminate: validation of material model with experimental data from Sánchez *et al. (*2002).

The stress-strain response at a strain-rate of 860 s^{-1} is shown in Fig. 4.12. For comparison, its quasi-static behaviour is also simulated and the calculated response is plotted on the same graph. It can be seen that the high-strain-rate response of the CFRP laminate was captured reasonably accurately. The peaks and troughs in the FE curve can be attributed to the stress rise and element-deletion upon reaching the threshold level of stresses.

4.9 Summary

A continuum-level dynamic failure model is proposed for a laminated composite that is capable of modelling accurately its through-thickness stress response, its strain-rate sensitive behaviour at different loading rates, the non-linear behaviour of matrix, damage-initiation in the laminate and its progressive failure along with the degradation. The primary motivation behind the development of this model is to analyse the mechanical behaviour of laminated composites in high-loading-rate regimes such as ballistic-impact and blast.

This model combines the advantages of two previously proposed damage models: by Hashin (1980) and by Puck and Schürmann (1998). These criteria were suitably modified to model a through-thickness stress response of a composite laminate and its strain-rate-sensitive behaviour. The damage evolution is modelled to facilitate material degradation using a concept of equivalent displacement and stress at the failure strain. This mitigated the problems associated with mesh-sensitivity in damage modelling by incorporating the characteristic length of a finite element in the damage-evolution criteria.

The proposed dynamic failure criteria is implemented into the general-purpose FE software ABAQUS/Explicit that can efficiently handle FE simulations of dynamic events and progressive degradation of material's stiffness based on the damage accumulation.

Another advantage of this model lies in the fact that it can be applied to woven-fabric-reinforced composite laminates with slight modification in the terminology used to define elastic moduli and ply-level stresses. Moreover, the ability of this material model to capture linear and nonlinear types of behaviour allows the prediction of responses for materials developing nonlinearity at high-strain-rates as shown in the case of FE modelling of the dynamic compression response of the quasi-isotropic CFRP laminate.

In the next chapter, development of a ply level finite-element model of ballistic impact on the woven fabric composites will be presented. This will be followed by details of analysis, and discussion of results.

CHAPTER 5

FINITE-ELEMENT ANALYSIS OF BALLISTIC-IMPACT RESPONSE OF WOVEN-FABRIC COMPOSITES

5.1 Introduction

In recent years, woven-fabric-reinforced polymer-matrix composites (PMCs) have been used increasingly in defence-related applications due to their higher energy absorption capacity, high through-thickness stiffness and strength properties. Additionally, their shape and properties can be tailored to meet the needs of variety of applications. In ballistic-impact, PMCs demonstrate different damage modes such as permanent deformation, delamination, fibre breakage and shear between layers hindering projectile's penetration by absorbing its kinetic energy. In this process they often suffer complete penetration that compromises the safety features of the base structure. The condition for perforation, also called the *ballistic limit velocity* (V_{50}) is one of the most important factors for design of a suitable protective structure in this regard (Naik *et al.*, 2008; Pandya *et al.*, 2013). It is defined as the incident impact velocity of a projectile that would lead to a complete penetration of a target structure accompanied by the complete loss of kinetic energy of the projectile (Naik *et al.*, 2008). It represents an average of the equal number of highest partial-penetration velocities and lowest complete-penetration velocities of a projectile for a specific velocity range, resulting in 50% probability of partial penetration and perforation of a target (Naik *et al.*, 2008; Pandya *et al.*, 2013).

A significant research has been carried out on the ballistic-impact behaviour of composite materials; few representative studies can be mentioned: Zhu *et al.*

(1992) investigated the response of woven Kevlar/polyester laminates of varying thickness to quasi-static and dynamic penetration by cylindro-conical projectiles. Ballistic limits were also determined and terminal velocities measured. It was reported that deliberately introduced delamination and changes in the volume fraction of fibres did not result in significant changes in the impact resistance. They also revealed that a damage pattern in composites under dynamic loading was significantly different from that in the corresponding quasi-static penetration conditions.

Cheng *et al.* (2003) developed a model for high-velocity impact of thick composites based on a continuum orthotropic constitutive behaviour with stress-based failure criteria and a simplified degradation model of failure. The model was implemented into a hydrodynamic finite-element code. Punching, fibre breakage, and delamination were the major energy-absorbing mechanisms of the penetration processes. Silva *et al.* (2005) carried out experiments to study the effect of ballistic-impact on Kevlar-29 impacted with simulated fragments. Numerical modelling was used to obtain an estimate for the limit perforation velocity (V_{50}) and simulate modes of failure and damage. Naik and Doshi (2008) studied the ballistic-impact behaviour of typical woven fabric E-glass/epoxy thick composites analytically. It was reported that shear plugging was the major energy-absorbing mechanism in these laminates.

Design of a fabric-reinforced composite structure capable to withstand ballistic-impact is a conceptually difficult task for a designer. Unlike metallic components that can yield and dissipate energy by undergoing plastic deformation, these can only dissipate energy through various damage processes that usually degrade stiffness of structural components. Hence, an advanced modelling tool that can adequately model such events is essential in the design process. However, due to the complexity involved in this process, most models attempt to provide acceptable trade-off in performance analysis. To model a woven-fabric down to a level of crossovers of individual yarn would certainly be

preferred in order to study the underlying frictional and crimping effects, but such studies are computationally impracticable for dynamic problems.

In this regards, this chapter discusses development of the FE model of ballistic-impact response of woven-fabric-reinforced composites. The experimental studies are discussed first, followed by a detailed description of the FE model. The results and discussion are presented after that.

5.2 Experimental studies

The experimental studies were conducted at IIT Bombay, India by our project partners Mr Kadar Pandya and Professor NK Naik. A short description of the ballistic-impact test facility and the specimen details are provided below.

5.2.1 Ballistic-impact test apparatus

A ballistic-impact test apparatus operated by a single-stage gas-gun (Fig. 5.1) was used to carry out experimental studies. It consisted of a projectile-propelling mechanism, a chronograph for velocity measurement, a support stand for holding the specimen, a containment chamber, safety devices and a strain-measuring facility. Compressed air was used as a propellant in the system. The main components of this propelling mechanism were a cylindrical barrel to guide the projectile, a quick release valve to relieve the trapped air and a nitrogen gas-driven solenoid valve to operate this valve. The cylindrical barrel (through which a bullet is propelled) was 1.5 m long. Its inner diameter was chosen to suit a projectile used in this experiment.

In ballistic impact events, three potential scenarios can be expected regarding the interaction between the projectile and the target structure:

— A projectile impacts the target structure and bounces off due to lack of kinetic energy and/or due to the highly stiff nature of a target.

— A projectile impacts the target and penetrates it just enough to lose its kinetic energy and as a result, its residual velocity at the end of this event is zero.

— A projectile impacts the target, perforates through and leaves the structure with a measurable residual velocity.

The second scenario is much more complex compared to other two and provides significant information on PMC's ability to absorb projectile's energy by undergoing damage. Contribution of these damage modes to the kinetic energy absorbed can be assessed using a validated FE model. Thus experimental scheme is prepared to achieve this scenario (Table 5.1).

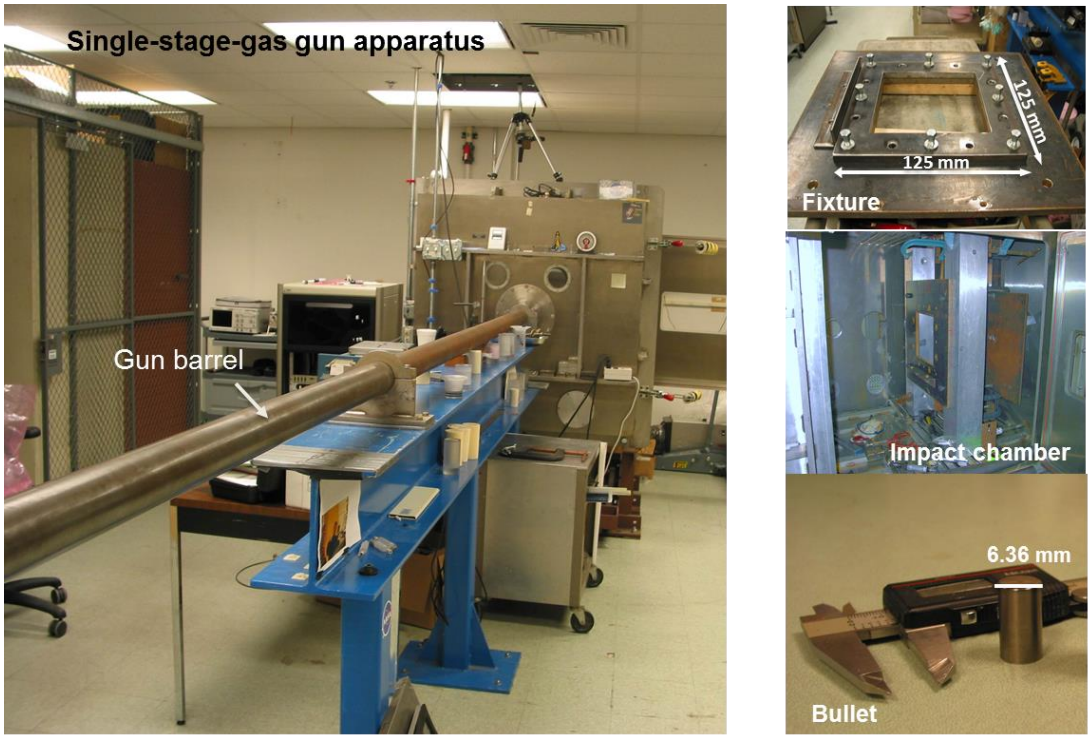

Figure 5.1 Ballistic-impact test apparatus

In this regard, a speed of the projectiles varied up to 200 m/s by changing the air pressure in the cylinder. Experimental studies were carried out on flat specimens with dimensions 125 mm × 125 mm with different thicknesses (Table 5.1). The specimen's dimensions were chosen such that they can be

accommodated into the fixture (Fig. 5.1) designed as an integral part of the ballistic-impact test apparatus. The mass of flat-end cylindrical projectiles made of hardened steel and its diameter was kept constant for all the tests (Table 5.1). Experiments were carried out on at least four specimens for each impact condition to ensure repeatability.

In order to assure the safety of a user from accidental stray firings, a hollow cylindrical shield was employed to enclose the projectile after propulsion. The barrel, hollow shield, chronograph and centre of the clamped specimen were in the perfect alignment. The ballistic-impact tests and projectile configurations were confirmed to ASTM standard for ballistic-impact studies at laboratory level (ASTM F1233-08, 2008).

5.2.2 Specimen details

Four symmetric cross-ply woven fabric composites: plain-weave E-glass fabric/epoxy, 8H satin-weave T300 carbon fabric/epoxy and their hybrids were studied. Specifications of tows/stands, fabrics, resin and composites for plain weave E-glass/epoxy and 8H satin-weave T300 carbon/epoxy composites are presented in Tables 5.1 and 5.2, and specimen's details are given in Table 5.3. For simplicity, these composite laminates are designated as *E, C, H4* and *H5,* respectively, from here onwards. The ply architecture of H4 and H5 is shown in Figs. 5.3 a and b, respectively.

Table 5.1 Scheme of ballistic tests (target surface dimensions: 125 ×125 mm, projectile diameter, dp = 6.36 mm)

Sr. No.	Projectile mass, m_p (g)	Projectile length, l_p (mm)	Target thickness, h (mm)
(A)	Plain-weave E-glass epoxy		
1	6.42	25.3	2.5

2	6.42	25.3	3.0
3	6.42	25.3	4.5
4	6.42	25.3	5.0
(B)	8H satin-weave T300 carbon/epoxy		
1	6.42	25.3	3.0
(C)	Hybrid (H4 and H5)		
1	6.42	25.3	3.0
2	6.42	25.3	3.0

Table 5.2 Specifications of tows/strands, fabrics, resin and composites (Pandya *et al.,* 2013)

Property	T300 carbon/epoxy	E-glass/epoxy
Reinforcement	T300 carbon	E-glass
Weave type	Plain-weave	Satin-weave
No. of counts (per cm)	7.16[a]	12.1[a]
Crimp (fibre waviness) (%)	0.1[a]	0.9[a]
Fabric thickness (mm)	0.32	0.28
Fabric areal weight (g/m^2)	312	388
Fibre volume fraction	0.56	0.51
Matrix material	Epoxy LY556 with hardener HY951	
Process used	Matched die moulding	

[a] along both warp and fill

Crimp is measured in percentage and obtained from two values – straightened thread length and distance between ends of the thread within the fabric. ASTM standard D3883 explains the procedure to measure this. In this study, the magnitude of the crimp was provided by the manufacturer. It should be noted that the present FE models do not account for crimp.

Table 5.3 Specimen details Specifications of tows/strands, fabrics, resin and composites (Pandya *et al.,* 2013)

Type	Configuration	V_f	V_c	V_g	V_f^c	V_f^g
Parent composites						
Plain-weave E-glass/ epoxy	$[G]_n$	0.51	-	1	-	1
8H satin-weave carbon/epoxy	$[C]_n$	0.56	1	-	1	-
Hybrid composites						
H4	$[C_2G_2]_s$	0.53	0.55	0.45	0.57	0.43
H5	$[G_2C_2]_s$	0.53	0.55	0.45	0.57	0.43

Here, V_f is fibre volume fraction; V_c is a volume fraction of *C*; V_g is a volume fraction of *E*; while V_f^c and V_f^g represent volume of one type of reinforcement to the total volume of reinforcement in *H4* and *H5*.

5.3 Constitutive model for fabric-reinforced composites

Development of a ply-level constitutive model to analyse a mechanical response of the fabric/epoxy composite is discussed in Chapter 4. This model was implemented as a material subroutine; VUMAT in ABAQUS (Hibbit *et al.*, 2011) as discussed in Section 4.8. Each ply was modelled as a homogeneous orthotropic elastic material with the potential to sustain progressive stiffness degradation due to fibre/matrix cracking and plastic deformation under shear loading. Delamination between the neighbouring plies was also modelled using the cohesive-zone-element (CZE) technique. The material properties for the simulated specimen are listed in Table 5.4.

5.4 Delamination modelling

Delamination was modelled using CZEs available in ABAQUS/Explicit. The location of CZEs in the meshed assembly of target structure and projectile is shown in Fig.5.2.

CZEs offer ability to capture initiation and propagation of delamination by employing an approach that allows modelling failure in terms of progressive degradation of material's stiffness. The elastic response of cohesive elements was characterised using elastic stiffness, calculated with an empirical formula suggested by Turon *et al.* (2006, 2010):

$$K = \frac{\alpha E_{33}}{t} \ . \tag{5.1}$$

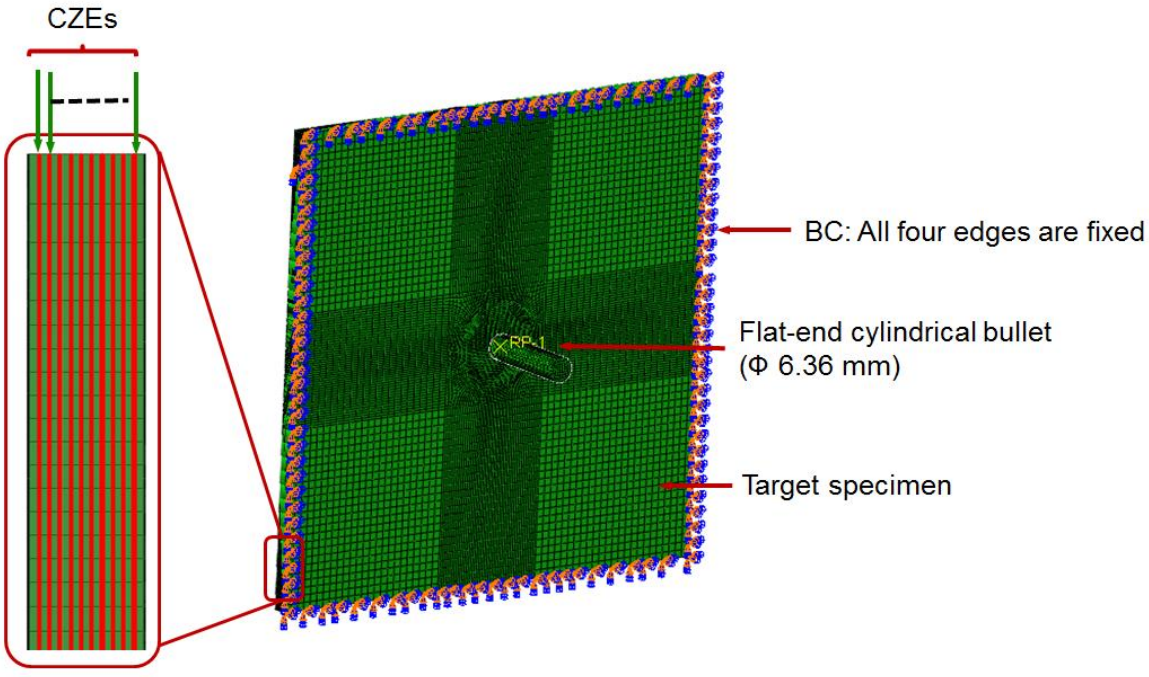

Figure 5.2 FE model setup and location of CZEs

Here, K is interface stiffness, E_{33} is the Young's modulus of CFRP laminate in the thickness direction, t is the thickness of individual ply and α is the adjusting

parameter such that for its values greater than 50, the loss of stiffness due to the presence of interface is less than 2%. In our simulations, we assume, α = 55 (Turon, 2009).

Delaminations initiate and propagate under the combined influence of normal and shear stresses. This mode-mixity was accounted for by employing a bi-linear traction–separation response (Section 3.6.3) using the quadratic nominal-stress criterion having following form:

$$\left[\frac{t_n}{t_n^0}\right]^2 + \left[\frac{t_s}{t_s^0}\right]^2 + \left[\frac{t_t}{t_t^0}\right]^2 = 1 \tag{5.2}$$

Here, t_n, t_t and t_s and are the instantaneous components of normal and shear traction at the interface, while t_n^0, t_s^0 and t_t^0 represent the peak values of nominal stress when the deformation is either purely normal to interface or purely in the first or the second shear direction, respectively. These properties are usually difficult to determine experimentally with good accuracy; therefore, they can be used as calibration parameters, if required. In the present work, the variation of the damage-initiation parameters within 15% from the typical values given in Table 5.4 did not influence significantly the overall analysis results. It should be noted that experimental determination of material properties typically yields a variation of ~15%.

Once the damage-initiation condition is fulfilled, delamination starts and stiffness begins to degrade linearly, linked to a damage variable D :

$$D = \frac{\delta_m^f(\delta_m^{\max} - \delta_m^0)}{\delta_m^{\max}(\delta_m^f - \delta_m^0)}. \tag{5.3}$$

The dependence of fracture energy on mode-mixity was defined using a power-law fracture criterion:

$$\left[\frac{G_n}{G_n^c}\right]^{\beta} + \left[\frac{G_s}{G_s^c}\right]^{\beta} + \left[\frac{G_t}{G_t^c}\right]^{\beta} = 1 . \quad (5.4)$$

Here, G_n, G_s and G_t are the instantaneous fracture energies in normal, and shear directions; whereas G_n^c,G_s^c and G_t^c refer to the critical fracture energies required to cause failure in the normal, the first, and the second shear direction respectively. The elastic-traction values were estimated from Eq. (5.1), while maximum values of stress and fracture energy were taken from Sokolinsky (2013), Naik *et al.* (2006) and Ullah *et al.* (2013) due to identical composite systems.

5.5 Description of finite-element model

5.5.1 Materials

As discussed in Section 5.2.2, four woven fabric composites, - E, C, H4 and H5- were modelled. The fundamental difference between hybrids H4 and H5 was linked to their ply architecture (Figs. 5.3 a and b), e.g. the stacking sequence of H4 was $[C_2G_2]_s$ while that of H5 was $[G_2C_2]_s$, Thus, for H4, carbon-fibre layers are at the exterior of the laminate, and glass-fibre layers are at the exterior of H5. The ballistic response of parent composites (C and G) was also analysed to compare their response with their hybrids under similar loading conditions.

5.5.2 Damage modelling

The in-plane and through-thickness responses of the fabric plies were modelled using the constitutive model described in Section 3. The input to the FE model consisted of elasticity constants that include the Young's moduli in three directions, principal Poisson's ratios, and in-plane shear modulus. The damage-initiation coefficients accounted for tensile and compressive strengths along the fibre directions and shear strength at the onset of shear damage. The values of the elastic properties of studied materials at quasi-static and high-strain-rate

loading conditions are listed in Tables 5.4 and 5.5 while their strengths at quasi-static and high-strain-rate loading are listed in Table 5.6 and 5.7, respectively. The shear plasticity parameters are listed in Table 5.8. The damage-evolution coefficients are characterised by tensile and compressive fracture energies per unit area along the fibre directions. These can be determined through a testing procedure described in (Pinho *et al.*, 2006), though for the present work these properties were taken from Ullah *et al.* (2013), Pandya *et al.* (2013) and Pinho *et al.* (2006). It should be noted that material properties used in the simulation were taken from literature and belonged to the same material system.

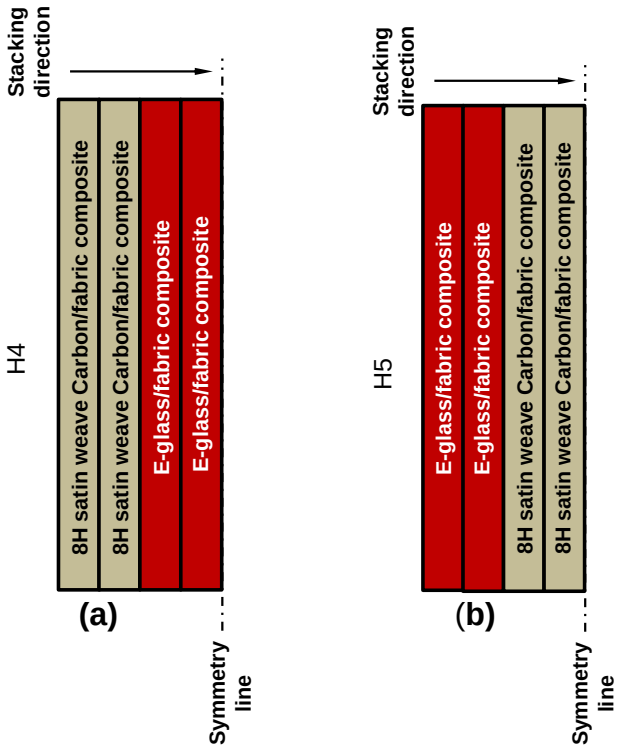

Figure 5.3 Architecture of hybrid composite laminates – (a) H4 (b) H5

5.5.3 Modelling perforation

In simulations, failed finite elements were removed from the model to represent the perforation of the material. The damage-based element deletion was

activated when any damage variable along the fibre direction or the equivalent plastic strain due to shear deformation reached a maximum specified value. Additionally, detached composite fragments were deleted when they moved far away from the impact zone to prevent non-physical numerical distortions.

Table 5.4 Elastic properties of studied composites under quasi-static loading (Pandya *et al.,* 2013; Naik *et al.*, 2006, 2008)

Material	E_x (GPa)	E_y (GPa)	E_z (GPa)	G_{xy} (GPa)	G_{xz} (GPa)	G_{yz} (GPa)	υ_{xy}	$\upsilon_{xz} = \upsilon_{yz}$	ρ (kg/m^3)	V_f (%)
T300 carbon / epoxy	(39.0) [21.9]	(39.0) [21.9]	(6.3) [8.9]	3.1	3.4	3.4	0.073	0.071	1435	56
E-glass / epoxy	(12.5) [12.0]	(12.5) [12.0]	(6.2) [8.8]	3.0	3.3	3.3	0.189	0.276	1850	51
H4	(30.8) [21.1]	(30.8) [21.1]	(6.2) [8.8]	3.1	3.4	3.4	0.145	0.182	1610	53
H5	(40.0) [23.2]	(40.0) [23.2]	(6.3) [8.9]	3.2	3.4	3.4	0.073	0.071	1435	56

The quantities in round brackets indicate values for tensile loading and in square brackets indicate values for compressive loading. Specimen nominal thickness = 3 mm

Table 5.5 Elastic properties of studied composites under high strain rate loading (Pandya *et al.,* 2013; Naik *et al.*, 2006, 2008)

Material	E_x (GPa)	E_y (GPa)	E_z (GPa)	G_{xy} (GPa)	G_{xz} (GPa)	G_{yz} (GPa)	υ_{xy}	$\upsilon_{xz} = \upsilon_{yz}$	ρ (kg/m^3)	V_f (%)

T300 carbon / epoxy	40.2) [24.2]	(40.2) [24.2]	(6.8) [11.3]	3.1	3.4	3.4	0.073	0.071	1435	56
E-glass / epoxy	(14.5) [20.5]	(14.5) [20.5]	(7.2) [9.9]	3.0	3.3	3.3	0.189	0.276	1850	51
H4	(33.2) [22.0]	(33.2) [22.0]	(7.0) [13.6]	3.1	3.4	3.4	0.145	0.182	1610	53
H5	(40.5) [24.8]	(40.5) [24.8]	(6.8) [11.3]	3.2	3.4	3.4	0.073	0.071	1435	56

The quantities in round brackets indicate values for tensile loading and in square brackets indicate values for compressive loading. Strain rate for compressive, tensile and shear loading was 1500 per sec, 400 per sec and 800 per sec, respectively.

Table 5.6 Strength properties of studied composites under quasi-static loading (Pandya *et al.,* 2013; Naik *et al.*, 2006, 2008)

Material	X_t (MPa) [ε_{xt}^{ult} (%)]	Y_t (MPa) [ε_{yt}^{ult} (%)]	Z_t (MPa) [ε_{zt}^{ult} (%)]	X_c (MPa) [ε_{xc}^{ult} (%)]	Y_c (MPa) [ε_{yc}^{ult} (%)]	Z_c (MPa) [ε_{zc}^{ult} (%)]	S_{12} (MPa) [γ_{12}^{ult} (%)]	$S_{13} = S_{23}$ (MPa) [$\gamma_{13}^{ult} = \gamma_{23}^{ult}$ (%)]	ρ (kg /m^3)	V_f (%)
T300 carbon / epoxy	511 [1.36]	511 [1.36]	49.5 [1.01]	242 [1.31]	242 [1.31]	220 [1.20]	67 [0.82]	66 [0.80]	1435	56
E-glass / epoxy	322 [3.75]	322 [3.75]	27.1 [2.60]	204 [1.60]	204 [1.60]	140 [3.85]	29 [1.54]	28 [1.52]	1850	51

H4	456 [2.41]	456 [2.41]	43.2 [1.08]	234 [1.33]	234 [1.33]	185 [1.30]	36 [0.93]	35 [0.90]	1610	53
H5	520 [1.78]	520 [1.78]	50.2 [1.02]	249 [1.47]	249 [1.47]	225 [1.22]	67 [0.82]	66 [0.80]	1435	56

The quantities in square brackets indicate % ultimate strain. Specimen nominal thickness = 3 mm

Table 5.7 Strength properties of studied composites under high strain rate loading (Pandya *et al.,* 2013; Naik *et al.*, 2006, 2008)

Material	X_t (MPa) [ε_{xt}^{ult} (%)]	Y_t (MPa) [ε_{yt}^{ult} (%)]	Z_t (MPa), [ε_{zt}^{ult} (%)]	X_c (MPa), [ε_{xc}^{ult} (%)]	Y_c (MPa), [ε_{yc}^{ult} (%)]	Z_c (MPa), [ε_{zc}^{ult} (%)]	S_{12} (MPa), [γ_{12}^{ult} (%)]	$S_{13} = S_{23}$ (MPa), [$\gamma_{13}^{ult} = \gamma_{23}^{ult}$ (%)]	ρ (kg /m^3)	V_f (%)
T300 carbon / epoxy	555 [1.32]	555 [1.32]	52.0 [1.01]	355 [1.45]	355 [1.45]	621 [1.90]	67 [1.62]	66 [1.60]	1435	56
E-glass / epoxy	525 [3.37]	525 [3.37]	30.1 [2.61]	278 [1.65]	278 [1.65]	725 [5.00]	46 [3.06]	45 [3.00]	1850	51
H4	545 [2.45]	545 [2.45]	49.0 [1.08]	348 [1.58]	348 [1.58]	675 [1.95]	56 [1.72]	55 [1.70]	1610	53
H5	558 [2.48]	558 [2.48]	52.1 [1.10]	359 [1.63]	359 [1.63]	632 [2.00]	67 [1.83]	66 [1.80]	1435	56

The quantities in square brackets indicate % ultimate strain. Strain rate for compressive, tensile and shear loading was 1500 per sec, 400 per sec and 800 per sec, respectively.

Table 5.8 Shear plasticity coefficients (Naik *et al.* 2006, 2008, Ullah *et al.*, 2013)

Parameter	Symbol	E-glass fabric composite	8H carbon fabric composite
Initial effective shear yield stress (MPa)	$\tilde{\sigma}_{y0}$	150	178
Hardening coefficient (Eq. 4 .15 – refer to Section 4.4.4)	C	1125	1039
Exponent (Eq. 4 .15) Eq. 4 .15 – refer to Section 4.4.4)	p	1.05	0.6

5.6 Finite elements and mesh sensitivity

In the rectangular composite plate modelled, each ply was represented by an eight-node solid element C3D8R, with one integration point. Details of this type of element can be found in Section 4.5.

A full 3D model was used instead of a quarter-symmetric model to avoid computational difficulties related to element deletion at the symmetric boundaries. The mesh-sensitivity study is very important in simulations involving high deformations and a non-linear material behaviour. The optimum mesh size was found (Fig 5.4) as a function of the ballistic limit velocity (V_{50}) to allow a reasonable trade-off between a reliable solution and computational resources.

The results converged for the element size of 0.2 mm. Thus, a planar mesh (X-Y plane) of size 0.2 mm × 0.2 mm was employed in the vicinity of the impact area, while a coarser mesh of 1.25 mm × 1.25 mm was used in the area away from the zone of interest (Fig. 5.6) to reduce computing clock time. The nominal thickness of each laminate was 3 mm. As mentioned above, each ply of a laminate had three elements through its thickness. At each ply interface 8-node,

3D cohesive elements of type COH3D8 were embedded and used to model delamination initiation and growth (mesh study is shown in Fig. 5.5), with the failure criterion discussed in Section 5.4. To capture the interface damage growth accurately, a reasonable mesh density is needed. For this purpose, a mesh convergence study for CZEs was performed by developing four FE models of E-glass-fabric reinforced composite with different mesh sizes in the plane ranging from 0.15 mm x 0.15 mm to 0.3 mm x 0.3 mm to capture a damage response under the impact load (projectile velocity = 100 m/s).

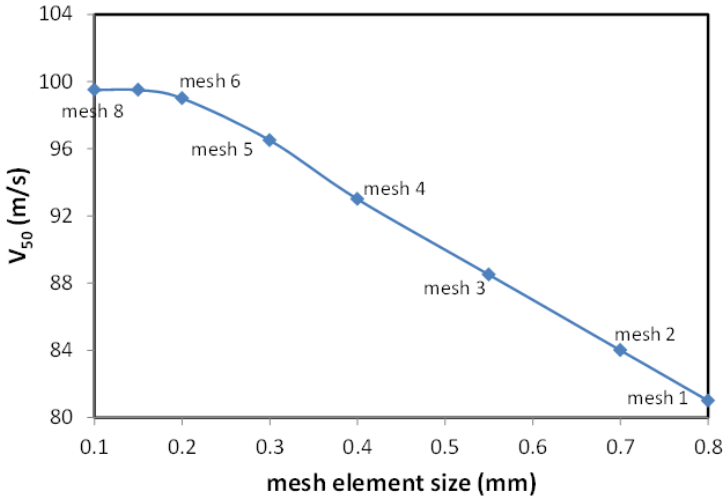

Figure 5.4 Mesh convergence study – ply

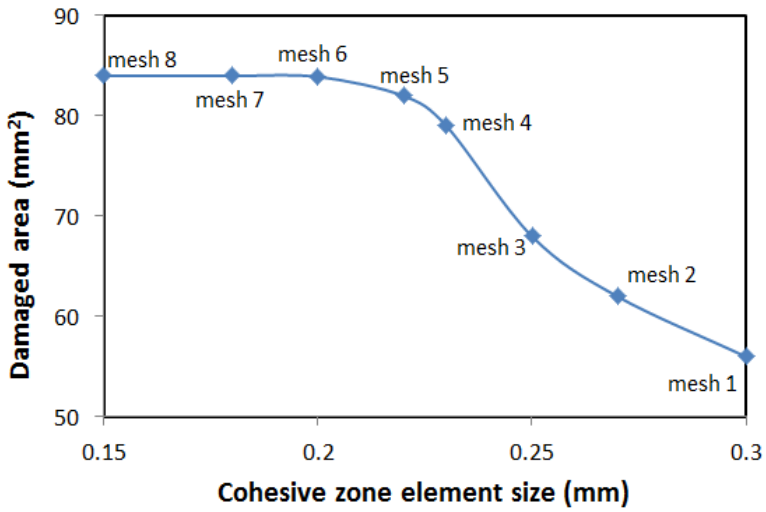

Figure 5.5 Mesh convergence study - CZE

The damaged area at the impact location of the mid layer is plotted against the size of CZEs in Fig. 5.6. Here, mesh convergence was achieved with interface elements of size 0.2 mm x 0.2 mm and 10 μm thickness and selected for simulations in other FE models.

The degradation parameters were set to 0.99, and the failed cohesive elements were removed from the FE model, once the failure criteria were satisfied. Localised stiffness reduction due to internal damage can cause excessive element distortion that could lead to difficulties in numerical convergence. To resolve this numerical issue, distortion control was used in ABAQUS. Damage variables were restricted to a maximum value of 0.999, to retain some residual stiffness in order to avoid numerical instabilities.

5.7 Load, contact and boundary conditions

A schematic of the developed FE model is shown in Fig. 5.2. Both the woven-fabric-reinforced plate and the bullet were modelled as 3D deformable solids. The dynamic explicit solver was used in simulations to account for the time-dependent loading and complex interaction between the target and the projectile.

A 3 mm-thick symmetric cross-ply laminate was modelled. It consisted of 5 plies each with a thickness of 0.32 mm for *C* and 0.28 mm for *G*. The local co-ordinate systems were defined to account for orientations of individual plies. In experimental trials, a cylindrical bullet of mass 6.42 g and length 25.3 mm impacts the centre of the workpiece in the axial direction. This was achieved using a pre-defined velocity boundary condition. Contacts between the bullet and the composite plate and all contacted plies of the laminate were defined by the general contact algorithm available in ABAQUS/Explicit. This algorithm generated the contact forces based on the penalty-enforced contact method. The friction coefficient μ is used to account for the shear stress of the surface traction with contact pressure p and can be represented as $\tau = \mu p$. In this

case, the frictional contact between a bullet and composite laminate was modelled with a constant coefficient of friction of 0.3 (Klinkova *et al.*, 2011). The models require on average 12 hours on 24 Intel quad-core processors with 48 GB RAM each to finish the analysis using the High Performance Computing (HPC) facility available at Loughborough University.

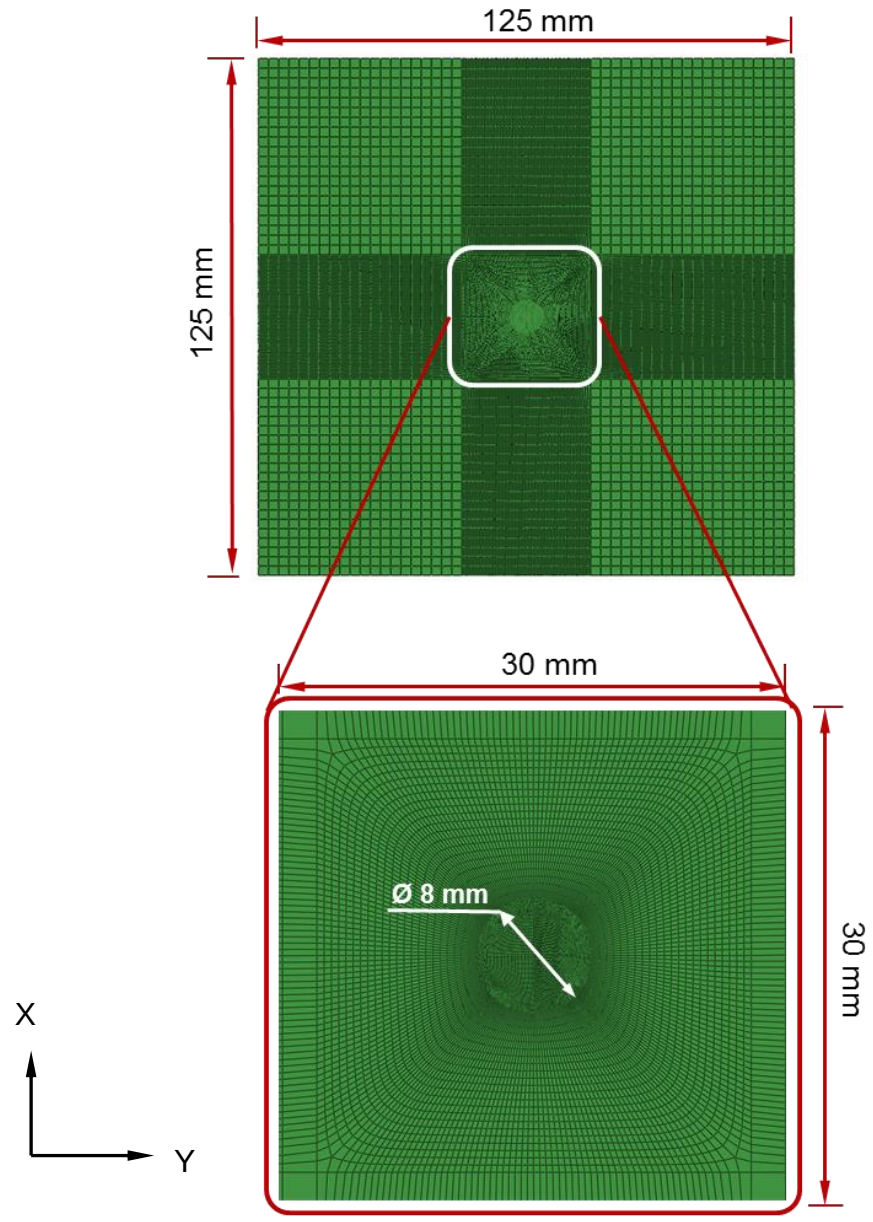

Figure 5.6 Typical meshed specimen in ballistic-impact simulations (t = 3mm)

5.8 Results and discussions

5.8.1 Penetration/perforation studies

The finite-element models of ballistic-impact on studied composite laminates were validated using experimental results that included the ballistic limit velocity (V_{50}) and energy absorbed by a laminate. The ballistic limit velocity (V_{50}) was assessed for the same thickness of laminates, impactor geometry and mass to provide an assessment of their relative ballistic-impact performance.

It should be noted that, though, thickness of all the studied laminates was the same, the areal weight of the underlying fabric materials (E-glass plain-weave and carbon satin-weave) was different. Thus, more viable comparison of their ballistic performance was provided in terms of V_{50} per unit areal weight of the target.

The fracture mechanisms in these laminates were also studied, and the contribution of these to absorption of incident impact energy is discussed below. Secondly, the ballistic-impact resistance of the studied hybrid composite laminates (H4 and H5) was analysed parametrically using the FE model by varying their thicknesses to elucidate the effect of hybridisation. The residual velocity of bullet was also calculated for varying ballistic-impact velocities within this parametric study. These results are discussed next.

5.8.2 V_{50} for same target thickness

In FE simulations, V_{50} was calculated at the reference point R_f tied to a bullet using an equation constraint to reduce the computational efforts. Figure 5.7 presents ballistic limit velocity V_{50} for *G, C, H4* and *H5* composites. It should be noted that each simulation was carried out under similar loading and boundary conditions.

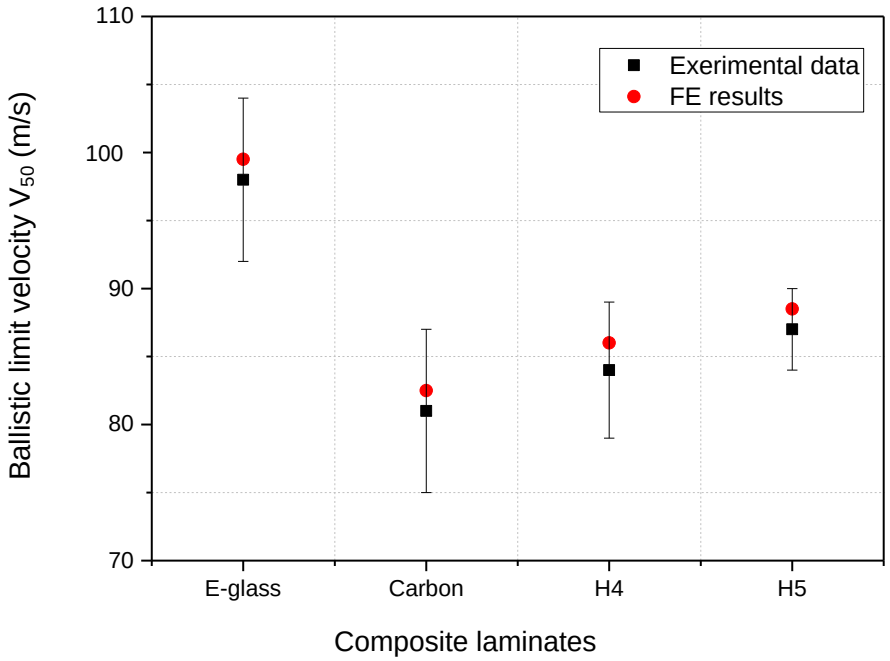

Figure 5.7 Ballistic limit velocity for studied composite laminates for same thickness (projectile mass 6.42 g, projectile length 25.3 mm, target thickness 3 mm)

It was observed that the ballistic limit velocity (V_{50}) had following hierarchy:

Plain-weave E-glass/epoxy G > Hybrid composite H5 > Hybrid composite H4 > 8H satin-weave T300 carbon/epoxy. (18)

It can be observed that V_{50} for *E* is 21% higher than that for the carbon/epoxy composite, while the hybrid laminates exhibited intermediate responses. It was evident from these results that for the hybrid composite laminates, placing glass-fibre layer at the exterior provided better ballistic-impact resistance than that of the inversed lay-up since V_{50} for H5 was 3.6% higher than for H4. Moreover, it should be noted that hybrid composites performed better than the carbon/epoxy composite with the same thickness of the target. It may be argued that the effect of hybridisation resulted in low in-plain strength of a ply when compared to their parent composites, though ultimate strain to failure seemed to be increased.

Later, it was identified that a better assessment of these composites was possible in terms of the ballistic limit per unit areal weight of the laminate, since the areal density of underlying fabric material was different for parent composites. This is discussed next.

5.8.3 V50 for the same areal density of the target

The results obtained for the normalised ballistic limit are shown in Fig. 5.8. It is interesting to note that the hierarchy of the ballistic limit velocity (V_{50}) normalised with the areal density of the target composite laminates is different from that in (18) due to difference in the areal weights of the underlying fabric materials:

8H satin-weave T300 carbon/epoxy > Plain-weave E-glass/epoxy G > Hybrid composite H5 > Hybrid composite H4 (19)

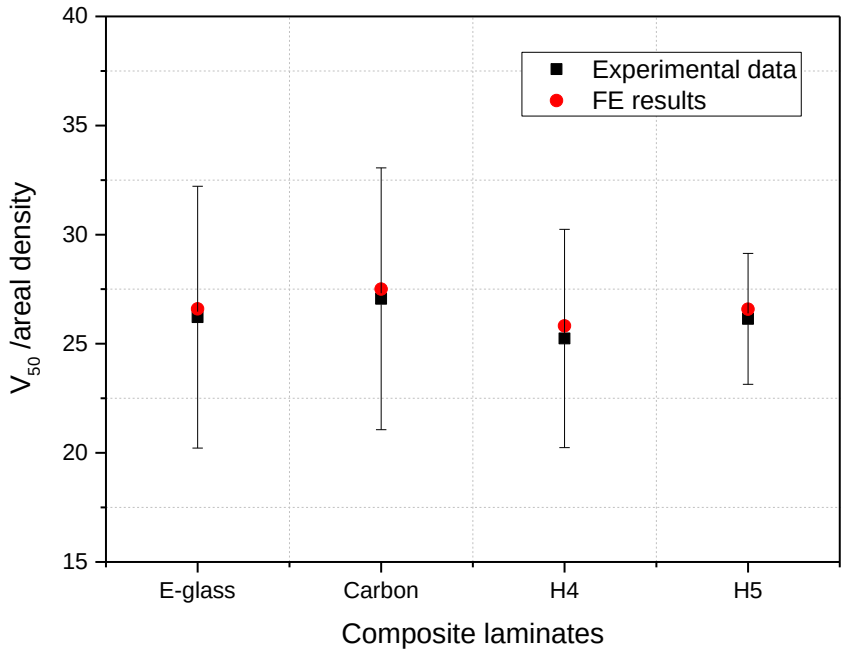

Figure 5.8 Ballistic-impact velocities per unit areal density for studied composite laminate (projectile mass 6.42 g, projectile length 25.3 mm)

Moreover, along the similar line, if the criterion for the ballistic-impact performance of these composites is changed to be ballistic limit velocity/energy absorbed, still another hierarchy different from (18) and (19), was obtained:

Plain-weave E-glass/epoxy G > Hybrid composite H5 > 8H satin-weave T300 carbon/epoxy > Hybrid composite H4 (20)

5.8.4 Fracture mechanisms

Damage assessment in the studied composites laminates subjected to ballistic-impact conditions was carried out using the developed FE model. The strategy adopted for this is discussed next. Three sections perpendicular to the plies of the C, E, H4 and H5 laminate with thickness of 3mm under respective ballistic-limit velocities were taken. They were obtained at various distances from the impact axis in order to attain useful information about the fracture processes when the laminate was subjected to different deformation levels: at distance 8 mm (1) 4mm (2) from the impact axis and at the impact axis (3) shown in Fig. 5.9.

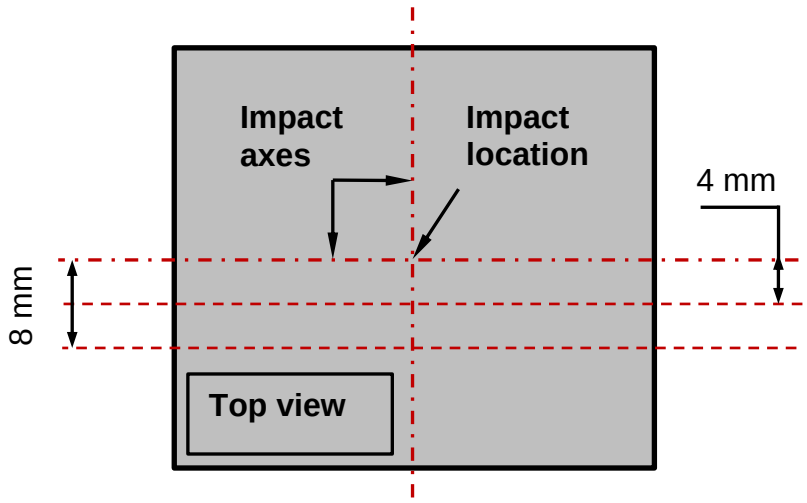

Figure 5.9 Schematic showing locations of sections cut in laminate

The damage mechanism in G and C laminates was observed to be similar, though overall damage at the front and back face of G was more pronounced than that of C due to low stiffness of glass-fibre plies (Fig. 5.15 A and B). The damage mechanism for C is discussed here.

At cross-section away (i.e., at 8 mm) from the impact axis, damage was observed in the form of tensile fracture of the back plies (Fig. 5.10). Intra-ply cracks formed at the back plies propagated through the lamina until they were deflected at the interply interface, and delamination progressed until interply cracks were deflected by matrix cracking in the upper plies. In this case the damaged zone was larger near the back plies.

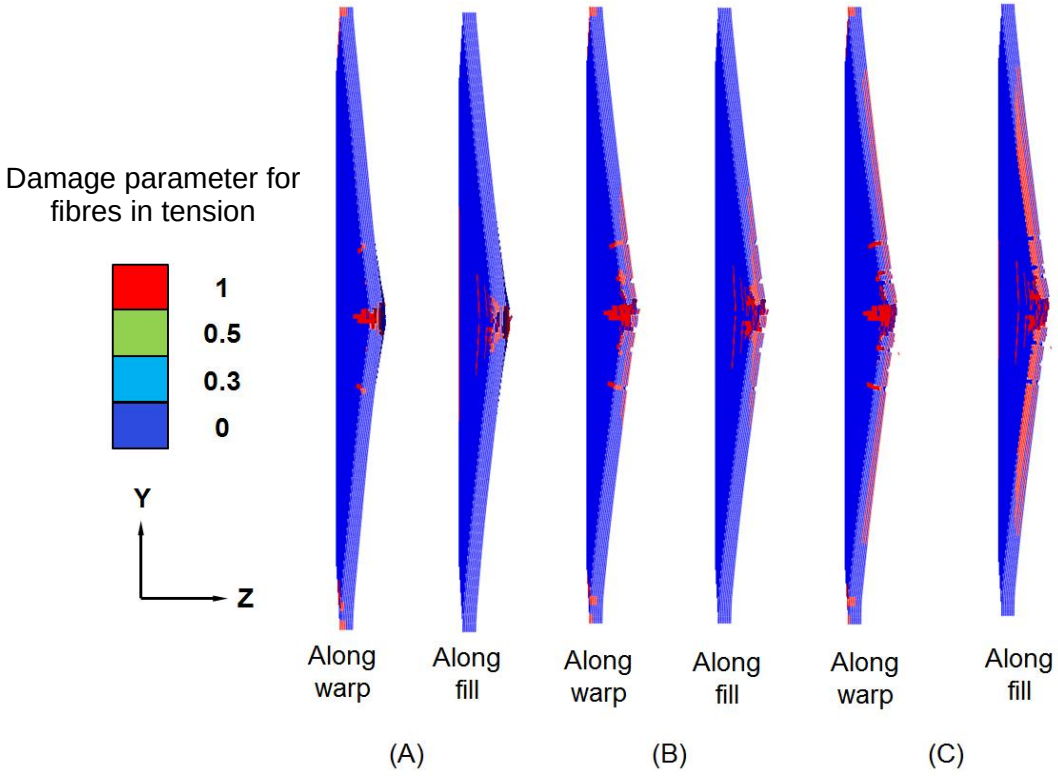

Figure 5.10 Fibre damage in tension for 8H satin-weave carbon/epoxy panel (t = 3 mm, V_{50} = 82.5 m/s) in different cross-sections: (A) 8 mm from impact axis; (B) 4 mm from impact axis; (C) at impact axis

The section of laminate at 4 mm from the impact axis (Fig. 5.11B) showed extensive damage near the back plies caused by delamination and intraply fracture since the stiff carbon plies were not able to withstand large strains induced by the impact.

The section located just below the impactor (Fig. 5.11C) showed formation of a crack developing through the laminate's thickness as a result of coalescence of interply cracks generated in the front and back plies. The conical shape of the damaged region was also evident in the section (Fig. 5.12).

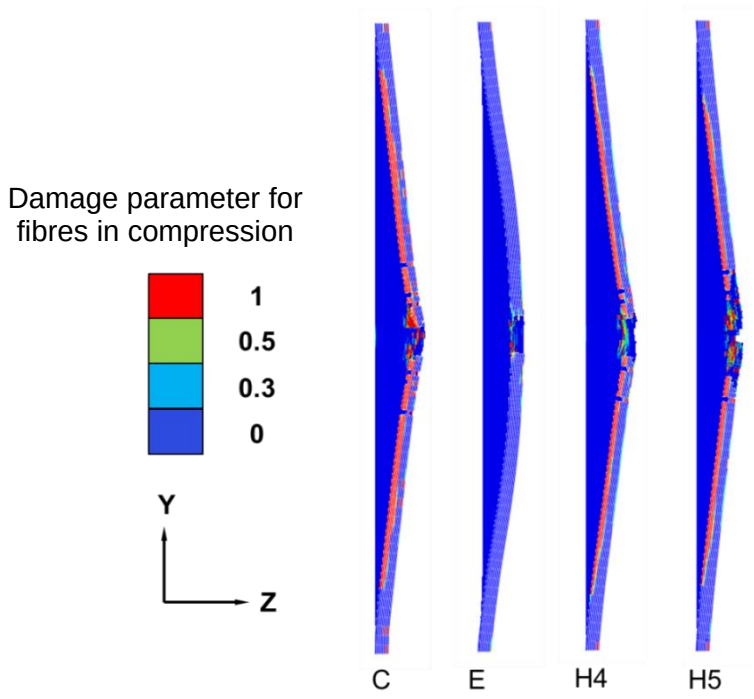

Figure 5.11 Fibre crushing damage in front plies of studied laminates at their respective V_{50} velocities [G - plain-weave E-glass/epoxy composites (V_{50} = 82 m/s); C - 8H satin-weave T300 carbon/epoxy composites (V_{50} = 99.5 m/s), H4 - Hybrid H4 (V_{50} = 86 m/s), H5 - Hybrid, H5 (V_{50} = 88 m/s), (laminate thickness = 3mm)]

In addition, failure by crushing was seen in the front plies. The intraply cracks generated by crushing were deflected at the interfaces and led to the development of interface cracks between the upper plies (Fig. 5.11). Damage

was, however, more localized near the front plies and the overall damaged zone had a conical shape.

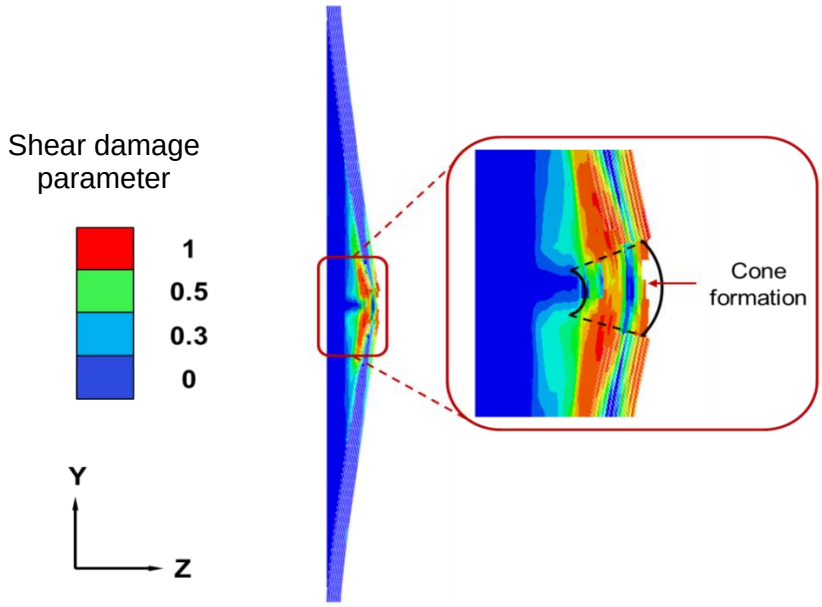

Figure 5.12 Shear damage in E-glass/epoxy composite and cone formation (t = 3mm, V_{50}=99.5 m/s)

(A) Effect of hybridisation on damage mechanism

Hybridisation of *G* and *C* laminate could possibly give a rise to either improved or reduced material properties. This would depend significantly on the position of these plies within a laminate as discussed in Sections 5.8.2 and 5.8.3.

In case of *H4* (hybrid laminate with exterior *G* plies), the dominant damage processes were the same as found in *C* and *G*, namely, tensile fracture of the back plies and crushing of the front plies under the impactor. The intraply cracks in the front and back plies grew upwards and downwards, respectively, leading to development of delamination cracks, and final fracture took place by formation of a crack through the laminate thickness (Fig. 5.12).

However, the amount of damage at the back face of *H4* laminate was far lower than in *G* and moderately less than in *C* under equivalent impact conditions

(Figs. 5.14 (A), (B) and (C)). Damage initiated due to intraply fracture at the back plies while delamination was localized in the carbon plies as E-glass plies were able to hold the laminate together. Fracture of the laminate only began when the E-glass plies were finally broken by shear similar to its parent composite, *E* (Fig. 5.12). The higher level of strain to failure of the E-glass plies thus helped to sustain higher deformations before laminate's fracture by percolation of a through-thickness crack and resulted in the improved load-bearing capability of the composite. In addition, the E-glass plies failed at higher strains than the carbon ones and absorbed more energy, significantly improving energy dissipation under impact. It should be noted that the higher deformability of the E-glass plies also inhibited propagation of interface cracks. These differences were not caused by changes in the interply toughness (which was mainly controlled by the epoxy properties) but were also a consequence of higher deformability of the E-glass plies. In the absence of cracking, delamination did not develop between *C* and E plies while intraply cracks in the *C* plies acted as stress concentrators, which promoted delamination between the *C* plies.

Extensive delamination between the *C* plies did not enhance the overall energy dissipation, and, hence, the contribution of intraply failure to the total energy dissipated was far higher than that provided by interply delamination. In this respect, the location of the glass fibre plies (near to but not on the front and back laminate's surfaces) helped to increase the laminate's performance in impact. The maximum load was controlled by fracture of the carbon ply at the back, though intraply cracks did not propagate into the laminate but were stopped at the E-glass ply, and a similar process occurred with cracks formed by crushing on the front ply (Fig. 5.11). In addition to stopping the intraply cracks, the glass-fibre plies accommodated the impact deformation, and the inner carbon plies in the hybrid composite did not fail at low strains although they experienced extensive delaminations to accommodate the deformation of the glass-fibre plies. This behaviour is in contrast with the brittle behaviour of

the composites without glass-fibre plies, in which extensive ply cracking was observed away from the impact axis (Fig. 5.11 A and B).

On the other hand, in case of *H5* (the hybrid laminate with *C* plies at the exterior), apart from ply fracture at the back and crushing at the front, large deformation in the stiff carbon plies led to extensive delamination and intraply fracture that grew rapidly towards the back. Ply fracture due to crushing at the front also accelerated this process resulting in greater damage on the back face of *H5* (Fig. 5.14 (D)).

Variations in the laminate thickness did not alter the dominant deformation mechanisms, although the volume of the conical damage zone increased with the thickness and the corresponding energy dissipated increased accordingly. Damage patterns obtained at the front and the back face of studied composite laminates are shown in Fig 5.14. Damage was visible on the either faces of the composite panels and was measured along both warp (l_{dw}) and fill (l_{df}) directions from the centre of specimens where they were impacted (refer Figs. 5.13 a and b) and compared with those obtained from FE analysis (Fig. 5.15).`

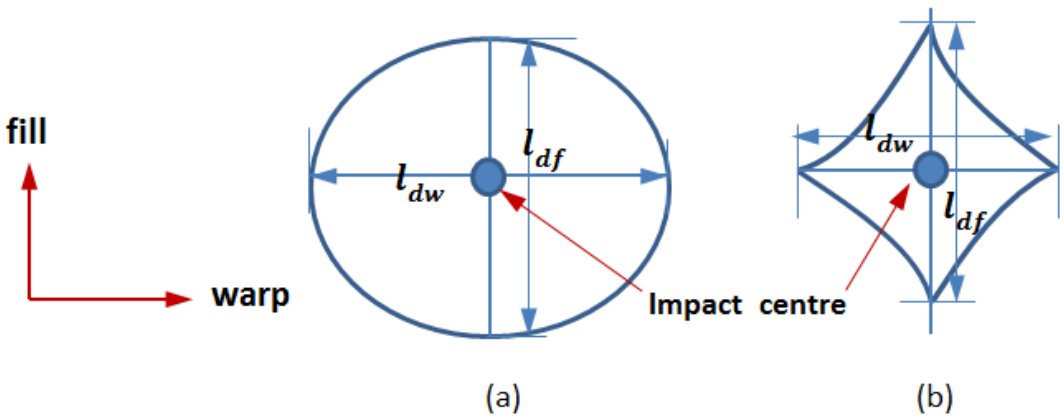

Figure 5.13 Schematic showing measurement of damage on the faces of composite panels: (a) a typical damage pattern for e-glass/epoxy based woven fabric composites (b) a typical damage pattern for carbon/epoxy based woven fabric composites

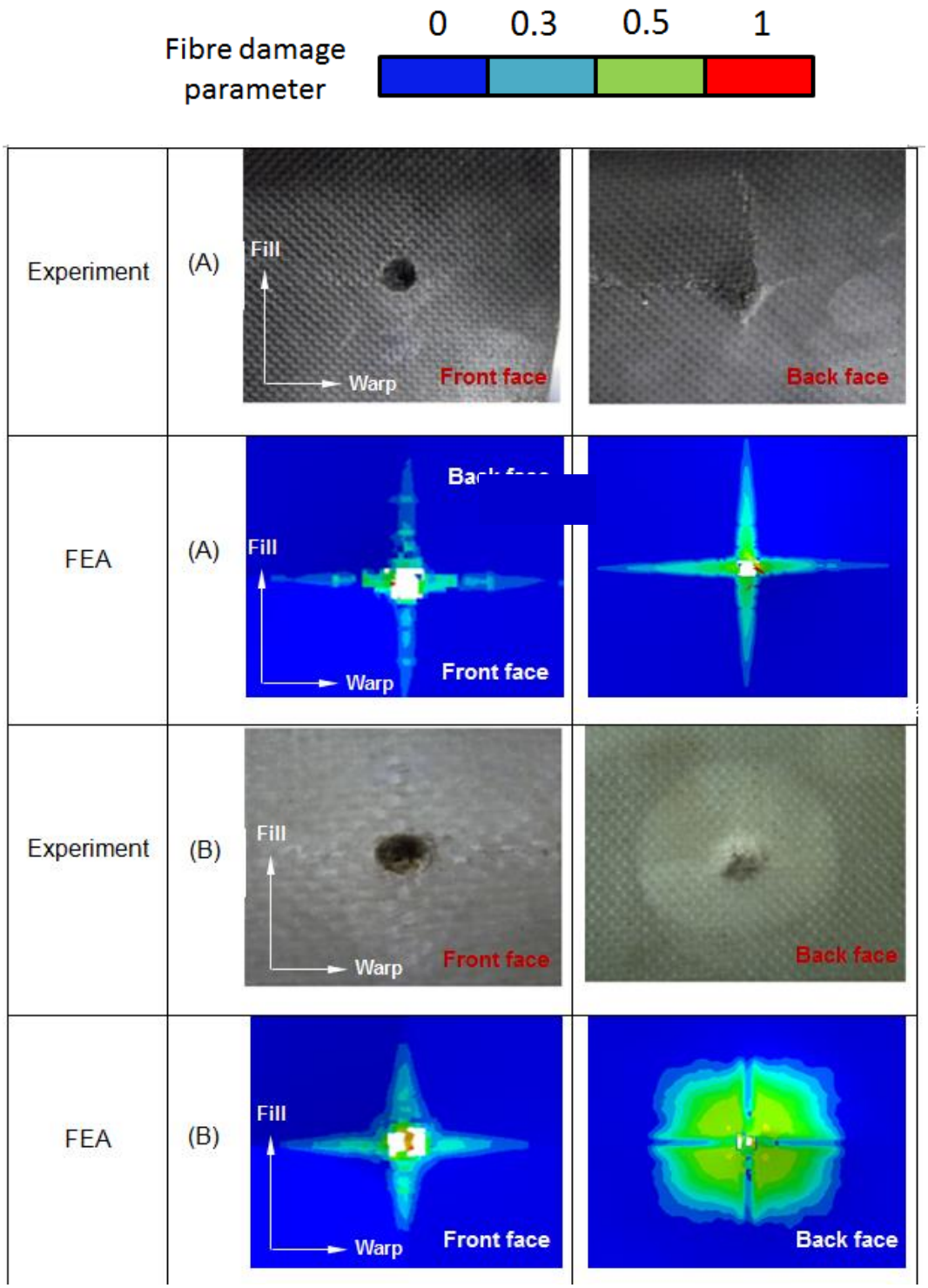

Figure 5.14 Damage patterns on the front and back faces of composite panels: (A) 8H satin-weave T300 carbon/epoxy composites (V_{50} = 99.5 m/s) (B) Plain-weave E-glass/epoxy composites (V_{50} = 82 m/s) (laminate thickness = 3mm)

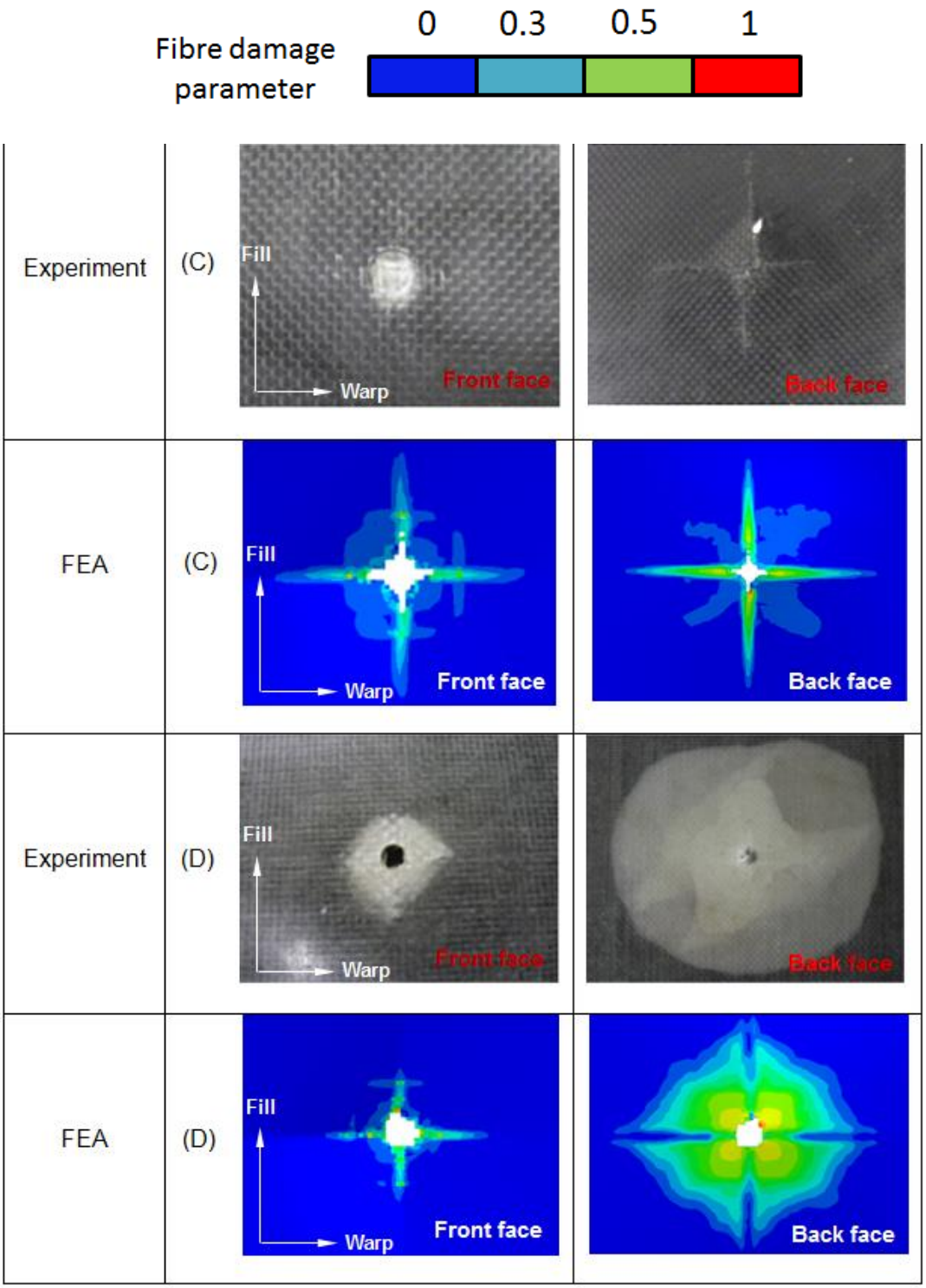

Figure 5.14 Damage patterns on the front and back faces of composite panels: (C) Hybrid H4 (V_{50} = 86 m/s) (D) Hybrid, H5 (V_{50} = 88 m/s) (laminate thickness = 3mm)

It can be observed that extent of damage in plain-weave E-glass/epoxy composite is more than that of carbon/epoxy composite laminate on both front and back faces.

This may be explained by the ductile nature of glass-fibres undergoing strain-hardening that allows damage to grow beyond the region of impact absorbing more energy. On the other hand, brittle carbon fibres restrict the damage growth in the laminate to a relatively localised region. This effect can also be observed in the hybrid composite laminates, where *H5* exhibits pronounced damage growth compared to *H4*. The results of FE simulations demonstrated that damaged area of the back face of the E-glass/epoxy composite consisted of two distinct regions, with the quasi-circular contours where severity of damage reduced towards the outer region. In case of carbon/epoxy composites, the cracks were seen along the warp and fill directions on both front and back surfaces.

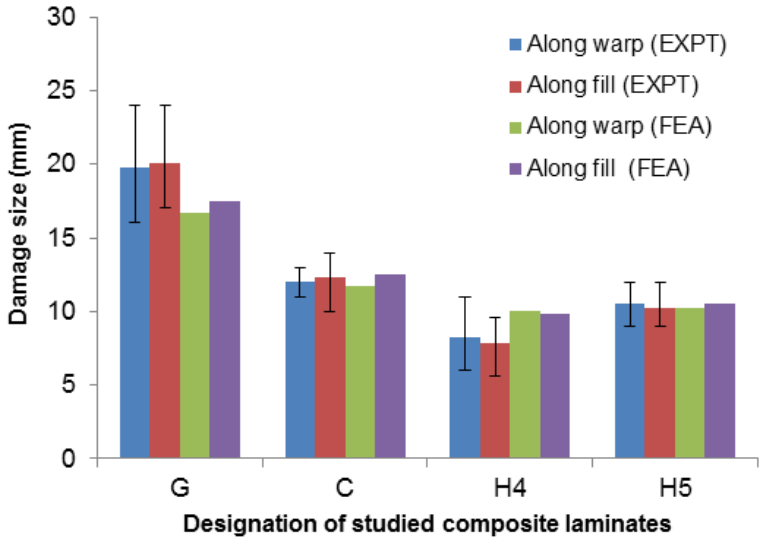

Figure 5.15 Damage size for studied composite laminates at their front face [G - plain-weave E-glass/epoxy composites (V_{50} = 82 m/s); C - 8H satin-weave T300 carbon/epoxy composites (V_{50} = 99.5 m/s), H4 - Hybrid H4 (V_{50} = 86 m/s), H5 - Hybrid, H5 (V_{50} = 88 m/s), (laminate thickness = 3mm)]

The petalling process was also observed at the back face. A damage pattern for *H5* was similar to that in the E-glass/epoxy laminate, though damage at the back face was more severe. The damage pattern in the *H4* laminate was like that in the carbon/epoxy laminate, though its intensity was lower. The size of these damage patterns are compared in Figs. 5.15 and 5.16.

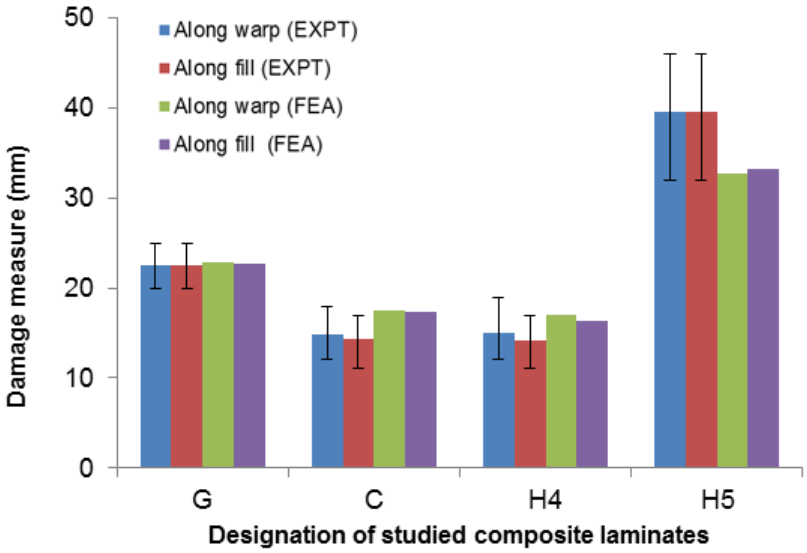

Figure 5.16 Damage size for studied composite laminates at their back face [G - plain-weave E-glass/epoxy composites (V_{50} = 99.5 m/s); C - 8H satin-weave T300 carbon/epoxy composites (V_{50} = 82 m/s), H4 - Hybrid H4 (V_{50} = 86 m/s), H5 - Hybrid, H5 (V_{50} = 88 m/s), (laminate thickness = 3mm)]

(B) Contribution of damage modes to the energy absorption

Ballistic-impact is a low-mass, high-velocity impact phenomenon, and its effect on the target structure is highly localised as the contact duration between the projectile and target structure is very small. During this event, kinetic energy of the projectile is transferred to the target, in this case - a composite laminate that absorbs this energy through permanent deformation accompanied by various damage mechanisms such as matrix cracking, delamination and fibre failure as discussed earlier. The contribution of these mechanisms towards the total energy absorbed by a laminate is critical for the improved design of structures

and explained here with the example of plain-weave E-glass/epoxy composite system with ballistic impact velocity (V_{50}) of 101 m/s, where partial penetration of target structure was observed.

The total kinetic energy (E_{TOTAL}) of the projectile lost during ballistic impact is the total energy absorbed by the target and is given by,

$$E_{TOTAL} = E_{KE} + E_{DE} + E_{DL} + E_{MC} + E_F, \tag{21}$$

Where E_{KE} is the kinetic energy of the projectile, E_{DF} is the energy absorbed due to the deformation of yarns, while E_{DL}, E_{MC} and E_F are the energies absorbed in delamination, matrix cracking and fibre failure.

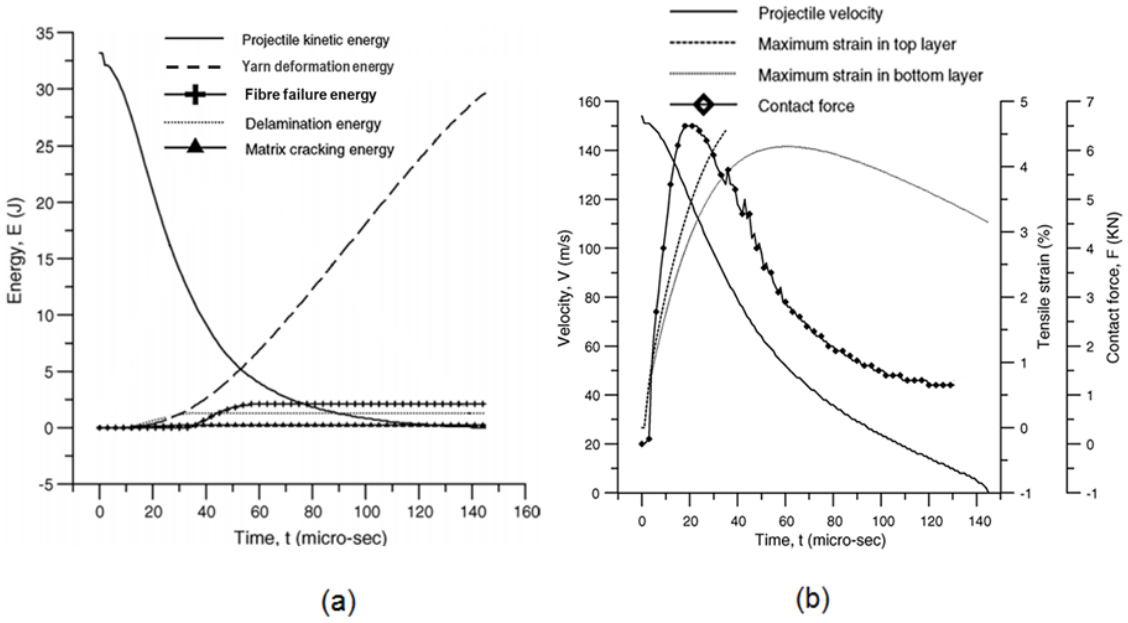

Figure 5.17 (a) Energy absorbed during ballistic event (b) Projectile velocity, strain and contact force variation - V_i = 100 m/s, plain-weave E-glass/epoxy laminate thickness = 3 mm, projectile diameter, dp = 6.36 mm

For V_i = 100 m/s as shown in Figs. 5.17 a and b, the maximum strain in the bottom layer is lower than the ultimate strain limit. Hence, the lower layers do not fail and kinetic energy of the projectile is zero at the end of ballistic impact

event. A significant portion of projectile's kinetic energy is absorbed due to the deformation of the secondary yarns (here, yarns directly below the projectile are termed as the primary yarns, while those away from the impacted region are termed as secondary yarns). The energy absorbed due to deformation of secondary yarns has two components: strain energy stored within the secondary yarns and the energy absorbed because of possible matrix cracking and delamination. After the projectile velocity reaches to zero, projectile may rebound from the target owing to the release of strain energy stored in the secondary yarns. This energy would be converted into kinetic energy of the projectile. Some energy is absorbed in the form of yarn/fibre tensile failure (E_F). In this particular case, layers in the upper half have failed in the form of fibre tensile failure. Layers in the lower half have not failed, while the energy absorbed due to matrix cracking (E_{mc}) and delamination (E_{DL}) is marginal. It should be noted that in FE analysis of ballistic impact events, these energy outputs were requested by selecting sets of elements pertaining to a particular damage mode (e.g. delamination- set of all cohesive elements; matrix cracking and fibre failure – set of elements where damage criteria met); while the contact force was calculated at the contact between the projectile and plate surface using a reference point (R_f) tied to the projectile where impact velocity was applied.

Next, kinetic energy of the projectile absorbed by the composite laminates during ballistic-impact at their V_{50}s is plotted against the duration of this event (Figs. 5.18 a-d). It should be noted that all these laminates were partially penetrated just enough to arrest the motion of a projectile. These show contribution of different damage modes in absorbing kinetic energy of projectile.

The trends of energy absorption mechanisms in studied laminates are quite similar to each other, where a majority of incident kinetic energy was absorbed due to the deformation of secondary yarns, while energy absorption due to primary yarn/fibre failure was relatively low and that due to matrix cracking and

delamination was marginal. It may be explained owing to the highly transient nature of this event (contact time between projectile and target ~150 microns) and highly localised deformation of target, where damage initiates in the form of fibre failure directly below the projectile and has hardly any time to diffuse through the laminate before projectile penetrates through it.

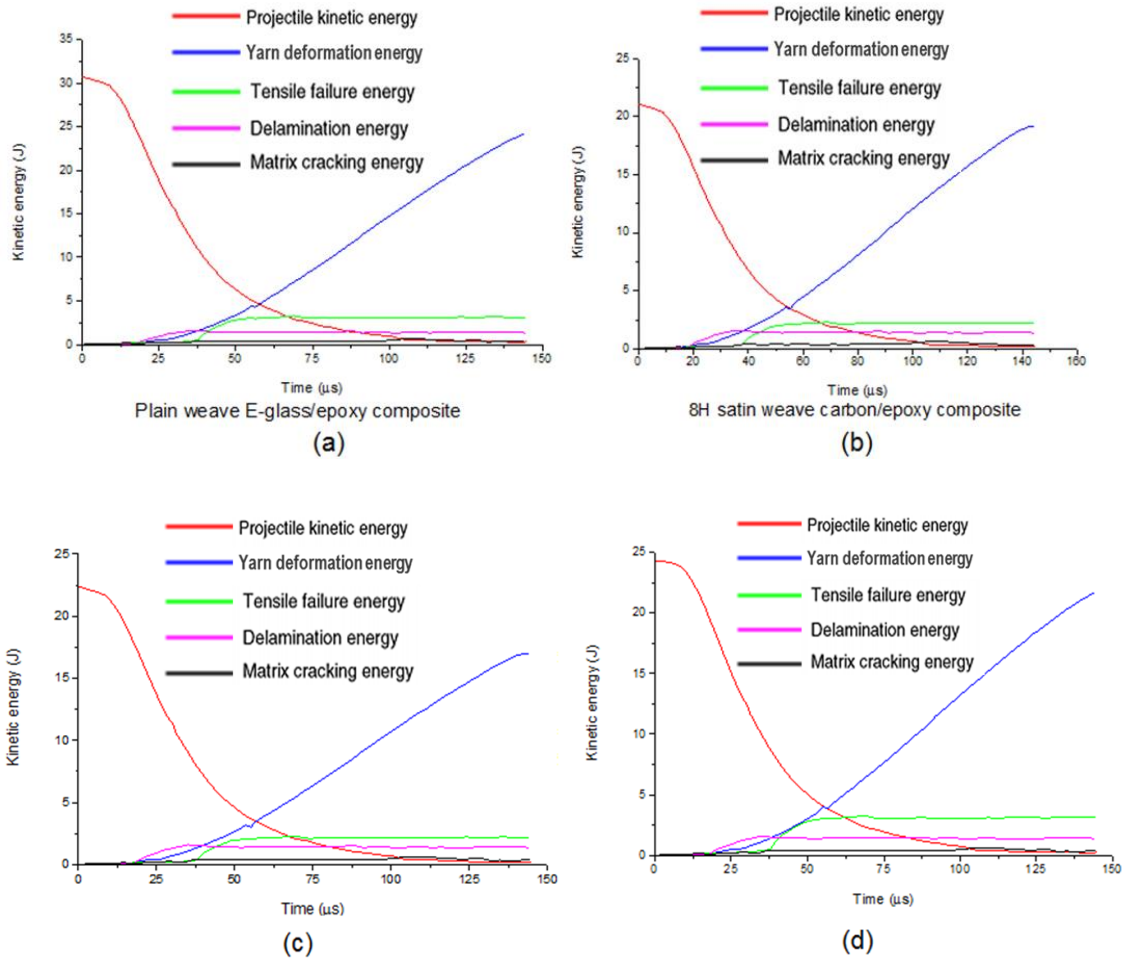

Figure 5.18 Contribution of damage modes to kinetic energy absorption - (a) plain-weave E-glass/epoxy composite (V_{50} = 99.5 m/s); (b) 8H satin-weave carbon/epoxy composite (V_{50} = 82 m/s); (c) hybrid composite H4 (V_{50} = 86 m/s); (d) hybrid composite H5 (V_{50} = 88 m/s), laminate thickness = 3 mm

These results support the argument made in Section 5.8.4 (A) that the contribution of intraply failure to the total energy dissipated was significantly higher than that provided by delamination.

5.9 Parametric study

It is interesting to study the ballistic-impact behaviour of hybrid composite laminates under varying parameters such as their thickness, mass and geometry of projectile to further analyse effects of their hybridisation. This is discussed next.

5.9.1 Effect of laminate thickness

During impact, stress waves travel in all the directions within the target structure. For thin laminates, this effect is not dominant along the thickness direction. However, if their thickness is increased, a stress-wave-induced deformation behaviour would be different at different locations along the thickness direction. It is normally observed that the damage in thick laminates show a pine-tree-like pattern compared to an inverse pine-tree damage pattern observed in thin laminates (Abrate, 2011), as shown in Figs. 5. 20a and b which was also observed during simulations.

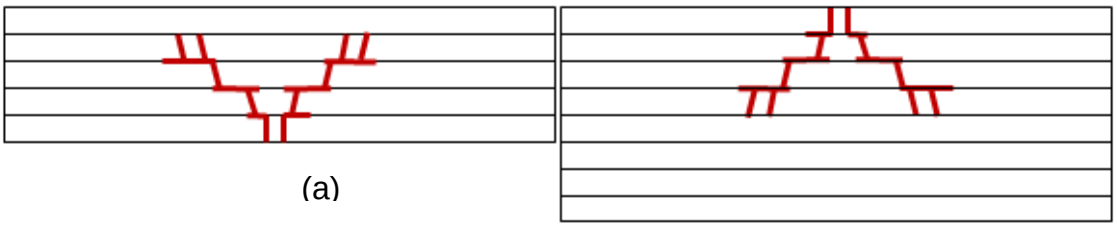

Figure 5.19 Damage patterns: (a) thin laminate (inverse pine-tree damage pattern); (b) thick laminate (pine-tree damage pattern) (Abrate, 2011)

Different energy-absorbing mechanisms would be observed including compression of the target directly below the projectile, reverse bulge formation

on the front face, friction between the projectile and the target, shear plugging, delamination and matrix cracking.

These mechanisms may depend on many parameters such as projectile size, shape, its mass and velocity as well as target material's properties, geometry and its potential area under impact. Here, this effect was analysed by varying the thickness of *H4* and *H5* laminates from 3 mm to 10 mm for the same projectile mass and diameter. The corresponding ballistic limit velocities are plotted against the target thicknesses in Fig. 5.21.

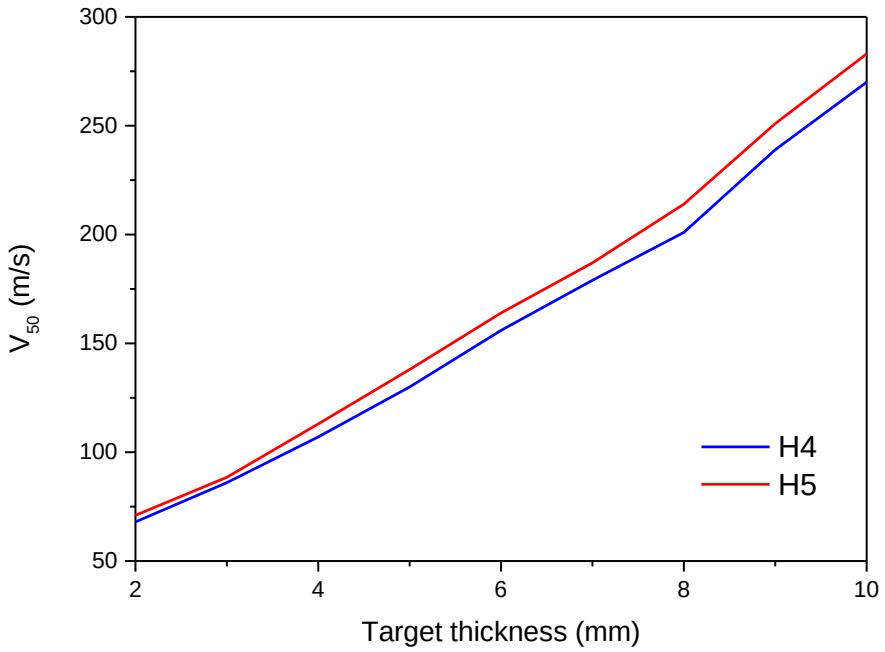

Figure 5.20 Effect of target thickness on V_{50}

5.9.2 Incident impact velocity

Residual velocity (V_R) of a projectile as a function of the incident ballistic-impact velocity is presented for the H4 and H5 laminates in Fig. 5.22. Previous simulation parameters employed here e.g. laminate thickness; mass and geometry of projectile were maintained.

The ballistic limit velocity for *H4* is 86 m/s (Fig. 5.8). This indicates that complete perforation would not take place until the projectile's incident velocity reaches this magnitude. It was noted that the residual velocity increased linearly till certain extent (till the impact velocity of 88 m/s for H4 and 92 m/s for H5 – Fig. 5.22) with the ballistic-impact energy, though interestingly enough; just after this, this increase is steeper and not linear.

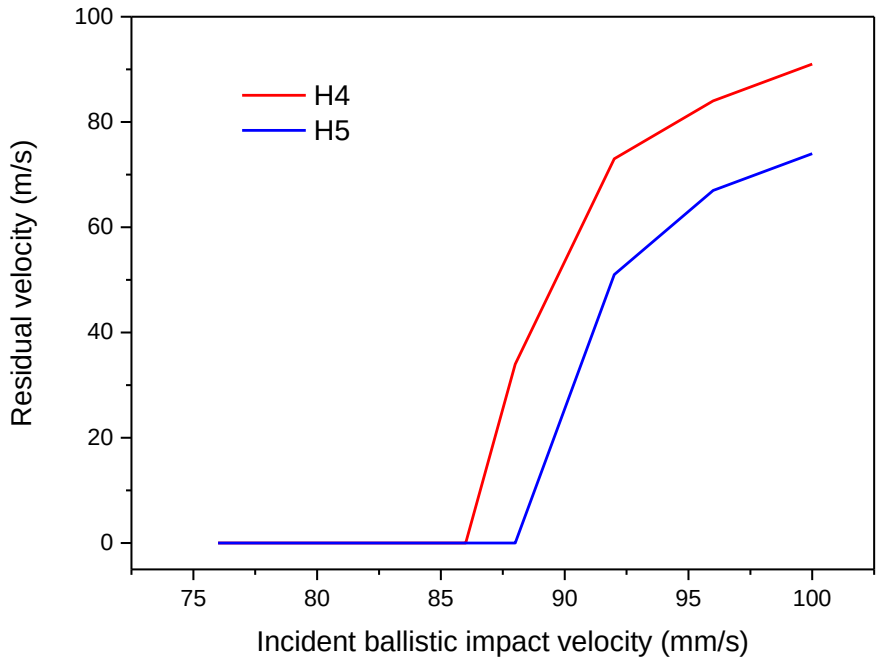

Figure 5.21 Effect of incident impact velocity on the residual velocity of a projectile for same target thickness

For example, until the incident velocity of 88 m/s, no penetration was observed, though at 88 m/s, laminate was fully penetrated and projectile emerged with the residual velocity of 35 m/s.

5.10 Summary

A ballistic-impact response of four woven fabric composite laminates *E, G, H4* and *H5* was studied using the developed finite-element model. Their ballistic-impact response was characterised in terms of limit velocities (V_{50}) for the same

thickness. Further comparison of V_{50} was facilitated for the unit areal density to obtain a more precise solution. Damage modes in these laminates were also studied. The effect of hybridisation on damage modes and their contribution to energy-absorption capacity of a laminate was also discussed. The FE model successfully captured the global response, e.g. (V_{50}), as well as local one (damage) both quantitatively and qualitatively. Some fundamental observations based on this study are listed below.

- The ballistic-impact velocity (V_{50}) was highest for *E* and lowest for *C*, while it was of intermediate magnitude for hybrids *H4* and *H5* for the same laminate thickness. This hierarchy was not maintained when their performance was analysed based on the same areal density of laminates. In that case, C had better impact resistance; while *H4* performed the worst.
- The main deformation and damage mechanisms of the studied hybrid laminates were independent of the presence of glass fibres. The maximum load carried by the composite was controlled by tensile fracture of the back carbon ply of the laminate subjected to bending and increased with its thickness. In addition, intraply fracture by crushing below the impactor was also initiated in the front plies. Intraply cracks formed in the front and back plies propagated through the lamina until they were deflected at the interply interface.
- Delamination progressed until interply cracks were deflected by matrix cracking into upper or lower plies. The final damage zone presented a conical shape and the overall energy dissipated by each material scaled with the volume of damaged material.
- Improvements in the behaviour under impact by hybridization were due to the higher strain to fracture of the E-glass-fibre plies located near the front and back laminate surfaces. These plies were able to sustain higher deformations before fracture and hindered propagation of damage to the inner plies from the broken plies on the front and back surfaces,

increasing the maximum load-bearing capability of the composite. Thus, it may be claimed that the hybridisation provided a reasonable trade-off between in-plain strength and failure strain that resulted in better ballistic-impact resistance properties compared to high-modulus fibre-reinforced composites. In addition, the presence of E-glass fibres helped to sustain higher deformations before laminate fracture by the percolation of a through-thickness crack, significantly improving the energy dissipated under impact. Most of the benefits of the E-glass fibre could be attributed to the plies located near the laminate surfaces. The presence of inner plies provided more limited improvements, particularly in terms of specific properties.

Next chapter presents the finite-element study on blast response of curved CFRP panels. A comparative study is performed where the effect of panels' curvature on their blast mitigation properties is studied.

CHAPTER 6

MODELLING BLAST RESPONSE OF CURVED CFRP PANELS

6.1 Introduction

Controlled and accidental explosions or detonations cause huge intensity dynamic loading on structures in the immediate vicinity of the event. Thus it becomes imperative to critically assess the blast resistance of structures which may not have been designed to resist explosions, such as, crucial civilian as well as governmental and defence buildings and structures.

It is no surprise that in recent years FRP composites, especially CFRP composites subjected to blast loading has drawn the attention of the research community (Rajendran and Lee, 2002; Tekalur *et al.*, 2008; Arora *et al.,* 2011; Kumar *et al.* 2012; Ochola *et al.*, 2004; LeBlanc and Shukla, 2011, Mohamed *et al.*, 2012) CFRP composites are widely used in protective structural applications, often retrofitted to existing structures to improve its resistance to blast. This is primarily due to their excellent mechanical properties such as high strength-to-weight ratio, durability and high impact resistance.

Composite structures need not be limited to flat geometries with several applications requiring curved geometries, such as, the use of composites shells in submarine hulls (Mohamed *et al.*, 2012; LeBlanc and Shukla, 2011). Effect of curvature of these structures on their blast mitigation properties has been the subject of interest of some studies (Tekalur *et al.*, 2008; Arora *et al.,* 2011; Kumar *et al.* 2012; Ochola *et al.*, 2004; LeBlanc and Shukla, 2011, LeBlanc *et*

al., 2007),only the most relevant studies are mentioned here. Rajendran and Lee (2009) conducted a detailed review of the phenomena of air blast explosions and their effects on plane plates. They found that the peak overpressure and the impulse generated during blast were the parameters that affected the mechanical behaviour of these plates. Tekalur *et al.* (2008) analysed the effect of different fibres reinforced in the epoxy based composite panels on their blast response. They used two different fibre materials: E-glass and carbon, and exposed those composite panels to high strain rates and quasi-static loading. Under dynamic loading, the carbon-fibre composites showed catastrophic failure, while E-glass-fibre composites exhibited progressive damage behaviour. Arora *et al.* (2011) studied a blast response of glass-fibre sandwich composite panels fixed at their edges and exposed to real explosives at varying stand-off distances. They used high-speed photography and digital image-correlation (DIC) analysis to characterise the blast response of these panels. Damage was observed to initiate in the form of a crack in the front skin, leading to localised delamination around the cracked region and shear-induced failure at the core. Interfacial failure between the front skin and the core was also observed. This analysis also involved a finite-element study to verify experimental observations such as transient boundary conditions. Recently, Kumar *et al.* (2012) reported the effect of transient boundary conditions in their study, where the dynamic response of curved CFRP panels was analysed using high-speed photography and 3D DIC technique followed by a post-mortem analysis. They found that curvature had a profound effect on the blast response of the CFRP panels. Ochola *et al.* (2004)] reported on strain-rate sensitivity of CFRP and glass fibre-reinforced polymer (GFRP) composites by testing a single-laminate configuration with a strain-rate varying from10^{-3} s^{-1} to 450 s^{-1}. The results showed that dynamic material strength for GFRP increased with the increasing strain rate while the strain to failure for both CFRP and GFRP decreased. LeBlanc and Shukla (2011) analysed the blast response of

curved composite panels with the aim to study the energy distribution during this event.

In this chapter, a dynamic response of quasi-isotropic CFRP panels with three different radii of curvature exposed to blast loading was studied. A shock tube was employed to impart blast load on these panels. A real-time analysis was carried out using the 3D DIC technique to measure the out-of-plane deflection on the back face of these panels. A finite-element (FE) model of blast response of these panels was developed in ABAQUS 6.11 and validated using the experimental findings. The FE model was further utilised to suggest the optimal panel curvature of studied composites to improve their blast resistance.

6.2 Experimental details

6.2.1 Material and specimen

Panels with three different radii of curvature (Fig. 1) were utilized in the experiments: infinite (i.e. flat; Panel A), 304.8 mm (Panel B) and 111.8 mm (Panel C).

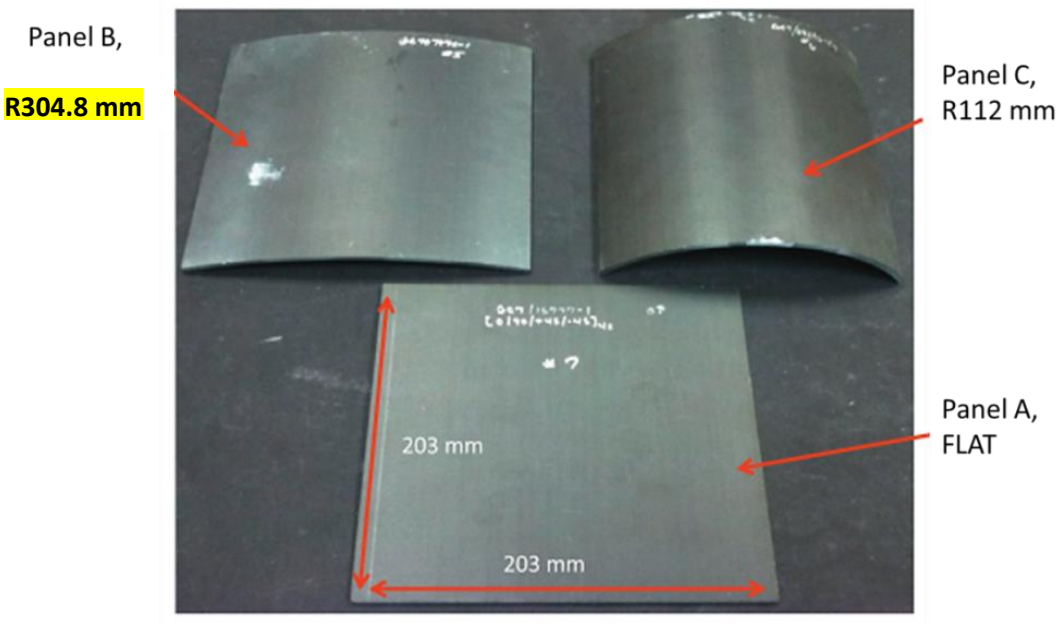

Figure 6.1 Specimen geometry (Kumar *et al.*, 2013)

The specimens were fabricated using unidirectional AS4/3501-6 prepreg (fibre volume fraction of 60%) manufactured by the Hercules Corporation of Magna, Utah. The stacking sequence of this composite laminate was selected to have quasi-isotropic properties ($[0^0/90^0/+45^0/-45^0]_{4s}$). The specimens were 203 mm × 203 mm × 2 mm in size, made out of 32 layers of unidirectional (UD) plies. For the curved panels, arc lengths of curved edges correspond to the plate length of 203 mm.

6.2.2 Shock loading apparatus and loading conditions

In experiments, blast load can be imposed onto a structure using two different methods – either by the controlled detonation of explosives or with the use of shock tubes. The use of real explosives is dangerous and produces spherical wave fronts and pressure signatures, which are spatially complex and difficult to measure. On the contrary, a shock-tube offers the advantage of planar wave fronts so that wave parameters may be easily controlled. Furthermore, the loading conditions are easy to replicate from a finite-element modelling point of view. Thus, the shock-tube apparatus was the preferred choice in the application of the blast load in our experiments. The shock-tube apparatus used in this study and locations of pressure transducers are shown in Figs. 6.2a and b respectively. The shock tube consisted of a long rigid cylinder divided into a high-pressure driver section and a low pressure driven section separated by a diaphragm. Helium (He) was found to be the most suitable inert gas to replicate blast loading conditions and also offered the advantage of repeatability. A driver section of a shock tube was pressurised by the gas flow that created a pressure difference across a diaphragm. When this pressure difference reached a critical value, it ruptured the diaphragm. This resulted in a rapid release of gas creating a shock wave that travelled down the shock tube and ultimately imparted a blast load on the composite laminate.

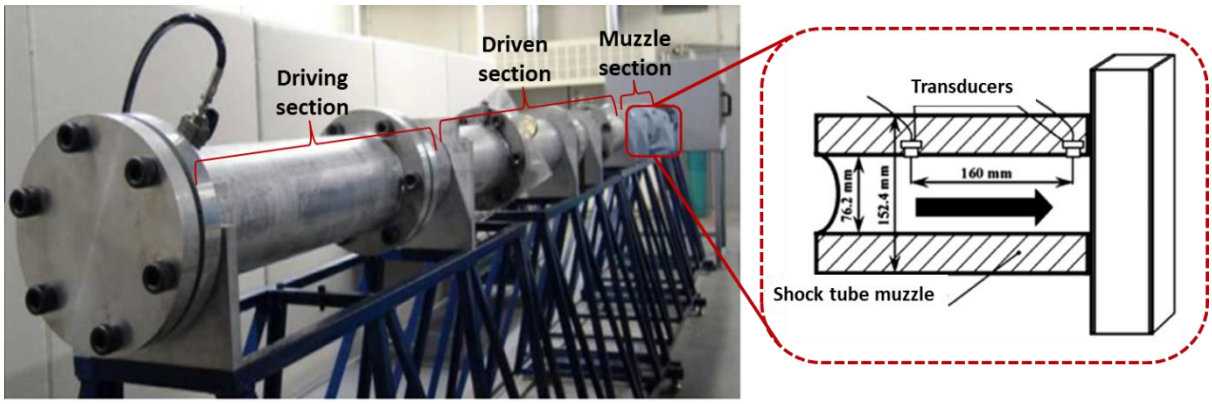

Figure 6.2 (a) Shock tube (b) Muzzle section showing location of transduces (Kumar *et al.*, 2012)

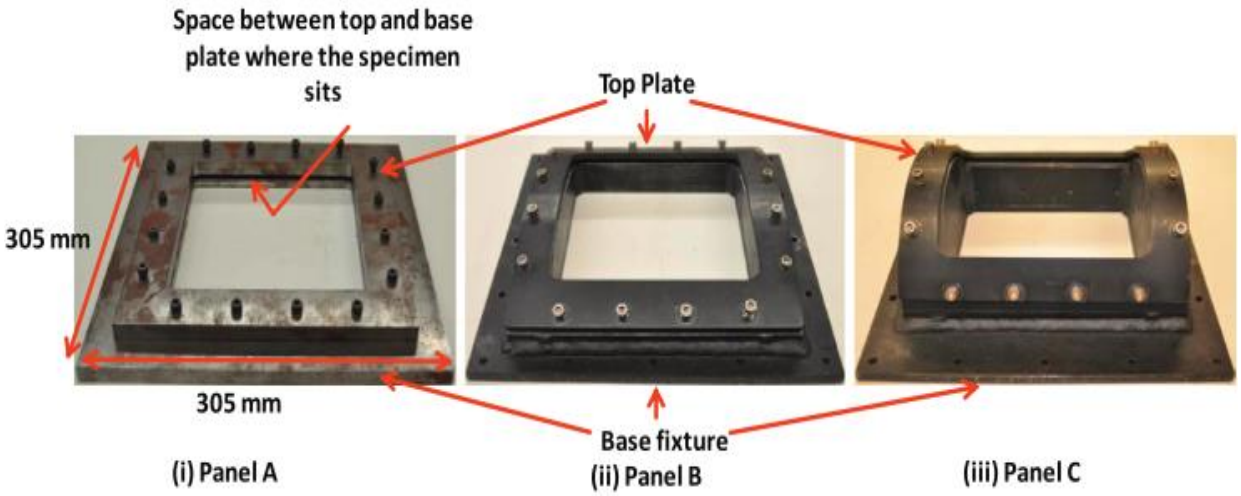

Figure 6.3 Fixtures for studied panels (Kumar *et al.*, 2012)

The theoretical details on the relevant equations for the state of the shock front generated from the gas flow and blast energy distribution have been previously established in the literature (Wright, 1961) and are briefly discussed here. Using conservation of energy, mass, and momentum as described by Wright (1961), following relationships for pressure, temperature, and density across a shock front was derived:

$$\frac{P_2}{P_1} = \frac{2\gamma M_1^{\,2} - (\gamma - 1)}{(\gamma + 1)} \tag{6.1}$$

$$\frac{T_2}{T_1} = \frac{\left\{2\gamma M_1^{\,2} - (\gamma - 1)\right\} - \left\{(\gamma - 1)M_1^{\,2} + 2\right\}}{(\gamma + 1)^2 M_1^{\,2}} \tag{6.2}$$

$$\frac{\rho_2}{\rho_1} = \frac{M_1^{\,2}(\gamma + 1)}{(\gamma - 1)M_1^{\,2} + 2}\ , \tag{6.3}$$

where P_1 , T_1, ρ_1 are pressure, temperature, and density of the gas located behind the incident shock wave, while P_2 , T_2 , ρ_2 are the pressure, temperature, and density behind the reflected shock wave front. γ is an adiabatic constant, while M_1 is a Mach number of the shock wave relative to the driven gas. The pressure imparted on the specimen can be controlled by varying the above parameters in eq. (6.1- 6.3).

Fundamentally, the energies associated with the gas in the shock tube that play a vital role in the blast loading process comprise of the incident energy , i.e. the energy stored in the gas behind the incident shock wave and the remaining energy, i.e. the energy stored in the gas behind the reflected shock wave (Wang and Shukla, 2010). As the incident shock wave impacts the specimen located at the muzzle end, the reflected shock wave is generated. This shock wave may travel in all possible directions away from the specimen upon its reflection and lose its original intensity in this process. The energy located behind this reflected shock wave then imparts the secondary loading on the specimen. This change in the magnitude of energy during the interaction of the reflected shock wave with the incoming gas is defined as the energy lost and it corresponds to the difference between the incident energy and the remaining energy.

Here, in general, the energy stored in the gas can be subdivided in three categories: (1) the internal energy, (2) the translational energy, and (3) the work

done by the gas during its propagation in the shock tube. These energies are calculated using Eq 6.4 (Wang and Shukla, 2010).

$$\begin{aligned} dE_{\text{internal}} &= \left[\frac{p(t).S\left|u_1(t)\right|}{(\gamma-1)} \right] dt \\ dE_{\text{translational}} &= \frac{1}{2}\left[p(t).S\left|u_1(t)\right| \right].\left|u_1(t)\right|^2 dt = \frac{1}{2} p(t).S\left|u_1(t)\right|^3 dt \\ dE_{work} &= p(t).S\left|u_1(t)\right| dt \end{aligned} \tag{6.4}$$

The total energy associated with the gas is the summation of these three individual components and can be calculated using Eqs. (6.5) and (6.6).

$$\begin{aligned} E_{incident} &= \left[\int \left\{ dE_{INTERNAL}^{INICIDENT} + dE_{TRANSITION}^{INCIDENT} + dE_{WORK}^{INCIDENT} \right\} \right] \\ &= \int S.\left|u_1(t)\right| \left[\frac{\gamma.\, P_1(t)}{(\gamma-1)} + \frac{1}{2}\rho_1(t).\left|u_1(t)\right|^2 \right] dt \end{aligned} \tag{6.5}$$

$$\begin{aligned} E_{remaining} &= \left[\int \left\{ dE_{INETRNAL}^{REMAINING} + dE_{TRANSITION}^{REMAINING} + dE_{WORK}^{REMAINING} \right\} \right] \\ &= \int S.\left|u_2(t)\right| \left[\frac{\gamma.\, P_2(t)}{(\gamma-1)} + \frac{1}{2}\rho_2(t).\left|u_2(t)\right|^2 \right] dt \ , \end{aligned} \tag{6.6}$$

where $\left|u_1(t)\right|$ is the absolute value of the particle velocity of the gas behind the incident shock front, $\left|u_2(t)\right|$ is the absolute value of the particle velocity of the gas behind the reflected shock front, γ is an adiabatic exponent of gas, and S is the cross-section area of shock tube. The detailed derivation of these equations has been discussed by Erheng and Shukla (Wang and Shukla, 2010).

In this study, the shock tube had an overall length of 8 m, consisting of driving, driven, and muzzle sections (Fig. 6.2a). The diameter of the driving and driven section was 0.15 m. The final muzzle diameter was 0.07 m. Two pressure transducers (Fig. 6.2b), mounted at the end of the muzzle section measured the incident shock pressure and the reflected shock pressure during the experiment. The pressure transducers were oriented along the horizontal line of

symmetry of the specimen. The specimens were clamped on all four edges. Appropriate fixtures were designed and manufactured to hold the specimens (Fig. 6.3). Blast loads were imparted on the specimens at three different pressures varying from 3 MPa to 8 MPa. The experiments were repeated three times under same conditions. The pressure profiles obtained at the transducer locations closer to the specimens are shown in Figs.6.4-6.6.

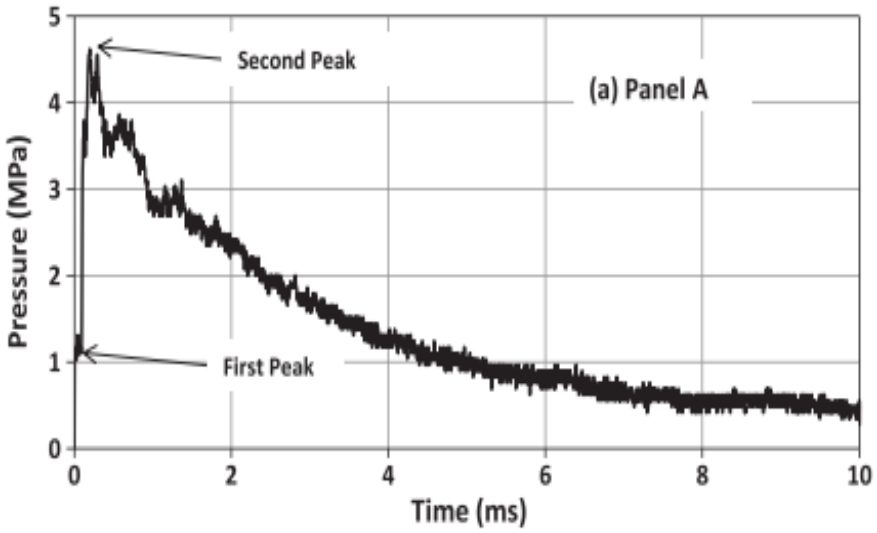

Figure 6.4 Pressure profile for panel A at failure load

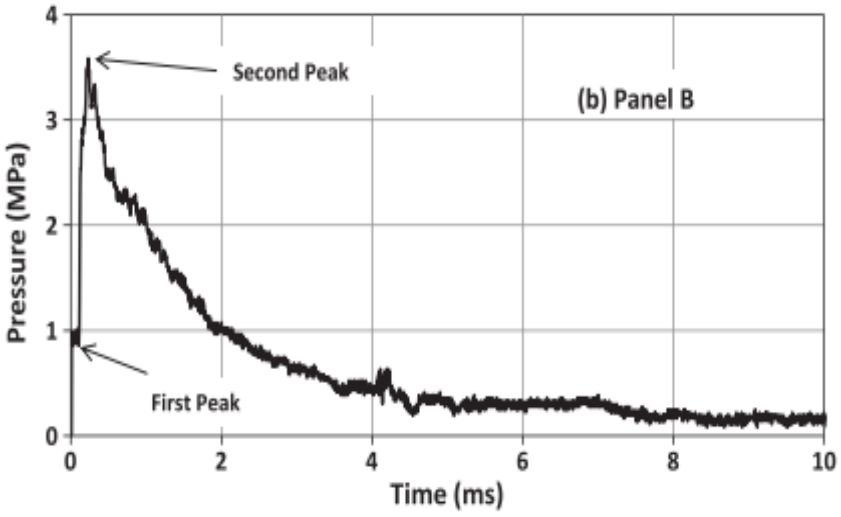

Figure 6.5 Pressure profile for panel B at failure load

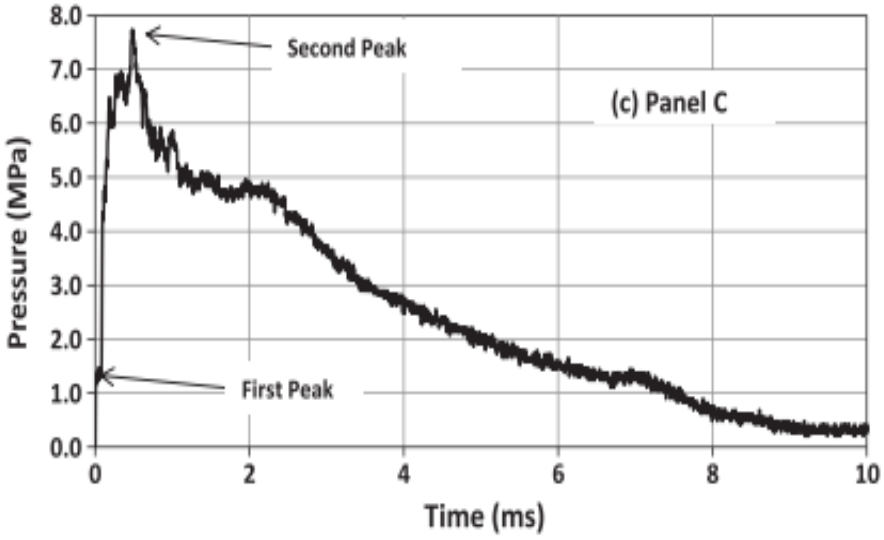

Figure 6.6 Pressure profile for panel C at threshold load

Here, first peak represents the peak (maximum) pressure measured by transducer owing to the incident shock wave, and second peak represents the peak (maximum) pressure measured by transducer exerted by the reflected shock wave.

6.2.3 Digital Image Correlation

Digital image correlation (DIC) is a non-contact optical method for analysing full-field measurements of deformation and strains (Tiwari *et al.*, 2009). Here, the DIC technique was employed to measure in-plane strains and out-of-plane deflection at the centre of the back face of all the studied specimens. A real-time deformation of the panels was captured using two high-speed digital cameras, Photron SA1s, positioned behind the shock tube apparatus. The cameras were able to capture synchronized images at 20,000 frames per second (inter-frame time of 50 μs). The images of deformed and undeformed specimens were analysed using DIC software to correlate the images from the two cameras and generate histories of real-time in-plane strain, out-of-plane deflection and velocity. A schematic of DIC set-up used in this study is shown in Fig. 6.7 and its experiments procedure explained below.

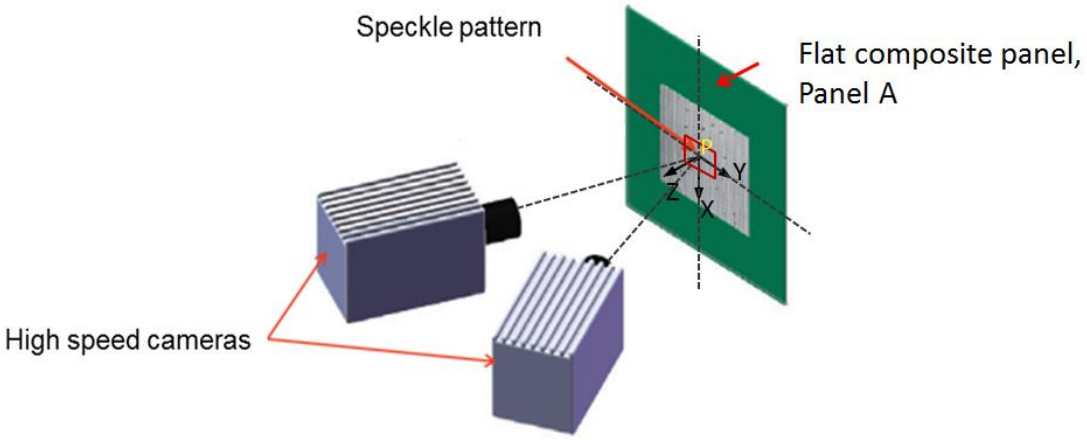

Figure 6.7 Schematic of DIC system (Kumar *et al.*, 2012)

First, composite panels were painted white, over-sprayed with black paint to apply a high contrast random pattern and then bolted into the fixtures (Fig. 6.3). Second, the specimens were placed against the shock tube to perform blast experiments. Thirdly, after mounting the cameras on the back side of specimen, the cameras were rotated and repositioned to view the specimen and maximize the common field of view on the specimen. Fourth, the specimen is removed from its designated position and a grid specimen (specimen marked with grid) was used to calibrate the stereo-vision system. Fifth, adjustable supports are attached to the corners of the plate so that shock wave impacts specimen exactly in its centre. Sixth, shock tube was pressurised to produce blast loading on the composite panel. Two high speed digital cameras, Photron SA1s, were positioned behind the shock tube apparatus to capture the real-time deformation and displacement of the panel. The high speed cameras were set to capture synchronized images at 20,000 frames per second (inter frame time of 50 μs). During the blast loading event, as the panel responded, the cameras recorded the speckles on panel's back face.

Before each of the experiment separate system camera calibration was performed to ensure the accuracy of the results. The grid used in the calibration

process consists of a series of circular speckle patterns arranged in a pre-determined manner, during the calibration process this grid is moved (translated and rotated) in and out of plane and several synchronized calibration images are acquired by both the cameras. Once the images are acquired, coordinates of the centre of the dots in the calibration are extracted using suitable edge detection method for all calibration images from both cameras. Once the camera calibration process was completed, actual digital image correlation is performed using undeformed and deformed image pairs to match common image subsets within the speckle patterns using VIC-3D software package. In this study, 15×15 pixel subsets are selected and matching is performed using an affine subset shape function. Subset spacing was 1 pixel, resulting in matching image positions for up to 20,000 positions. Once an image subset was matched (a) between undeformed image pairs and (b) between deformed image pairs and also between undeformed and deformed image pairs, the stereo-vision system parameters are used to estimate the 3D position of points on the undeformed panel (initial profile) and also on each deformed panel's position.

Dynamic experiments have been done in the past (Gardener *et al.*, 2012) to compare the back face deflection from the real-time transient image and DIC to verify the accuracy of the DIC results. The difference between the maximum deflection from the DIC and real-time transient images was within 4%. The DIC system and high-speed camera used by Gardener *et al.* (2012) was employed in this study which ensured the reliability of its results.

There were two key assumptions used in this study to convert images to experimental measurements of objects geometry, deflection, and strain. First, it was assumed that there is a direct correspondence between the motion of the points in the image and that in the object. This ensured that the displacement of points on the image have a correlation with the displacement of points on the

object. Second, it is assumed that each sub-region has adequate contrast so that accurate matching can be performed to define local image motion.

The Lagrangian strain field on the object is obtained by least squares fitting of a quadratic function to each component of the displacement data using a 9 × 9 set of displacement measurements. Here, the coordinate system shown in Fig. 6.7 was used to define the (x, y, z) directions, with (u, v, w) defining the object displacements in the (x, y, z) directions. By differentiating the local surface fit at the centre point P, to define the displacement gradients for each component, Eq. (6.7) is used to obtain the local strain components (Tiwari *et al.*, 2009).

$$\varepsilon_{xx}\big|_P = \frac{\partial u}{\partial x}(P) + \frac{1}{2}\left[\left(\frac{\partial u}{\partial x}(P)\right)^2 + \left(\frac{\partial v}{\partial x}(P)\right)^2 + \left(\frac{\partial w}{\partial x}(P)\right)^2\right]$$

$$\varepsilon_{yy}\big|_P = \frac{\partial v}{\partial y}(P) + \frac{1}{2}\left[\left(\frac{\partial u}{\partial y}(P)\right)^2 + \left(\frac{\partial v}{\partial y}(P)\right)^2 + \left(\frac{\partial w}{\partial y}(P)\right)^2\right] \tag{6.7}$$

$$\varepsilon_{xy}\big|_P = \frac{1}{2}\left(\frac{\partial u}{\partial y}(P) + \frac{\partial v}{\partial x}(P)\right) + \frac{1}{2}\left[\left(\frac{\partial u}{\partial x}(P)\frac{\partial u}{\partial y}(P)\right) + \left(\frac{\partial v}{\partial x}(P)\frac{\partial v}{\partial y}(P)\right) + \left(\frac{\partial w}{\partial x}(P)\frac{\partial w}{\partial y}(P)\right)\right]$$

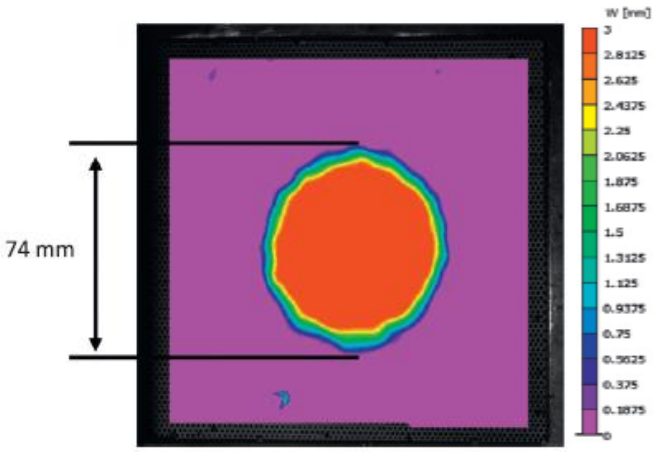

Figure 6.8 DIC analysis showing the loading area during shock impingement on a flat panel at t = 50 μs (Kumar *et al.*, 2013)

The shock tube used in this study provides a uniform pressure pulse over a circular area of 4562 mm^2 (muzzle area). This is verified by the DIC image of the out-of-plane displacement on the flat plate during shock impingement as shown in Fig. 6.8.

The image taken at 50 μs shows that the Panel A (flat panel) had a uniform deflection of 3 mm ± 0.2 mm within a central region of diameter 70 mm. The full-field history of deformation of all three composite panels is shown in Fig. 6.13, it can be observed from Fig. 6.15-6.17, that out-of-plane deformations, velocities and in-plane strains at the centre of the back face of CFRP panels measured from DIC technique correlates reasonably accurately to those calculated with FE analysis.

6.3 Development of finite-element model

6.3.1 Material model

A user-defined damage model (VUMAT) with 3D continuum elements was developed and implemented to predict the damage characteristics through the laminate's thickness under the blast load, as discussed in Chapter 4. The model is able to characterise damage in a composite laminate by employing a stiffness-degradation concept with the help of an element-deletion approach based on the initiation and evolution of damage in the meshed domain (Hibbit *et al.*, 2011). Another damage mode – interply delamination – is simulated using cohesive elements inserted between the adjacent plies of the laminate. The general-contact algorithm in ABAQUS/Explicit was used to model the contact conditions between the shock wave and the composite laminate, and between the laminae by defining appropriate contact-pair properties. The results of numerical simulations were evaluated using comparison with the experimental data.

(A) Strain–rate sensitivity

The polymer matrix material in a CFRP composite demonstrates strain-rate-sensitivity at high strain rates (~ 10^3 s^{-1}), which are typical for a blast event. This effect becomes significant, particularly for transverse directions, in cases where polymer matrix is the primary load-bearing member (Gómez-del Rio *et al.*, Ochola *et al.*, 2004; Raimondo *et al.*, 2012; Koerber *et al.*, 2010; Daniel *et al.*, 2011). Many test methods have been developed to facilitate the dynamic characterisation of composite materials at high deformation rates. Previous test studies highlighted the increase in stiffness and strength of composites with an increasing strain rate in matrix-dominated regions (Puck *et al.*, 1998; Gómez-del Rio *et al.*, Ochola *et al.*, 2004; Raimondo *et al.*, 2012; Koerber *et al.*, 2010). In some cases, explicit empirical relations were formulated to derive such material properties at corresponding strain-rates (Koerber *et al.*, 2010; Daniel *et al.*, 2011). The composite laminate used in our experiments – AS4/3501-6 – was shown to exhibit a strain-hardening behaviour at high loading rates (Daniel *et al.*, 2011). The response of AS4/3501-6 laminate at various biaxial stress states e.g. combined transverse compression and shear, at strain rates varying from 10^{-4} s^{-1} to 400 s^{-1} was characterised. Stress-strain data at failure, initial moduli, and strength were also recorded. Empirical relationships between the matrix-dominated properties and strain rates under high-strain rate deformation were as follows:

- for in-plane shear and transverse moduli:

$$E(\dot{\varepsilon}) = E(\dot{\varepsilon}_0)\left[m_e \log\left(\frac{\dot{\varepsilon}}{\dot{\varepsilon}_0}\right)+1\right]$$
$$m_e = 0.045,\ \dot{\varepsilon}_0 = 10^{-4}s^{-1} \tag{6.8}$$

- for in-plane shear and transverse strength:

$$F(\dot{\varepsilon}) = F(\dot{\varepsilon}_0)\left[m_f \log\left(\frac{\dot{\varepsilon}}{\dot{\varepsilon}_0}\right)+1\right]$$
$$m_f = 0.057,\ \dot{\varepsilon}_0 = 10^{-4} s^{-1} \quad (6.9)$$

Here, $E(\dot{\varepsilon})$ and $F(\dot{\varepsilon})$ are the instantaneous in-plane moduli of elasticity and shear strength at a strain-rate of $\dot{\varepsilon}$, respectively, $\dot{\varepsilon}_0$ = 10^{-4} s^{-1} is the reference strain-rate, which corresponds to quasi-static loading, while m_e = 0.045 and m_f = 0.057 are curve-fitting parameters. Eqs. (6.7 - 6.8) form the basis of the dynamic material properties used in our simulations.

The average maximum strain rates for the studied composite panels under blast loading were analysed, initially without specifying strain-rate-dependent properties, with our FE simulations. They were observed to be in the range of 2200 s^{-1} to 2400 s^{-1} for panel A, 3500 s^{-1} to 3800 s^{-1} for panel B and, 1500 s^{-1} to 1800 s^{-1} for panel C. The matrix-dominated properties reported by Daniel *et al.* (2011) for a similar composite were suitably extrapolated to match these strain rates (Table 6.1).

(B) Delamination

The interply delamination was modelled using cohesive zone element (CZE) approach as discussed in Sections 3.6.3 and 5.4.The mechanical properties of cohesive elements used in these simulations are listed in Table 6.1. The magnitude of elastic traction was estimated from eq. (5.1), while maximum stress and fracture energy values were taken from Song (2008) owing to the same material system.

Table 6.1 Mechanical properties of AS4/3501-6 UD composite laminate (Ochola *et al.*, 2004; Daniel *et al.*, 2011)

Elastic moduli	$E_{xx}=147$ GPa, $E_{yy}=11.2$ GPa, $E_{xy}=7$ GPa				
Tensile strength in fibre direction, X_{1t}	2004 MPa				
Compressive strength in fibre direction, X_{1c}	1197 MPa				
Tensile strength in transverse direction, X_{2t}	65 MPa				
Compressive strength in transverse direction, X_{2c}	285 MPa				
In–plane shear strength, S	80 MPa				
Stiffness of cohesive zone, K (N/mm^3)	5×10^6				
Interlaminar traction in normal direction, τ_n(MPa)	53.78				
Interlaminar traction in shear-1 and 2 direction, $\tau_s = \tau_t$(MPa)	86.88				
Mode-I critical fracture energy, G_{IC} (N/mm)	0.08				
Mode II critical fracture energy, G_{IIC}(N/mm)	0.55				
Power law coefficient, β	1.8				
Strain-rate dependent properties	Average strain-rates, $\dot{\varepsilon}$ (s^{-1})				
	0.0001	1	400	2400	3800
Transverse modulus, E_2(GPa)	11.2	12.9	14.5	[14.8]	[14.96]
Shear modulus, G_{12}(GPa)	7	8.2	9	[9.3]	[9.4]
Transverse tensile strength, F_{2t}(MPa)	65	80	90	[94]	[95]

Transverse compressive strength, F_{2c} (MPa)	285	345	390	[405]	[409]

Note: Numbers in brackets denote extrapolated values.

6.3.2 FE model and boundary conditions

The 3D finite-element model developed in ABAQUS 6.11 (Hibbit *et al.*, 2011) consisted of a shock-tube wall and a CFRP panel. The shock tube was modelled with shell elements with five integration points through its thickness. The elements of the wall had an edge length of 2 mm and shell thickness of 25.4 mm. The CFRP panels were modelled as a solid continuum with mechanical properties listed in Table 6.1. These panels were meshed with eight-node, one-integration-point hexahedral elements C3D8R with an optimised mesh size of 0.2 mm (Fig.6.9) along the length, while each ply was assigned one element though its thickness. There were a total of 1.7 million elements in this structural domain.

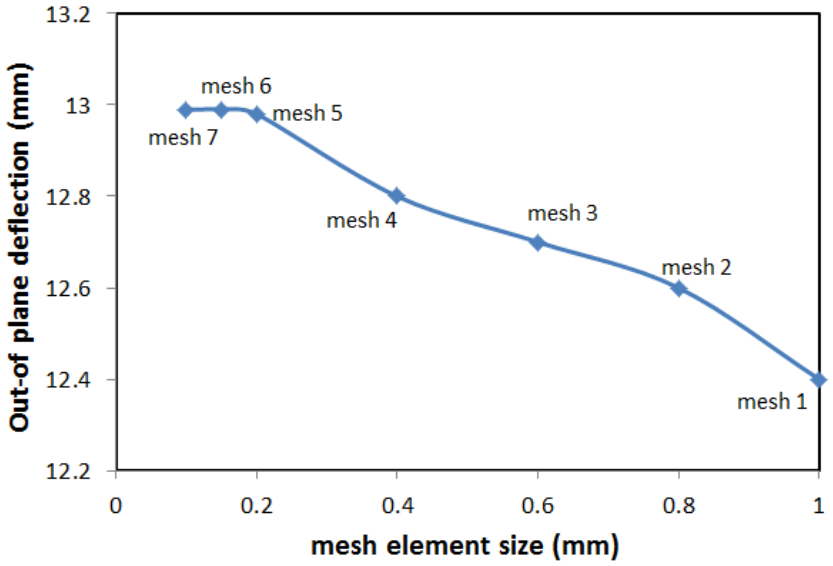

Figure 6.9 Mesh study – ply (Panel A)

The material co-ordinate system was assigned to the panel such that it captured a discrete orientation of each element accurately following the curvature. The

schematic for meshed CFRP panel C is shown in Fig. 6.10. The boundary conditions employed in this model reflected the physical constraints applied in the experiments. All edges of the panels were fully constrained. All the degrees of freedom at the shock tube wall were also fully constrained, since it was considered rigid in simulations. All three panels in our simulations were positioned against the wall of the shock tube as shown in Fig. 6.11.

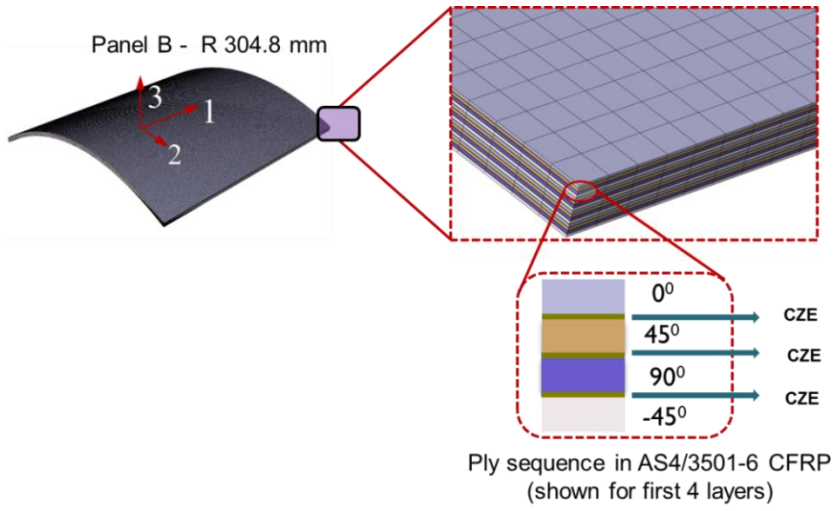

Figure 6.10 Meshed CFRP panel C and locations of cohesive elements

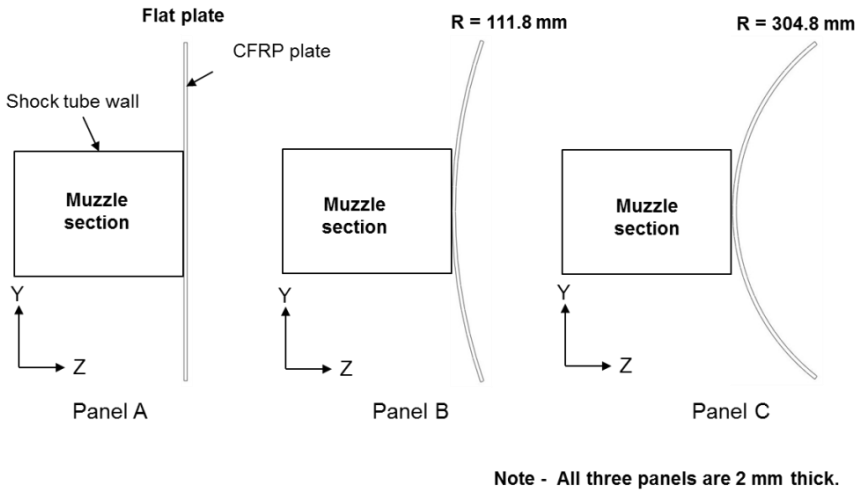

Figure 6.11 Orientation of specimens

6.3.3 Fluid-structure coupling and shock-wave loading

The fluid model consisted of the air inside and outside the shock tube as well as the air surrounding the plate as shown in Fig. 6.11. The air outside the tube was modelled in an Eulerian domain as a cuboid with a domain size of 400 mm × 400 mm in X-Y plane and 2000 mm along the tube axis.

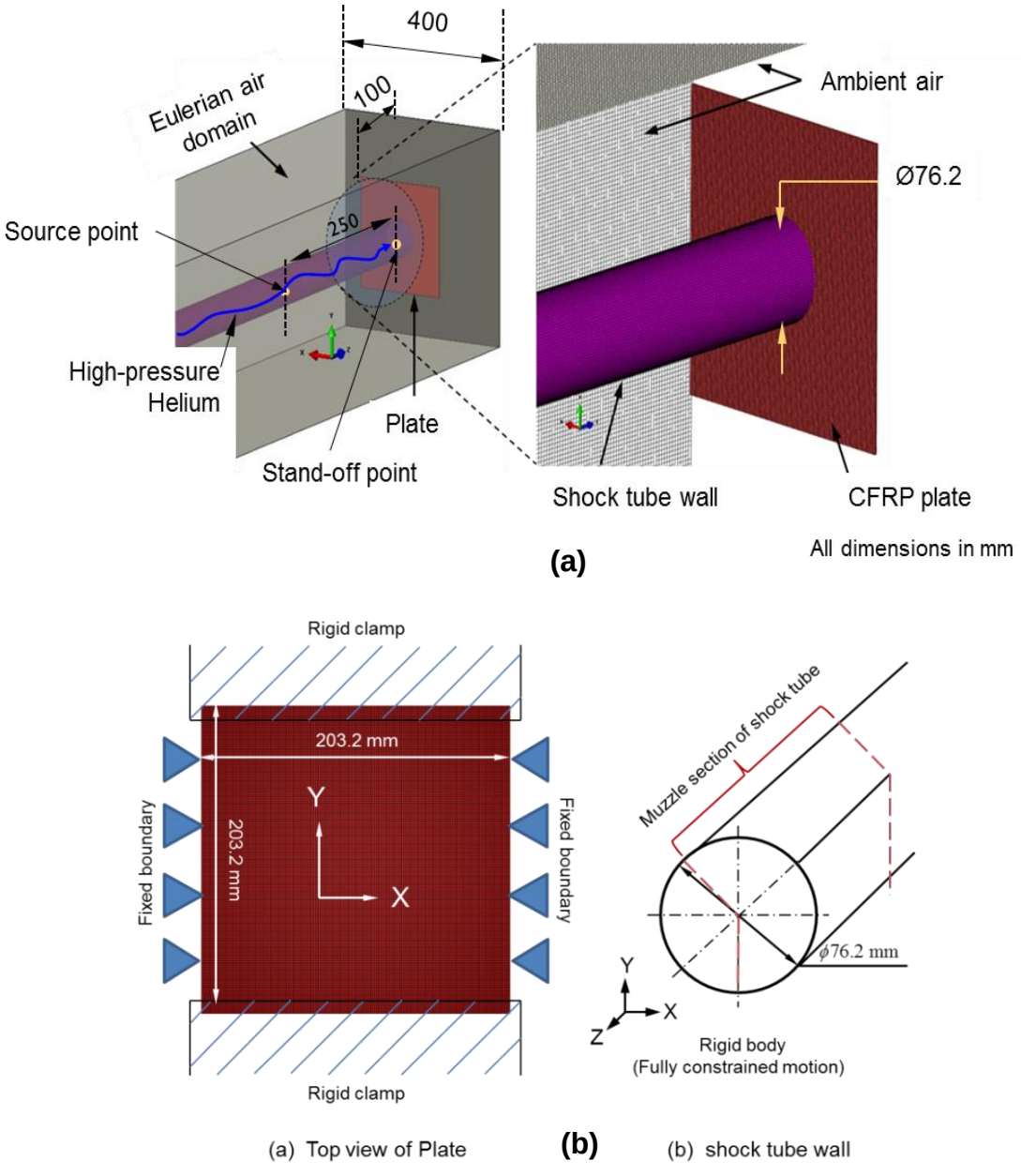

Figure 6.12 FE model setup (a) solid and fluid regions (b) Boundary conditions

The model had 100 mm of air along the tube axis behind the plate to ensure that the plate remained in air during deformation caused by shock-wave load. The air inside the tube was also modelled in the Eulerian domain with the element size of 3 mm.

All the fluid elements were meshed with the Eulerian eight-node, one-integration-point hexahedral elements EC3D8R. The acoustic structural coupling between acoustic pressure of the fluid mesh and structural displacements of the CFRP panel was accomplished with a surface-based tie constraint at the common surface.

The master-slave type of contact was established between the annular surface of the shock tube in contact with the CFRP panel and the front surface of the panel. The surface of the external fluid at the interface was designated as the master surface. The incident wavefront was assumed to be planar. For a planar wave, two reference points, namely, the standoff point and the source point were defined (Fig. 6.12a). The relative positions of these two reference points were used to determine the direction of travel for the incident shock wave; the pressure history at the standoff point was used to drive it.

The ‘amplitude’ definition in ABAQUS/Explicit (Hibbit *et al.*, 2011) was employed to specify the shock load on the front surface of the CFRP panel using the pressure-history data. The entire analysis was divided into two steps pertaining to the wave incidence and reflection, with appropriate magnitudes of average shock-wave velocity and density were used. Linear fluid mechanics was used for the entire model. The observed total pressure in the fluid was divided into two components: the incidents wave itself, which was known, and a calculated wave field in the fluid due to reflections at the fluid boundaries and interactions with the solid.

6.4 Results and discussion

The results obtained in this numerical study are discussed below. The FE analysis was employed to compute the out-of-plane deflections of CFRP panels, energy distributions during blast, and damage in the panels. A parametric study was carried out to suggest the optimal curvature of CFRP panel for improved blast resistance.

6.4.1 FE model validation

The FE model allows for the observation of interaction of shock front with the CFRP panels and their deformation under shock loading. The deflection, velocity and strain data acquired using the DIC technique (Kumar *et al.*, 2012; Ochola *et al.* 2004) was used as a basis to validate the FE model. Initially, the flat panel (Panel A) had a uniform deflection within a central region of loading. This out-of-plane deflection decayed gradually towards the edges. When the radius of curvature was increased, the effective loading area changed its shape from circular to elliptical.

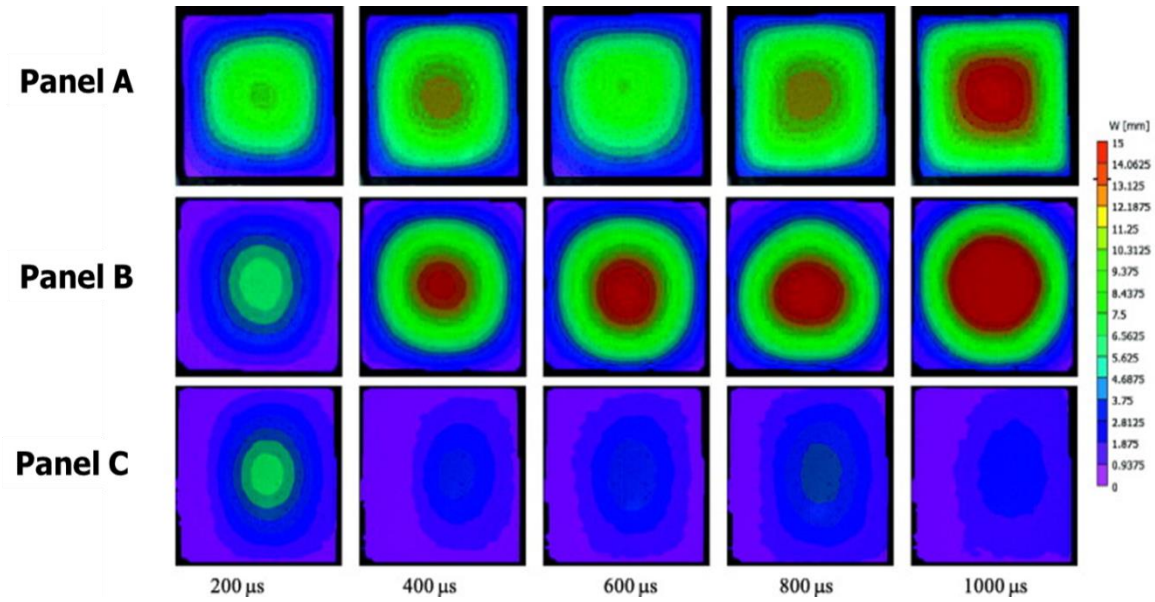

Fig. 6.13 Deflection contours obtained using DIC at the back face of studied CFRP panels (Kumar *et al.*, 2013)

For the curved panels, shock loading primarily acted upon the projected area unlike the circular area as in case of flat panel, which caused this change in a shape. During the early stages of shock loading, contours of out-of-plane deflection were not affected by the boundary conditions. Deflection of Panel A started as a circular region, which continued until 150 μs. This was a localized circular deflection contour, which had roughly the same diameter as that of the muzzle (at t = 50 μs). At t = 150 μs, the boundary conditions started to affect the development of deflection contours in the panel. The stress waves generated in the specimen travelled outwards and were reflected by the boundary. This reflected stress wave caused the change in the shape of the deflection contours. The full-field deflection at the failure loading for these panels is shown in Fig.6.13.

6.4.2 Modes of deflection in CFRP panels

The FE analysis demonstrated that deflection of the studied CFRP panels was the combined result of two deflection modes, namely, the indentation mode and the flexure mode. It was seen that all the panels started deflecting in the indentation mode initially (Fig. 6.14). In the flat panel (Panel A), the global flexural mode quickly began dominating the deflection process. This was confirmed by the continuous nature of displacement contours that show a monotonic increase in deflection from the edge to the centre of the specimen after t = 200 μs. Deflection of Panel B continued in the indentation mode up to about 400 μs, after which it changed to the global flexural deflection mode.

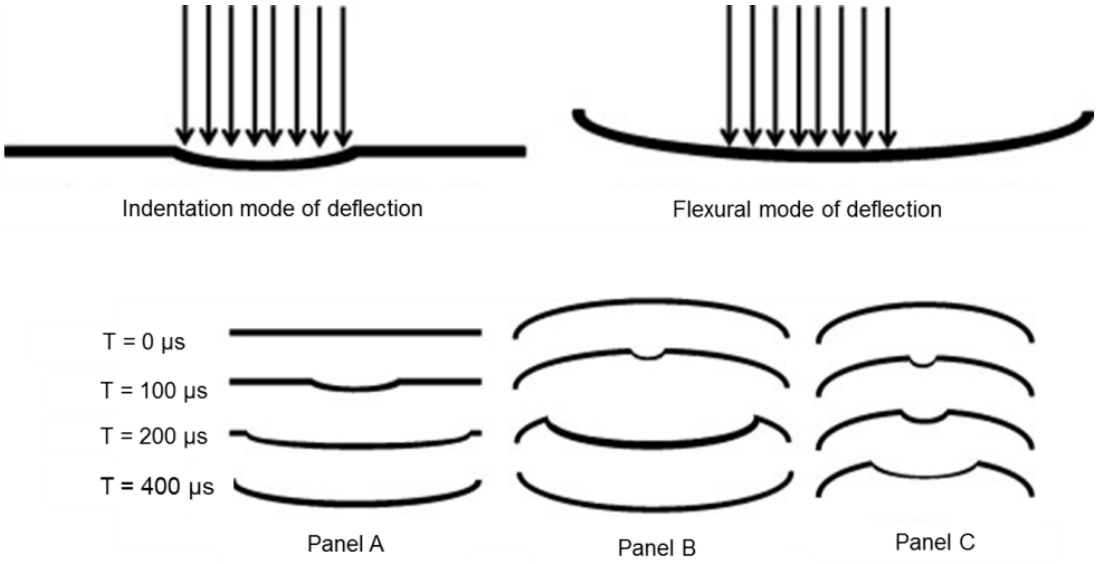

Figure 6.14 Modes of indentation of CFRP panels (blast pressure for Panel A =4.6 MPa, Panel B = 3.5 MPa and Panel C =7.8 MPa)

These deflection contours (Fig.6.14) show a continuous increase in deflection from the edge to the centre of panel and the transition from elliptical contours back to the circular shape. In Panel C, the deflection was observed to be less than that in Panels A and B since only the central loading region was affected. In addition to the out-of-plane deflection, velocities and in-plane strain data were also extracted from FE model at the centre point of the back of the studied CFRP panels (Figs. 6.15 - 6.17). The in-plain strain output was requested for a set of four elements located at the centre of the back face of panels and its average magnitude was calculated. Figure 6.15 shows that the deflection rate (35 m/s), for the initial 200 μs, was almost the same for all the three panels, though Panels A and B attained a higher deflection as compared to Panel C. This means that the Panel C was stiffer than the other two panels since it sustained a higher pressure and had a lower deflection. Panels A and B showed similar trends up to 1000 μs. At this time, damage was observed to initiate in Panel B, which explains the rapid increase in its deflection.

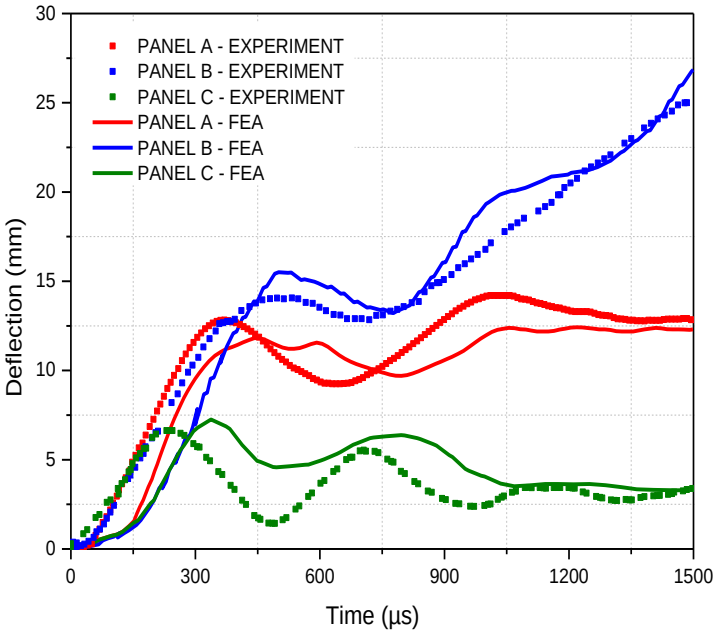

Figure 6.15 Experimental and numerical results: out-of-plane deflections at the centre of the back face of CFRP panels (blast pressure for Panel A =4.6 MPa, Panel B = 3.5 MPa and Panel C =7.8 MPa)

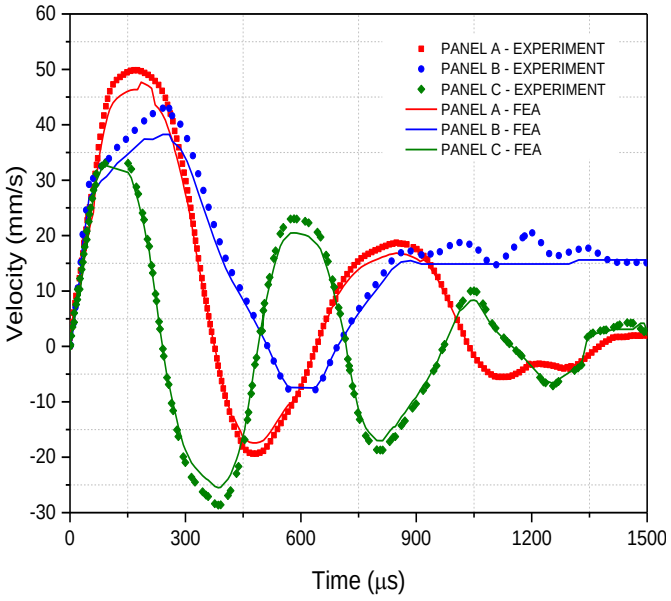

Figure 6.16 Experimental and numerical results: out-of-plane velocities at the centre of the back face of CFRP panels (blast pressure for Panel A =4.6 MPa, Panel B = 3.5 MPa and Panel C =7.8 MPa)

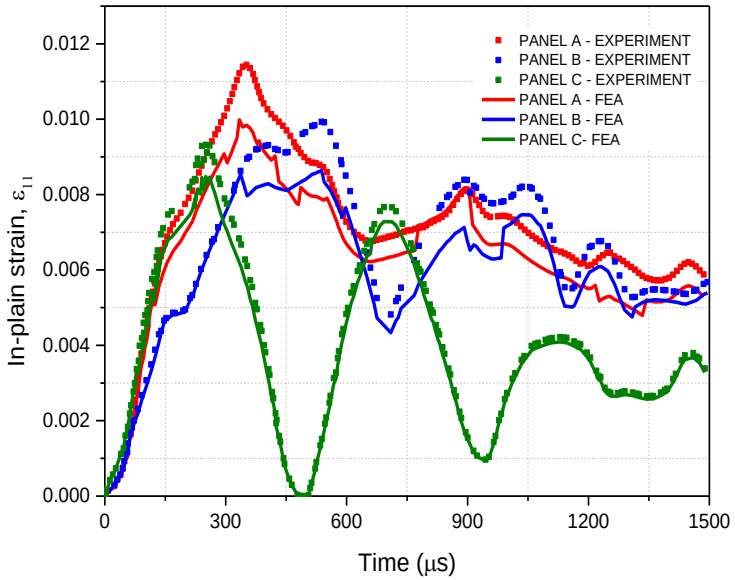

Figure 6.17 Experimental and numerical results: in-plain strain at the centre of the back face of CFRP panels (blast pressure for Panel A =4.6 MPa, Panel B = 3.5 MPa and Panel C =7.8 MPa)

It should be noted that in Fig. 6.16, the in-plane strain (ε_{11}) was calculated experimentally using DIC from Eq. (6.7) at the centre of the back face of the CFRP panels. This was then compared to the average strain obtained at the centre of the back face of the CFRP panels as discussed in Section 6.4.2.

The lower out-of-plane velocity (Fig. 6.16) and in-plane strain (Fig. 6.17) in Panel C showed that this panel had higher flexural rigidity. Panel B exhibited higher in-plane shear strain which led to its catastrophic failure.

6.4.3 Damage in CFRP panels

The damage initiation for panel A is discussed below with the help of stress component in fibre direction. It should be noted that the blast is a highly dynamic event and a relatively small magnitude of pressure exerted on the composite panel with very high velocity (the velocity of sound in Helium gas at room temperature (20^0C) is 927 m/s; and in general, speed of shock wave is higher than that of sound (Davison (2008)) can generate high stresses in the

vicinity of the constraints applied to the specimens and can be of the order of the strength of laminates in fibre directions. The pressure filed generated by a shock wave is of transient dynamic nature. Thus a relatively small magnitude of pressure (when compared to the strength of a CFRP laminate) exerted to a CFRP panel can lead to its damage – e.g., in this study it was observed that Panel B with laminate strength of ~ 2GPa in fibre direction failed at a peak pressure of 7.8 MPa. This is discussed below.

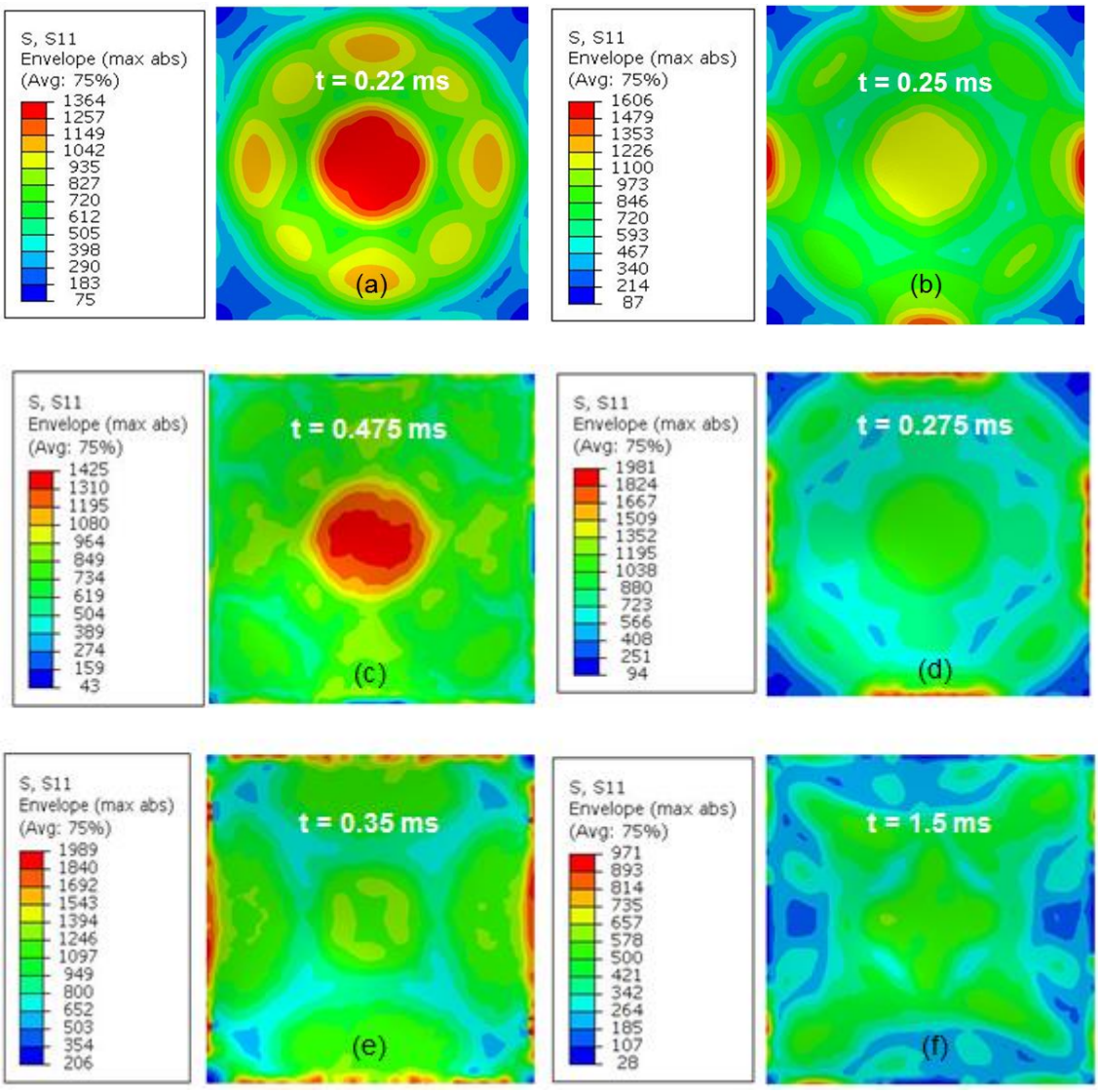

Figure 6.18 Time history of longitudinal (fibre-direction) stress component of Panel A during blast (peak pressure = 4.6 MPa)

The component of stress in fibre direction is shown for Panel A in Figs. 6.18 (a)-(f). It can be seen that as soon as the blast wave impacts Panel A, the region directly below the loading area is subjected to high stress concentration till 250 μs when it undergoes a considerable out-of-plane deflection (refer Fig. 6.15) of magnitude 12 mm. Here, it should be noted that out-of-plane deflection was measured at the centre point of the back face of the panel. Beyond this time period, the stress wave travels down the fully constrained edges of the plate. This results in higher stress concentration at the edges (Fig. 6.18 (b), (c), and (d)). At 400 μs, the magnitude of the stress exceeds (~2 GPa) the longitudinal (fibre-direction) strength of ply in tension at which point the fibre damage takes place directly below the clamped edges (Fig. 6.19).

This is followed by the reflection of the stress wave by the clamped edges which again results in loading the central region of the plate, though the stress magnitude never exceeds the ply strength in fibre direction till 2 ms, and thus no subsequent damage is observed at the centre of the Panel A during this time period. The similar phenomenon is responsible of damage initiation in Panel B and C where these panels were initially highly stressed directly under the loading region.

Thus a large deflection is seen at the centre of these panels till 250 μs (Fig.6.15). At this time in case of Panel C, the stress waves travel towards clamed edges and reflected back towards its centre, when its out-of-plane deflection drops to 2 mm. This process continues till the end 1.5 ms since the ply stresses never reach the level at which damage may initiate. Panel B has the highest out-of-plane deflection at 250 μs ~12 mm among all studied panels (Fig.6.15). Damage initiates at the clamped edges upon stress wave reaching the constrained boundaries, at the same time damage starts initiating in the centre of the panel and couples with that growing from the edges and it fails at ~800 μs.

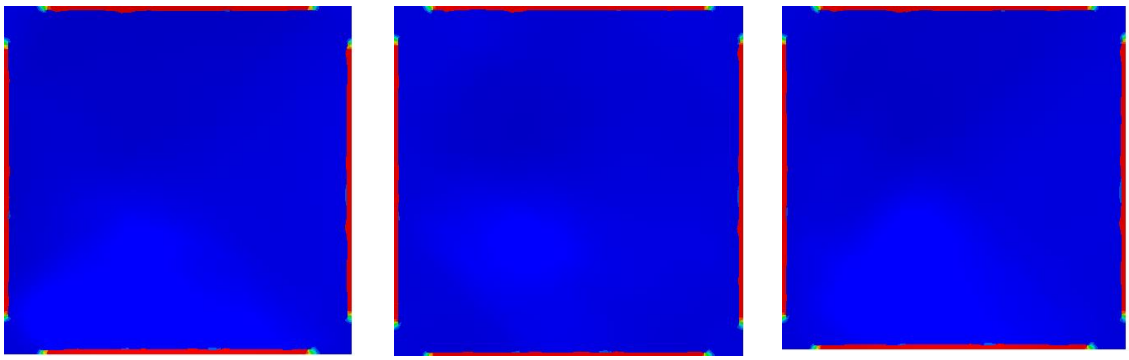

400 µs 800 µs 1200 µs

Figure 6.19 Damage initiation and evolution in plates under blast loading: fibre breakage in front face of Panel A at failure load (blast pressure = 4.6 MPa)

The observed variability of spatio-temporal evolution of deflections in the panels under blast load resulted in different realisation of damage modes. The damage development in Panel A at failure loading is shown in Fig. 6.19. Apparently, fibre breakage was the dominant damage mode.

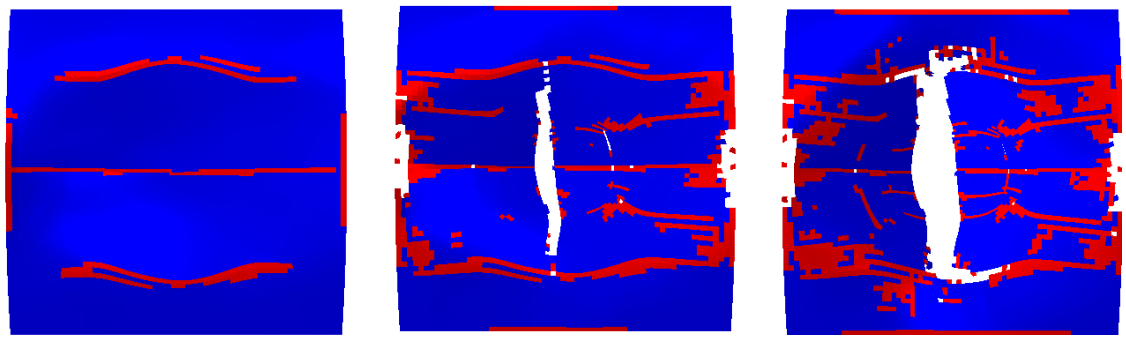

400 µs 800 µs 1200 µs

Figure 6.20 Damage initiation and evolution in plates under blast loading: Panel B at failure load (blast pressure = 3.5 MPa)

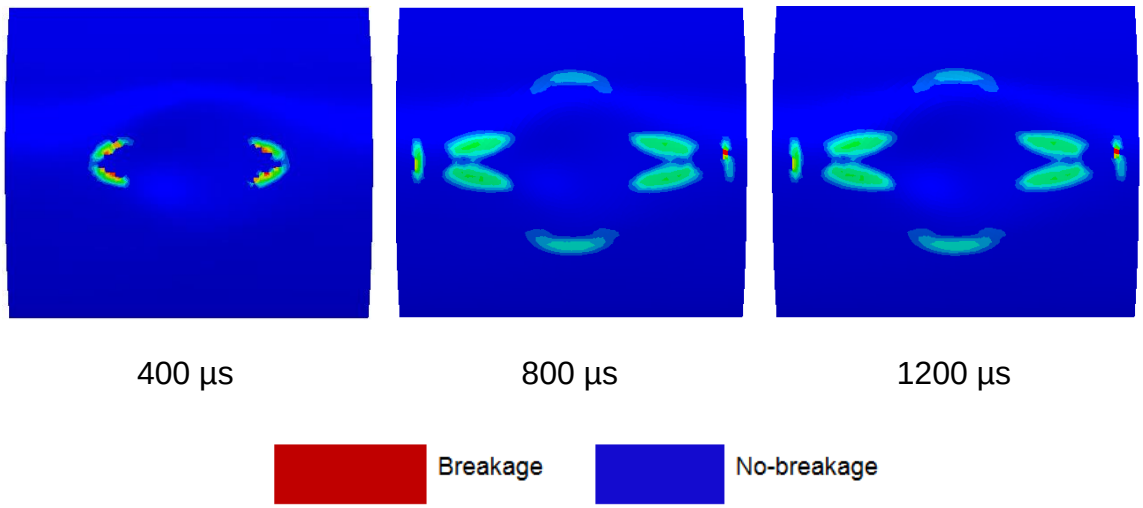

Figure 6.21 Damage initiation and evolution in plates under blast loading: Panel C at threshold load - no global fracture is observed (blast pressure = 7.8 MPa)

The damaged regions were primarily located along the clamped edges, due to the constraints imposed, exposing the underlying fibres to the excessive tensile loading. The extent of damage was near about the same at clamped edges though varied along their thickness.

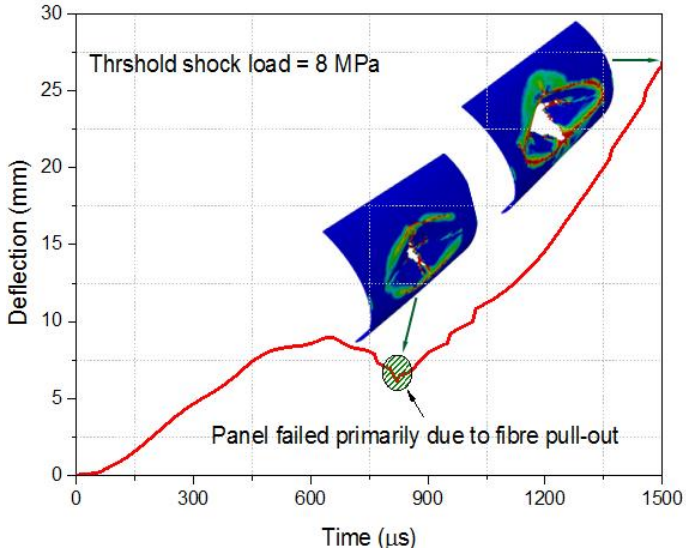

Figure 6.22 Calculated response of Panel C at failure load (8 MPa): deflection

In Panel B similar trend as was observed, though on a larger scale. Fibre breakage was the governing damage mode, though a large-scale delamination was also observed. Damage initiated in the form of fibre breakage at the clamped boundaries and propagated towards the mid-region, where Panel B failed (Fig. 6.19). The damage in Panel C at threshold loading is shown in Fig.6.20, where no fibre breakage or delamination was observed.

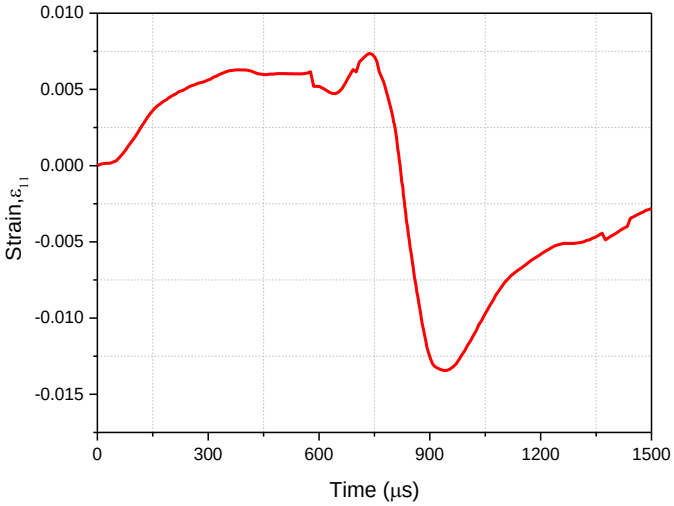

Figure 6.23 Calculated response of Panel C at failure load (8MPa): in-plain strain

Using the developed FE model, this panel was then exposed to a higher pressure of 8 MPa, where it failed catastrophically at around 1000 μs, following the similar damage trend as observed in Panel B. The deflection, and in-plane strain data at the centre point of the Panel C at this load (8 MPa) is shown in Figs. 6.22-6.23.

6.4.4 Energy distribution during blast

The incident and remaining energies associated with the shock loading intensities were analysed with the developed FE models. The energy lost was obtained by subtracting the remaining energy from the incident energy. The magnitudes of energies (incident, remaining, and lost) for all the three loading cases are shown in Figs. 6.24-6.26. Panel C was subjected to the highest

intensity of shock loading and so the incident energy was the highest for this panel. The energy remaining in the gas is identical with impact energy as this is the actual energy that the panel experienced due to shock loading. Since Panel C reflected a major part of the incident shock energy, it was exposed to lower impact energy while Panel B was subjected to the highest impact energy.

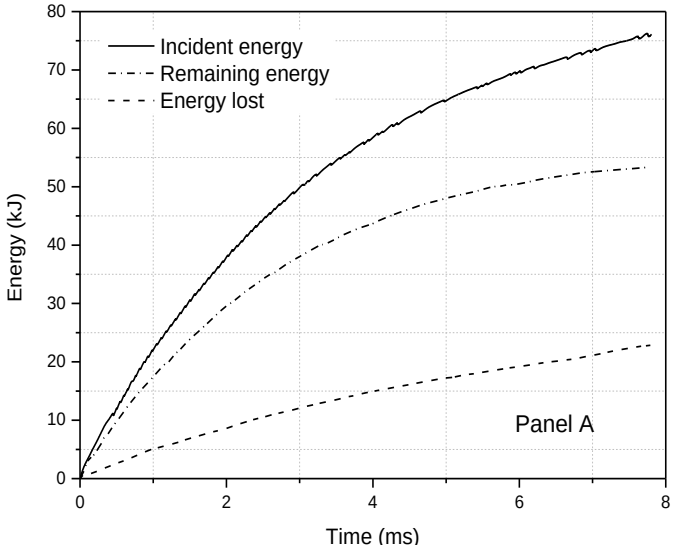

Figure 6.24 Energy distribution during blast: Panel A (blast pressure = 4.6 MPa)

The ratio of impact energy (remaining energy in the gas) to the incident energy was considered as an indication of the blast mitigation ability of studied CFRP panels. Panel C had the lowest ratio of impact to incident energy, which indicates its enhanced blast mitigation capacity. Consequently, Panel B with the highest ratio demonstrates its poor blast mitigation capacity.

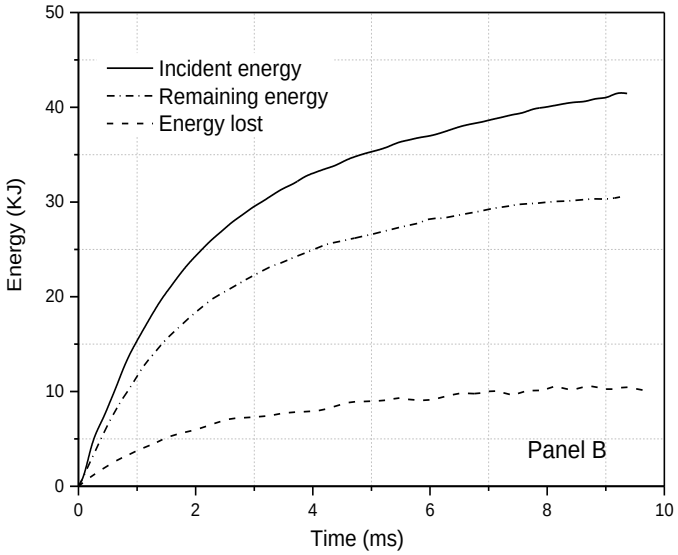

Figure 6.25 Energy distribution during blast: Panel B (blast pressure = 3.5 MPa)

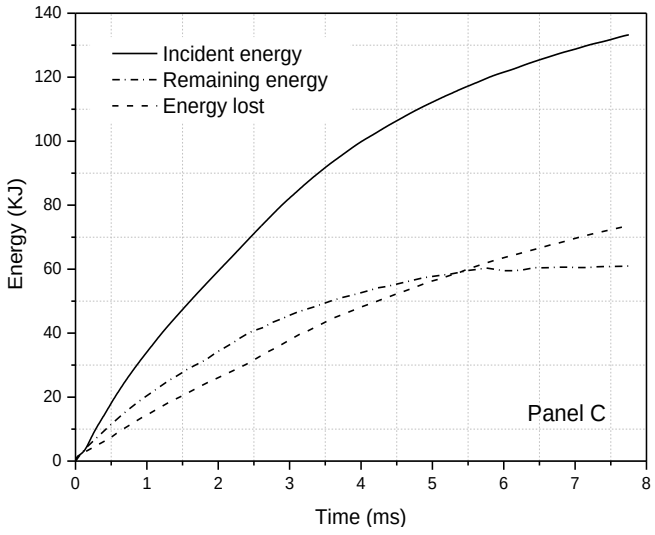

Figure 6.26 Energy distribution during blast: Panel C (blast pressure = 7.8 MPa)

To clarify, energy evolution analysis for all three panels was performed at the same loading pressure. The panels had different levels of energy dissipation capacities. Again, Panel C had the lowest ratio of impact to incident shock energy whereas the Panel B had the highest.

6.4.5 Parametric study and predictions

An important finding resulting from both experimental and numerical studies into the effect of composite panel's curvature on its blast response was the existence of the optimum curvature for maxim blast load. Ideally it may be expected that the out-of-plane deflection and damage exhibited by Panel A (flat) would be the worst among the studies panels, though different observations were as discussed in Section 6.4.2 and 6.4.3. Given the reasonably accurate correlation between the predicted results for Panel B (R304.8 mm) and Panel C (R111.8 mm), there is no reason to believe that the predicted results for flat panel are in any way anomalous or an artefact of the numerical modelling.

The observed aberrant trend in results can be explained using the strain energy theory for deformed shells (Ugural, 1998). This discussion is restricted to the impact not resulting into creation of new surfaces (fracture) for simplicity and the energy of deformation of the panels during blast is referred as their strain energy. The studied composites plates are considered as shells due to their small thickness (2 mm) compared to other relevant dimensions.

The components of strain-energy of a deformed shell are the bending –strain energy U_b and the membrane strain energy U_m.The membrane strain energy is associated with the mid-surface stretching of shells. It is assumed that the shell resists the transverse loading manly through bending action and that the membrane strain energy is small enough to be neglected. The bending strain energy U_b for a thin shell fixed at its ends is expressed by Ugural (1998) as follows:

$$U_b = \frac{1}{2} D \iint_A \left[\left(\chi_x + \chi_y \right)^2 - 2(1-\upsilon)(\chi_x \chi_y - \chi^2{}_{xy}) \right] dxdy \qquad (6.10)$$

Where A represents the surface area of the shell and χ_x , χ_y represent changes in curvatures upon loading. D is the flexural rigidity of the shell given

by, $D = \frac{Et^3}{12}(1-\upsilon^2)$, where E, t and υ are the elastic modulus, thickness and Poisson's ratio respectively. Eq. (6.10) provides first subtle insight into the manifestation of curvature effects. Since the bending-strain energy of deformed shell is a function of a change in radius of shell due to loading and not merely of its initial curvature, there is a potential for the existence of non-monotonic relationships with respect to the curvature. From Fig. 6.14, it can be seen that during the impact, Panel B undergoes a large deformation resulting in a drastic change of its initial curvature, while Panel A only shows a moderate degree of change in its initial curvature for given pressure load. Thus according to eq.(6.10) it can be concluded that Panel B exhibits higher bending strain and undergoes higher damage compared to other two panels. This was observed in Figs.6.15-6.17

This can be further explained using an example - consider the impact process where a fixed plate deforms elastically under loading. During impact, the plate deforms elastically and shock wave is reflected. Elastic stress wave propagates through the plate transforming stress and strain states and induce changes in its motion. The reflected shock wave then impacts the plate before its strain energy completely relaxes. Thus bending-strain energy being a function of change in panel's curvature under loading, there exists a potential for an ideal configuration state i.e. initial radius of curvature that would maximise panel's ability to resist blast. While no proof has been provided to support this ideal configuration to support the ideal configuration state hypothesis, the aim of this discussion was to demonstrate that the effects of curvature are represented in governing equation of motion of plates and that the amount of energy stored in a deforming plate is affected by both initial curvature and more importantly, its change of curvature under loading.

The developed numerical model was utilised to investigate the optimum curvature of the CFRP panel that would result in better blast-mitigation

properties. The incident shock energy was maintained as before for comparability. Since Panel C outperformed the other two, it was considered as a basis for the optimisation. Here CFRP panels with radii of curvature varying between 105 mm to 76 mm (105 mm, 100 mm, 90 mm, 87 mm, 80 mm and 76 mm) were simulated. It was observed that, as the radius of curvature of the CFRP panel was reduced (from 110 mm to 76 mm); the shock wave glided over the exposed surface, and almost no noticeable out-of plane deflection was observed. In case of CFRP panel with the radius of curvature of 76 mm (Panel D), the major portion of shock energy was reflected by the panel towards the shock-tube wall and partially vented outside the fluid-structure domain.

Furthermore, the shock wave, reflected back from the shock-tube wall towards the CFRP panel, was reduced by the air surrounding the panel, and no significant out-of-plane deflection was observed. In this case, no damage was found on the exposed surface of, as well as within, the CFRP panel. The impact energy was noted to be as small as 30% of the incident energy. The pressure load was then gradually increased to 9.5 MPa (i.e. exceeding the failure level for Panel C) where the panel failed catastrophically due to fibre breakage. The critical blast pressure was about 19% higher than that responsible for failure in Panel C. The panels with radii of curvature below 76 mm were not simulated since their shape closely represents that of a closed cylinder where the application of appropriate boundary conditions could not be maintained.

Table 6.2 Results of parametric study: Blast load sustained by panels before their failure

Panel radius (mm)	76	80	87	90	100	105
Threshold blast load (MPa)	9.4	9.2	9.1	8.8	8.4	8.2

Also, the further reduction in the curvature would lead to the situation with the projected area of the shock tube spreading beyond the contour of the panels.

The magnitude of maximum blast load sustained by the simulated panels just before their catastrophic failure is listed in Table 6.2.

6.5 Conclusions

The effect of curvature of composite panels on their blast-mitigation capacity was studied using a shock-tube apparatus. The performance of these panels under blast loading was characterised in terms of their out-of-plane deflection, in-plain stress and the damage and failure scenarios. A finite-element model was developed to simulate blast loading of curved CFRP panels and validated using the 3D DIC data coupled with high-speed photography. This model accurately accounted for the interaction between the shock wave, curved panels, shock tube and surrounding air. After validation, the FE model was employed to predict the optimum panel curvature that would demonstrate superior blast-mitigation properties using the envelope of parameters not covered by the experimental conditions. The following conclusions were drawn:

1. The experimental analysis based on macroscopic post-mortem assessment and the DIC data for deflection, velocity, and in-plane strain showed that Panel C (radius of curvature - 112 mm) was capable of sustaining the highest threshold failure load, though a further optimisation study using a validated FE model revealed that a panel with 76 mm radius of curvature (Panel D) performed better than Panel C reflecting about 90% of the incident shock energy.
2. There were two main deformation modes contributing to deflection of the studied panels under shock loading: flexural and indentation. Flexural deformation decreased and indentation deformation increased as the radius of curvature was reduced. The indention mode was found to be more severe since it led to the damage-initiation in the panels.
3. Fibre breakage was the dominant mode of damage observed in the studied panels at the failure loading and was captured reasonably accurately with the developed FE model.

Next chapter outlines the conclusions of this research work and summarises its advantages and outcomes. The research outlook and future work is also discussed.

CHAPTER 7

CONCLUSIONS AND OUTLOOK

7.1 Conclusions

The study presented in this thesis has resulted in the formulation of a failure model for FRP composite materials based on a combined work of Hashin (1980) and Puck (1998). It provides a robust numerical implementation. This dynamic failure model takes into account the mechanical behaviour of a composite laminate and is capable of modelling its through-thickness stress response, strain-rate sensitive behaviour at different loading rates, non-linear behaviour of matrix, damage-initiation and its progressive failure along with the erosion. These failure criteria are implemented into a general purpose FE software ABAQUS/Explicit that can efficiently handle FE simulations aimed at modelling dynamic events and progressive degradation of material stiffness based on the damage propagation.

Another advantage of this model lies in the fact that it can be applied to multi-directional as well as woven fabric composite laminates with the slight modification in the terminologies used to define elastic moduli and ply level stresses in failure criteria. Moreover, the ability of this material model to capture linear and nonlinear loading allows the prediction of material behaviours developing nonlinearity at high strain rates. To explore these characteristics finite-element models are developed and mechanical behaviour of laminated composites under high load-rate phenomena: ballistic-impact and blast was studied.

A ballistic-impact response of four woven fabric composite laminates was studied using a finite-element model. It was characterised in terms of ballistic limit velocities (V_{50}) based on the same thickness. Further comparison of V_{50}

was facilitated for the unit areal density of a laminate to obtain more precise solution. Damage modes in these laminates were studied. The effect of hybridisation on damage modes and contribution of these to energy absorption capacity of a laminate was also discussed. The FE model successfully captured the global response e.g. (V_{50}) as well as local response (damage) both quantitatively and qualitatively. Some fundamental observations based on this study are listed below.

- Ballistic-impact velocity (V_{50}) was the highest for low-modulus, high strain-to failure fibre laminates and lowest for high-modulus, low strain-to failure fibre laminates while it was of intermediate magnitude for their hybrids for the same laminate thickness. This hierarchy was different when their response was analysed for the same areal density. Thus appropriate criteria of their selection in design of such structures depend on the requirement of the application, for example – minimum weight and /or maximum impact resistance.
- The main deformation and damage mechanisms of studied laminates were fibre failure and delamination governed by high-modulus, low strain-to failure fibre laminates. The tensile fracture of the rear ply of the laminate subjected to bending was observed leading to damage imitation. In addition, intraply fracture by crushing below the impactor was also initiated in the front plies. Intraply cracks formed in the front and rear plies propagated through the lamina until they were deflected at the interply interface.
- Improvements in the behaviour under impact by hybridization were due to the higher strain-to-fracture of the low-modulus fibre plies located near the front and back laminate surfaces. Hybridisation provided a reasonable trade-off between in-plain strength and failure strain that resulted in better ballistic-impact resistance properties compared to high modulus fibre composites.

- To design hybrid composite structures with improved ballistic resistance, it is preferred to build a laminate in such a way that high strain-to failure fibre plies encompass those with low strain-to-failure. This will ensure better in-plain strength of a laminate combined with its better energy absorbing capacity.

In case of numerical study of blast, the effect of curvature of composite panels on their blast-mitigation capacity was studied using a shock-tube apparatus. The performance of these panels under blast loading was characterised in terms of their out-of-plane deflection, in-plain stress and the damage and failure scenarios. A finite-element model was developed to simulate blast loading of curved CFRP panels and validated using the 3D DIC data coupled with high-speed photography. This model accurately accounted for the interaction between the shock wave, curved panels, shock tube and surrounding air. After validation, the FE model was employed to predict the optimum panel curvature that would demonstrate superior blast-mitigation properties using the envelope of parameters not covered by the experimental conditions. The following conclusions were drawn:

- FE models showed that the blast resistance of curved CFRP panels increased as their radii of curvature were reduced (for the studied range). This was concluded to be due to the alterations in the projected area of the curved panels in contact with a shock tube.
- There were two main deformation modes contributing to deflection of the studied panels under shock loading: flexural and indentation. Flexural deformation decreased and indentation deformation increased as the radius of curvature was reduced. The indention mode was found to be more severe since it led to the damage-initiation in the panels.
- Fibre breakage was the dominant mode of damage observed in the studied panels at the failure loading and was captured reasonably accurately with the developed FE model.

- Parametric studies performed using FE model revealed that further optimisation of CFRP panel's curvature was possible and would further improve its design (geometry) to blast load.

7.2 Outcomes

The potential outcomes of this study are listed below.

(A) Proposition of a generalised form of a failure criteria

- The 3D failure criteria proposed in this study can adequately capture the global failure response of a variety of polymer composite laminates under various impact scenarios - from low to high velocity. This provided a convenient virtual tool for the assessment of critical failure mechanisms of a structure made of such materials and can be of great interest to the industrial community, especially aviation and defence industry, for example,. to optimise the layup of composite structures, as in case of hybrid composites and to build and assess their dynamic response beforehand to save manufacturing costs.
- The FE modelling methodology employed in this work can be incorporated into the routine design process within the industry.

(B) Understanding response of laminated composites under different impact scenarios

A better understanding of deformation and damage behaviour of polymer matrix composites to impact loading is gained in this study. For the research community, it is important to understand the response of laminated composites under various dynamic loading scenarios to help improve their structural design. In this regard, this study provided an insight into the air blast and ballistic impact behaviour of polymer composites laminates, underlying damage modes and their interactions. The detailed outcomes are listed below.

- 3D FE models based on ply-by-ply approach enables determination of the through-thickness stress-state within laminates. This allows analysis of interlaminar delamination and damage in thickness direction.
- The account for strain-rate dependent behaviour of composite laminates helped in reasonably accurate prediction of global response of structure as well as local damage modes.
- The FE models considered complex contact interactions during the ballistic-impact and blast events reasonably accurately without compromising accuracy yet were computationally economical.
- A numerical model of ballistic-impact provided deeper understanding of the effect of hybridisation on composites laminates and its potential use in design of such structures with improved resistance.
- Further to this, these FE models can be used to conduct parametric studies in order to help optimising geometric features of structures under severe dynamic loading. For example, in blast study for CFRP panels, a validated FE model was employed to estimate their optimised curvature.

Besides the advantages and potential uses of this study, it is also imperative to recognise the areas that require further attention both in terms of improving numerical efficiency and prediction capability. In this regard, following areas have been identified:

(A) Account for discrete geometry of constituents

- FE models developed in this study are based on the 3D homogeneous formulation of a laminate and do not account for its constituents discretely. This may compromise the efficiency of the numerical prediction. For example, in this study, for simulations involving woven fabric laminates - modelling friction between interlaced fabric tows is not possible due to homogeneous formulation of the problem. Thus estimation of higher V_{50}s in these simulations may be attributed to the reduced in-plane strength in the absence of this friction.

(B) Strain-rate dependant behaviour for CZE in delamination study

Strain-rate dependency of resin-rich areas represented by CZEs is not considered in simulations. There are two reasons for this: first, the experimental data for high strain-rate behaviour of interfaces is not available for studied laminates. Secondly, in all the studied simulations, the dominant damage mode was fibre failure, resulting in the penetration of the structure under impact. For example, in FE model of ballistic-impact, different damage modes contributing to energy absorption capacity of a laminate were evaluated and that of delamination was found to be the lowest.

7.3 Future work

It is believed that the present study can be further improved with the proper attention to the following research areas:

(A) Microstructure analysis and randomness

- Though continuum level FE modelling approach presented in this study appears sufficient to model damage of FRP panels at the relevant length scale (i.e. meso-scale), it is possible to assess the damage of the laminated composites in more details by modelling their microstructures where a proper geometry of individual constituents will be accounted for. This is a challenging task from the point of view of the computational efficiency, though it may provide a better idea of the damage modes and their interaction during impact loading conditions.
- In the current model, it was assumed that the fibres in a ply are uniformly distributed, which in general, is not a case. The fibres are often randomly distributed in a ply which generally affects its overall strength. In this regards, microscopic analysis of the studied laminates needs to be performed. The randomness scatter can be analysed using statistical

techniques. Finally using Weibull's theory (1951) a randomness parameter can be generated that can be later linked to the ply strength.

(B) Hydro-dynamic response

- It is envisaged that the capability of the proposed material model can be further extended to analyse the hyper-velocity impact (HVI) loading on to the composite structures.
- It is commonly known fact that under HVI, structures behave as a fluid and strength of material upon impact is very small compared to the inertial stresses often governed by its hydrodynamic response. A proper mathematical formulation is needed to incorporate this effect in the current FE model.

(C) Numerical cost

The numerical effectiveness of the current FE model can be analysed by employing several other numerical schemes, such as: extended finite-element method (XFEM) and smooth particle hydrodynamics (SPH) as discussed in Chapter 3. For example, XFEM method can be utilised to model propagating cracks, and provide reasonably accurate results even for the coarse meshes due to added degree of enrichment ahead of the crack tip. Also SPH consist of single node particles bounded by a volume and can be very useful for modelling large deformation events.

These improvements to the numerical simulation studies may lead to more reliable and efficient use of advanced composite material models. This in turn, has the potential to improve safety and reduce development cost of protective composite structures. Finally, the interesting results obtained in Chapter 6 regarding the curvature of composite panels can be investigated further.

REFERENCES

ABAQUS. (2010). *ABAQUS 6.10 Theory manual*. Dassault System, UK.

Abdel, G. F. (2000). *A three-phase constitutive model for macrobrittle fatigue damage of composites*. PhD thesis, College of Engineering and Mineral Resources at West Virginia University.

Abdel-Wahab, A. A., Maligno A. R. and Silberschmidt V. V. (2012) Micro-scale modelling of bovine cortical bone fracture: Analysis of crack propagation and microstructure using X-FEM. *Computational Materials Science*. 52(1), pp.128-35.

Abrate, S. (1991). Impact on laminated composite materials. *Applied mechanics review*. 44(4), pp. 155-190.

Abrate, S. (2011). *Impact engineering of composite structures*: Springer.

Adams, D. F, Carlsson, L. A. and Pipes, R.B. (2003.) *Experimental characterization of advanced composite materials*: CRC Press.

Adumitroaie, A. and Barbero, E. J. (2011). Beyond plain weave fabrics – II. Mechanical properties. *Composite Structures.* 93, pp. 1449-62.

Airoldi, A., Sala, G. and Bettini, P. (2009). Evaluation of a numerical approach for the development of interlaminar damage in composite laminates. *Composites Science and Technology*. 34, pp. 45-53.

Alfano, G. and Crisfield, M. A. Finite element interface models for the delamination analysis of laminated composites: mechanical and computational issues. *International Journal for Numerical Methods in Engineering*. 200150(7), pp. 1701-36.

Allix, O. and Blanchard, L. (2006). Meso-modelling of delamination: towards

industrial applications. *Composites Science and Technology*. 66(6), pp. 731-44.

Arora, H., Hooper, P. A. and Dear, J. P. (2011). Dynamic response of full-scale sandwich composite structure subject to air-blast loading, *Composites: Part A*. 42, pp. 1651-62.

Arora, H., Hooper, P., Dear, J. P. (2010). *Impact and blast resistance of glass fibre reinforced sandwich composite materials*. In: Proceedings of IMPLAST.

ASTM F1233-08 (2008). Standard test method for security glazing systems and materials.

Azzi, V. and Tsai, S. (1965). Anisotropic strength of composites. *Experimental Mechanics*. 5(9), pp. 283 – 288.

Bažant, Z. P. and Oh, B.H. (1983). Crack band theory for fracture of concrete. *Materials and structures*.16, pp.155-77.

Barbero, E. J. (2010) *Introduction to composite materials design*: CRC press.

Barbero, E. J. and Lonetti, P. (2002). An inelastic damage model for fibre reinforced laminates. *Journal of Composite Materials*. 36(8), pp. 941-62.

Barbero, E., Lonetti, P. and Sikkil, K. (2006). Finite element continuum damage modelling of plain weave reinforced composites. *Composites Part B: Engineering*. 37(2-3), pp. 137 – 47

Barenblatt, G. I. (1962). The mathematical theory of equilibrium cracks in brittle fracture. *Advances in applied mechanics*. 7(55-129), pp.104-09.

Belytschko, T. and Black, T. (2006). Elastic crack growth in finite elements with minimal remeshing. *International Journal for Numerical Methods in Engineering*. 45(5), pp. 601-20.

Benzeggagh, M. L and Kenane, M. (1996). Measurement of mixed-mode delamination fracture toughness of unidirectional glass/epoxy composites with mixed-mode bending apparatus. *Composites Science and Technology*. 56(4), pp. 439-49.

Böhm, H. J. (2005). *Mechanics of microstructured materials*. New York: Springer.

Brunner, A. J., Blackman, B. R. K. and Davies, P. (2008). A status report on delamination resistance testing of polymer-matrix composites. *Engineering Fracture Mechanic*s. 75(9), pp. 2779-94.

Bunsell, A. R. and Renard, J. (2005). *Fundamentals of fibre reinforced composite materials*: Taylor & Francis.

Camanho, P. P. and Davila, C. G. (2002). *Mixed-mode decohesion finite elements for the simulation of delamination in composite materials*. NASA-Technical Paper. 211737.

Camanho, P. P., Davila, C. G. and De Moura, M. F. (2003). Numerical simulation of mixed mode progressive delamination in composite materials. *Journal of Composite Materials*. 37(16), pp. 1415.

Cantwell, W. J. and Morton, J. (1991). The impact resistance of composite materials – a review. *Composites Part A: Applied science and manufacturing*. 22(5), pp.347-362.

Cantwell, W. J., Curtis, P. T and Morton, J. (1986). An assessment of the impact performance of CFRP reinforced with high-strain carbon fibres. *Composite Science and Technology*. 25, pp.133-148.

Chaboche, J. (1988). Continuum damage mechanics: general concepts. Transactions of the ASME*. Journal of Applied Mechanics*. 55(1), pp. 59 – 64.

Chang, F. K. and Chang, K. Y. (1987). Post-failure analysis of bolted composite joints in tension or shear-out mode failure. *Journal of Composite Materials*. 21(9), pp. 809–33.

Chang, F. K. and Chang, K. Y. (2006). A progressive damage model for laminated composites containing stress concentrations. *Journal of Composite Materials*. 21(9), pp. 834-42.

Chawla, K. K. (2007). *Composite materials: Science and Engineering*. Third Ed. New York: Springer.

Cheng, W. L, Langlie S., and Itoh, S. (2003). High velocity impact of thick composites. *International Journal of Impact Engineering*. 29, pp.167–84.

Clegg, R. A., White D.M., Riedel W. and Harwick W. (2006). Hypervelocity impact damage prediction in composites: Part I—material model and characterisation. *International Journal of Impact Engineering*. 33(1–12), pp. 190-200.

Cook, R. D., Malkus, D. S., Plesha, M. E. and Witt, R. J. (2001). *Concepts and applications of finite element analysis*: John Wiley & Sons, Inc.

Cox HL. (1952). The elasticity and strength of paper and other fibrous materials. *Journal of applied physics*. 3:72-79.

Cox B. and Flanagan G. (1997). *Handbook of analytical methods for textile composites,* NASA, USA.

Cox, B. and Yang, Q. (2006). In quest of virtual tests for structural composites. Science. 314(5802), pp. 1102-7.

Crisfield, M. (1994). *Non-linear finite element analysis of solids and structures*: John Wiley & Sons.

Cui, W. and Wisnom, M. (1993). A combined stress-based and fracture-mechanics-based model for predicting delamination in composites. *Composites*. 24(6), pp.467-74.

Cui, W., Wisnom, M. and Jones, M. (1992). A comparison of failure criteria to predict delamination of unidirectional glass/epoxy specimens waisted through the thickness. *Composites*. 23(3), pp.158-66

Cuntze, R. (2004). The predictive capability of failure mode concept-based strength criteria for multi-directional laminates - part B. *Composites Science and Technology*. 64(3-4), pp. 487 – 516.

Cuntze, R. and Freund, A. (2004). The predictive capability of failure mode concept-based strength criteria for multidirectional laminates. *Composites Science and Technology*. 64(3-4), pp. 343 – 77.

Daggumati, S., De Baere, I., Van Paepegem, W., Degrieck, J., Xu, J. and Lomov, S. V. (2010). Local damage in a 5-harness satin-weave composite under static tension: Part I - Experimental analysis. *Composites Science and Technology*. 70, pp. 1926-33.

Daniel, G., Suong, V. H. and Stephen, W. (2003). *Composite Materials: Design and Applications*: CRC Press, 2nd ed.

Daniel, I. M., Werner, B. T. and Fenner, J. S. (2011). Strain-rate-dependent failure criteria for composites. *Composites Science and Technology*. 71(3), pp. 357-364.

Daudeville, L., Allix, O. and Ladeveze, P. (1995). Delamination analysis by damage mechanics: some applications. *Composites Engineering*. 5(1), pp.17-24.

Davison, L. (2008). *Fundamentals of shock wave propagation in solids*. USA,

Springer.

Dávila, C. G. and Camanho, P. P. (2003). *A failure criterion for FRP laminates in plane stress*. Technical Report NASA/TM-2003-212663.

De Carvalho, N. V., Pinho, S. T. and Robinson, P. (2012). Analytical modelling of the compressive and tensile response of woven composites. *Composite Structures*. 94(9), pp.2724-35.

De Carvalho, N.V, Pinho, S.T and Robinson, P. (2011). An experimental study of failure initiation and propagation in 2D woven composites under compression. *Composites Science and Technology*. 71(10), pp.1316-25.

De Carvalho, N.V., Pinho, S.T. and Robinson, P. (2012). Numerical modelling of woven composites: Biaxial loading. *Composites Part A: Applied Science and Manufacturing*. 43(8), pp.1326-37.

Dugdale, D. S. (1960). Yielding of steel sheets containing slits. *Journal of Mechanics and Physics of Solids*. 8(2), pp.100-4.

Edlund, U. and Volgers, P. (2004). A composite ply failure model based on continuum damage mechanics. *Composite Structures*. 65(3-4), pp. 347 – 355.

Ernst, G., Vogler, M., Hühne, C. and Rolfes, R. (2006). Multiscale progressive failure analysis of textile composites. *Composites Science and Technology*. 70(1), pp.61-72.

ESI (2004). *PAM-CRASH User's Manuals*. ESI/PSI, Inc, Paris, France.

Fang, X. J, Yang, Q. D, Cox, B. N and Zhou Z. Q (2011). An augmented cohesive zone element for arbitrary crack coalescence and bifurcation in heterogeneous materials. *International Journal for Numerical Methods in Engineering*. 88(9), pp. 841-61.

Fang, X. J, Zhou, Z. Q, Cox, B. N and Yang Q. D. (2011). High-fidelity simulations of multiple fracture processes in a laminated composite in tension. *Journal of Mechanics and Physics of Solids*. 59(7), pp. 1355-73.

Floyd, A. M. (2004). *An Engineering Approach to the Simulation of Gross Damage Development in Composite Laminates*. PhD thesis. University of British Columbia.

Gardner, N., Wang, E., Kumar, P. and Shukla, A. (2012). Blast Mitigation in a Sandwich Composite Using Graded Core and Polyurea Interlayer. *Experimental Mechanics*. 52(2), pp. 119-133.

Garg, A. C. (1988) Delamination-a damage mode in composite structures. *Engineering Fracture Mechanics*. 29(5), pp. 557-84.

Gómez-del Río, T., Barbero, E., Zaera, R. and Navarro, C. (2005). Dynamic tensile behaviour at low temperature of CFRP using a split Hopkinson pressure bar. *Composites Science and Technology.* 65(1), pp. 61-71.

Gözlüklü, B. and Coker, D. (2012). Modelling of the dynamic delamination of L-shaped unidirectional laminated composites. *Composite Structures*. 94(4), pp.1430-42.

Hallett, S. R., Jiang, W. G., Khan, B. and Wisnom, M. R. (2008). Modelling the interaction between matrix cracks and delamination damage in scaled quasi-isotropic specimens. *Composites Science and Technology*. 68(1), pp. 80-9.

Halquist (2006). *LS-DYNA Theory Manual V971*. Livermore Software Technology Corporation.

Hansbo A. and Hansbo P. (2004) A finite element method for the simulation of strong and weak discontinuities in solid mechanics. Computer Methods in *Applied Mechanics and Engineering*. 193(33), pp. 3523-40

Harper, P. W. and Hallett, S. R. (2008). Cohesive zone length in numerical simulations of composite delamination. *Engineering Fracture Mechanics*. 75(16), pp. 4774-92.

Hashin, Z. (1980). Failure criteria for unidirectional fibre composites. *Journal of Applied Mechanics. 47,* pp. 321-329.

Hashin, Z. (1985). Analysis of cracked laminates: a variational approach. *Mechanics of materials*. 4(2), pp. 121-36.

Hashin, Z. and Rotem, A. (1973). A fatigue failure criterion for fibre reinforced materials. *Journal of Composite Materials*. 7, pp.448 – 64.

Hibbit, Karlsson and Sorensen (2011). *Abaqus User's Manual Version 6.11*. Michigan, USA.

Highsmith, A. L and Reifsnider K. L. (1982). *Stiffness reduction mechanisms in composite laminates in Damage* in Composite Materials: ASTM International. pp. 103–17.

Hill, R. (1963). Elastic properties of reinforced solids – some theoretical principles. *Journal of Mechanics and Physics of Solids*. 11(5), pp. 357 – 372.

Hinton, M. J. and Soden, P. D. (1998). Predicting failure in composite laminates: the background to the exercise. *Composites Science and Techn*ology. 58(7), pp. 1001-10

Hochard, C., Payan, J. and Bordreuil, C. (2006). A progressive first ply failure model for woven ply CFRP laminates under static and fatigue loads. *International Journal of Fatigue*. 28(10), pp. 1270 – 6.

Hoffman, O. (1967). Brittle strength of orthotropic materials. *Journal of Composite Materials*. 1(2), pp. 200 – 206.

Hsiao, H., Daniel, I., and Cordes, R. (1999). Strain rate effects on the transverse compressive and shear behaviour of unidirectional composites. *Journal of composite materials*, 33(17):1620 – 42.

Iannucci, L. (2006). Progressive failure modelling of woven carbon composite under impact. *International Journal of Impact Engineering*. 32(6), pp.1013-43.

Irwin, G. R. (1957). Analysis of stresses and strains near the end of a crack traversing a plate. *Journal of Applied Mechanics* ASME, New York.

Jackson, M., Shukla, A. (2011). Performance of sandwich composites subjected to sequential impact and air blast loading. *Composites Part B: Engineering*. 42(2), pp.55-66.

Johnson, A. (2001). Modelling fabric reinforced composites under impact loads. *Composites Part A: Applied Science and Manufacturing*, 32(9), pp.1197 – 206.

Johnson, A., Pickett, A. and Rozycki, P. (2001). Computational methods for predicting impact damage in composite structures. *Composites Science and Technology*; 61(15), pp.2183-92.

Johnson, H.E, Louca, L.A and Mouring, S., Fallah A.S. (2009). Modelling impact damage in marine composite panels. *International Journal of Impact Engineering*. 36(1), pp.25-39.

Jones, R.M. (1999). *Mechanics of composite materials*: Taylor and Francis, 2nd ed.

Kashtalyan, M. and Soutis, C. (2005). Analysis of composite laminates with intra and interlaminar damage. *Progress in Aerospace Sciences*. 41(2), pp.152-73.

Kästner, M., Haasemann, G. and Ulbricht, V. (2011). Multiscale XFEM-modelling and simulation of the inelastic material behaviour of textile-reinforced

polymers. *International Journal for Numerical Methods in Engineering*. 86(4-5), pp. 477-98.

Key, C. T., Schumacher, S. C. and Hansen, A. C. (2007). Progressive failure modelling of woven fabric composite materials using multicontinuum theory. *Composites Part B: Engineering*. 38(2), pp. 247 – 257.

Klinkova, O., Rech, J., Drapier, S., and Bergheau J. M. (2011). Characterization of friction properties at the workmaterial/cutting tool interface during the machining of randomly structured carbon fibres reinforced polymer with carbide tools under dry conditions. *Tribology International*. 44(12), pp. 2050-8

Koerber H., Xavier J. and Camanho, P. P. (2010). High strain rate characterisation of unidirectional carbon-epoxy IM7-8552 in transverse compression and in-plane shear using digital image correlation. *Mechanics of Materials*. 42(11), pp. 1004-19.

Kosevich, A. M., Lifshitz, E. M., Landau, L. D. and Pitaevskii, L. P. (1984). *Theory of Elasticity*: Butterworth-Heinemann, 3rd edition.

Krueger, R. (2004). Virtual crack closure technique: History, approach, and applications. *Applied Mechanics Reviews*. 57(2), pp.109-43.

Kumar, P., LeBlanc, J., Stargel, D. S. and Shukla, A. (2012). Effect of plate curvature on blast response of aluminium panels. I*nternational Journal of Impact Engineering*. 46, 74-85.

Ladeveze, P. (1995) A damage computational approach for composites: Basic aspects and micromechanical relations. Computational Mechanics. 17(1), pp. 142-50.

Ladevèze, P. and Dantec, E. L. (1992). Damage modelling of the elementary ply for laminated composites. *Composites Science and Technology*. 43(3),

pp.257 – 67.

Lapczyk, I. and Hurtado, J.A. (2007).Progressive damage modelling in fibre-reinforced materials. *Composites Part A: Applied Science and Manufacturing*. 38, pp.2333-41.

LeBlanc, J. and Shukla, A. (2011). Dynamic response of curved composite panels to underwater explosive loading: Experimental and computational comparisons. *Composite Structures*. 93, pp.3072-81.

LeBlanc, J., Shukla, A., Rousseau, C. and Bogdanovich, A. (2007). Shock loading of three dimensional woven composite materials. *Composite Structures* 79, pp. 344–55.

Li, S., Thouless, M., Waas, A., Schroeder, J. and Zavattieri, P. (2005). Use of mode-I cohesive-zone models to describe the fracture of an adhesively-bonded polymer matrix composite. *Composites Science and Technology*. 65(2), pp. 281-93.

Li, Z. and Lambros, J. (2000). Dynamic thermomechanical behaviour of fibre reinforced composites. *Composites Part A: Applied Science and Manufacturing*. 31(6), pp. 537-547.

Ling, D., Yang, Q. and Cox, B. (2009). An augmented finite element method for modelling arbitrary discontinuities in composite materials. *International journal of fracture*. 156, pp. 53-73.

Liu, P. F. and Zheng J. Y. (2010). Recent developments on damage modelling and finite element analysis for composite laminates: A review. *Materials and Design*. 31(8), pp.3825-34.

López-Puente, J. and Li, S. (2012) Analysis of strain-rate sensitivity of carbon/epoxy woven composites. International Journal of Impact Engineering.

48(0), pp.54-64.

Lua, J., Gregory, W. and Sankar, J. (2006). Multi-scale dynamic failure prediction tool for marine composite structures. *Journal of Materials Science*, 41(20), pp.6673 – 92.

Maimi, P., Camanho, P. P, Mayugo, J. A and Davila, C. G. (2006). *A thermodynamically consistent damage model for advanced composites*. Technical report NASA/TM-2006-214282, NASA; 2006.

Maimí, P., Camanho, P. P, Mayugo, J. A and Dávila, C. G. (2007). A continuum damage model for composite laminates: Part I - Constitutive model. *Mechanics of Materials*. 39(10), pp. 897-908.

Marsh, G. (2008). *Airbus takes on Boeing with composite A350 XWB*. http://www.reinforcedplastics.com/view/1106/airbus-takes-on-boeing-with-composite-a350-xwb/. (Accessed on 10/09/2013).

Matthews FL, Davies GA, Hitchings D and Soutis C. (2000). Finite element modelling of composite materials and structures: Woodhead Pub Ltd. Cambridge, UK

Matzenmiller, A., Lubliner, J., Taylor, R. L. (1986). A constitutive model for anisotropic damage in fibre-composites. *Mechanics of Materials*. 20(2), pp.125-52.

Melenk J. M. and Babuška I. (1996). The partition of unity finite element method: basic theory and applications. *Computer Methods in Applied Mechanics and Engineering*. 139(1):289-314.

Meo M. and Thieulot E. (2005). Delamination modelling in a double cantilever beam. *Composite Structures*. 71(3), pp. 429-34.

Mergheim J., Kuhl E. and Steinmann P. (2005). A finite element method for the

computational modelling of cohesive cracks. *International Journal for Numerical Methods in Engineering*. 63(2), pp. 276-89.

Mi, Y., Crisfield, M., Davies, G. and Hellweg, H. (1998). Progressive delamination using interface elements. *Journal of Composite Materials*. 32(14), pp.1246-72.

Moës, N. and Belytschko, T. (2002). Extended finite element method for cohesive crack growth. *Engineering Fracture Mechanics*. 69(7), pp. 813-33.

Mohamed G, Soutis C and Hodzic A. (2012). Blast Resistance and Damage Modelling of Fibre Metal Laminates to Blast Loads. *Applied Composite Materials*. 19(3-4), pp. 619-36.

Motamedi D. and Mohammadi S. (2012). Fracture analysis of composites by time Independent moving-crack orthotropic XFEM. *International Journal of Mechanical Sciences*. 54, pp. 20-37.

Mouritz, A. P. (2001). Ballistic-impact and explosive blast resistance of stitched Composites. *Composites Part B: Engineering*. 32, pp. 431–9.

Mouritz, A. P. The effect of underwater explosion shock loading on the fatigue behaviour of GRP laminates. (1995). *Composites*. 26, pp. 3–9.

Mourtiz, A. P. The effect of underwater explosion shock loading on the flexural properties of GRP laminates. (1996). *International Journal of Impact Engineering*. 18, pp. 129–39.

Naghipour, P., Schneider, J., Bartsch, M., Hausmann, J. and Voggenreiter, H. (2009). Fracture simulation of CFRP laminates in mixed mode bending. *Engineering Fracture Mechanics*. 76(18), pp. 2821-33.

Naik, N. and Doshi, A. (2008) Ballistic-impact behaviour of thick composites:

parametric studies. *Composite Structures*. 82, pp.447–64.

Naik, N. K., Shrirao, P. and Reddy, B. C. K. (2006) Ballistic-impact behaviour of woven fabric composites: Formulation. *International Journal of Impact Engineering*. 32(9), pp. 1521-1552.

Nairn J. A. (2000). Matrix Microcracking in Composites. *Polymer Matrix Composites*. 5, pp.403-432

Nairn, J. A and Hu, S. (1992). The initiation and growth of delaminations induced by matrix micro cracks in laminated composites. *International Journal of Fracture*. 57(1), pp. 1-24.

Nairn, J. A. (1989). The strain energy release rate of composite microcracking: a variational approach. *Journal of Composite Materials*. 23(11), pp. 1106 -29.

Needleman, A. A. (1987). A continuum model for void nucleation by inclusion debonding. *Journal of Applied Mechanics*. 54(3), pp. 525-31.

Nemes, J. and Speciel, E. (1996). Use of a rate-dependent continuum damage model to describe strain-softening in laminated composites. *Computers and Structures*. 58(6), pp. 1083 – 92.

Norris G. and Wagner M. (2005). *Airbus A380: Superjumbo of 21st century*: Zenith press, China.

Nurick, G. and Shave, G. (1996). The deformation and tearing of thin square plates subjected to impulsive loads – an experimental study. *International Journal of Impact Engineering*. 18, pp. 99–116.

Nurick, G., Olson, M., Fagnan, J., and Levin, A. (1995). Deformation and tearing of blast loaded stiffened square plates. *International Journal of Impact Engineering*. 16, pp. 273–91.

O'Brien T. K. (1982). Characterization of delamination onset and growth in a composite laminate. *Damage in Composite Materials: ASTM International*. pp. 140–67.

Ochoa, O.O. and Reddy, J.N. (1992). *Finite element analysis of composite laminates*. Springer.

Ochola, R. O., Marcus, K., Nurick, G. N. and Franz, T. (2004). Mechanical behaviour of glass and carbon fibre reinforced composites at varying strain rates. *Composites Structures*. 63, pp. 455-467.

Orifici, A. C., Herszberg, I. and Thomson, R. S. (2008). Review of methodologies for composite material modelling incorporating failure. *Composite Structures*. 86 (1-3), pp.194-210.

Pagano, N. J., Schoeppner, G. A., Anthony, K. and Carl, Z. (2000). *Delamination of Polymer Matrix Composites: Problems and Assessment in Comprehensive Composite Materials*. Oxford: Pergamon. pp. 433-528.

Pandya, K. S., Pothnis, J. R., Ravikumar G. and Naik, N. K. (2013). Ballistic-impact behaviour of hybrid composites. *Materials & Design*. 44(0), pp. 128-135.

París, F. (2001). *A study of failure criteria of fibrous composite materials*. Technical Report NASA/CR 2001-210661.

Parvizi, A. and Bailey, J. E. (1978). On multiple transverse cracking in glass fibre epoxy cross-ply laminates. *Journal of Materials Science*. 13(10), pp. 213-6.

Parvizi, A., Garrett, K. W. and Bailey, J. E. (1978). Constrained cracking in glass fibre reinforced epoxy cross-ply laminates. *Journal of Materials Science.* 13(1), pp. 195-201.

Pereira, A. B., de Morais, A. B. and de Moura, M. F. S. F. and Magalhães, A. G.

(2005). Mode I interlaminar fracture of woven glass/epoxy multidirectional laminates. *Composites Part A: Applied Science and Manufacturing*. 36 (8), pp.1119-27.

Pindera M. J., Khatam H., Drago A. S. and Bansal Y. (2009). Micromechanics of spatially uniform heterogeneous media: A critical review and emerging approaches. *Composites Part B: Engineering*. 40(5), pp. 349-78.

Pinho, S., Dàvila, C.G., Camanho, P. P., Iannucci, L. and Robinson, P. (2005). *Failure models and criteria for FRP under in-plane or three-dimensional stress states including shear non-linearity*. NASA Technical Memorandum. 213530.

Pinho, S., Iannucci, L. and Robinson, P. (2006) Formulation and implementation of decohesion elements in an explicit finite element code. *Composites Part A: Applied Science and Manufacturing*. 37(5), pp. 778-89.

Pinho, S.T., Robinson, P. and Iannucci, L. (2006). Fracture toughness of tensile and compressive fibre failure modes in laminated composites. C*omposite Science and Technology*. 66(13). pp. 123-30.

Puck, A. (1992). Fracture criteria for highly stressed fibre-plastics composites which meet requirements of design practice. Kunststoffe, *German plastics*, 82(2), pp.149 – 155.

Puck, A. (1996). *Festigkeitsanalyse von Faser-Matrix-Laminaten*. Hanser Fachbuch.

Puck, A. and Schneider, W. (1969). On failure mechanisms and failure criteria of filament-wound glass-fibre/resin composites. *Plastics and Polymers*. 37(127), pp. 33– 44.

Puck, A. and Schürmann, H. (1998). Failure analysis of FRP laminates by means of physically based phenomenological models*. Composites Science and*

Technology, 58(7), pp. 1045-67.

Raimondo, L., Iannucci, L., Robinson, P., Curtis, P. T. (2012). Modelling of strain rate effects on matrix dominated elastic and failure properties of unidirectional fibre-reinforced polymer–matrix composites. *Composites Science and Technology.* 72(7), pp. 819-827.

Rajendran, R. and Lee, J. M. (2009). Blast loaded plates. *Marine Structures*. 22, pp. 99-127.

Randles, P. and Nemes, J. F. (1992). Continuum damage model for thick composite materials subjected to high-rate dynamic loading. *Mechanics of Materials*. 13(1):1 – 13

Reeder, J. R. (1992). *An evaluation of mixed-mode delamination failure criteria*. Technical Memorandum-1992-104210: NASA Langley Research Centre.

Rice, J. R. (1968). A path independent integral and the approximate analysis of strain concentration by notches and cracks. *Journal of applied mechanics*. 35(2), pp. 379-86.

Riedel, W., Nahme, H., White D.M. and Clegg R. A. (2006). Hypervelocity impact damage prediction in composites: Part II—experimental investigations and simulations. International *Journal of Impact Engineering.* 33(1–12), pp. 670-680.

Römelt, P., Cunningham, P. R. (2012). A multi-scale finite element approach for modelling damage progression in woven composite structures. *Composite Structures*. 94(3), pp. 977-86.

Rybicki, E. F. and Kanninen, M. F. (1977). A finite element calculation of stress intensity factors by a modified crack closure integral. *Engineering Fracture Mechanics*. 9(4), pp. 931-8.

Sánchez-Sáez, S., Gómez-del Río, T, Barbero, E., Zaera, R. and Navarro, C. (2002). Static behaviour of CFRPs at low temperatures. *Composites B*: *Engineering*, 33, pp. 383–90.

Santiuste, C., Sánchez-Sáez, S. and Barbero, E. (2010). A comparison of progressive-failure criteria in the prediction of the dynamic bending failure of composite laminated beams. *Composite Structures*. pp. 92(10):2406-14.

Schubel, P. M., Luo, J. and Daniel, I. (2007). Impact and post-impact behaviour of composite sandwich panels. *Composites Part A: Applied Science and Manufacturing*. 38, pp. 1051–7.

Schweizerhof, K., Weimar, K., Münz, T., and Rottner, T. (1998). *Crashworthiness analysis with enhanced composite material models in Ls-dyna merits and limits*. Proceedings of the 5th International LS-DYNA Users Conference, Dearborn MI.

Segurado, J. and Llorca, J. (2006). Computational micromechanics of composites: The effect of particle spatial distribution. *Mechanics of Materials*. 38(8-10), pp.873-83.

Shi, Y., Swait, T., Soutis, C. (2012). Modelling damage evolution in composite laminates subjected to low velocity impact. *Composite Structures*. 94(9), pp. 2902-2913.

Shindo, Y., Takeda, T., Narita, F., Saito, N., Watanabe, S. and Sanada, K. (2009). Delamination growth mechanisms in woven glass fibre reinforced polymer composites under Mode II fatigue loading at cryogenic temperatures. *Composites Science and Technology*. 69(11–12), pp. 1904-11.

Silberschmidt, V. V. (2006). Effect of micro-randomness on macroscopic properties and fracture of laminates. *Journal of Materials Science*. 41(20), pp.

6768-76.

Silberschmidt, V. V. (2008). *Account for random microstructure in multi-scale models* in Multiscale modelling and simulation of composite materials and structures: Springer, New York.

Silva, M. (2005). Numerical simulation of ballistic-impact on composite laminates. *International Journal of Impact Engineering*. 31, pp. 289–306.

Simo, J. and Ju, J. (1987). Strain- and stress-based continuum damage models: formulation. *International Journal of Solids and Structures*. 23(7), pp.821 – 40.

Sokolinsky, V. S., Indermuehle, K.C. and Hurtado, J. A. (2011). Numerical simulation of the crushing process of a corrugated composite plate. *Composites Part A: Applied Science and Manufacturing*. 42(9), pp. 1119-1126.

Song, K. *Guidelines and Parameter Selection for the simulation of Progressive Delamination*. 2008. NASA, Langley Research Centre.

Soutis, C. (2000). *Finite element modelling of composite materials and structures*: Woodhead Pub Ltd.

Sound speed in gases - Hyperphysics. (2013). http://hyperphysics.phy-astr.gsu.edu/hbase/sound/souspe3.html (Accessed on 26/01/2014).

Talreja R. (1985). A continuum mechanics characterization of damage in composite materials. *Proceedings of the Royal Society of London A Mathematical and Physical Sciences*. 399(1817), pp.195-216.

Talreja, R. (1985). Transverse cracking and stiffness reduction in composite laminates. *Journal of Composite Materials*. 19(4):355 – 75.

Talreja, R. (1986). Stiffness properties of composite laminates with matrix cracking and interior delamination. Engineering Fracture Mechanics. 25(5-6),

pp. 751-62.

Talreja, R. (2006). Multi-scale modelling in damage mechanics of composite materials. *Journal of Materials Science*. 41(20), pp. 6800-12.

Talreja, R., and Singh C. (2008) *Multi-scale modelling for damage analysis in Multiscale modelling and simulation of composite materials and structures*. New York: Springer.

Talreja, R., and Singh, C. (2012). *Damage and failure in composite materials*: Cambridge University Press, New York.

Tay, T. E. (2008) Characterization and analysis of delamination fracture in composites: an overview of developments from 1990 to 2001. *Applied Mechanics Review*. 56(1), pp.1-32.

Tekalur, A.S., Shivakumar, K. and Shukla, A. (2008). Mechanical behaviour and damage evolution in E-Glass vinyl ester and carbon composites subjected to static and blast loads. *Composites Part B: Engineering.* 39, pp. 57–65.

Thollon, Y. and Hochard, C. (2009). A general damage model for woven fabric composite laminates up to first failure. *Mechanics of Materials*. 41(7), pp.820 – 827.

Tiwari, V., Sutton, M. A., McNeill, S. R, Xu, S., Deng, X. and Fourney WL. (2009). Application of 3D image correlation for full-field transient plate deformation measurements during blast loading. *International Journal of Impact Engineering*. 36, pp. 862–74.

Tsai, S. (1965). *Strength characteristics of composite materials*. Technical Report. NASA/CR-224.

Tsai, S. and Wu, E. (1971). A general theory of strength for anisotropic

materials. *Journal of Composite Materials*. 5, pp. 58 – 80.

Turon, A., Camanho P. P., Costa, J. and Dávila, C. G. (2006). A damage model for the simulation of delamination in advanced composites under variable-mode loading. *Mechanics of Materials*. 38(11), pp.1072-89.

Turon, A., Camanho, P. P., Costa, J. and Renart, J. (2010). Accurate simulation of delamination growth under mixed-mode loading using cohesive elements: definition of interlaminar strengths and elastic stiffness. *Composite Structures*. 92(8), pp.1857-64.

Turon, A., Dávila, C. G., Camanho, P. P. and Costa, J. (2007). An engineering solution for mesh size effects in the simulation of delamination using cohesive zone models. *Engineering Fracture Mechanics*. 74(10), pp. 1665-82.

Tvergaard, V. and Hutchinson, J. W. (1992). The relation between crack growth resistance and fracture process parameters in elastic-plastic solids. *Journal of Mechanics and Physics of Solids*. 40(6), pp.1377-97.

Ugural, A.C. (1998). *Stresses in Beams, Plates, and Shells*. Third Edition (Computational Mechanics and Applied Analysis). CRC press.

Ullah, H., Harland, A. R and Silberschmidt, V. V. (2013). Damage and fracture in carbon-fabric reinforced composites under impact bending. *Composite Structures*. 101(0):144-156.

Van der Meer, F. and Sluys, L. (2009). A phantom node formulation with mixed mode cohesive law for splitting in laminates. *International Journal of Fracture*. 158(2), pp.107-24.

Van der Meer, F. and Sluys, L. (2010). Mesh-independent modelling of both distributed and discrete matrix cracking in interaction with delamination in composites. *Engineering Fracture Mechanics*. 77(4), pp. 719-35.

Van Der Meer, F. P. and Sluys, L. (2009) Continuum models for the analysis of progressive failure in composite laminates. *Journal of Composite Materials*. 43(20), pp. 21-31.

Van der Meer, F., Sluys, L., Hallett, S. and Wisnom, M. (2012) Computational modelling of complex failure mechanisms in laminates. J*ournal of Composite Materials*. 46(5), pp. 603-23.

Wang, A. S. D, Kishore N. N. and Li C. A. (1895). Crack development in graphite-epoxy cross-ply laminates under uniaxial tension. *Composite Science and Technology*. 24(1), pp. 1-31.

Wang, E. and Shukla, A. (2010). Analytical and experimental evaluation of energies during shock wave loading. *International Journal of Impact Engineering*. 37, pp.1188–96.

Weibull, W. (1951). Statistical distributions function of wide applicability. *Journal of Applied Mechanics-Transactions of ASME.* 18 (3), pp. 293–297

Whitney J.M. (1971). Analysis of rail shear test - applications and limitations. *Journal of composite materials*. 5, pp. 23-30.

Williams, K. V., Vaziri, R. and Poursartip, A. (2003). A physically based continuum damage mechanics model for thin laminated composite structures. *International Journal of Solids and Structures*. 40(9), pp. 2267 – 2300.

Wimmer, G., Schuecker, C. and Pettermann, H. E. (2009). Numerical simulation of delamination in laminated composite components-A combination of a strength criterion and fracture mechanics. *Composites Part B*. 40(2), pp. 158-65.

Wisnom, M. and Chang F. K. (2000). Modelling of splitting and delamination in notched cross-ply laminates. *Composites Science and Technology*. 60(15), pp.

2849-56.

Wisnom, M. R. (2010). Modelling discrete failures in composites with interface elements. *Composites Part A: Applied Science and Manufacturing*. 41(7), pp. 795-805.

Xiao, J. R., Gama, B.A. and Gillespie Jr. J.W. (2007). Progressive damage and delamination in plain weave S-2 glass/SC-15 composites under quasi-static punch-shear loading. *Composite structures*. 78(2), pp.82-96.

Yamada, S. and Sun, C. (1978). Analysis of laminate strength and its distribution. *Journal of Composite Materials*. 12, pp. 275 – 84.

Yang, Q. and Cox, B. (2005). Cohesive models for damage evolution in laminated composites. *International Journal of Fracture*. 133(2), pp. 107-37.

Yen, C. F. (2002). *Ballistic-impact modelling of composite materials*. Proceedings of the 7th International LS-DYNA Users Conference. pp. 15–25

Zheng, X., Goldberg, Robert, K., Binienda, Wieslaw, K. and Roberts, Gary, D. (2003). *Ls-dyna implementation of polymer matrix composite model under high strain rate impact*. Technical Report NASA/TM-2003-212583.

Zhou, Z., Fang, X., Cox, B. and Yang, Q. (2010). The evolution of a transverse intra-ply crack coupled to delamination cracks. *International Journal of Fracture*. 165(1), pp.77-92.

Zhu, G., Goldsmith, W. and Dharan, C. K. H. (1992). Penetration of laminated Kevlar by projectiles: Experimental investigation. *International Journal of Solids and Structures*. 29, pp. 399–420.

Zou, Z., Reid, S. R and Li, S. (2003). A continuum damage model for delaminations in laminated composites. *Journal of Mechanics and Physics of*

Solids. 51(2), pp. 333-56.

Zureick, A. H. and A. T. Nettles (2002). *Composite Materials: Testing, Design, and Acceptance Criteria*, Issue 1416, ASTM International.